Application of Computational Fluid Dynamics To the Biopile Treatment of Hydrocarbon Contaminated Soil

Tong Wu

A thesis submitted for the degree of Doctor of Philosophy

The University of Edinburgh

Jan 2009

Dedicated to my parents

Declaration

I hereby declare that this thesis came into shape solely by myself under the supervision of Dr. Martin Crapper; and the work involved herein was accomplished by myself, except where due reference has been made. Moreover, this thesis contains no material, which has been accepted for the award of any other degree or professional qualification.

Tong Wu

Abstract

Biopiles are a common treatment for the ex-situ remediation of contaminated soil. Much research has been carried out on understanding and modelling of bioremediation techniques related to biopiles, but hitherto no study has attempted to model the effect on a biopile by its ambient surroundings. A hydraulics-based approach to simulating a biopile in the context of its ambient surroundings is presented in this study, taking into account physical, chemical and biological processes within the pile, external conditions of wind and temperature, the location of aeration pipes and venting pressure, and considering the spatial distribution of treatment as well as contaminant within the pile.

The simulation approach was based upon a fluid flow model which couples Eulerian multiphase flow model and Darcy's Law for immiscible fluid flow through porous media, a species transport model integrating advection, diffusion/dispersion and biodegradation, and a heat transfer model considering the interphase temperature equilibrium.

A Computational Fluid Dynamics (CFD) system has been developed to solve this set of mathematical models by applying the commercial CFD package FLUENT, and various trial simulations have been carried out to examine the potential of the hydraulics approach for practical applications.

The simulation produces reasonable results: the biodegradation process relates to the temperature within the pile, and the temperature in turn relates to wind speed and aeration details; due to the various fluid flow patterns, the contribution of each remediation mechanism (contaminant loss to atmosphere via pile surface, contaminant loss to aeration pipe and biodegradation) varies according to the aeration method; contaminant interphase transfer between different pairs of phases have greatly different impacts on contaminant removal. A number of counter-intuitive results are presented, indicating that simulations of this type will give valuable insight into the practical design of biopiling systems. The simulation system also allows the total environmental footprint of biopiling to be considered, examining not just degradation of contaminant but also its removal via volatilization and the energy used in heating air for venting. Further, the application of the approach formulated in this

study is not limited to biopiles, but can also be expanded to related in situ bioremediation techniques.

Acknowledgements

My dissertation would not have come into shape without the support and help from many people and from the University of Edinburgh.

As a natural starting point, I would like to express my deep gratitude to my supervisor, Dr. Martin Crapper, who is so responsible, responsive and dedicated. He has tirelessly offered insightful comments, suggestions, and constant help throughout my study here. Whenever I faced any hurdle in my work, he never hesitated to give his help immediately, and always encouraged me to keep pressing on. I have benefited greatly from the many discussions I have had with him, and this thesis would not have been in the present form without his constructive suggestions and revisions.

I would also like to thank Prof. Andrew Barry and Mr. Colin Cunningham. Both of them helped me a great deal in setting the direction of this research, and were always willing to guide me and share their knowledge. I am also indebted to Miss Rachel Verdon for proofreading my thesis even when she was very busy preparing for her final exams.

I am also grateful to my colleagues in the institute, who made my life in Edinburgh more enjoyable, and to the guys on the Inch Park basketball court for keeping me balanced with sports during my studies, long may it continue.

I would also like to express my appreciation for the assistance from a NERC/Dorothy Hodgkin Postgraduate Award which enabled me to pursue whatever interested me and to explore my full potential as a graduate student.

Lastly and most importantly, I would like to express my gratitude to my family: to my mother and father for their love, selfless support and dedication; to my wife's parents for their love; and most of all, to my dear wife, Haiping, for always being there encouraging me and helping me achieve my full potential in everything I set out to accomplish.

Contents

List of Figures

List of Tables

Notation

A variable can be assumed to be dimensionless where units are not shown.

$\vec{a}$	acceleration vector (m/s^2)
A	surface area of heat transfer (m^2) or cross sectional area (m^2)
b_{ca}	air utilization coefficient (kg/kg)
b_{cw}	water yield coefficient of water due to microbial metabolism (kg/kg)
B_{a_c}	net rate of species c consumed by biological transformation per unit total volume occurring in aqueous phase (mol/m^3 s)
c_c	specific heat capacity of the composting material (m^2/s^2 K)
C	contaminant concentration in the fluid (mol/m^3 or kg/m^3)
C_{ac}	concentration of species c in aqueous phase (kg/m^3)
C_{O_2}	concentration of oxygen in composting matrix (kg O^2/ m^3 dry air)
C_p	specific heat of different phases($J/[kg \cdot K]$=m^2/s^2 K)
D	species hydrodynamic dispersion coefficient (m^2/ s)
$\underline{D}$	species hydrodynamic dispersion tensor (m^2/ s)
D_h	species mechanical dispersion coefficient (m^2/ s)
D_0	species diffusion coefficient (m^2/ s)
D_s	species effective diffusion coefficient in porous media (m^2/ s)
D_{sh}	species effective hydrodynamic dispersion coefficient (m^2/ s)
E_{pqc}	mass transfer rate of species c from q to p phase per unit pore volume (mol/ s m^3)
$\overline{F}$	body force vector (kg/m^2 s^2)
F_{c_l}	consumption coefficient of species c with substrate l degradation(mol c/kg l)
$\overline{F}_{lift}$	lift force vector (kg/m^2 s^2)
$\overline{F}_{vm}$	virtual mass force vector (kg/m^2 s^2)
$\vec{g}$	gravity acceleration vector (m/s^2)
g_{O_2}	oxygen consumption coefficient (kg O^2/ kg degradable composting mass)
G	air flow rate (kg/s)
h_c	heat transfer coefficient between phases (kg m^2/s^3 K)
h_{evp}	latent heat of water vaporization (J/ kg=m^2/s^2)

h_q	specific enthalpy of the phase q (J/ kg=m^2/s^2)
h_{pq}	interphase enthalpy (J/ kg=m^2/s^2)
H_c	combustion heat of biodegradable substrate (J/ kg=m^2/s^2)
H_{input}	inlet gas enthalpy (J/ kg=m^2/s^2)
H_l	reaction enthalpy of substrate l degradation (J/ kg=m^2/s^2)
H_{output}	exit gas enthalpy (J/ kg=m^2/s^2)
I	unit tensor or inhibition function
J	hydraulic gradient
$\overline{J}$	hydraulic gradient vector
J_a	species advection flux (mol/ m^2 s or kg/ m^2 s)
J_h	species mechanical dispersion mass flux (mol/ m^2 s or kg/ m^2 s)
J_0	species diffusive mass flux (mol/ m^2 s or kg/ m^2 s)
J_{sh}	species hydrodynamic dispersion flux (mol/ m^2 s or kg/ m^2 s)
k	intrinsic permeability (m^2)
$\underline{k}$	intrinsic permeability tensor (m^2)
k_l	maximum specific substrate utilization rate (kg l/kg biomass s)
k_r	relative permeability
k_t	thermal conductivity (w/m k =kg m/ s^3 K)
k_T	first order rate coefficient for biodegradation at temperature T (1/s)
K	hydraulic conductivity (m /s)
$\underline{K}$	hydraulic conductivity tensor (m /s)
K_d	decay coefficient of the microorganisms (1/s)
K_{fc}	Freundlich isotherm parameters for species c adsorption $(m^3/kg)^{nc}$
K_H	Henry's Law constant (Pa= kg/ms^2)
K_{pq}	interphase momentum exchange rate between phase p and q (kg/s)
K_{pqc}	mass transfer coefficient for species c from q to p phase (1/s)
K^e_{pqc}	species equilibrium partition coefficient between phase p and q
K_s	half-velocity constant of Monod equation (kg/m^3)
m	mass of composting material (kg) or fitting variable for van Genuchten equation
m_a	air dry mass (kg)
m_c	compost dry mass (kg)

M_c	molecular weight of species *c* (kg/mol*)*
m_{cw}	compost water (kg)
m_{evp}	evaporation rate of water (kg/s)
m_{in}	mass flow rate of the inlet air (kg/d)
m_{out}	mass flow rate of the outlet air (kg/d)
$\dot{m}_{pq}$	mass transfer from the *p* phase to *q* phase (kg/m^3 s)
m_s	mass of biodegradable substrate
n	fitting variable for van Genuchten equation
n_c	Freundlich isotherm parameters for species *c* adsorption
n_{pore}	volumetric porosity
p	pressure (Pa=kg/m s^2)
p_c	capillary pressure (Pa=kg/m s^2)
p_{nw}	pressure in the nonwetting phase (Pa=kg/m s^2)
p_{gc}	partial pressure of the species c of the gas phase (Pa=kg/m s^2)
p_{vc}	vapour pressure of species *c* (Pa=kg/m s^2)
p_w	pressure in the wetting phase (Pa=kg/m s^2)
q	specific fluid discharge (m/s)
$\bar{q}$	specific fluid flux vector (m /s) or conductive heat flux (kg/s^3)
Q	heat content of the composting (J=kg m^2/s^2) or flow rate (m^3/s)
$Q_{ambient}$	heat flow to ambient air via the surface of the composter (J=kg m^2/s^2)
Q_{bio}	generation of bioreaction heat (J=kg m^2/s^2)
Q_c	convective heat transfer from solid-liquid to gas (J=kg m^2/s^2)
Q_{evp}	heat loss rate by evaporation (J/s= kg m^2/s^3)
Q_{input}	heat flow via the input air (J=kg m^2/s^2)
$\bar{Q}_{pq}$	heat exchange intensity between the phase *p* and q (kg/m s^3)
Q_{output}	heat flow via the output air (J=kg m^2/s^2)
R	universal gas constant 8.314472 (J/K mol= kg m^2/s^2 K mol)
$\bar{R}_{pq}$	interaction force between phases *p* and *q* (kg m /s^2)
S	source or sink term in governing equations (unit variable for different equations) or substrate concentration (kg/m^3)
$\bar{S}_a$	normalized aqueous saturation
S_m	solid content of the composting mixture

S_q	saturation of fluid q
S_r	residual saturation
T	temperature of the composting material (°C or K)
u	velocity in the x-direction (m/s)
U	overall heat transfer coefficient from composting to ambient surroundings ($kw/m^2K=1000kg/s^3$ K)
v	air velocity (m/s) or velocity in the y-direction (m/s)
V	composting pile volume (m^3) or velocity (m/s)
$\overline{V}$	fluid velocity vector (kg/m^3)
$\overline{V}_{pq}$	interphase velocity vector (m/s)
Vol_q	volume of phase q in a multi phases system (m^3)
$VOLPO2$	volume percentage of oxygen in the exhaust gas
w	velocity in the z-direction (m/s)
$w_{as,in}$	absolute humidity of saturated inlet air (kg/kg)
$w_{as,out}$	absolute humidity of saturated outlet air (kg/kg)
$x_{al}^{\max}$	inhibitory aqueous phase mole fraction of substrate l
$x_{al}^{\min}$	the minimum detectable aqueous phase mole fraction of substrate l
$x_{aN}^{\max}$	inhibitory aqueous phase mole fraction of nutrient N
$x_{aO_2}^{\min}$	limiting aqueous phase oxygen mole fraction
x_{qc}	mole fraction of species c in phase q
x_{pqc}^{e}	p phase mole fraction of species c in equilibrium with the q phase mole fraction of species c
X	biomass concentration (kg/m^3)
$X_{\min}$	indigenous microbial population in uncontaminated material (kg/m^3)
$X_{\max}$	maximum allowable biomass (kg/m^3)
Y_l	biomass yield coefficient for metabolism of substrate l (kg biomass/kg l)
α_q	phase q volume fractions in a multi phases system
γ_{oc}	activity coefficient of species c in the organic phase
Γ	control boundary
Γ_q	diffusion coefficient tensor for fluid q (m^2/ s)
ε	fitting variable for van Genuchten equation (Pa^{-1})
ε_a	air filled porosity of the composting (%)
θ	volume fraction

θ_r	residual volume fraction
λ_q	bulk viscosity of phase q (kg/m s)
μ	dynamic viscosity (kg/m s) or specific biomass growth rate (s^{-1})
ρ	density (kg/m^3)
ρ^m	molar density ($mole/m^3$)
$\hat{\rho}_q$	effective density of phase q (kg/m^3)
σ	fluid stress tensor (kg/m s^2)
τ	fluid shear stress tensor (kg/m s^2) or tortuosity effect
$\overline{\overline{\tau}}$	fluid stress tensor (kg/m s^2)
φ	piezometric head (m)
φ'	potential function (m)
ϕ	field variable
ϕ_g	gravity potential function
χ	temperature of gas in composting (K)
ω_c	species c sorbed to soil (kg c/kg soil)

Subscripts

a	immiscible fluid phase or aqueous phase
b	immiscible fluid phase
g	gas phase
l	degradable substrate
N	nutrient
O_2	oxygen
p, q	different fluid phases
s	solid phase

Superscripts

e	equilibrium status

Chapter 1 Introduction

1.1 Introduction

Pollution caused by non-degradable organic contaminants is becoming increasingly significant. Since many of these contaminants are mutagenic, teratogenic and carcinogenic, this kind of pollution is not only harmful in the long-term to people's living conditions, but can also seriously threaten health directly, especially considering its cumulative effect. Therefore, methods for the treatment of this form of pollution are developing swiftly.

A major source of organic contamination is initiated by leakage and spills of fuels or solvents from underground storage tanks into soil, and their subsequent migration into groundwater. This can occur as a result of the malfunction or misoperation of process equipment, and other kinds of accidents [1, 2]. Over the past few decades, people have spent billions of pounds in order to clean up sites contaminated in this way [3]. During this time, numerous treatment methods have been developed. The three most widely adopted solutions for treatment are disposal to landfill, combustion and bioremediation. However, landfill and combustion have some obvious disadvantages, for instance, landfill cannot reduce harmful substances quickly although it may allow such matters to degrade over time, and combustion requires high levels of investment. Comparatively, bioremediation is an environmentally friendly option for the low cost recycling of contaminated soils.

Bioremediation can be defined as a process that uses the inherent ability of certain living microorganisms, heterotrophic bacteria and fungi, to degrade hazardous organic materials and heavy metals into harmless materials such as carbon dioxide, methane, water, inorganic salts and biomass. The carbon and energy required for microorganism growth is taken from the biodegradation of organic contaminants during the bioremediation process. Complex, synthetic chemicals can also be transformed by co-metabolism [4].

Bioremediation treatment can be roughly divided into two categories: in situ and ex-situ. In situ

bioremediation techniques do not require the excavation of contaminated soil from sites before treatment [5], while ex-situ techniques involve the removing and relocation of wastes and contaminated soil to alternative land disposal facilities [3]. Some examples of in situ processes include bioventing, soil vapour extraction and air sparging. Ex-situ techniques include slurry reactors, composting and biofilters.

Although the development of bioremediation techniques originated from ex-situ processes, due to the excavation process involved, current research is predominantly focused on in situ solutions. However, ex-situ treatment displays remarkable advantages for some applications. The soil excavation and relocation not only enables the original site to recover quickly, but also allows for simpler and easier operational control of subsequent processes. Treatment can be more efficiently monitored, enabling unsuccessful processes to be avoided to the maximum extent. Additionally, some enhanced remediation methods, for instance surfactant and acid leaching, can be applied freely without needing to consider the polluting surrounding uncontaminated soil by mobilized contaminants [3].

Aside from the above advantages, a well-designed ex-situ bioremediation system is not a single functional process, but an integrated multifunctional complex, which supports sequential remediation processes. Normally, the contaminating source within a soil or industrial sludge is not single component, but consists of both various organic (volatile/non-volatile) and inorganic (soluble/nonsoluble or sorbed/unsorbed) pollutants. This mixture of pollutants can not be degraded with a single process. Most in situ process are only effective for a part of the pollutant, and still leave a significant quantity of contaminant unresolved with in the soil. Additionally, because of the high expense and equipment demand of in situ technologies, it is impossible to develop sequential in situ processes. However, for a well designed ex-situ bioremediation system, by changing the operating conditions, various processes can be achieved and eventually lead to a better treatment result [3]. Among various ex-situ methods, biopiles, also known as biocells, bioheaps, biomounds, and compost piles, are becoming an ever increasingly popular treatment technology, especially for petroleum hydrocarbon contaminated sites [6-8].

A biopile is actually a form of composting technique, which is an artificially controlled process of microbial aerobic decomposition, which results in the production of stabilized organic end products

which may be used as soil conditioners and/or organic fertilizers [9-13]. With biopile treatment, contaminated soils or industrial sludge are heaped into piles, and aerobic microorganism activity is stimulated within these piles by aeration and/or addition of minerals, nutrients, and moisture. The enhanced microorganism activity and accelerated metabolism process leads to the swift degradation of contaminants within the soils or sludge [14]. Meanwhile, volatile organics can be readily removed from the soil via the aeration process. Thus, even a basic biopile carries out not only a single degradation process but incorporates an additional evaporation process. Figure 1.1 shows industrial sludge biopiles in practice.

Figure 1.1 Ex-situ biopiles
(Photo © M. Crapper 2004)

A biopile system consists of at least three components: an aeration system, irrigation/nutrient injection system and a leachate collection system. An aeration system supplies oxygen to the microorganisms. Biopiles are frequently aerated by injection or extraction through slotted or perforated pipes, placed throughout the pile. An irrigation/nutrient injection system provides nutrients and moisture following pile construction: this is usually a spray or drip irrigation system built on the pile surface. Finally, a

leachate collection system controls excess moisture emanating from the pile. The leachate collection system consists of a containment berm or structure around the pile, perforated pipes at low points in the fill, a leachate collection pump connected to the drain piping, and a collection tank [15]. Figure 1.2 [3] presents a schematic description of such a soil biopile running concept.

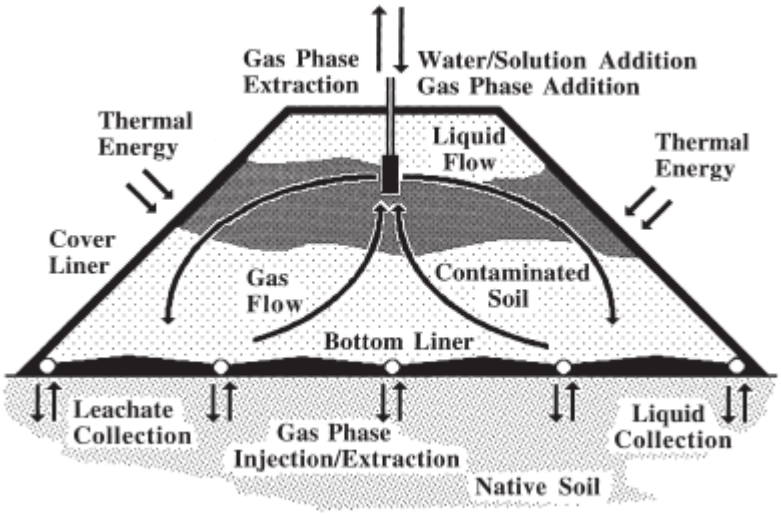

Figure 1.2 Conceptual geometry of an ex-situ biopile [3]

1.2 Key factors in biopile treatment

Though biopiles are a multifunctional method for the treatment of contaminated soils, the key microbial and environmental factors, which influence the treatment effect, are the same as common bioremediation technologies, or composting. These factors include environmental parameters (temperature, moisture content, pH and aeration), and parameters related to the nature of the substrate (C/N ratio, particle size, and nutrient content) [16, 17].

Oxygen (Aeration)

Oxygen is the preferred electron acceptor and is necessary for aerobic biodegradation of organic contaminants. Normally, oxygen is supplied by the injection or extraction of air through pipes within the pile. The aeration rate is very important for pile performance, and it is considered as “the most important factor in composting systems” [16]. If the aeration rate is too high, heat transfer within the

composting pile will become accelerated, thus temperature within the pile will decrease. If the aeration rate is inadequate, oxygen supply will decrease [18]. If the oxygen rate drops to an insufficient level, anaerobic processes will occur [19]. Therefore constant oxygen concentration must be maintained within the pile. It is suggested that a minimum oxygen concentration of 5% within the pore space of the composting pile is necessary for aerobic conditions [20]. Various aeration rates have been used in previous studies, e.g., 0.34-1.10 l air/ min·kg_{om} (litre air per minute per kilogram of organic material) [21], 0.3-0.9 l air/ min·kg_{om} [22], 0.69 l air/ min·kg_{om} [23] and 0.4 l air/ min· kg_{om} [17]. Aside from this, volatile contaminants in the pile can also be removed through volatilization into and flowing out with the air. Such a process is actually a primary remediation method in some in situ bioremediation techniques, such as soil vapour extraction.

Water

Water is essential for microorganisms, since they rely on water as a habitat for growth and survival. Water also provides a medium for the transfer of contaminants and affects the overall bioavailability of the contaminants. While low moisture content can inhibit microbial growth and mobility, excessive moisture will clog soil pores, thereby restricting necessary airflow. For a soil pile, water content should be maintained at 25 to 85% of the soil field capacity[*] [24] to sustain microbial activity. Optimal soil water content is generally 75% or higher of field capacity [4].

Nutrients

Biopiles use organic contaminants as a source of carbon and energy to build biomass. Typically the contaminants in a biopile provide an adequate amount of carbon, but the availability of other essential nutrients needed for microbial metabolism may be insufficient compared to the quantity of carbon [15]. The nutrients required for microbial proliferation include nitrogen, phosphorous, potassium, sulfur, magnesium, calcium, manganese, iron, zinc, and copper. Nitrogen and phosphorous are more likely to be deficient in a hydrocarbon contaminated pile. These nutrients can be applied in solid or liquid form during the pile construction or can be introduced through a drip irrigation system during

[*] Soil field capacity is the percentage of moisture remaining in a soil horizon 23 days after being saturated (by rainfall or irrigation) and after free drainage has ceased [24].

operation. Typically, the C:N:P ratio should be brought to within the range of 100:10:1 to 100:10:0.5 [14].

pH

pH is a measure of the hydrogen ion concentration. A neutral to slightly alkaline pH is the best condition for growth of most hydrocarbon bacteria. Hence, pH levels should be maintained around 7, and is restricted within the range of 5 to 9 to insure an effective bioremediation treatment [25]. pH adjustment is required if it lies outside the desired range prior to biopile operation. Soil pH can be raised through the addition of lime, and lowered by adding elemental sulfur during biopile construction [14].

Temperature

Temperature also affects the biodegradation rate. Although biological systems can operate over a wide range of temperatures, microbial activity declines as temperature decreases. At the temperatures below 10°C, microbial activity decreases considerably, and virtually ceases below 5°C. The microbial activity of most bacteria required for petroleum hydrocarbon biodegradation also fails at temperatures greater than 45°C. Within the range of 10°C to 45°C, the rate of microbial activity typically doubles for every 10°C rise in temperature [14]. On the other hand, when microbes digest hydrocarbons, heat is generated within the piles, causing the temperature of the pile to rise.

Microbial Population

For the successful implementation of a biopile, there must be an acclimatized, indigenous population of microorganisms within the pile which are capable of degrading the objective contaminants [4]. Normally, there are large numbers of various microorganisms existing in soil, including bacteria, algae, fungi, protozoa, and actinomycetes. People have found that in well drained soils, which are most appropriate for biopiles, these organisms are generally aerobic, and among these organisms, bacteria are the most abundant and biochemically active group, particularly at low oxygen levels [14].

1.3 Importance of aeration

Biopiles, as a kind of aerobic composting process, decompose organic substrates in the presence of oxygen [26]. Oxygen is considered essential for the microbial activity in composting, since it is an aerobic process [17]. The products of microbiological metabolism are primarily carbon dioxide, water, and heat [27]. The principal aeration techniques employed to provide O_2 during a composting process include: allowing it to percolate naturally through a static pile; physically turning the mass of soil at intervals; or in biopiles, passive and/or active aeration [28]. Natural aeration is the simplest and most cost effective method, as it requires no installations due to the process occurring only by diffusion and convection, and is regulated by the exposed surfaces of the pile [29]. Passive and active aeration techniques require the installation of ducts within the piles to enhance the convective forces. Passive aeration is then created by the temperature differences between the composting material and the ambient air [30] whilst active aeration requires fans to drive air into the ducts and consequently through the piles [20]. With active aeration, the aeration rate is usually controlled according to the pile temperature, since excessive aeration cools the piles and leads to large N losses, while inadequate aeration prevents the appropriate temperatures from residing in the pile as well as preventing adequate oxygen supply for microorganism biodegradation [31].

The important role of aeration in bioremediation has attracted great attention. Many researchers have explored the impacts of various aeration schemes on the bioremediation process.

With a one-month field trial, Li et al. [5] compared the performances of biopiles consisting diesel-contaminated soils using two different aeration pipe settings; one comprising two perforated vertical pipes with wind-driven turbines and the other a standard pile configuration with two horizontal perforated pipes. The data from a thirty day treatment showed that the normalized degradation rate of the biopile with vertical aeration pipes was significantly higher (1.26 times) than that found in the biopile with horizontal aeration pipes, with a considerably higher suction pressure in vertical pipes than in horizontal pipes. These authors also suggested investigating different aeration methods by means of modelling.

In a lab experiment studying agricultural waste composting, Kulcu and Yaldiz [17] applied four

different aeration rates (0.1, 0.2, 0.4, 0.8 l air/ min·kg_{om}) in four vertical forced aeration type reactors and one vertical natural convection type reactor. The results revealed that the highest organic matter degradation and temperature value were obtained at the aeration rate of 0.4 l air/ min·kg_{om} and not at the biggest aeration rate.

By comparing the performance of three aeration systems for pilot composting of swine manure from an economic perspective, Zhu et al. [32] suggested that passive aeration systems were suitable for a small scale swine farm, and forced aeration systems should be applied in medium and large scale swine farms with a high level of industrialization.

Shi et al. [33] evaluated the value of mature compost from dairy waste (faeces and urine of dairy cows with bedding material and additional straw) as soil nitrogen fertilizer, and found that composts treated with frequent turning, which is a form of aeration methods, had higher N mineralization potentials and mineralization rate constants (38 μg/g and 42e-3/d respectively) than composts without turning treatment (28 μg/g and 31e-3/d respectively).

Rhykerd et al. [34] examined the impact of bulking agents (non-bulked, hay, sawdust and vermiculite) which can lower the soil's bulk density, increase porosity, and may also enhance oxygen diffusion when added to soils, and the impact of various aeration methods (static, tillage and forced aeration) on remediation of oil contaminated soil. They concluded that tilling increased the rate and extent of remediation more than in soils receiving forced aeration or left static. After 12 weeks of composting, tilled-hay treatment decreased 82% of the total petroleum hydrocarbons contaminants, while non-bulked-static treatment removed only 33%.

In Hwang's work [35], three intermittent aeration modes were compared with a continuous aeration mode with respect to the degradation rate of diesel oil in a composting process for contaminated soil. Intermittent aerations were found to be more effective treatment methods for the degradation of both total petroleum hydrocarbons (TPH) and normal alkanes than continuous aeration. The highest efficiency of diesel oil degradation took place with the 1 hour aeration/3 hour rest mode among three intermittent aeration modes which were tested. In a 15 day treatment, 1 h aeration/3 h rest mode removed 89.5 TPH and 100.0% normal alkanes, while these two values were 86.3% and 98.6%

respectively for continuous aeration.

Godoby [36] studied an aged contaminated mixture of desert mining soil and sawdust with fuel oil at a laboratory scale. Since the soil had a high salinity and metal content, it was not clear whether it was suitable for bioremediation. However the researcher found that the aerated in-vessel composting method was feasible for the bioremediation of such contaminated soils and the highest contaminant removal amount reached 59%.

Yeung et al. [37] carried out field bioremediation on soil collected from a pipeline break site contaminated with crude oil. Four treatment conditions with different aeration and heating schemes were considered. The results showed that forced aeration (0.4 $l/min \cdot m^2$) apparently enhanced the biodegradation rate of hydrocarbon.

Cegarra et al. [38] performed field experiments on composts of a solid olive-mill by-product using two aeration methods; one by mechanical turning only, and the other by intermittent forced ventilation coupled with mechanical turning. With identical mechanical turning operations, the compost involving the forced ventilation completed the treatment in less time, while the other compost achieved similar results after a slight delay. In terms of economic value and desired composition of the end-product, the authors recommended mechanical turning alone for practical applications.

Due to its significance on bioremediation treatment efficiency, aeration is addressed as a key issue in this study.

1.4 Literature review on modelling of the bioremediation process

1.4.1 General

Following the development of computer science, mathematical modelling has become widely used in science and engineering. This relatively new technology can help people understand the operation of systems, test new theoretical ideas, predict performance of a process, and advantageously assist in industrial design problems. Furthermore, models can also take the part of or even the whole place of

physical experimentation, giving a more economical and laboursaving option.

Although in this study, the objective point of investigation is biopiling, it is better to broaden the review to the modelling of composting, not only because biopiling is a branch of composting, but also because research work on composting is more developed, and closely related to biopiles. Mathematical models of the composting process originally appeared in literature in 1976 [39]. Since then, research work on this topic has become more and more numerous. Researchers have developed a large number of models, covering a very big range, from microcosmic reaction models to macroscopical models which can simulate the performance of a compost system. In addition, achievements in modelling studies of wider fields, including groundwater contaminant, in situ bioremediation techniques such as soil vapour extraction (SVE) and bioventing (BV), and even food engineering, supply knowledge relevant to the understanding and prediction of composting system.

1.4.2 Modelling of composting

All composting models are based on the solution of heat and mass balance in time. The universal concept for analysis is [39]:

$$\text{Accumulation} = \text{input-output} \pm \text{transformation} \qquad (1.1)$$

Most composting models adopt a deterministic approach, while a few of them use a stochastic method [40, 41] or a statistical method [42]. Generally, researchers treat the composting system on a macroscale, which means the status of the entire compost is taken as homogeneous throughout the treatment process, and as a result, research has been focussed on the compost as a whole. Therefore, in such models, there is no difference between any two points in the composting system. However, a few other researchers [3, 43, 44] have included spatial simulation functionality within their models. They solve the problem from a microscale point of view where the entire compost is not treated as a whole, and although the particles of a composting pile are connected to each other, the changes of different parts vary from each other since they are located at distinct positions of a compost system.

(1) Variables simulated

The most important factors for composting treatment are the same as those for biopile treatment as mentioned in Section 1.2. Temperature is the first concern of most models. Nearly all models predict composting temperature except those models starting from the microcosmic perspective [3]. Normally, temperature is modelled from an unsteady state procedure which means that the temperature of composting changes with time during the whole treatment process; while some other research [20] treats the composting process as a continuous series of discrete steady state sections, each section accounts for a short period of the whole process and only stands for a particular temperature. Furthermore, in microscale models, temperature is modelled from the point of view of energy transport [43].

Moisture content is also simulated in most models. In macroscale models, moisture content is simulated from mass balance considerations, while in microscale models, moisture content, considered as an mobile phase, is modelled from equations of fluid flow in a porous medium [43].

Oxygen concentration is another common state variable simulated by many models [45-47].

Although the three variables stated above are key factors in the bioremediation process, microbial population (i.e. biomass concentration) is another contributing factor, which has only been considered by a few models. [43, 46-48]. In addition to this, pH and nutrient levels are further contributing factors, of which no existing models have investigated extensively.

Additional variables which have been predicted or considered include substrate concentration [46, 47], oxygen uptake rate [43, 46, 49], carbon dioxide evolution [42, 48, 50], water evolution [51-53], dry exit gas mass and exit gas water vapour [20], total solids/dry mass [42, 45, 52] and product solids composition [20, 47, 48]

(2) Mass balance considerations

Mass balance considerations are widely used for many variables, including air flow, moisture content and oxygen consumption.

The moisture content is associated with inlet air moisture content, outlet air moisture content and biodegradable mass conversion to water. Water produced from microbial transformation is always evaluated from yield factors based on compost mass removal or substrate biodegradation [45, 48, 53]. For example in Ekinci's work, compost water is simulated by the following expressions:

$$\frac{dm_{cw}}{dt} = w_{as,in} m_{in} - w_{as,out} m_{out} + b_{cw} \frac{dm_c}{dt} \qquad (1.2)$$

where m_{cw} is compost water (kg), $w_{as,in}$ and $w_{as,out}$ are the absolute humidity of saturated inlet and outlet air respectively (kg/kg), m_{in} and m_{out} are the air mass flow rate of the inlet and outlet (kg/d), b_{cw} is the yield coefficient of water due to microbial metabolism (kg/kg), and m_c is compost dry mass (kg).

A similar approach is used to analyze air balance, oxygen consumption and also carbon dioxide production [39]. The air balance expression should consider air utilization [54]:

$$\frac{dm_a}{dt} = m_{in} - m_{out} - b_{ca} \frac{dm_c}{dt} \qquad (1.3)$$

where m_a is the air dry mass (kg), and b_{ca} is air utilization coefficient (kg/kg).

The governing equation for oxygen concentration should include terms of oxygen accumulation, oxygen in and out of the composting matrix and consumption due to biodegradation [55]:

$$\varepsilon_a V \frac{dC_{O_2}}{dt} = C_{O_2,in} A v_{in} - C_{O_2,out} A v_{out} + g_{O_2} \frac{dm_c}{dt} \qquad (1.4)$$

where ε_a is the air filled porosity of the composting (%), V is composting pile volume (m^3), C_{O_2} is the concentration of oxygen in composting matrix (kg O^2/ m^3 dry air), v is the air velocity (m/d) and g_{O_2} is the oxygen consumption coefficient (kg O^2/ kg degradable composting mass).

(3) Heat balance

The attitudes towards temperature are quite different for the two types of composting models. For

macroscale models, excepting only a few models [56], most involve temperature as an important state variable and make predictions of it; whilst, among the small number of microscale models, only one model [43] was found to include an energy consideration.

Four different terms constitute the energy balance model for composting [39]. The accumulation term is represented by sensible heating of composting material. Input terms include sensible heat of inlet dry air, sensible and latent heat of inlet water vapour, sensible heat of supplementary water and radiation. Output terms include sensible heat of dry exit gas, sensible heat of exit water vapour, conductive/ convective losses, radiation losses and latent heat of evaporation. The last term, transformation, is predominantly biologically generated heat.

A typical heat balance model is as follows [48]:

$$\frac{dQ}{dt} = \frac{dQ_{bio}}{dt} - \frac{dQ_{ambient}}{dt} + \frac{dQ_{input}}{dt} - \frac{dQ_{output}}{dt} \qquad (1.5)$$

where Q is the heat content of the composting (J), Q_{bio} is the generation of bioreaction heat (J), $Q_{ambient}$ is the heat flow to ambient air via the surface of the composter (J), Q_{input} is the heat flow via the input air (J) and Q_{output} is the heat flow via the output air (J).

Every term within Equation *(1.5)* can be expressed in detail [39, 42, 48, 51]:

$$\begin{cases} Q = mc_c T \\ \dfrac{dQ_{ambient}}{dt} = UA(T - T_a) \\ \dfrac{dQ_{input}}{dt} = GH_{input} \\ \dfrac{dQ_{output}}{dt} = GH_{output} \\ \dfrac{dQ_{bio}}{dt} = H_c \dfrac{dm_s}{dt} \end{cases} \qquad (1.6)$$

where m is the mass of composting material (kg), c_c is the specific heat capacity of the composting material (J/kg °C), T is the temperature of the composting material (°C), U is the overall heat transfer coefficient from composting to ambient surroundings (kW/m^2°C), A is the surface area of

heat transfer (m^2), G is air flow rate (kg/s), H_{input} and H_{output} are the inlet and exit gas enthalpies (J/kg). m_s is the mass of biodegradable substrate and H_c is the combustion heat of biodegradable substrate.

If evaporation is involved in a heat balance model, a negative term due to evaporation should be added in to the right side of Equation *(1.5)* [42, 52]

$$\frac{dQ_{evp}}{dt} = -m_{evp}h_{evp} \qquad (1.7)$$

where m_{evp} is the evaporation rate of water and h_{evp} is the latent heat of water vaporization.

Where some research treats the composting material as a single matter [45, 57], and consequently "mc" as a constant term [39, 57], some other research take the composting material as a combination of different components, normally with dry mass (solid component) and water included. Sometimes, dry mass can also be divided into organic/non organic or biodegradable/non biodegradable. Air is included in some researchers' work [48, 53], but is absent from this combination in some others' research [42, 52]. In the majority of the models, the composting material or its components are variable and are simulated by mass balance equations. In any of the conditions discussed above, all components are considered to be at the same temperature.

For most current research, heat generated by biodegradation is monitored by a linear equation with biodegraded mass, as shown in Equation *(1.6)*. The coefficient is either referred to as the heat of combustion [39, 45, 52, 58] or reaction enthalpy [51, 57]. Some researchers have assumed that biological heat generation is proportional to oxygen consumption rate [47] and not to biodegraded mass. Other kinds of heat generation equation were also adopted based on the regression analysis of experiment data [42, 47].

The gas enthalpies at inlet and exit of the pile are always considered as a whole, regardless of dependence on humidity. If water vapour is included, saturated humid gas at the exit and a representative value of humidity or the humidity at ambient temperature is used for the inlet gas [20, 59].

Heat losses from the compost surface or reactor wall were incorporated in the majority of models, but not all [52, 53, 57]. Three different heat transfer methods, convection, conduction and radiation are considered for heat losses, whilst in all existing models, discrimination between these three reactions was not implemented and an integrated approach was introduced. Such an approach is shown in Equation *(1.6)* representing the overall heat losses which were adopted by most researchers [42, 47, 48, 51]. Ndegwa's model [58], only considers convective heat loss, but uses the same expression as the integrated heat loss equation mentioned above. Ekinci treated the conductive heat flux as a sum of two components in different directions in a cylindrical coordinate system [45]. Moreover, Mason pointed out that although only one single heat loss term named conduction heat loss was used in many models, this conduction actually represented overall heat loss [39]. Radiation is seldom mentioned as a separate term, or is defined as zero [45].

There are also a number of researchers who have developed heat balance equations for each single phase or for some combined phases [47, 51]. In their work, temperatures of different phases are not uniform, and two kinds of interphase heat transfer are considered. The first one is lead by the mass transfer between phases. The other type is the convective heat transfer from a solid-liquid unified phase to the gas, and modelled by Newton's equation:

$$\frac{dQ_c}{dt} = h_c(T - \chi) \qquad (1.8)$$

where Q_c is the convective heat transfer from solid-liquid to gas (J), h_c is the heat transfer coefficient between phases (J/s K), T and χ are the temperatures of the solid-liquid phase and gas respectively (K).

(4) Biodegradation kinetics

Biodegradation kinetic modelling is the core of composting models. The biodegradation processes have been illustrated explicitly by biodegradable volatile solids decomposition, or implicitly by oxygen consumption or carbon dioxide evolution [39]. Generally, kinetic formulations of composting biodegradation can be divided into three different categories: first order kinetic relationships, Monod type biomass production expressions and empirical equations. For both first order kinetic models and

Monod type models, the reaction rate coefficients are subject to correction for variation of some state variables, including temperature, moisture content, oxygen concentration and free air space (FAS).

The first order formulation is the most widely utilized kinetic model describing degradation processes. Normally, it can be set up on three basic targets: volatile solids degradation [17, 20, 40, 52, 54, 56, 58, 60], oxygen consumption [61], or carbon dioxide generation [50, 53]. Most first order kinetic equations directly adopt substrates as their foundation, as this is more straightforward.

A large amount of research has been done on first order kinetic modelling to make it more suitable for practical application. Many correction functions regarding environmental factors have been made for kinetic reaction rate coefficients. Among these works, Haug [20] developed the most comprehensive model, which has been further inspected by many subsequent studies [45, 52, 58, 62]. Haug's model was set up for a continuous-feed and well mixed composting reactor. The whole process was divided into multiple stages, with the output of each stage used as the input of the next stage. The corrections for temperature, moisture content, oxygen concentration and FAS were made as follows:

$$
\begin{aligned}
k_T &= k_{20}\left[1.066^{(T-20)} - 1.21^{(T-60)}\right] \\
f(H_2O) &= \frac{1}{e^{\left[-17.684\times(1-S_m)+7.0622\right]}+1} \\
f\left(O_2\right) &= \frac{VOLPO2}{VOLPO2+2} \\
f(FAS) &= \frac{1}{e^{\left[-23.675\times FAS+3.49451\right]}+1}
\end{aligned}
\qquad (1.9)
$$

where k_T and k_{20} are first order rate coefficient at temperature T or 20 °C respectively; $f(H_2O)$, $f\left(O_2\right)$ and $f(FAS)$ are corrections for moisture, oxygen and FAS; S_m is the solid content of the composting mixture and $VOLPO2$ is the volume percentage of oxygen in the exhaust gas.

Some others also used environmental condition relationships on first order kinetic rates. Finger [61] gave an Arrhenius equation[**] [63] for temperature dependency. Based on composting data, Smith and

[**] Arrhenius equation: $k = Ae^{-E_a/RT}$. An equation represents the dependence of the rate constant of a reaction on the absolute temperature and activation energy [63].

Eilers [64] created two corrections in exponential expressions, separately, for temperature and moisture content. Mohee [65] developed a polynomial equation with regard to temperature to calculate first order kinetic rate, and also an exponential expression regarding moisture which is similar to Smith and Eilers' formulation for the rate correction. From experimental data, Rosso [66] formulated the temperature effect based on minimum, maximum and optimum temperatures for microbial growth. This model was compared with some other correction models for temperature [20, 67], and was found to have the most stable parameters over the whole course of degradation [50]. This model was further adopted by Higgins and Walker and corroborated with a Monod type oxygen correction function, in which the half reaction rate constant is related to temperature and moisture content [53].

In addition to setting up correction relations for environmental factors on a constant first order kinetic rate, some researchers also found empirical functions of temperature, moisture content and carbon dioxide rate to depict the kinetic rate in various situations [17, 56, 60, 68].

All first order models, which are the most common type of kinetic mode, originate from experimental data, and the modelling forms of kinetic rates determined are totally based on this existing data. Thus, the parameters obtained in this method are only suitable for the same conditions in which the parameters have been experimentally determined. This kind of method is considered as inductive by some researchers. The first drawback of this model is its restricted applicability. In order to get a set of exact parameters, many relevant factors need to be examined, and therefore substantial experimental work is needed. This limits the model's utilization. Another limitation is that first order kinetics basically ignore the biological influence on the composting process and therefore cannot achieve the simulation of biomass transformation [47, 69].

Monod type expressions are the second most commonly used composting function. In such methods, models were developed by integrating the basic theories of physics, chemistry and biology. Hence, this kind of model is regarded as a mechanistic or deductive model [69].

The Monod theory was used to describe the substrate utilization, and then transformed to illustrate the biomass growth. Used in composting modelling, it was further extended to simulate carbon dioxide

evolution [48], oxygen consumption [46] and ammonia consumption [47]. There are not many corrections accounting for environmental effects made for Monod type kinetics. Three temperature corrections were made from empirical knowledge of microbial growth [46, 48, 49], while Saucedo-Castaneda et al. [70] used an Arrhenius-type temperature correction in their work. Stombaugh and Nokes also made a correction of the rate coefficient for moisture content [49]. Other compounds that can take part in substrate degradation as reactants, such as oxygen, ammonia and other nutrients, can also contribute to kinetic rate, and Monod type adjustment functions can be used to reflect their effect [47, 49]. Correction functions for substrate or reactants' availability and inhibition were used in some research work [3, 47].

An advantage of Monod type kinetics is that this method can be used to make more detailed and accurate simulations of a multi-substrate degradation process. For instance, Kaiser modelled four substrate decomposition by four different microbes [48]. Sole-Mauri further developed such work by considering hydrolysis and stoichiometry for six polymeric substrates in a specialized degradation process involving six different microbial populations [47].

As these deductive models start from basic theories, there are many elementary parameters appearing in such models. However, some of these parameters are hard to distinguish or test for. This shortcoming has limited the application of Monod type kinetic models to a certain extent [69].

There are also some empirical models used for composting kinetic foundations. Adopting correction functions for environmental factors of other researcher works, Petric and Selimbasic [51] and Briski [57] used kinetic models with an uncertain order, after exploiting experimental data on substrate degradation, they made regression analysis to determine the order of kinetic models. Kishimoto [42] modelled the substrate degradation implicitly by simulating the heat generated by microorganisms. The model of heat generation is a polynomial of temperature, water content, aeration rate and accumulation of the generated heat. From pilot scale experimental oxygen depletion rate and temperature data, VanderGheynst [71] developed an exponential model of oxygen consumption to simulate the composting of a dog food substrate. Temperature correction in this model was found in power law expression. Many other researchers [72-74] also developed many empirical models based on experimental data.

1.4.3 Modelling of in situ bioremediation

Composting and biopiles, although both are ex-situ bioremediation techniques, share some of the fundamental theory of with in situ bioremediation processes for contaminated soil as well as contaminated groundwater. Therefore, models developed for in situ bioremediation processes are highly relevant to modelling biopiles. The in situ bioremediation techniques with which researchers have been most concerned are primarily SVE, BV, and air sparging (AS). All these methods account for contaminant removal by presenting aeration which can not only alter the bioreaction rate but also cause the volatilization of organic matters. These methods are theoretically almost identical to biopiles. Furthermore, in groundwater bioremediation, the contaminant transfer and reaction processes are also similar to that of soil bioremediation. For these reasons, the modelling developments of in situ bioremediation, especially for SVE, BV and AS, will be discussed in this section.

Generally, models for in situ bioremediation were developed on the basis of fluid flow and species transport equations, and solved numerically after temporal and spatial discretization. There are a large number of mathematical models given in the literature, and they are highly variable in their complexity, and in the processes they set out to describe.

The first and simplest case is modelling gas flow behaviour in the contaminated domain for SVE and BV systems. These models can be solved analytically for the examination of pneumatic pump tests and the design of SVE [75, 76], or numerically to simulate the gas phase advection in SVE [77] and BV [78, 79]. However, since only gas flow is considered in this group of models, they cannot predict the contaminant transport and transformation, and can only be used for very simple design analysis.

A more complex group of models was developed for the processes of species transport with a hypothetic steady state gas flow. A few models analytically solved the transport equations [80, 81] whereas most of others used numerical solutions [82-85]. On the basis of Wilson's model, a great deal of work was done to investigate the effect of different permeability conditions on SVE/BV systems, including impermeable caps, anisotropic permeability, variable permeability, spatially variant permeability and areas of low permeability. Some other aspects were also investigated, such as evaporative cooling, and system geometry [86-92]. Some models of this group were extended to

include complexities accounting for species reaction and biodegradation processes. DePaoli [82] simplified the biodegradation relationship to zero order kinetics, and predicted the oxygen profiles in the soil. With the assumption of chemical equilibrium between organic compounds in four phases, vapour, NAPL, water and soil, El-Beshry et al. [83] simulated SVE performance of a jet-fuel spill site by applying a coupled flow and transport code, VENT3D. Rahbeh and Mohtar developed a numerical model for the design and operation of AS/SVE. [84]. They treated both the interphase mass transfer and biodegradation as kinetic processes, and applied first order formulations for them. Some models of this group also inspected influences of soil heterogeneities [84, 93]. However, due to the intrinsic deficiency of single phase steady state flow assumptions, this kind of model is not capable of comprehensively modelling the in situ bioremediation process [94].

The complexities of in situ models were further advanced by integrating transient single phase gas flow and species transport. Pennington et al. [95] simulated in situ gas venting processes by using adaptive numerical solution software for SPRINT2. In their model, NAPL was considered kinetically partitioned in different phases and the relative permeability of gas varied according to the NAPL removal. The adaptive method proved to be computationally efficient, with the same accuracy as fixed mesh methods. In Campagnolo and Akgerman's model for SVE, heterogeneity of soil, kinetic interphase mass transfer and a Monod expression of biodegradation kinetics were all considered [1]. Rathfelder et al. [96] developed a 2D numerical model incorporating transient single phase gas flow and multicomponent transport, and explored both equilibrium phase partitioning and kinetic mass transfer conditions. Schulenberg and Reeves [97] presented a 2D axis-symmetric model to simulate SVE processes and improved their model's ability by accounting for soil fracturing. Lingineni and Dhir [98] formulated a 1D non-isothermal model to describe soil venting systems. This work focused on the evaporation rate of organic contaminants in unsaturated soil. Their work is remarkable in that they accounted for temperature variations in the soil due to heat absorbed during the evaporation process and due to the provision of heat sources to enhance soil remediation.

All the above models assumed that only gas was mobile in the in situ bioremediation systems. However, in practice some of other phases, water, NAPL and even biomass, are also mobile. Hence, more comprehensive models should involve multiphase flow. Stephanotos [99] developed a 2D finite

element model to simulate single volatile organic species transport in a two phase (air and water) flow system. A 1D multicomponent transport model is presented by Baehr et al. [100] which can predict not only air, NAPL and water flow but also vapour flux. Kaluarachchi and Parker [101] developed a 2D finite-element model to predict the coupled transient flow of gas, water and oleic phase, and multicomponent transport of organic chemicals. These models were not directly pertinent to simulate SVE, BV or AS, their focus being fluid flow and species transport. Mass transfers between phases were all assumed to be in equilibrium and biotransformations were not included.

Some researchers carried out more straightforward modelling work on bioremediation processes. Integrating two existing modelling packages, T2VOC for fluid (air, water and NAPL) flow and heat transport in porous and fractured media with variably-saturated conditions, and M^2NOTS for multicomponent transport and equilibrium partitioning between phases, Webb an Phelan [102] performed 3D simulations for soil heated vapour extraction. Travis and Rosenberg [103] applied a computer code, TRAMPP, which they developed to simulate in situ bioremediation of TCE. Their model accounted for unsteady water and air flow, multicomponent transport, chemical equilibrium partitioning between air and water, first order kinetic adsorption process, and Monod kinetics of microbial degradation. Yoon et al. [104] conducted 2D simulations to test the effect of strongly layered heterogeneous porous media during soil vapour extraction. They incorporated rate limiting mass transfer models for trapped NAPL to aqueous and slow sorption/desorption between soils and aqueous, which were both simulated using first order kinetics, with an existing multiphase flow and transport simulator called STOMP.

For modelling research on SVE and BV systems, Abriola and her group conducted a series of important studies. They firstly developed a model for gas and aqueous phase advection, multicomponent transport and equilibrium interphase mass exchange [105, 106], and then improved this model by incorporating a linear kinetic equation for mass exchange between phases [107]. A more complex model [108] was introduced and applied to model 2D BTX biotransformation and transport in the subsurface. Four phases were involved in this model: water, air, soil and biophase. The hydrocarbon was treated as a solute in each phase. Solutes in air, water and solid were in equilibrium, whilst transfer between water and the biophase was governed by a linear driving force expression.

Monod type kinetics were applied to microbial degradation and biomass growth. The most comprehensive model developed was called MISER which was a 2D model designed for simulation field scale SVE and BV systems [94, 109]. The model covered five phases, including two mobile phases of gas and water, and three immobile phases of soil, organic and biophase. The processes integrated in this model consisted of multiphase flow, multicomponent compositional transport with nonequilibrium first order kinetic interphase mass transfer, and kinetic (Monod type) aerobic biodegradation. This model was extended in many subsequent works to explore surfactant enhancement [110]; porous media heterogeneities [111]; textural and wettability variations [112]; effects of ethanol addition [113]; and hydraulic property correlation [114].

Although research on the modelling of in situ bioremediation processes is a very important field of study, with an enormous number of models having been developed, and although temperature greatly affects bioreaction rate and volatilization rate, there are, nevertheless only a few models [2, 98, 102, 115] which focus on energy aspects and which can predict temperature changes. In addition, these models all focus on thermal venting (heated SVE or heated soil venting). Commonly, in these models, heat energy transport analysis is modelled by phase-summed effective thermal properties under thermodynamic equilibrium conditions.

In comparison with the bioremediation of contaminated soil, groundwater bioremediation normally only includes single phase (water) saturated flow, and consequently mass transfer to or from the gas phase is not required in such models. Therefore, more research has been dedicated to the study of kinetic processes of biodegradation and chemical reactions taking place in the water. Mohammed and Allayla [116] used different kinetics (first order, zero order, Monod and non-growth associated Monod) to simulate 1D biodegradation of BTX compounds in saturated sandy soil. El-Kadi [117] investigated water saturation and heat inhibition effects on hydrocarbon biodegradation in tidal aquifers within variably-saturated groundwater flow conditions. Huang et al.[118] combined substrate competition, inhibition and aerobic co-metabolism functions with Monod kinetics for modelling enhanced in situ bioremediation processes. Prommer, Barry and their colleagues developed numerical models which coupled advective-dispersive transport of organic and inorganic solutes with the geochemical equilibrium package PHREEQC and a biodegradation module. PHREEQC was used to

illustrate the inorganic solute concentration change due to precipitation/dissolution of minerals and chemical speciation. The activity of multiple bacterial groups and their biochemical effects were represented by the biodegradation module. This model was firstly developed for 1D modelling [119] and then adapted to 3D to investigate the role of ferric iron during biodegradation of dissolved petroleum hydrocarbon compounds at a field site [120]. Finally, in one conclusive paper [121], they provided a comprehensive modelling framework, including biogeochemical reactions and interphase mass transfer processes such as sorption/desorption, non-aqueous phase liquid dissolution and mineral precipitation/dissolution, and microbiological transformation/degradation. All of these processes can be in equilibrium or kinetically modelled by first order reaction or Monod expression (for microbiological transformation/degradation).

Some researchers also studied specific factors affecting biodegradation processes. For example, Zysset et al. [122] developed a 1D macroscopic model for the transport of dissolved substances in a groundwater-biofilm system. Their study emphasized the effect of the biofilm and assumed that the diffusion within biofilm dominated chemical interphase transfer. Their work successfully recreated the transport of nitrate and sulphate in two laboratory column experiments. Gallo and Manzini [123] conducted 2D modelling of the bioremediation processes occurring in heterogeneous saturated soils. Their results showed that heterogeneity could strongly affect dissolved oxygen delivery and consequently influence contaminant degradation.

Unlike the models introduced above which can predict the temporal and spatial variation of component concentrations, some researchers have developed models to evaluate the prediction of the overall performance of bioremediation processes. Hence, such models only account for kinetic reaction processes, and do not include fluid flow and species transport aspects. Rashid and Kaluarachchi [124] used a multi-term Monod expression for non-linear reactions between the hydrocarbon, oxygen, nitrate, and a heterotrophic facultative microbial population in their model. Mulder et al. [125] investigated bioremediation periods for PAH soil pollutants. Their model only involved mechanistic models for first order dissolution, desorption and biodegradation. In the work of Li et al. [126], the processes they concentrated on for mathematical modelling were first order oxygen transfer from the air, oil transfer from the soil and Monod kinetics for the bioreaction in the aqueous

phase.

There were also some unique models made from specialized perspectives. For instance, Cornelissen and Sijm [127] built their biodegradation model from an energy balance viewpoint and the model was set upon the energy budget for bacterial cellular growth, cometabolism, maintenance, as well as heat loss and substrate degradation. By applying Monte Carlo analysis, Barnes and McWhorter [128] studied the effects of SVE system operation time and permeability variance on the uncertainty of mass removal rates which were predicted by a numerical model.

1.4.4 Other related models

Some models developed in other fields are also instructive for this study, especially those models relevant to fluid flow and heat transfer in porous media. Furman [129] reviewed current research works on modelling surface-subsurface flow systems. By giving the governing equations for each component of the coupled system, the physics and mathematics of five differing categories of boundary condition were introduced. Three coupling schemes were identified in numerical solution methods, with a review of their application. Datta [130], from the field of food engineering, analysed the applicability of different momentum governing equations for porous media according to the variation of pores size. Vafai and Tien [131, 132], studying in the field of mechanical engineering, integrated Darcy's Law and the Navier-Stokes equations and created a steady state model to simulate flow and heat transfer in porous media. Their work was further extended by Khaled and Vafai [133] to simulate the case of an unsteady state. Incorporating inertia and transient effects, this model was successfully applied to the simulation of flow in biological tissues. Lian et al. [134] implemented a computational fluid dynamics (CFD) model, which was set up for a generalized Darcy equation acquired from a volume averaged analysis method, to simulate the tea fermentation process. Pak et al. [135] also adopted CFD techniques for modelling crossflow filtration in tubular membranes. In this work, 2D equations for coupled Navier-Stokes, Darcy's Law and mass transfer were developed first, and numerically solved by a control volume based finite difference method. Using the commercial CFD package FLUENT, Saidi et al. [136] develop a 3D model for static and forward smouldering combustion in a packed bed of plant materials. This model not only simulated fluid flow but also heat

transfer and species transport.

The works mentioned above are all relevant for the study of modelling fluid flow and heat transfer through a porous media system, such as contaminated soil or other solid waste, which are the primary constituents of a biopile.

1.4.5 Conclusion

Generally, research into the modelling of bioremediation processes is flourishing, and many models have been developed. For ex-situ bioremediation techniques (composting/biopiles), macroscopic models based on mass and heat balance are dominant; for in situ bioremediation techniques, microscopic models based on fluid flow through porous media and component transport are more popular. Both models can incorporate contaminant reaction processes either in the form of chemical equilibrium or kinetic expressions. In the kinetic reaction models, interphase mass transfer is always illustrated by first order models, and biological reactions are mostly depicted by Monod type expressions.

No matter how simple or complex these models are, intrinsic deficiencies of each exist. The macroscopic ex-situ bioremediation models can only make general predictions on the whole composting pile, and cannot give results for a specific location within the pile. These models may fit laboratory or small scale experiments very well, but cannot reliably simulate a field scale bioremediation process, since large scale geometries will inevitably lead to performance variations at different positions of the pile. Furthermore, the effect of an aeration system for the whole biopile is unlikely to be homogenous.

On the other hand, ex-situ bioremediation models normally only account partially for chemical reactions taking place in bioremediation processes. Volatilization of organic components is ordinarily included, while other interphase mass transfer is ignored in such models. Whilst in situ bioremediation models take into account more processes, and thus can more particularly and comprehensively describe the real bioremediation processes. Temperature, a very important factor for bioreaction, is seldom incorporated in this type of model. Moreover, the solution approaches for in situ

bioremediation models are commonly very complex, requiring time and spatial discretization and numerical computation. Hence, a profound amount of coding work always accompanies the development of such models, and these codes are normally unpublished. As a result, subsequent progress made to such works is limited.

In addition to the deficiencies of each model discussed above, to date, researchers have only given their attention to the bioremediation material itself, and have not account for any effects by the interaction between a bioremediation process and its surroundings.

1.5 Aims and objectives

The ultimate goal of this project is to investigate the feasibility of applying CFD techniques to develop a numerical model for aiding the design and operation of aerated/un-aerated biopiles for organic contaminated materials in the context of its ambient surroundings. Unlike previous work in this field, which has predominantly focused on the biopile itself, the effects of ambient environmental conditions on the biopile will be examined in this project.

The work covered by this thesis involves preparing a set of governing equations that effectively represent the physical, chemical and biological reactions that take place in aerated/un-aerated biopile treatment. It also includes the formulation of boundary conditions which are suitable for the physical processes and work well with the CFD solution. To solve the mathematical models, the commercial CFD package FLUENT is applied. FLUENT, a general CFD package, although very efficient, cannot depict entire set of processes studied in this work with only its built in functions, and thus a number of User Defined Functions (UDFs) are created to fill these gaps. Several biopile treatments with different operating conditions are then simulated using the developed model incorporating the solver of FLUENT, and the modelling results are examined to reveal the effect of the various conditions.

This work should ultimately lead to the development and testing of a model capable of giving a deeper understanding of the flow, transport and reaction processes that dominate biopile treatment. Moreover, although this work is based on an ex-situ bioremediation technique, biopiles, the findings can also be applied to modelling in situ bioremediation processes, such as SVE and BV. In addition, in

comparison with creating ones own numerical solver, the research methodology used in this study can be easily followed and repeated by others, which in the author's opinion, can accelerate the research development of this field.

1.6 Layout of thesis

This thesis is divided into seven chapters in total. In the previous sections, a generalised introduction regarding the scope of relevant research has been provided.

The second chapter derives the comprehensive governing equations for immiscible fluid flow in a porous media and normal fluid flow by combining Navier-Stokes equations and Darcy's Law for variably-saturated flow.

Chapter 3 emphasizes the species processes involved in the biopile treatment. The species transport formulation is presented in this chapter. All the reactions that species take part in, including inter-phase mass transfer and biotransformation are also set out in mathematical expressions.

Chapter 4 provides the energy governing equations for biopile treatment.

Chapter 5 introduces the modelling setup procedures and the numerical solution method in FLUENT. The author's experiences of using the software to carry out the modelling are also given at the end of this chapter.

The sixth chapter reveals the influences of various operating conditions on biopiles by presenting the modelling results of a number of cases run under various conditions.

Chapter 7 summarizes the conclusions based on the preceding chapters and also makes recommendations for further work.

Chapter 2 Immiscible Fluid Flow

2.1 Introduction

As mentioned in Section 1.5, the work of this thesis includes applying CFD to model biopile treatments and exploring the influence of ambient environmental conditions on biopiles which is supported by Mason. Mason has suggested that it would be worthwhile to carry out investigation into natural ventilation aeration for the improvement of current models of composting processes [39]. Hence, in this chapter, the integrated equations for governing both Multiphase flow in porous media and normal single-phase flow will be formulated first, followed by the method used to incorporate these governing equations with CFD package FLUENT.

Traditionally, Richard's equation, which is built on unsaturated Darcy's law and the principle of mass conservation is the only mathematical equation used to illustrate unsaturated or variably-saturated fluid flow in porous media [109, 130]. In this chapter, several independent fluid flow theories including simple, single-phase fluid flow, Eulerian multiphase flow, and immiscible fluid flow in porous media are first introduced. The coupling processes of all the above models are then addressed. The resulting coupled model is suitable for immiscible fluid flow in porous media as well as single-phase fluid problems. The advantage of this model is that when applied to bioremediation simulation, research can be carried out extending from contaminated materials (porous media zone) to their surroundings, giving a broader perspective on the issue. By using this method, the physical boundary of biopile is no longer the boundary of the research objective. The scope of the research objective can be extended to include both the biopile itself and its ambient surroundings. Therefore, the flow pattern of the wind around biopiles can be predicted simultaneously with the simulation of biopile performance and other ambient conditions, such as temperature and moisture of the wind, which can also be taken into account.

To the author's knowledge, the goal and method of modelling fluid flow in bioremediation processes

of this study are unique and novel, no other model was found to simulate the bioremediation processes in a similar method and no work was found to include interaction between the remediation site and ambient wind.

2.2 Basic fluid flow

The governing equations for very common single fluid flow can be achieved by applying the conservation principle. In this study, the Eulerian method is adopted to formulate the equations within a Cartesian frame of reference, studying the velocity field as a function of position and time, therefore, describing the flow at every fixed point at different times.

2.2.1 Conservation principle

Applying Euler's approach, the standard method employed to derive the governing equations of fluid flow is to focus attention on a definite volume, fixed in space, referred to as the control volume or control box. The shape of the control volume is arbitrary. The boundaries of the control volume are referred to as control surfaces and always form a closed surface in space. The quantity and identity of matter in the control volume may change with time, while the shape and position of the control volume remain fixed.

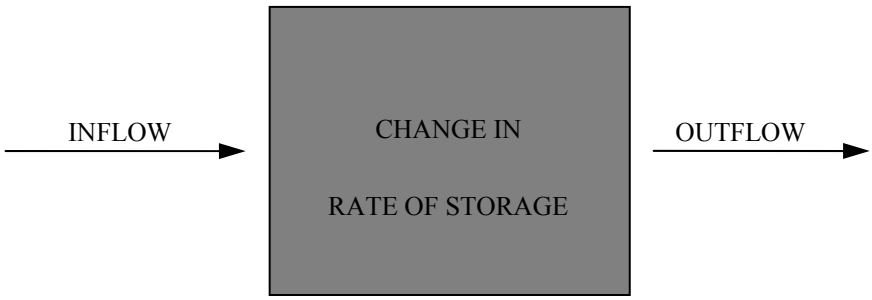

Figure 2.1 Control volume principle

The general form of the conservation principle applied to the control volume is shown in Figure 2.1, that is: the change in rate of storage of the conserved quantity is equal to the inflow minus the outflow of the quantity, plus the rate of its production or minus the consumption in the control volume. The

conservation principle can be used for:

- Mass
- Momentum
- Energy
- Species

2.2.2 Conservation of mass

To derive the mass conservation equation in differential form for an Eulerian system, a control volume *dx dy dz* can be considered. The point *0*, is the middle of the control box, as shown in Figure 2.2, and at time t,

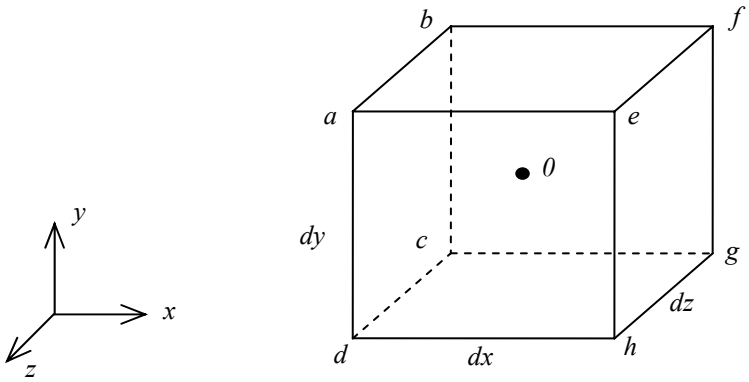

Figure 2.2 Elemental control volume for derivation of the differential form of the mass conservation equation

$$\begin{cases} u = \overline{V_x} = u_0 \\ v = \overline{V_y} = v_0 \\ w = \overline{V_z} = w_0 \\ \rho = \rho_0 \end{cases} \qquad (2.1)$$

u, v and *w* are the *x*-component, *y*-component and *z*-component of velocity respectively. ρ represents

the fluid density. Summing up the contributions over all six faces, the total net mass outflow can be expressed as:

$$\text{Total net mass outflow in time } dt = \left[\frac{\partial(\rho u)}{\partial x} + \frac{\partial(\rho v)}{\partial y} + \frac{\partial(\rho w)}{\partial z} \right] dx\, dy\, dz\, dt$$

The total net mass outflow must be equal to the decrease in mass contained in this volume during the same time interval, according to mass conservation, so that:

$$\left[\frac{\partial(\rho u)}{\partial x} + \frac{\partial(\rho v)}{\partial y} + \frac{\partial(\rho w)}{\partial z} \right] dx\, dy\, dz\, dt = -\, dx\, dy\, dz \frac{\partial \rho}{\partial t} dt$$

That is:

$$\frac{\partial(\rho u)}{\partial x} + \frac{\partial(\rho v)}{\partial y} + \frac{\partial(\rho w)}{\partial z} = -\frac{\partial \rho}{\partial t} \qquad (2.2)$$

It can be simplified, in terms of the divergence operator:

$$\nabla \cdot \rho \vec{V} = -\frac{\partial \rho}{\partial t} \qquad (2.3)$$

Alternatively, the above equation can also be expanded to give:

$$u\frac{\partial \rho}{\partial x} + \rho\frac{\partial u}{\partial x} + v\frac{\partial \rho}{\partial y} + \rho\frac{\partial v}{\partial y} + w\frac{\partial \rho}{\partial z} + \rho\frac{\partial w}{\partial z} = -\frac{\partial \rho}{\partial t} \qquad (2.4)$$

Applying the total derivation symbol *D/Dt*:

$$\frac{D}{Dt} = \frac{\partial}{\partial t} + u\frac{\partial}{\partial x} + v\frac{\partial}{\partial y} + w\frac{\partial}{\partial z}$$

to Equation *(2.4)*

$$\frac{\partial u}{\partial x} + \frac{\partial v}{\partial y} + \frac{\partial w}{\partial z} = -\frac{1}{\rho}\frac{D\rho}{Dt}$$

or:

$$\nabla \cdot \vec{V} = -\frac{1}{\rho}\frac{D\rho}{Dt} \qquad (2.5)$$

For an incompressible fluid which is a fluid with constant density during its motion, $D\rho / Dt = 0$. Thus, the mass conservation or continuity equation for incompressible fluid can be expressed as:

$$\nabla \cdot \vec{V} = 0 \qquad (2.6)$$

2.2.3 Conservation of momentum

(1) Euler equation

When the fluid is inviscid, its momentum equation in differential form is called the Euler equation. To derive Euler equation, consider a fixed control volume of infinitesimal size with fluid flows through the six faces of the volume. Surface forces and body forces act on the fluid particle that occupies the volume at a particular instance in time. The only surface force taken into account is that due to pressure differences, and the only body force considered is that due to gravity. The volume element *dx dy dz* is similar to that used to derive the continuity equation. Figure 2.3 shows a single face of the control volume, and this face has an arbitrary orientation with respect to the gravitational vector $\vec{g}$. The point *0* is located at the centre of the control volume.

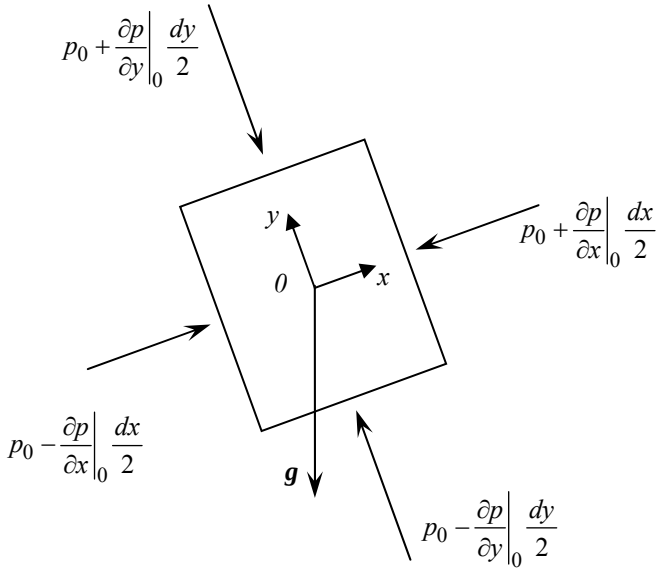

Figure 2.3 Elemental control volume for derivation of the differential form of the momentum equation

Summing up the pressure over all six faces of the control unit, the force action on one unit volume fluid $\vec{F}$ can be expressed as:

$$\vec{F} = -\nabla p + \rho \vec{g} \qquad (2.7)$$

Newton's second law of motion states:

$$\vec{F} = m\vec{a}$$

where $\vec{F}$ is force, m is mass and $\vec{a}$ is acceleration. $\vec{F}$ is equal to the rate of change of momentum following a fluid particle. For a velocity field in an Eulerian system, the acceleration following a fluid particle is given by $D\vec{V}/Dt$, so that

$$\rho \frac{D\vec{V}}{Dt} = -\nabla p + \rho \vec{g} \qquad (2.8)$$

Equation *(2.8)* is the differential form of the linear momentum equation in vector form for an inviscid fluid, referred to as the Euler equation. It holds for compressible and incompressible fluid flow. The term on the left side of the equation represents the inertia force, while the first term on right side is the

surface force due to pressure differences and the second term on right side is the body force due to gravitational attraction. By defining a potential function ϕ_g, applying gravitational force, such that

$$\bar{g} = -g\nabla\phi_g$$

where ϕ_g represents altitude or elevation and $\nabla\phi_g$ is a unit vector that points in the direction opposite to the vector $\bar{g}$, the Euler Equation *(2.8)* can be written as:

$$\frac{D\bar{V}}{Dt} = -\frac{1}{\rho}\nabla p + \bar{g} = -\frac{1}{\rho}\nabla p - g\nabla\phi_g \qquad (2.9)$$

Hence, in Cartesian coordinates:

$$\begin{aligned}
&\frac{\partial u}{\partial t} + u\frac{\partial u}{\partial x} + v\frac{\partial u}{\partial y} + w\frac{\partial u}{\partial z} = -\frac{1}{\rho}\frac{\partial p}{\partial x} - g\frac{\partial \phi_g}{\partial x} \\
&\frac{\partial v}{\partial t} + u\frac{\partial v}{\partial x} + v\frac{\partial v}{\partial y} + w\frac{\partial v}{\partial z} = -\frac{1}{\rho}\frac{\partial p}{\partial y} - g\frac{\partial \phi_g}{\partial y} \\
&\frac{\partial w}{\partial t} + u\frac{\partial w}{\partial x} + v\frac{\partial w}{\partial y} + w\frac{\partial w}{\partial z} = -\frac{1}{\rho}\frac{\partial p}{\partial z} - g\frac{\partial \phi_g}{\partial z}
\end{aligned} \qquad (2.10)$$

(2) Navier-Stokes equations

The momentum equation for viscous fluid flow is known as the Navier-Stokes equations. For viscous fluid, the total resultant force on the control volume is not only made up of pressure gradients and body forces, but also viscous forces. Table 2.1 shows the nine stress components associated with the fluid in the control volume.

Table 2.1 Stress components

	x plane	*y* plane	*z* plane
x direction	σ_{xx}	σ_{yx}	σ_{zx}
y direction	σ_{xy}	σ_{yy}	σ_{zy}
z direction	σ_{xz}	σ_{yz}	σ_{zz}

Stress shown in Table 2.1 includes both surface force due to pressure differences and viscous stress:

$$\sigma_{ij} = -p\delta_{ij} + \tau_{ij} \tag{2.11}$$

where, p is the pressure, δ is the Kronecker delta and τ_{ij} is the shear stress caused by fluid viscosity. Table 2.2 shows the change in stress component over the three dimensions i.e. the force per unit volume.

Table 2.2 Force per unit volume

	x plane	y plane	z plane
x component	$\frac{\partial \sigma_{xx}}{\partial x}$	$\frac{\partial \sigma_{yx}}{\partial y}$	$\frac{\partial \sigma_{zx}}{\partial z}$
y component	$\frac{\partial \sigma_{xy}}{\partial x}$	$\frac{\partial \sigma_{yy}}{\partial y}$	$\frac{\partial \sigma_{zy}}{\partial z}$
z component	$\frac{\partial \sigma_{xz}}{\partial x}$	$\frac{\partial \sigma_{yz}}{\partial y}$	$\frac{\partial \sigma_{zz}}{\partial z}$

The momentum equation for viscous fluid flow can be expressed in vector form as:

$$\rho \frac{D\bar{V}}{Dt} = -\nabla \cdot \sigma + \rho \bar{g} \tag{2.12}$$

In Cartesian coordinates, the equation becomes:

$$\begin{aligned}
\rho \frac{Du}{Dt} &= -\frac{\partial p}{\partial x} + \frac{\partial \tau_{xx}}{\partial x} + \frac{\partial \tau_{yx}}{\partial y} + \frac{\partial \tau_{zx}}{\partial z} - \rho g \frac{\partial \phi_g}{\partial x} \\
\rho \frac{Dv}{Dt} &= -\frac{\partial p}{\partial x} + \frac{\partial \tau_{xy}}{\partial x} + \frac{\partial \tau_{yy}}{\partial y} + \frac{\partial \tau_{zy}}{\partial z} - \rho g \frac{\partial \phi_g}{\partial y} \\
\rho \frac{Dw}{Dt} &= -\frac{\partial p}{\partial x} + \frac{\partial \tau_{xz}}{\partial x} + \frac{\partial \tau_{yz}}{\partial y} + \frac{\partial \tau_{zz}}{\partial z} - \rho g \frac{\partial \phi_g}{\partial z}
\end{aligned} \tag{2.13}$$

For a Newtonian fluid, the viscous shear stress τ_{ij} can be related to the deformation of the fluid through velocity gradients using Stokes' hypothesis, considering the shear stresses to be proportional to rates of angular deformation. The fluid is isotropic for this hypothesis. The stress action on the

control volume is shown in Figure 2.4.

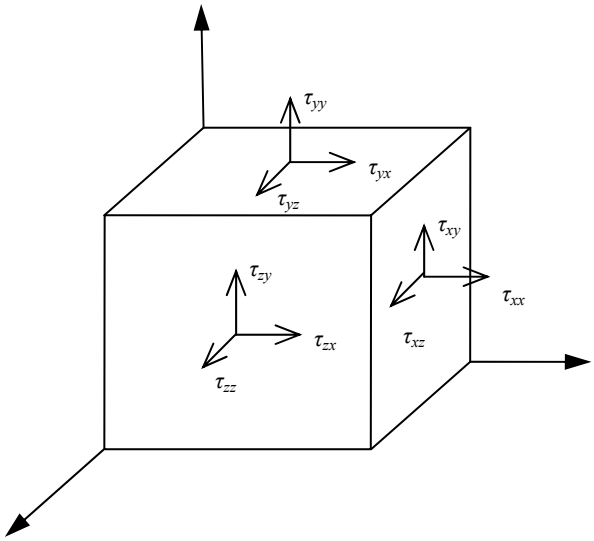

Figure 2.4 Orientation of principle axes in the control volume

The components of these shear stresses can be written as:

$$\tau_{yx} = \tau_{xy} = \mu\left(\frac{\partial v}{\partial x} + \frac{\partial u}{\partial y}\right)$$
$$\tau_{zy} = \tau_{yz} = \mu\left(\frac{\partial w}{\partial y} + \frac{\partial v}{\partial z}\right)$$
$$\tau_{xz} = \tau_{zx} = \mu\left(\frac{\partial u}{\partial z} + \frac{\partial w}{\partial x}\right)$$

and

$$\tau_{xx} = 2\mu\frac{\partial u}{\partial x} - \frac{2}{3}\mu\nabla\cdot\bar{V}$$
$$\tau_{yy} = 2\mu\frac{\partial v}{\partial y} - \frac{2}{3}\mu\nabla\cdot\bar{V}$$
$$\tau_{zz} = 2\mu\frac{\partial w}{\partial z} - \frac{2}{3}\mu\nabla\cdot\bar{V}$$

where μ is the dynamic viscosity.

Thus, Equation *(2.13)* can be rewritten to:

$$\rho\frac{Du}{Dt}=-\frac{\partial p}{\partial x}+\frac{\partial}{\partial x}\left[\mu\left(2\frac{\partial u}{\partial x}-\frac{2}{3}\nabla\cdot\vec{V}\right)\right]+\frac{\partial}{\partial y}\left[\mu\left(\frac{\partial u}{\partial y}+\frac{\partial v}{\partial x}\right)\right]+\frac{\partial}{\partial z}\left[\mu\left(\frac{\partial w}{\partial x}+\frac{\partial u}{\partial z}\right)\right]-\rho g\frac{\partial\phi_g}{\partial x}$$
$$\rho\frac{Dv}{Dt}=-\frac{\partial p}{\partial x}+\frac{\partial}{\partial y}\left[\mu\left(2\frac{\partial v}{\partial y}-\frac{2}{3}\nabla\cdot\vec{V}\right)\right]+\frac{\partial}{\partial z}\left[\mu\left(\frac{\partial v}{\partial z}+\frac{\partial w}{\partial y}\right)\right]+\frac{\partial}{\partial x}\left[\mu\left(\frac{\partial u}{\partial y}+\frac{\partial v}{\partial x}\right)\right]-\rho g\frac{\partial\phi_g}{\partial y} \qquad (2.14)$$
$$\rho\frac{Dw}{Dt}=-\frac{\partial p}{\partial x}+\frac{\partial}{\partial z}\left[\mu\left(2\frac{\partial w}{\partial z}-\frac{2}{3}\nabla\cdot\vec{V}\right)\right]+\frac{\partial}{\partial x}\left[\mu\left(\frac{\partial w}{\partial x}+\frac{\partial u}{\partial z}\right)\right]+\frac{\partial}{\partial y}\left[\mu\left(\frac{\partial v}{\partial z}+\frac{\partial w}{\partial y}\right)\right]-\rho g\frac{\partial\phi_g}{\partial z}$$

Equation *(2.14)* gives the set of motion equations for viscous fluid in differential form, also referred to as the Navier-Stokes equations.

For incompressible fluid, density is constant and $\nabla\cdot\vec{V}=0$, thus Equation *(2.14)* can be simplified:

$$\rho\frac{Du}{Dt}=-\frac{\partial p}{\partial x}+\mu\nabla^2u-\rho g\frac{\partial\phi_g}{\partial x}$$
$$\rho\frac{Dv}{Dt}=-\frac{\partial p}{\partial x}+\mu\nabla^2v-\rho g\frac{\partial\phi_g}{\partial y} \qquad (2.15)$$
$$\rho\frac{Dw}{Dt}=-\frac{\partial p}{\partial x}+\mu\nabla^2w-\rho g\frac{\partial\phi_g}{\partial z}$$

In vector form, it is:

$$\rho\frac{D\vec{V}}{Dt}=-\nabla p+\mu\nabla^2\vec{V}+\rho\vec{g} \qquad (2.16)$$

or:

$$\rho\frac{\partial\vec{V}}{\partial t}+\rho(\vec{V}\cdot\nabla)\vec{V}=-\nabla p+\mu\nabla^2\vec{V}+\rho\vec{g} \qquad (2.17)$$

2.2.4 Governing equations in FLUENT

For all kinds of flow, FLUENT solves conservation equations for mass and momentum. The governing equations for laminar flow are:

Continuity:
$$\frac{\partial\rho}{\partial t}+\nabla\cdot(\rho\vec{V})=S \qquad (2.18)$$

where *S* is source or sink term.

Momentum: $$\frac{\partial}{\partial t}\left(\rho\vec{V}\right)+\rho(\vec{V}\cdot\nabla)\vec{V}=-\nabla p+\nabla\cdot\left(\bar{\bar{\tau}}\right)+\rho\vec{g}+\vec{F} \qquad (2.19)$$

where $\vec{F}$ is external body force, and $\bar{\bar{\tau}}$ is the stress tensor, given by

$$\bar{\bar{\tau}}=\mu\left[\left(\nabla\vec{V}+\nabla\vec{V}^{T}\right)-\frac{2}{3}\nabla\cdot\vec{V}I\right]$$

I: unit tensor

2.3 Multiphase flow – Eulerian model

2.3.1 Introduction

Many kinds of flow encountered both in nature and technology, such as those flows that occur during biopile treatment, are in mixture of phases. Physical phases of matter are gas, liquid, and solid, but the concept of phase in a multiphase flow system can be applied in a broader sense. In multiphase flow, a phase can be defined as an identifiable class of material that has a particular inertial response to and interaction with the flow and the potential field in which it is immersed.

There are several models supplied by FLUENT for modelling multiphase flow: the discrete phase model, the volume of fluid (VOF) model, the mixture model, and the Eulerian model. Each one has different applicability. For the modelling work of this study, the Eulerian model was adopted as it is the most suitable among all these models.

2.3.2 Eulerian model applicability

The Eulerian model is the most complex of the multiphase models in FLUENT. It solves a set of momentum and continuity equations for each phase. Coupling of each phase is achieved through the pressure and interphase exchange coefficients. FLUENT's user-defined functions can also be used to customize the calculation of the interphase exchange [137].

The phases in the Eulerian model can be liquids, gases, or solids in nearly any combination. The solution of the Eulerian model can be adopted if the flow case fits the following criteria [137]:

- A single pressure is shared by all phases.
- Momentum and continuity equations are solved for each phase.
- Interphase drag coefficient functions are available, which are appropriate for various types of multiphase regimes.
- Turbulence models are available, and may apply to all phases or to the mixture.

2.3.3 Eulerian model conservation equations

Eulerian model conservation equations are derived from the governing equations for basic fluid flow. To change from a single-phase model, where a single set of conservation equations for momentum, continuity and heat are solved, to a multiphase model, additional sets of conservation equations must be introduced for each phase. In the process of introducing additional sets of conservation equations, the original set must also be modified. The modifications involve the introduction of the volume fractions for the multiple phases, as well as mechanisms for the exchange of momentum, heat, and mass between the phases.

The description of multiphase flow as interpenetrating continua incorporates the concept of phase volume fractions, denoted by α_q. Volume fractions represent the space occupied by each phase, and the laws of conservation of mass and momentum are satisfied by each phase individually. The derivation of the conservation equations can be done by ensemble averaging the local instantaneous balance for each of the phases, or by using the mixture theory approach [137].

In a system with *n* phases, the volume of phase *q*, Vol_q, is defined by

$$Vol_q = \int_{Vol} \alpha_q dVol \qquad (2.20)$$

where:

$$\sum_{q=1}^{n} \alpha_q = 1 \qquad (2.21)$$

The effective density of phase q is:

$$\hat{\rho}_q = \alpha_q \rho_q \tag{2.22}$$

where ρ_q is the density of q.

The continuity equation for phase q is

$$\frac{\partial}{\partial t}(\alpha_q \rho_q) + \nabla \cdot (\alpha_q \rho_q \vec{V}_q) = \sum_{p=1}^{n} (\dot{m}_{pq} - \dot{m}_{pq}) + S_q \tag{2.23}$$

where $\vec{V}_q$ is the velocity of phase q. $\dot{m}_{pq}$ and $\dot{m}_{qp}$ characterizes the mass transfer from the p phase to q phase and mass transfer from the q phase to p phase respectively. S_q is the mass source term for q phase.

The momentum balance for phase q yields:

$$\frac{\partial}{\partial t}(\alpha_q \rho_q \vec{V}_q) + \nabla \cdot (\alpha_q \rho_q \vec{V}_q \vec{V}_q) = -\alpha_q \nabla p + \nabla \cdot \bar{\bar{\tau}}_q + \alpha_q \rho_q \vec{g} + \sum_{p=1}^{n} (\vec{R}_{pq} + \dot{m}_{pq} \vec{V}_{pq} + \dot{m}_{qp} \vec{V}_{qp}) + (\vec{F}_q + \vec{F}_{lift,q} + \vec{F}_{vm,q}) \tag{2.24}$$

where $\bar{\bar{\tau}}_q$ is the q phase stress-strain tensor:

$$\bar{\bar{\tau}}_q = \alpha_q \mu_q (\nabla \vec{V}_q + \nabla \vec{V}_q^T) + \alpha_q (\lambda_q - \frac{2}{3}\mu_q) \nabla \cdot \vec{V}_q I \tag{2.25}$$

where μ_q and λ_q are the shear and bulk viscosity of phase q, $\vec{F}_q$ is an external body force, $\vec{F}_{lift,q}$ is a lift force, $\vec{F}_{vm,q}$ is virtual mass force, $\vec{R}_{pq}$ is an interaction force between phases, and p is the pressure shared by all phases.

$\vec{V}_{pq}$ is the interphase velocity, defined as follows. If $\dot{m}_{pq} > 0$ i.e., phase p mass is being transferred to phase q, $\vec{V}_{pq} = \vec{V}_p$; if $\dot{m}_{pq} < 0$ i.e., phase q mass is being transferred to phase p, $\vec{V}_{pq} = \vec{V}_q$.

Likewise, if $\dot{m}_{qp} > 0$, then $\vec{V}_{qp} = \vec{V}_q$, if $\dot{m}_{qp} < 0$, then $\vec{V}_{qp} = \vec{V}_p$.

This interaction force between phases $\vec{R}_{pq}$ depends on the friction, pressure, cohesion, and other effects, and is subject to the conditions that $\vec{R}_{pq} = -\vec{R}_{qp}$ and $\vec{R}_{qq} = 0$. In FLUENT, $\vec{R}_{pq}$ is expressed as;

$$\sum_{p=1}^{n} \vec{R}_{pq} = \sum_{p=1}^{n} K_{pq}(\vec{V}_p - \vec{V}_q) \qquad (2.26)$$

where $K_{pq} = K_{qp}$ is the interphase momentum exchange.

2.4 Immiscible fluid flow in porous media

2.4.1 Darcy's law

In 1856, Henry Darcy investigated the flow of water in vertical homogeneous sand filters, as shown in Figure 2.5. From the experimental results, Darcy concluded that the rate of flow i.e. volume per unit time Q is:

- Proportional to the constant cross sectional area A
- Proportional to the piezometric head difference between face a and face b
- Inversely proportional the length L between face a and b

Thus, the Darcy's law is given:

$$Q = KA(\varphi_a - \varphi_b)/L \qquad (2.27)$$

where K is called hydraulic conductivity, φ is a piezometric head, and $(\varphi_a - \varphi_b)/L$ can be interpreted a hydraulic gradient. The above equation can also be expressed as:

$$q = Q / A = KJ \qquad J = (\varphi_a - \varphi_b) / L \tag{2.28}$$

where J denotes the hydraulic gradient, q is the specific discharge i.e. discharge per unit cross sectional area normal to the flow direction.

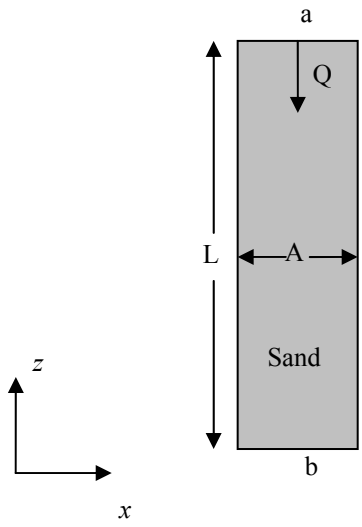

Figure 2.5 Darcy's experiment

The flow takes place from a higher piezometric head to a lower one and not from a higher pressure to a lower pressure. The relation of piezometric head and pressure is:

$$\varphi = z + p / \rho g \tag{2.29}$$

In the case of a porous media, when fluid flows through the column shown in Figure 2.5, the fluid only occupies part of the cross section, the pores, and the remaining part being occupied by the solid matrix of the porous media. Therefore the average velocity in the pore is given by:

$$V_{pore} = Q / n_{pore} A = q / n_{pore} \tag{2.30}$$

where V_{pore} and n_{pore} are average velocity in the pore and volumetric porosity respectively.

The above derived Darcy's law is limited to one dimensional flow. When the flow is three dimensional, the obvious formal generalization of Darcy's law is:

$$\vec{q} = K\vec{J} = -K\ grad\,\varphi \tag{2.31}$$

where $\vec{q}$ is the specific flux vector with components q_x, q_y, q_z in the directions of Cartesian *x, y, z* coordinates respectively, and $\vec{J} = -\ grad\,\varphi$ is the hydraulic gradient with components $J_x = -\partial\varphi/\partial x$, $J_y = -\partial\varphi/\partial y$, $J_z = -\partial\varphi/\partial z$ in the *x, y, z* directions respectively.

When the porous media is homogeneous isotropic, the hydraulic conductivity K is a constant scalar, and the above equation can be written in three separate equations:

$$\begin{aligned} q_x &= KJ_x = -K\frac{\partial\varphi}{\partial x} \\ q_y &= KJ_y = -K\frac{\partial\varphi}{\partial y} \\ q_z &= KJ_z = -K\frac{\partial\varphi}{\partial z} \end{aligned} \tag{2.32}$$

And also:

$$\begin{aligned} \vec{q} &= -\frac{k}{\mu}\left[\frac{\partial p}{\partial x}\vec{i} + \frac{\partial p}{\partial y}\vec{j} + \left(\frac{\partial p}{\partial x} + \rho g\right)\vec{k}\right] \\ &= -\frac{k}{\mu}\left(grad\ p + \rho g\vec{k}\right) \end{aligned} \tag{2.33}$$

where k is the intrinsic permeability which depends solely on properties of the solid matrix, and is independent of the properties of the fluid:

$$k = K\mu/\rho g \tag{2.34}$$

If we define a potential as the energy per unit mass of the fluid [138]

$$\varphi' = p/\rho + gz \tag{2.35}$$

Then:

$$\vec{q} = -\left(k\rho/\mu\right) grad\,\varphi' \tag{2.36}$$

For flow in the general case of a homogenous anisotropic medium, the relationship between the specific discharge and the hydraulic gradient can be written as:

$$\vec{q} = \underline{K} \cdot \vec{J} \quad or \quad q_i = K_{ij} J_j \tag{2.37}$$

where $\underline{K}$ is the hydraulic conductivity tensor and it is symmetrical i.e. $K_{ij} = K_{ji}$. The intrinsic permeability $\underline{k}$ is also a symmetrical tensor, due to its relation to hydraulic conductivity as described in Equation *(2.34)*.

2.4.2 Flow of immiscible fluids

Two types of flow can take place when two or more fluids in motion occupy a porous media domain. One is miscible displacement in which fluids are completely soluble in each other. The interfacial tension between fluids is zero and a distinct fluid-fluid interface does not exist. The other is immiscible displacement, in which there are simultaneous flows of two or more immiscible fluids or phases (e.g., oil, water and gas) in the porous medium domain. In this case, interfacial tension between the two fluids exists, and a distinct fluid-fluid interface separates the fluids within each pore. This results in a capillary pressure difference across the interface [139].

Although the fluids are described as either miscible or immiscible, in the macroscopic sense, an abrupt interface, which is a continuous surface completely separating fluids, does note exist in practice in either type, since hydrodynamic dispersion takes place immediately after different fluids contact each other no matter whether they are immiscible fluids or miscible fluids. Hence, a transition zone appears between these fluids instead of an abrupt interface.

However, because the transition zone is narrow relative to the size of the flow domain especially for immiscible fluids, for the sake of practicality, an imaginary abrupt interface may be assumed to separate the two fluids. On each side of the fictitious interface, there is only a pure single phase. Despite this being an approximation to reality, it is effective for the treatment of the multiphase flow problem in porous media. [139]

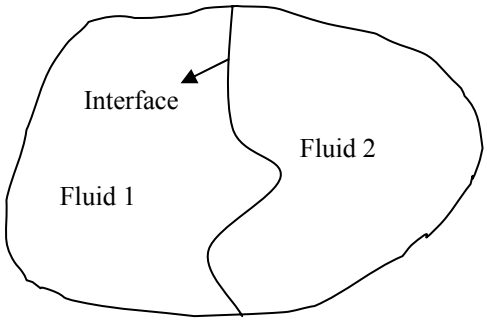

Figure 2.6 An abrupt interface separating two immiscible fluids

When immiscible fluid flow takes place, the different fluids contact with each other in the void space of the porous media, and across the interface separating them, the pressure is discontinuous. The magnitude of this discontinuity is related to the interface curvature and is also related to the nature properties of the solid matrix and fluids and the content of each fluid. The difference in pressure is called capillary pressure.

$$p_c = p_{nw} - p_w \tag{2.38}$$

where p_c is capillary pressure, p_{nw} is the pressure in the nonwetting phase and p_w is the pressure in the wetting phase. All these three terms are taken as a statistical average over the void space surrounding a considered point in the porous media.

When considering the simultaneous movement of two or more fluids, each of the fluids is treated as a continuum throughout the complete flow domain, and the various continual fluids occupy the entire flow domain simultaneously. In addition, a large amount of experimental research has been performed which discovered that when immiscible fluids flow through porous media, each fluid has it own pathway, which is a very stable channel [139]. With the above concepts, it is possible to extend the concept of permeability established for the flow of single phase fluid in porous media, and adjust it owing to the existence of other phases. Thus, Darcy's Law can be extended to describe the flow of each of the immiscible fluids flowing simultaneously through an anisotropic porous media:

$$q_{ia} = -\frac{k_{ija}}{\mu_a}\left(\frac{\partial p_a}{\partial x_j} + \rho_a g \frac{\partial z}{\partial x_j}\right) = -k_{ij}\frac{k_{ra}}{\mu_a}\left(\frac{\partial p_a}{\partial x_j} + \rho_a g \frac{\partial z}{\partial x_j}\right)$$
$$q_{ib} = -\frac{k_{ijb}}{\mu_b}\left(\frac{\partial p_b}{\partial x_j} + \rho_b g \frac{\partial z}{\partial x_j}\right) = -k_{ij}\frac{k_{rb}}{\mu_b}\left(\frac{\partial p_b}{\partial x_j} + \rho_b g \frac{\partial z}{\partial x_j}\right) \qquad (2.39)$$

where subscripts *a* and *b* denote two immiscible fluids, $\underline{k}_a$ and $\underline{k}_b$ re the two effective permeabilities of the media to fluids *a* and *b*, respectively. These depend on the structure of the porous media, on the permeability $\underline{k}$ of the media at a single phase fluid saturated status, and on the saturations of a different phase. k_{ra} and k_{rb} are the relative permeability to fluids *a* and *b*, respectively, and are given by the ratios of effective permeability to saturated permeability:

$$k_{ra} = k_a / k \qquad k_{rb} = k_b / k \qquad (2.40)$$

The relative permeability depends on the properties of the porous media on the wettability of the coexisting fluids and on the saturations, but is independent of the viscosities of the fluids and their specific discharges. In addition, it is also independent of direction. Figure 2.7 [140] illustrates the relationship between relative permeability and saturation.

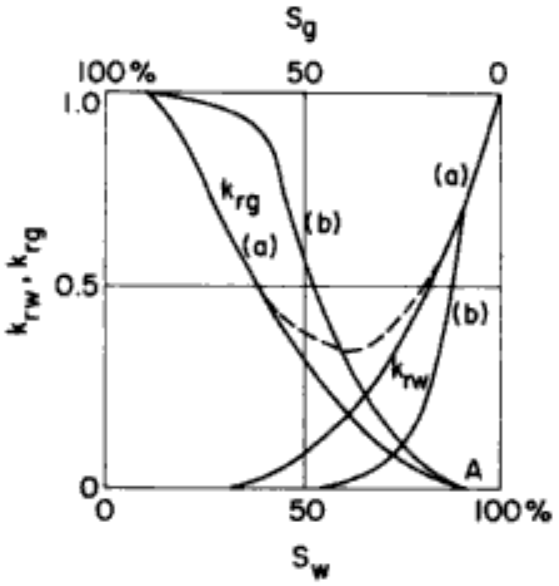

Figure 2.7 Typical relative permeability of gas and water (a) unconsolidated sand (b) consolidated sand [140]

For the immiscible fluids flowing simultaneously through isotropic porous media, the above equation can be simplified to:

$$\begin{aligned} q_{ia} &= -\frac{k_{ia}}{\mu_a}\left(\frac{\partial p_a}{\partial x_i}+\rho_a g\frac{\partial z}{\partial x_i}\right) = -k_i\frac{k_{ra}}{\mu_a}\left(\frac{\partial p_a}{\partial x_i}+\rho_a g\frac{\partial z}{\partial x_i}\right) \\ q_{ib} &= -\frac{k_{ib}}{\mu_b}\left(\frac{\partial p_b}{\partial x_i}+\rho_b g\frac{\partial z}{\partial x_i}\right) = -k_i\frac{k_{rb}}{\mu_b}\left(\frac{\partial p_b}{\partial x_i}+\rho_b g\frac{\partial z}{\partial x_i}\right) \end{aligned} \qquad (2.41)$$

Using this concept of effective permeability, the mass conservation equation was formed and for unsaturated liquid flow it is known as Richard's equation [141]:

$$\frac{\partial(\rho_q n_{pore} S_q)}{\partial t} = \frac{\partial}{\partial x_i}\left(\rho_q q_{iq}\right) \qquad (2.42)$$

where the subscription q denotes different fluid, S_q denotes saturation of fluid q in the pores. For an incompressible fluid, it can be simplified to:

$$\frac{\partial(n_{pore} S_q)}{\partial t} = \frac{\partial}{\partial x_i}\left(q_{iq}\right) \qquad (2.43)$$

2.5 Integrating immiscible fluid flow model with Eulerian multiphase model

The above analysis clearly shows that although normal fluid flow and porous media fluid flow problems share some similarities, the solution theories of each are set on differing fundamentals: the governing equations of normal fluid flow include continuity and momentum equations, while that of porous media flow includes only a continuity equation which is based on Darcy's Law. However, from the perspective of momentum and interaction between fluids and solid matrix, Darcy's Law and the Navier-Stokes equations can be unified. A generalized model for single incompressible fluid steady state flow through porous media was arrived at by Vafai and Tien [131, 132]:

$$\rho(\vec{V}\cdot\nabla)\vec{V} = -\nabla p + \mu\nabla^2\vec{V} + \rho\vec{g} - \frac{\mu n_{pore}\vec{V}}{k} - \frac{\rho F n_{pore}^3}{k^{1/2}}\vec{J} \qquad (2.44)$$

This model was extended to unsteady state flow by including a convective term [133]:

$$\rho\frac{\partial\vec{V}}{\partial t} + \rho(\vec{V}\cdot\nabla)\vec{V} = -\nabla p + \mu\nabla^2\vec{V} + \rho\vec{g} - \frac{\mu n_{pore}\vec{V}}{k} - \frac{\rho F n_{pore}^3}{k^{1/2}}\vec{J} \qquad (2.45)$$

In Equation *(2.44)* and *(2.45)*, F is the dimensionless inertia term coefficient and $\vec{J}$ is a unit vector oriented along the velocity vector. In these two equations, the fourth term on the right side of both equations are the Darcy term, which represent the Darcy resistance acting on the fluid by the solid matrix. The last term on the right side are inertia term, which can be neglected if the fluid velocity is very small and *Re* is no greater than 10 (discussed in Section 6.4.2).

In this study, the above model is extended to immiscible incompressible fluid flow through porous media:

$$\alpha_q\rho_q\frac{\partial\vec{V}_q}{\partial t} + \alpha_q\rho_q(\vec{V}_q\cdot\nabla)\vec{V}_q = -\alpha_q\nabla p_q + \alpha_q\mu_q\nabla^2\vec{V}_q + \alpha_q\rho_q\vec{g} - \alpha_q\frac{\mu_q\alpha_q\vec{V}_q}{k_q} - \alpha_q\frac{\rho_q F_q\alpha_q^3}{k_q^{1/2}}\vec{J_q} \qquad (2.46)$$

where q denotes the q phase fluid and α_q denotes the volumetric fraction of this q phase in the flow domain. Since the wetting fluid and nonwetting fluid endure different pressures, for the nonwetting phase:

$$\begin{aligned}&\alpha_{nw}\rho_{nw}\frac{\partial\vec{V}_{nw}}{\partial t} + \alpha_{nw}\rho_{nw}(\vec{V}_{nw}\cdot\nabla)\vec{V}_{nw}\\ &= -\alpha_{nw}\nabla p_{nw} + \alpha_{nw}\mu_{nw}\nabla^2\vec{V}_{nw} + \alpha_{nw}\rho_{nw}\vec{g} - \alpha_{nw}\frac{\mu_{nw}\alpha_{nw}\vec{V}_{nw}}{k_{nw}} - \alpha_{nw}\frac{\rho_{nw}F_{nw}\alpha_{nw}^3}{k_{nw}^{1/2}}\vec{J}_{nw}\end{aligned} \qquad (2.47)$$

and for the wetting phase:

$$
\begin{aligned}
&\alpha_w \rho_w \frac{\partial \vec{V}_w}{\partial t} + \alpha_w \rho_w (\vec{V}_w \cdot \nabla)\vec{V}_w \\
&= -\alpha_w \nabla p_w + \alpha_w \mu_w \nabla^2 \vec{V}_w + \alpha_w \rho_w \vec{g} - \alpha_w \frac{\mu_w \alpha_w \vec{V}_w}{k_w} - \alpha_w \frac{\rho_w F_w \alpha_w^3}{k_w^{1/2}} \vec{J}_w \\
&= -\alpha_w \nabla (p_{nw} - p_c) + \alpha_w \mu_w \nabla^2 \vec{V}_w + \alpha_w \rho_w \vec{g} - \alpha_w \frac{\mu_w \alpha_w \vec{V}_w}{k_w} - \alpha_w \frac{\rho_w F_w \alpha_w^3}{k_w^{1/2}} \vec{J}_w \\
&= -\alpha_w \nabla p_{nw} + \alpha_w \nabla p_c + \alpha_w \mu_w \nabla^2 \vec{V}_w + \alpha_w \rho_w \vec{g} - \alpha_w \frac{\mu_w \alpha_w \vec{V}_w}{k_w} - \alpha_w \frac{\rho_w F_w \alpha_w^3}{k_w^{1/2}} \vec{J}_w
\end{aligned}
\qquad (2.48)
$$

Comparing Equations *(2.47)* and *(2.48)* with Equation *(2.24)*, it is clear that these two equations have a similar form to the Eulerian multiphase model, with the exception of the Darcy term, inertial term and capillary pressure term; however, these terms can be presented by the external body force term of the Eulerian multiphase model. Hence, Equation *(2.47)* and *(2.48)* are combined models of the Eulerian multiphase model and the Darcy's Law based immiscible fluid flow model.

2.6 Mathematical models of immiscible fluid flow within/around biopile

2.6.1 Governing equations

A microcosmic conceptualization of a biopile system is shown in Figure 2.8. There are five phases involved in this system, and theoretically, to apply the Eulerian model to this system, a momentum governing equation should be set for every phase. However, the solid matrix used as the porous media is a fixed phase and is untransformable. In addition, the organic liquid phase (or oleic phase) is considered at residual content and the biophase should be fixedly attached to the solid matrix, thus these two phases are immobile. Furthermore, the quantity of these two phases are small, they only occupy a very small proportion of the total space volume, hence two more assumptions are made that the biomass growth does not affect the flow field, and the disappearance of the organic liquid phase caused by chemical, physical and biological processes does not affect the flow field either. This means that no matter how the biomass and organic liquid mass change, the volume in the flow domain they occupy maintain constant value. With these assumptions, the biomass and the organic liquid phases are treated as two virtual phases and integrated into the solid phase as a single immobile phase. Thus, the only mobile phases are the gas and aqueous phases.

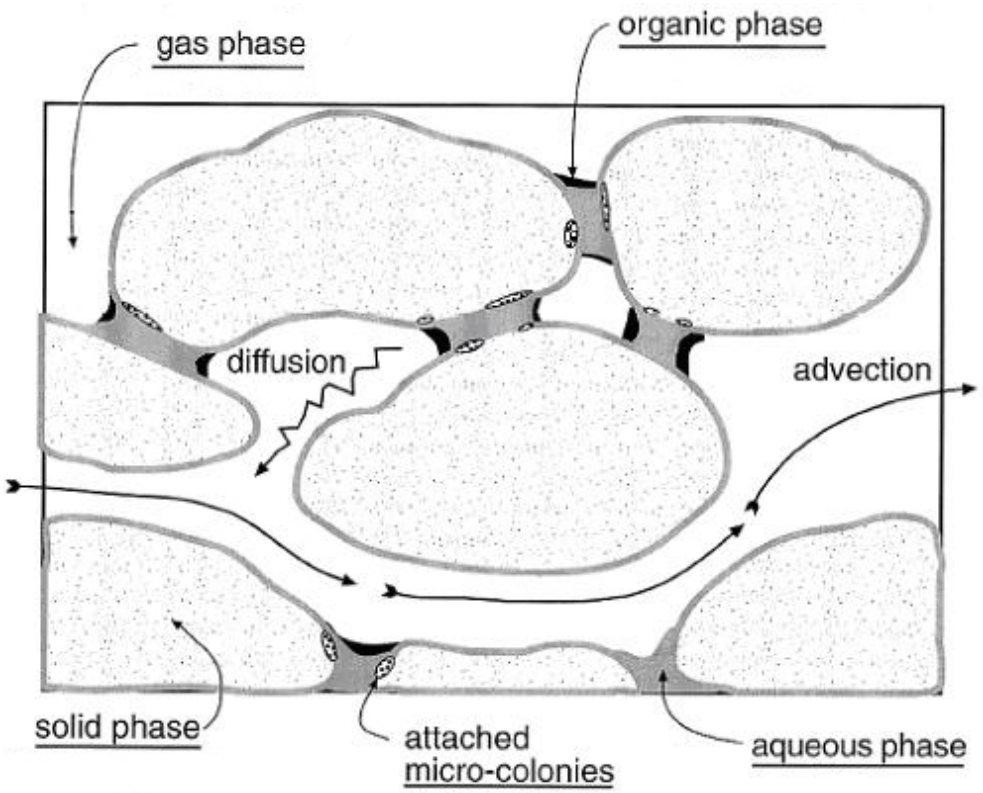

Figure 2.8 Conceptual representation of the biopile system [109]

Gas and aqueous phase flow within the biopile or its surroundings can be expressed by the equations acquired in Section 2.5. These governing equations of immiscible fluid flow in porous media are included in FLUENT's Eulerian model. Equation *(2.47)* and *(2.48)* also have their unique terms which are not covered by Equation *(2.24)*. To make the problem solvable by FLUENT, these unique terms need to be unified in the Eulerian model.

In this study, the velocities of gas and aqueous phases are very small and within an acceptable laminar flow range, so that Darcy's Law is valid to describe the interaction between phases (discussed in Section 6.4.2). Furthermore, although organic components can transfer between phases, since the organic component concentration in each phase is presumed to be very low, the fluid density change caused by this can be neglected. Also, in this study the pressure acting on the nonwetting phase, gas, changes within a very narrow range (discussed in Section 6.4.1), therefore, both the gas density and aqueous phase density are considered as constant. Therefore in this study, the governing equations solved by FLUENT are:

Continuity equation:

$$\frac{\partial}{\partial t}(\alpha_q) + \nabla \cdot (\alpha_q \vec{V}_q) = S_q \qquad q = gas, aqueous, solid \qquad (2.49)$$

Momentum equation:

$$\alpha_g \rho_g \frac{\partial \vec{V}_g}{\partial t} + \alpha_g \rho_g (\vec{V}_g \cdot \nabla)\vec{V}_g = -\alpha_g \nabla p_g + \alpha_g \mu_g \nabla^2 \vec{V}_g + \alpha_g \rho_g \vec{g} - \alpha_g \frac{\mu_g \alpha_g \vec{V}_g}{k_g} \quad \text{(gas phase)} \qquad (2.50)$$

$$\alpha_a \rho_a \frac{\partial \vec{V}_a}{\partial t} + \alpha_a \rho_a (\vec{V}_a \cdot \nabla)\vec{V}_a = -\alpha_a \nabla p_g + \alpha_a \nabla p_c + \alpha_a \mu_a \nabla^2 \vec{V}_a + \alpha_a \rho_a \vec{g} - \alpha_a \frac{\mu_a \alpha_a \vec{V}_a}{k_a} \quad \text{(aqueous phase)} \qquad (2.51)$$

By enabling or disabling the Darcy's term and/or capillary pressure term, the two equations above can be applied to fluid flow within the biopile or the normal fluid flow around the biopile.

The phase volume fractions are subject to the constraint:

$$\alpha_a + \alpha_g + \alpha_s = 1 \qquad (2.52)$$

Considering the application criteria described in Section 2.3.2, the fluid flow processes in this study will be modelled separately for each phase. A nonwetting phase pressure is shared by both phases. Interphase drag is substituted with Darcy's Law for unsaturated flow and relative permeability and also this study is now limited to laminar flow. Therefore, the Eulerian model is applicable to model the fluid flow of this study.

2.6.2 Capillary pressure

Capillary pressure, as a part of wetting fluid pressure, is one factor of wetting fluid motion and is related to fluid saturation. A widely used fitting function of the capillary retention data of a two-phase gas-aqueous system was delivered by van Genuchten [142]:

$$\overline{S}_a = [1 + (\varepsilon p_c)^n]^{-m} \qquad (2.53)$$

where $\overline{S}_a$ denotes the normalized aqueous saturation, ε , n and m are fitting variables. These variables are subjected to the following constrains:

$$m = 1 - 1/n \qquad (2.54)$$

$$\overline{S}_a = \frac{S_a - S_{ra}}{1 - S_{ra}} = \frac{\theta_a - \theta_{ra}}{n_{pore} - \theta_{ra}} \qquad (2.55)$$

where subscript a denotes aqueous phase, S_{ra} and θ_{ra} denote residual aqueous saturation and residual aqueous volume fraction respectively.

Van Genuchten only considers a two phase system, with aqueous phase as a wetting phase and gas as a nonwetting phase. In a biopile system, there are three phases existing in the pores: gas, aqueous phase and organic (or oleic) phase. The capillary pressure in such a three phase system is hard to measure. In 1987, Parker et al. established a parametric model to estimate three phase capillary pressure [143]. In this model, the organic phase was considered as an intermediate wetting phase and clearly segregated the gas and aqueous phases. Hence, the organic phase works as the key point for the saturation of each phase. This model was also extended for hysteresis by Kaluarachichi and Parker [144]. However, the application of this model is not practical due to the existence of many problems, primarily since it requires explicit evaluation of an organic liquid pressure which is difficult at organic immobile residual saturation [94].

Due to the difficulty mentioned above, in this study the capillary behaviour is assumed to be independent of the organic liquid pressure. Only the saturations of aqueous and gas phases are related to the gas-aqueous capillary pressure. Furthermore, hysteretic behaviour is also neglected since there were no widely acceptable mathematical equations to depict it.

With these assumptions, the capillary pressure of the wetting phase, aqueous, of the biopile system is also calculated from van Genuchten Equation *(2.53)*.

2.6.3 Relative permeability

A model developed by Parker et al. can be used to estimated the relative permeability for a three phase system [143]. In this model, the relative permeability of a fluid phase is assumed to be a function only of the saturation of this specific phase, regardless of the presence of other fluid phases. The functional forms for aqueous and gas phases are:

$$\begin{aligned} k_{ra} &= \bar{S}_a^{1/2}[1-(1-\bar{S}_a^{1/m})^m]^2 \\ k_{rg} &= \bar{S}_g^{1/2}(1-\bar{S}_t^{1/m})^{2m} \end{aligned} \qquad (2.56)$$

where $S_t = 1 - S_g$.

Chapter 3 Reactions on Contaminants

3.1 Introduction

The essential feature of the biopile treatment simulation is to actually model the migration and transformation processes of the pollutants, a process which is a very complex combination of physical, chemical and biological reactions. The main processes include contaminant transport within the fluid, contaminant transfer between different phases, and biotransformation of the contaminants. All these processes are inter-dependent, mutually constrained, and affect each other by sharing the contaminant concentration.

3.2 Interphase contaminant transfer

3.2.1 Contaminant concentration in phases

In this study, the author defines three actual phases and two virtual phases for the modelling of the biopile treatment process. The three actual phases are aqueous, gas and solid, which represents contaminant sorbed to the soil. The virtual phases are the oleic or organic phase, and the biophase. The mode of existence of the organic contaminant in each of these phases is different.

In the aqueous phase, the contaminant is actually a solute of the aqueous solution. In the gaseous and oleic phases, the volatilized gaseous and liquid organic contaminants are components of the phases, with the concentration in the gaseous phase being very small, and in the oleic phase being possibly very high. The unit of the organic contaminant concentration in these three phases is molar fraction, and is expressed as x_{qc}.

In the solid phase, the organic chemicals are adsorbed by the solid phase itself. The concentration unit is the nondimensional mass ratio of organic contaminant to solid matrix, and is expressed as ω_c.

An assumption about the contaminant concentration is made that regardless of how the contaminant concentration varies in each of the phases, it can not affect the density, including mass density and molar density, and volume fraction of a phase.

3.2.2 Interphase equilibrium

Species interphase equilibrium is the base of the species partition between phases, for either a dynamic process or an instantaneous equilibrium process. The equilibrium partitioning coefficients are typically developed under the assumption of ideal fluid behaviour.

Equilibrium partitioning between the organic and gas phases is given by Raoult's Law [83, 101], which states:

$$p_{gc} = \gamma_{oc} x_{oc} p_{vc} \qquad (3.1)$$

where p_{gc} is the partial pressure of the component c of the gas phase; γ_{oc} is the activity coefficient of component c in the organic phase and p_{vc} is the vapour pressure of component c as a pure chemical.

The activity coefficient is used to measure the nonideal behaviour caused by the interaction of dissimilar molecules. For a pure oleic substance and many common mixtures of hydrocarbons which are made up of components with similar chemical properties, the assumption of ideal behaviour of the organic phase, i.e. γ_{oc}=1, can be reasonably accepted [145, 146].

The partial pressure of component *c* can be expressed in the form of ideal gas law:

$$p_{gc} = \rho_g^m x_{gc} RT \qquad (3.2)$$

where ρ_g^m is the molar density of gas phase and R is universal gas constant. Integrating the above two equations using the assumption just mentioned, Raoult's Law is transformed:

$$\rho_g^m x_{gc} = \frac{x_{oc} p_{vc}}{RT} \qquad (3.3)$$

After rearranging this equation, the expression of organic-gas equilibrium partition coefficient, K_{goc}^e, can be obtained:

$$K_{goc}^e = \frac{x_{gc}}{x_{oc}} = \frac{p_{vc}}{\rho_g^m RT} \qquad (3.4)$$

Dissolution of the organic component in the aqueous phase is also assumed to be subject to ideal fluid behaviour. This assumption is valid for many common hydrophobic organic compounds with low aqueous solubility such that their activity coefficients remain constant over the range of possible concentrations [145, 146]. The equilibrium aqueous-organic partition coefficient is expressed as:

$$K_{aoc}^e = \frac{x_{ac}}{x_{oc}} = x_{ac}^{sol} \qquad (3.5)$$

where K_{aoc}^e is the aqueous-organic equilibrium partition coefficient, and x_{ac}^{sol} is the solubility limit for component c in aqueous phase.

The aqueous-gas equilibrium partition coefficient can be obtained by combining the partition coefficients of organic-gas and aqueous-organic:

$$K_{agc}^e = \frac{x_{ac}}{x_{gc}} = \frac{K_{aoc}^e}{K_{goc}^e} \qquad (3.6)$$

Expanding Equation *(3.6)* using the expression of K_{aoc}^e and K_{goc}^e gives:

$$p_{gc} = \frac{p_{vc}}{x_{ac}^{sol}} x_{ac} = K_H x_{ac} \qquad (3.7)$$

Equation *(3.7)* is the expression of Henry's Law, which states the relationship between the concentration of a chemical in liquid solution and its partial pressure in the gas phase. $K_H = \frac{p_{vc}}{x_{ac}^{sol}}$ is

the Henry's Law constant. Henry's Law is generally applied to solutes in dilute solutions, whilst some people have proved that its usage can be extended slightly, or even moderately soluble organic compounds with solute-solute interactions [94].

From Equations *(3.4)-(3.6)*, it is clear that K^e_{agc}, K^e_{aoc} and K^e_{goc} can be derived by calculation if Henry's Law constant and the vapour pressure of a compound are known.

The organic contaminant adsorbed by solid matrix is considered to only be related to the aqueous concentration in this study, and the equilibrium adsorption capacity is described by the Freundlich isotherm [147]:

$$\omega^e_{sc} = K_{fc}(C_{ac})^{n_c} \qquad (3.8)$$

where K_{fc} and n_c are the Freundlich isotherm parameters for component c adsorption, and C_{ac} is the solute aqueous concentration in the unit of mass of solute/volume of solution.

3.2.3 Dynamic interphase contaminant transfer

Although in previous research, models have used a chemical equilibrium hypothesis [2, 83, 95, 99-101], rate limited interphase contaminant transfer processes are more exact for depicting the contaminant reactions during biopile treatment [94]. When the contaminant exists in various phases out of equilibrium, transfer between the phases must take place as the system attempts to restore equilibrium conditions. As shown in Figure 3.1, in this study, such interphase transfer is considered to be occurring in four pairs of phases: organic and aqueous, organic and gas, aqueous and gas, aqueous and solid. Linear driving force models are adopted for modelling the interphase transfer processes, and such models are the most widely used in others previous works [84, 94, 96, 103, 104, 107].

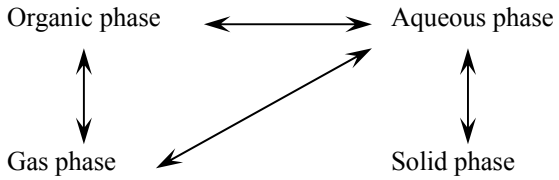

Figure 3.1 Interphase compound transfer paths

Interphase mass transfer involves three steps: the transfer of mass from the main bulk of one phase to that phases' interface, transfer across the interface into the second phase, and finally transfer to the main bulk of the second phase [148]. This process is illustrated in Figure 3.2 and can be explained by a two-resistance theory [149]. This theory has two principle assumptions: the rate of the mass transfer between the two phases is controlled by the rate of diffusion through the phases on each side of the interface, and no resistance is exerted on the mass transfer at the interface.

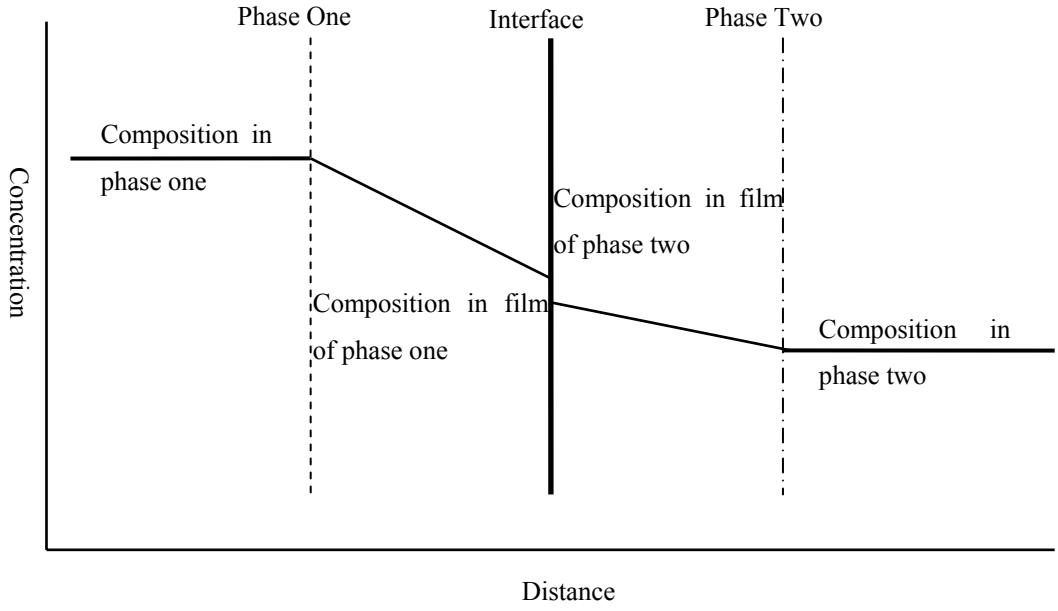

Figure 3.2 Interphase mass transfer process

Species diffusion resistances exist in both of the contacted phases. Within each of the phases, the species transfer can be expressed by a species transfer coefficient, and the combination of the two individual species transfer coefficients can be used to describe the overall process [149]. However, it is quite difficult to measure the partial pressure of the species, or concentration at the interface, and

the diffusion resistance on one side of the interface is frequently considered dominant. Therefore it is convenient to employ an overall species transfer coefficient based on an overall driving force between the species concentration and/or partial pressure [148].

The dominant resistance is assumed in the gas phase for the rate of organic phase volatilization. Evaluated with a linear driving force form, the transfer rate is expressed as [149]:

$$E_{goc} = \rho_g^m K_{goc}(x_{goc}^e - x_{gc}) \tag{3.9}$$

Here, K_{goc} is the effective gas-organic species transfer coefficient, x_{goc}^e is the gas phase mole fraction of species *c* in equilibrium with the organic phase mole fraction of species *c*. By applying Equation *(3.4)* to the equilibrium of species mole fraction in gas phase and organic phase, Equation *(3.9)* can be rewritten:

$$E_{goc} = \rho_g^m K_{goc}(K_{goc}^e x_{oc} - x_{gc}) \tag{3.10}$$

For species transfer rate between the organic phase and aqueous phase, a similar linear driving force model is adopted. In this study, the species transfer resistance of aqueous phase is assumed to be the controlling factor. By relating the equilibrium aqueous phase mole fraction of species *c* to the corresponding organic phase mole fraction, the expression becomes:

$$E_{aoc} = \rho_a^m K_{aoc}(K_{aoc}^e x_{oc} - x_{ac}) \tag{3.11}$$

where, ρ_a^m is the molar density of aqueous phase.

An assumption made for species transfer between the aqueous and gas phases is that this process is controlled by resistance in the aqueous phase. This assumption is proved to be valid for most volatile solutes [150, 151]. Under this assumption, the aqueous-gas transfer rate is:

$$E_{agc} = \rho_a^m K_{agc}(K_{agc}^e x_{gc} - x_{ac}) \tag{3.12}$$

The rate of species transfer between the aqueous and solid phases is also assumed to be controlled by

resistance in the aqueous phase:

$$E_{asc} = \rho_a^m K_{asc}(x_{asc}^e - x_{ac}) \tag{3.13}$$

where x_{asc}^e is the aqueous phase morel fraction in equilibrium with the solid phase concentration, and can be computed by Equation *(3.8)*and:

$$x_{asc}^e = \frac{C_{asc}^e}{\rho_a^m M_c} \tag{3.14}$$

where M_c is the molecular weight of species *c*.

3.3 Biotransformation

3.3.1 Monod equation

There are many expressions for substrate utilization in bioreaction, including zero-order model, first-order model etc. [152]. In this study, a Monod kinetic expression [153] is adopted as the fundamental model for substrate utilization and biomass production. The Monod equation was first introduced for biological treatment of wastewater by Lawrence and McCarty in 1970 [154]. Thereafter, it became widely used in the field of environmental biological treatment. The Monod equation is given by:

$$\mu = \frac{\mu_{\max} S}{K_s + S} \tag{3.15}$$

where μ and $\mu_{\max}$ are the specific biomass growth rate and the maximum specific biomass growth rate respectively, K_s is the half-velocity constant which is the substrate concentration at one-half the maximum specific biomass growth rate, and S is the substrate concentration. Here, substrate refers to the organic compounds or nutrients needed for the growth of microorganisms. A typical plot of specific growth rate against the concentration of a limiting substrate is shown in Figure 3.3 [154].

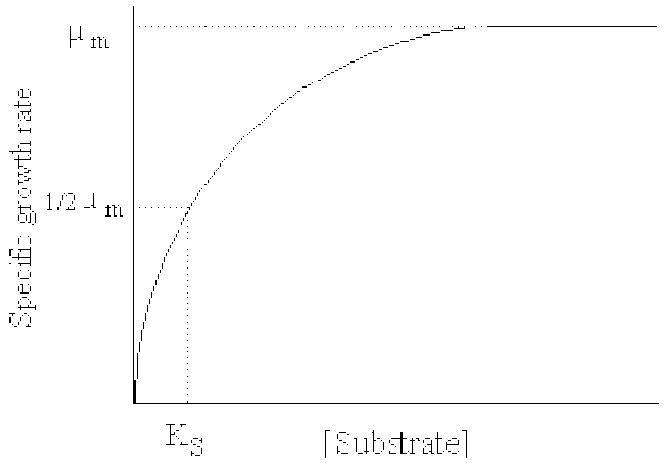

Figure 3.3 Monod growth rate as a function of limiting substrate concentration [154]

Since $\mu = \frac{dX/dt}{X}$, where X is the biomass concentration, the Monod type biomass growth kinetic model is:

$$\frac{dX}{dt} = \frac{\mu_{\max} SX}{K_s + S} \qquad (3.16)$$

If all the mass of the substrate can be converted to biomass, the rate of substrate utilization would be equal to the biomass production. However, the rate of substrate utilization is greater than the rate of biomass production due to conversion inefficiency, therefore:

$$\frac{dX}{dt} = -Y_l \frac{dS}{dt} \qquad (3.17)$$

where Y_l is the biomass yield coefficient for metabolism of substrate *l*.

Combining Equation *(3.16)* and *(3.17)*:

$$-\frac{dS}{dt} = \frac{(\mu_{\max}/Y_l)SX}{K_s + S} \qquad (3.18)$$

This is the substrate utilization rate model in which $\mu_{\max}/Y_l$ can be defined as maximum specific substrate utilization rate k_l.

3.3.2 Biodegradation

Although both aerobic and anaerobic bioreactions can take place in the biodegradation process, in this study, the concerned process is of an aerated biopile. Therefore it is assumed that aerobic bioreaction is dominant through the biopile operation. Moreover, bioreaction is assumed to only take place where aqueous phase contacts the soil surface to which biomass is attached. The biomass is considered as a kind of indigenous mixed microbial population which is attached to the solid phase (porous media) as micro colonies (Figure 2.8). The overall biodegradation model is an extended Monod-type expression which integrates the utilization of a substrate, oxygen as the electron acceptor and limiting nutrients [109, 155-157].

$$B_{a_c} = -F_{c_l} k_l X \left(\frac{x_{al}}{K_{sl} + x_{al}} \right) \left(\frac{x_{aO_2}}{K_{sO_2} + x_{aO_2}} \right) \left(\frac{x_{aN}}{K_{sN} + x_{aN}} \right) I_l I_{O_2} I_N I_S I_T \qquad (3.19)$$

where B_{a_c} is the net rate of component *c* consumed by biological transformation occurring in the aqueous phase; F_{c_l} is the consumption coefficient of component c with substrate l degradation; k_l is the maximum specific substrate utilization rate of substrate *l;* X is the active biomass concentration; x_{a1}, K_{s1}, x_{aO_2}, K_{sO_2}, x_{aN}, K_{sN} are the aqueous phase concentrations and half-velocity constants of substrate l, oxygen and nutrients, respectively; I_l, I_{O_2}, I_N and I_S are inhibition functions of substrate, oxygen, nutrients and moisture saturation; and I_T is the temperature effect function on biodegradation.

Normally, the contaminants of a biopile are very complex. When the contaminants are consumed as substrates in the aerobic bioreaction, oxygen and nutrients are needed for the microorganism metabolism as well. Equation *(3.19)* gives component *c* consumption by biological transformation of a single substrate *l*, in the case where component *c* is the substrate *l*, $F_{c_l} = M_c^{-1}$; if there are multiple substrates then the utilization of oxygen and nutrients must be summed over repeated applications of the equation, one for each substrate being degraded.

The above biodegradation model incorporates many effects on biokinetics, including organic substrate,

oxygen, nutrients, moisture saturation and temperature. The organic substrate and nutrients may potentially have inhibitory effects on biodegradation at excessively high or low concentrations [158-160]. Woods gave the expression for substrate inhibition [161]:

$$I_l = \left(1 - \frac{x_{al}^{\min}}{x_{al}}\right)\left(1 - \frac{x_{al}}{x_{al}^{\max}}\right) \qquad (3.20)$$

where $x_{al}^{\min}$ represents the minimum detectable mole fraction of substrate *l*, and $x_{al}^{\max}$ is the inhibitory mole fraction of substrate *l*.

Nutrient inhibition can be expressed in a similar way to Equation *(3.20)* [161]:

$$I_N = \left(1 - \frac{x_{aN}}{x_{aN}^{\max}}\right) \qquad (3.21)$$

where $x_{aN}^{\max}$ is the inhibitory mole fraction of nutrient *N*.

For aerobic degradation of aromatic hydrocarbons, in hypoxic conditions where alternative electron acceptors, such as nitrates, are absent, the reaction will be greatly decreased or entirely halted [162, 163]. An empirical inhibition function for hypoxic conditions is:

$$I_{O_2} = \left(1 - \frac{x_{aO_2}^{\min}}{x_{aO_2}}\right) \qquad (3.22)$$

where $x_{aO_2}^{\min}$ is the limiting oxygen mole fraction below which aerobic metabolism stops.

In an immiscible fluid flow process such as the biopile system, represented in this study, the moisture content influences the microbial activity also [164, 165]. However, due to a lack of data, this effect can not be accurately modelled. Abriola made an untested hypothetical saturation inhibition function in her research [94]:

$$I_S = \left(0.1 + 0.9 \frac{S_a - S_{ra}}{1 - S_{ra}} \right) \tag{3.23}$$

Although many bioremediation models do not take into account the effect of temperature, it has a significant influence on microbial growth. In the biodegradation process, the growth of organisms is restricted to the temperature range of 0-80 °C, with a maximum growth rate at about 40 °C. Only some bacteria are still active up to 80 °C, and the metabolism of other microorganisms cease at about 60 °C [48]. The expression regarding the effect of temperature is:

$$\begin{aligned} I_T &= \frac{T(80 - T)}{1600} \qquad 0\,°C \le T \le 80\,°C \\ I_T &= 0 \qquad\qquad\quad T < 0\,°C \;\; and \;\; T > 80\,°C \end{aligned} \tag{3.24}$$

3.3.3 Biomass metabolism

The Monod equation is only an expression of growth of microorganisms and does not treat their natural die-off. The death or decay of the microbial mass is generally assumed to be a first order expression [166]. Hence the overall biomass growth and decay expression is [167]:

$$\frac{dX}{dt} = \left[\sum_l Y_l \left(\frac{x_{al}}{K_{sl} + x_{al}} \right) \left(\frac{x_{aO_2}}{K_{sO_2} + x_{aO_2}} \right) \left(\frac{x_{aN}}{K_{sN} + x_{aN}} \right) I_l I_{O_2} I_N I_S I_T I_{\max} - K_d I_{\min} \right] X \tag{3.25}$$

where Y_l is the yield coefficient for metabolism of substrate l; K_d is the decay coefficient of the microorganism; $I_{\max}$ and $I_{\min}$ are functions preventing the biomass concentration from exceeding a maximum concentration or declining below a minimum concentration. The two functions are [94]:

$$I_{\max} = \left(1 - \frac{X}{X_{\max}} \right) \tag{3.26}$$

$$I_{\min} = \left(1 - \frac{X_{\min}}{X} \right) \tag{3.27}$$

where X_{min} reflects the indigenous microbial population in uncontaminated material, and X_{max} is the maximum allowable biomass.

3.4 Transport mechanisms

Contaminants such as leakage and spill of fuels and petroleum dissolved in the gaseous and aqueous phases, can be transported with these fluids in the biopile as well as in the surroundings. There are three physical transport mechanisms: advection, diffusion and mechanical dispersion.

3.4.1 Advection

Advection is contaminant mass transport caused by the bulk movement of the flowing phase [168]. The driving force is the pressure gradient. The advection flux is related to the fluid flux and the contaminant concentration:

$$J_a = qC = v\alpha C \qquad (3.28)$$

where J_a is the advection flux (mol/ m^2 s or kg/ m^2 s), q and v are the fluid flux, or Darcy velocity (m/s), and average pore velocity of the fluid respectively. α is the volume fraction of the fluid. C is the contaminant concentration in the fluid (mol/ m^3 or kg/m^3).

3.4.2 Diffusion

Diffusion is the process by which contaminants migrate from a zone of higher concentration to a zone of lower concentration. The driving force behind this is the random movement of ionic and molecular constituents under the influence of their kinetic activity, called Brownian motion [168]. Thus, diffusion does take place, even in the absence of fluid motion, and from a theoretical perspective, diffusion is driven by gradients in chemical potential rather than gradients in concentration [169]. Additionally it should be noted diffusion is irreversible.

The diffusion process is described by Fick's Law:

$$J_0 = -D_0 \frac{dC}{dx} \tag{3.29}$$

where J_0 and D_0 are diffusive mass flux (mol/ m^2 s or kg/ m^2 s) and diffusion coefficient (m^2/ s) respectively. The diffusion process, taking place in porous media flow, is affected by two additional effects. Firstly, since in porous media flow, every fluid occupies only a part of the pore space, it leads to the porosity effect; secondly, the path followed by a diffusing species is not straight, it has to swing its way around the matrix particles, resulting in the tortuosity effect [169]. Hence the diffusion in porous media flow can be expressed as:

$$J_0 = -\alpha D_s \frac{dC}{dx} \tag{3.30}$$

where α is the volume fraction of the fluid on which the species depends, it reflects the porosity effect, and D_s is the effective diffusion coefficient (m^2/ s) in porous media and reflects the tortuosity effect. The function of D_s is [170]:

$$D_s = \tau D_0 \tag{3.31}$$

And

$$\tau = \frac{\alpha^{7/3}}{n_{pore}^2} \tag{3.32}$$

Although normally the diffusion coefficient is very small, it can still have a significant impact on the overall contaminant transport over a long period of time.

3.4.3 Mechanical dispersion

As a result of the velocity distribution within each pore, variations of fluid local velocity results in mechanical dispersion. This variation is both in magnitude and direction, along the tortuous flow paths and between adjacent flow paths. The reasons for variation include velocity variation between the middle and the boundary of the flow paths, dissimilar pore sizes and different flow path

tortuosities. Such velocity variations cause initial species distributions within the flow domain to spread and occupy a continually expanding space in the flow domain. This process is considered as mechanical dispersion. It can also be described in the form of Fick's Law given below:

$$J_h = -\alpha D_h \frac{dC}{dx} \qquad (3.33)$$

where J_h and D_h are mechanical dispersion mass flux and mechanical dispersion coefficient respectively, and D_h is related to the fluid velocity. Since dispersion depends on pore geometry, it will generally not be uniform in all directions. Thus, the dispersion coefficient is a tensor rather than a scalar.

3.4.4 Hydrodynamic dispersion

Both diffusion and mechanical dispersion induce mixing and spreading, Due to difficulties in measuring the microscopic velocity and in clearly separating the influences of these two processes, diffusion and mechanical dispersion are usually treated synthetically, and referred to as hydrodynamic dispersion:

$$J_{sh} = D_{sh}(\alpha, v)\frac{dC}{dx} = -\alpha D \frac{dC}{dx} \qquad (3.34)$$

where J_{sh} is the hydrodynamic dispersion flux, D_{sh} is the effective hydrodynamic dispersion coefficient which is related to the volume fraction and velocity of the fluid, and D is the hydrodynamic dispersion coefficient.

3.4.5 Relationship of D_s, D_h and D

Many researchers have conducted experimental work to study the relationship between velocity distribution, diffusion and hydrodynamic dispersion. A dimensionless number, the Péclet number, is used to define the ratio between rate of transport by advection to the rate of transport by diffusion:

$$Pe = \frac{v \cdot d}{D_s} \qquad (3.35)$$

where d is the average diameter of the porous material particle or another characteristic length.

Kutilek and Nielsen [171], divided hydrodynamic dispersion into four zones according to the value of the Péclet number:

Table 3.1 Relationship of hydrodynamic dispersion and Péclet number

Zone 1	$Pe<0.3$	$D=D_s$	$D_h << D_s$
Zone 2	$0.3<Pe<5$	$D=D_s+D_h$	$D_h \approx D_s$
Zone 3	$5<Pe<20$	$D_h<D<(D_s+D_h)$	$D_h > D_s$
Zone 4	$Pe>20$	$D=D_h$	$D_h >> D_s$

Their conclusions reflect the relationship of hydrodynamic dispersion coefficient, velocity distribution, diffusion and properties of porous media. However, this was derived from a one-dimensional experimental study, and does not take into account the tensor characteristic of the dispersion coefficient. It can not properly justify the transversal and longitudinal dispersion coefficient in homogenous porous media, or the dispersion coefficient in heterogeneous porous media. However, it can be used to estimate which process (diffusion or mechanical dispersion) dominates the hydrodynamic dispersion.

3.4.6 Mathematical model for species transport

The total species flux is the sum of advection flux and hydrodynamic dispersion flux:

$$J = qC - \alpha D \frac{dC}{dx} = \alpha vC - \alpha D \frac{dC}{dx} \qquad (3.36)$$

Applying the elemental control volume scheme with the above expression of total species flux, without considering any source/sink term, the differential species transport equation can be obtained:

$$\frac{\partial}{\partial t}(\alpha_q \rho_q C_q) + \nabla \cdot \alpha_q (\rho_q C_q \bar{V}_q - \rho_q \underline{D}_{qc} \nabla C_q) = 0 \qquad (3.37)$$

where q denotes phase q.

3.5 Governing equations

A variable number of contaminants may be encountered in each of the phases. The transport and transformation of any individual contaminant in any of the mobile phases, aqueous or gaseous, can be described as:

$$\frac{\partial}{\partial t}(\alpha_a \rho_a^m x_{ac}) + \nabla \cdot \alpha_a (\rho_a^m x_{ac} \bar{V}_a - \rho_a^m \underline{D}_{ac} \nabla x_{ac}) = n_{pore} E_{ac} + B_{ac} \qquad (3.38)$$

$$\frac{\partial}{\partial t}(\alpha_g \rho_g^m x_{gc}) + \nabla \cdot \alpha_g (\rho_g^m x_{gc} \bar{V}_g - \rho_g^m \underline{D}_{gc} \nabla x_{gc}) = n_{pore} E_{gc} \qquad (3.39)$$

where the subscript c denotes the specific contaminant in the fluid phase, E_{ac} and E_{gc} are the net interphase transfer rate of contaminant c from other phases to the aqueous and gas phases respectively. B_{ac} is the net rate of contaminant c consumed by biological transformation and is restricted to the aqueous phase (see Section 3.3.2).

By multiplying Equation *(3.38)* and *(3.39)* by the molecular weight of aqueous and gas phase respectively, the following is obtained:

$$\frac{\partial}{\partial t}(\alpha_a \rho_a^m x_{ac} M_a) + \nabla \cdot \alpha_a (\rho_a^m x_{ac} \bar{V}_a M_a - \rho_a^m \underline{D}_{ac} \nabla x_{ac} M_a) = n_{pore} E_{ac} M_a + B_{ac} M_a$$

$$\frac{\partial}{\partial t}(\alpha_g \rho_g^m x_{gc} M_g) + \nabla \cdot \alpha_g (\rho_g^m x_{gc} \bar{V}_g M_g - \rho_g^m \underline{D}_{gc} \nabla x_{gc} M_g) = n_{pore} E_{gc} M_g$$

Since $\rho_a = \rho_a^m M_a$ and $\rho_g = \rho_g^m M_g$, the above equations can be transformed to:

$$\frac{\partial}{\partial t}(\alpha_a \rho_a x_{ac}) + \nabla \cdot \alpha_a (\rho_a x_{ac} \bar{V}_a - \rho_a \underline{D}_{ac} \nabla x_{ac}) = n_{pore} E_{ac} M_a + B_{ac} M_a \qquad (3.40)$$

$$\frac{\partial}{\partial t}(\alpha_g \rho_g x_{gc}) + \nabla \cdot \alpha_g (\rho_g x_{gc} \bar{V}_g - \rho_g \underline{D}_{gc} \nabla x_{gc}) = n_{pore} E_{gc} M_g \qquad (3.41)$$

Two other phases, oleic and solid, are considered immobile in this study. The contaminants dissolved in them are not subject to transport by advection. In addition, a further assumption is addressed in that the hydrodynamic dispersion transport of the contaminants in these two phases is considered negligible. Hence, the contaminant transport equations for these phases are:

$$\frac{\partial}{\partial t}(\alpha_o \rho_o^m x_{oc}) = n_{pore} E_{oc}$$

$$\frac{\partial}{\partial t}(\rho_s \frac{\omega_{sc}}{M_c}) = n_{pore} E_{sc}$$

Since the volume fraction and density of organic and porous media is assumed to be constant, the above two transport equations can be simplified:

$$\alpha_o \rho_o^m \frac{\partial}{\partial t}(x_{oc}) = n_{pore} E_{oc} \qquad (3.42)$$

$$\rho_s \frac{\partial}{\partial t}(\frac{\omega_{sc}}{M_c}) = n_{pore} E_{sc} \qquad (3.43)$$

Chapter 4 Heat Transfer

4.1 Introduction

Temperature is an important influencing factor of the biological reactions. During biopile treatment, aeration will result in heat loss or gain of the pile system due to the air flowing through it. Even without active aeration, heat exchange between the biopile and its surroundings can still take place. Since wind blowing over a biopile is a form of aeration, the effect of this will be examined in this study, as it has been unheeded in most previous studies, where focus was mainly centered on the contaminated material itself rater than its reactions with surroundings. Inside the biopile, heat will be exchanged between phases with differing temperatures. Moreover, the process of organic biodegradation is an exothermic reaction. All the above factors conduce to change of the temperature of each phase, and consequently affect the rate of biodegradation.

4.2 Heat transfer model in FLUENT

The heat transfer model in this study must correspond to the Eulerian multiphase flow model which has been chosen as the governing equation for the fluid flow. Therefore, the adopted heat transfer model is also an Eulerian multiphase type model, in which a separate enthalpy equation is written for each phase:

$$\begin{aligned} &\frac{\partial}{\partial t}\left(\alpha_q \rho_q h_q\right) + \nabla \cdot \left(\alpha_q \rho_q \vec{V}_q h_q\right) \\ &= -\alpha_q \frac{\partial p_q}{\partial t} + \bar{\bar{\tau}} \nabla \cdot \vec{V}_q - \nabla \cdot \vec{q}_q + S_q + \sum_{p=1}^{n} \left(\overline{Q}_{pq} + \dot{m}_{pq} h_{pq} - \dot{m}_{qp} h_{qp}\right) \end{aligned} \qquad (4.1)$$

where h_q is the specific enthalpy of the phase q, S_q is a source term that includes sources of enthalpy due to chemical reaction or radiation etc., $\overline{Q}_{pq}$ is the intensity of heat exchange between the phase p

and q, and h_{pq} is the interphase enthalpy. $\overline{\overline{\tau}}$ has already been defined in Equation *(2.25)*, and $\bar{q}_q$ is the conductive heat flux, and can be expressed as:

$$\bar{q}_q = k_t \nabla T \tag{4.2}$$

where k_t is thermal conductivity, T is temperature.

4.3 Heat generated from bioreaction

Both the processes of interphase contaminant transfer and organic contaminant biodegradation lead to heat consumption or production and accordingly result in variations in temperature. The physical, chemical and biological reactions are affected by temperature. Because it is widely consented that system temperatures are within the limits of microbial growth, but that interphase mass transfer is not [172], only the biodegradation reaction is considered to be pertinent to heat consumption/production. Moreover, due to the lack of a clear mathematic model and for the sake of model simplification, the interphase contaminant equilibrium partition coefficient and transfer coefficient are assumed to remain constant with temperature, while biodegradation rate is modulated by a temperature effect coefficient.

Biodegradation is an exothermic reaction, and is also modelled based on the Monod expression:

$$\begin{aligned} H &= -\sum H_l B_{a_l} \\ &= \sum H_l F_{l_l} k_l X \left(\frac{x_{al}}{K_{sl} + x_{al}} \right) \left(\frac{x_{aO_2}}{K_{sO_2} + x_{aO_2}} \right) \left(\frac{x_{aN}}{K_{sN} + x_{aN}} \right) I_l I_{O_2} I_N I_S I_T \end{aligned} \tag{4.3}$$

where H is the total energy generation rate, and H_l is the reaction enthalpy of substrate l degradation.

Chapter 5 Modelling Setup and Process

5.1 Introduction

FLUENT, a general purpose CFD package based on the finite volume method, is employed in this study. In this chapter, the cooperate method of the suitable FLUENT modules and the mathematical equations depicting the processes discussed in previous chapters are described first. Although FLUENT is a popular and competent CFD software package, if only its built- in functions are used, it would not be capable for modelling some processes in this study. Consequently, the author has developed a number of User Defined Functions (UDFs), which are programmed functions that can be dynamically loaded with the FLUENT solver, to compensate for the deficiencies of the standard features in the software, and to achieve comprehensive simulation of the concerned problems. Additionally, User Defined Scalars (UDSs) are also introduced to collaborate with the UDFs and other FLUENT modules in order to integrate the whole model.

The ordinary grid generation method, discretization and numerical solution method, and procedure of the finite volume method used in FLUENT are introduced, followed by an explanation regarding the detailed solution procedure of specific cases in this study. This chapter concludes with a summary of the experiences gained by the author by applying FLUENT to carry out this study.

The UDSs and UDFs created in this study are listed in Appendixes A and B respectively.

5.2 Setting proper FLUENT modules

FLUENT consists of many modules fitted for various fluid flow problems. In this study, the processes of concern are multiphase flow through the biopile and its surroundings, and contaminant transport with fluid flow and heat transfer. The governing equations of these processes and the proper FLUENT modules depicting them have been addressed in previous chapters. The settings for coordinating these

FLUENT modules with their corresponding governing equations will be introduced in this section.

5.2.1 Eulerian model for multiphase flow

The Eulerian multiphase flow module is adopted in this study. The general mass and momentum conservation equations of the Eulerian model are described in Section 2.3.3. Practically, the equations solved by FLUENT for the Eulerian model are as follows:

Continuity equation:

$$\frac{1}{\rho_{rq}}\left(\frac{\partial}{\partial t}(\alpha_q\rho_q)+\nabla\cdot(\alpha_q\rho_q\vec{V}_q)=\sum_{p=1}^{n}(\dot{m}_{pq}-\dot{m}_{pq})\right) \qquad (5.1)$$

where ρ_{rq} is the phase reference density, or the volume averaged density of the q phase in the solution domain. The solution of this equation for each secondary phase, along with the condition that the volume fractions sum to one, allows for the calculation of the primary-phase volume fraction.

Conservation of momentum for a fluid phase *q*:

$$\frac{\partial}{\partial t}(\alpha_q\rho_q\vec{V}_q)+\nabla\cdot(\alpha_q\rho_q\vec{V}_q\vec{V}_q)=-\alpha_q\nabla p+\nabla\cdot\bar{\bar{\tau}}_q+\alpha_q\rho_q\vec{g}+\sum_{p=1}^{n}(K_{pq}(\vec{V}_p-\vec{V}_q)+\dot{m}_{pq}\vec{V}_{pq}+\dot{m}_{qp}\vec{V}_{qp})+(\vec{F}_q+\vec{F}_{lift,q}+\vec{F}_{vm,q}) \qquad (5.2)$$

In this study, the fluid mass interphase transfer is not considered. In Equation *(2.50)* and *(2.51)*, the interaction between the solid matrix and fluid phase is defined by the Darcy resistance term, and the interaction between immiscible fluids is expressed by the relative permeability of each phase. Consequently, the Darcy resistance term in these two equations can replace the interaction force in Equation *(5.2)*. With these considerations, Equation *(2.49)*, *(2.50)* and *(2.51)* all fall in the form of Equation *(5.1)* and *(5.2)*.

The whole fluid zone is divided into sub-zones of the biopile and its surroundings. In the surroundings sub-zone, FLUENT solves the common momentum conservation equation. UDFs of source term type

expressing the Darcy term and/or the capillary pressure term are created and hooked to the biopile fluid zone for modelling immiscible fluid flow in porous media. The capillary pressure at each location in the biopile is recorded by a non-transported UDS and updated at the beginning of each time step, which is also achieved by a UDF.

Conservation equations are also defined for the solid phase. However, in this study, the solid phase is described as a packed bed, and its velocity is set to be constant at zero, hence such equations are not actually solved.

5.2.2 UDS transport model for contaminant transfer

In this study, since contaminants are only a kind of solute dissolved in fluid phases, and not treated as compositions of a fluid, the contaminant transfer would be unnecessarily complicated by using the species transport model in FLUENT. Hence, the UDS transport model of FLUENT is adopted to simulate the process of contaminant transport. Here, the contaminant concentration in each phase is defined by a UDS. UDSs for concentration in water and gas are dependent on the corresponding fluid phase, while UDSs for concentration in solid and oleic phases are dependent on the mixture of phases.

For a UDS which is dependent on a single phase in a multiphase flow system, its transport equation solved by FLUENT is:

$$\frac{\partial}{\partial t}(\alpha_q \rho_q \phi_q) + \nabla \cdot \alpha_q (\rho_q \phi_q \vec{V}_q - \Gamma_q \nabla \phi_q) = S \qquad (5.3)$$

where ϕ_q is the UDS which is dependent on the q phase, Γ_q is the diffusion coefficient in FLUENT, and S is a source term [137].

Equation *(5.3)* is clearly comparable with the governing equations *(3.40)* and *(3.41)* for contaminant transfer in this study, with Γ_q corresponding to $\rho_a \underline{D}_{ac}$ and $\rho_g \underline{D}_{gc}$. The hydrodynamic dispersion in this study is considered to be dominated by the diffusion process (discussed in Section 6.4.3), hence the effective diffusion coefficient replace both $\underline{D}_{ac}$ and $\underline{D}_{gc}$ in Equations *(3.40)* and *(3.41)*. Since the effective diffusion coefficient is a function of the volume fraction of a fluid phase, it changes with

time. Hence UDFs accounting for this variation are developed. In addition, the right hand terms of Equations *(3.40)* and *(3.41)*, including contaminant interphase transfer and biodegradation, are treated as a source/sink term, and expressed by UDFs. A UDS is employed to indicate the effect of temperature on biodegradation at any location, and is updated at the beginning of each time step by applying a UDF.

Contaminants in the solid and oleic phases are not transferred but instead its concentration changes due to interphase transfer. Also, although biophase is fixed in the soil, its mass changes due to metabolism. Hence transport models for corresponding UDSs are disabled in FLUENT, whereas calculations based on Equations *(3.25)*, *(3.42)* and *(3.43)* are executed at the end of each time step by applying UDFs.

In order to simplify the complex model for the whole biopile treatment and reduce the computational burden, only single contaminant biodegradation and transfer processes were simulated in this study. Simulations for multi contaminants cases can be made following the same method introduced above. Therefore, in this study, when modelling processes related to bioreaction (biodegradation, biomass metabolism and heat from biodegradation), only the effects of the substrate (i.e. contaminant) and temperature are considered. Other controlling and inhibiting functions, such as oxygen and nutrients, have a similar mathematical expression to that of the substrate, and can be included in a similar manner as that of the substrate in simulations of the case of multi contaminants to acquire more sophisticated results. However these were excluded from the simulations carried out in this study. This treatment apparently provides simulation results with increased biodegraded contaminant, in addition to more heat generated from the biodegradation process.

5.2.3 Heat transfer modelling

As described in Section 4.2, since the heat transfer model is to be coordinated with the selected model for fluid flow, and consequently the Eulerian model is also adopted for heat transfer modelling. Equation *(4.1)* is the heat governing equation, which is set for each individual phase (gas, water and soil), and the heat generated by bioreaction, illustrated by Equation *(4.3)*, is incorporated in the governing equation for water as a source term by a UDF.

A key point for modelling heat transfer in a multiphase system is interphase heat transfer. Meanwhile, such a process in a multiphase porous media flow problem is very complex. Although there are some models describing heat transfer between phases [133, 173-178], these have been derived by either considering only a two-phase system, or studying saturated flow through a fluid-bed whose particles were homogeneous. These models are therefore not compatible with immiscible fluid flow through porous media, such as petroleum contaminated soil or other organic contaminated material.

Due to the complexity and the absence of a reliable model, previous researchers have either neglected the effects of temperature in their model [1, 84, 179] or have assumed a thermodynamic equilibrium condition within all phases [2, 180], as Datta pointed out, "An important assumption made in almost all multiphase porous media studies is that the solid, liquid and gas (vapour+air) at any location are in thermal equilibrium, so there is only one temperature at any given location." [130]. In addition, in this study, the slow flow of each mobile phase (as discussed in 6.4.2) can make the thermo-equilibrium even more readily established at any given time step.

Therefore, in this study, the above assumption is also adopted, which means a thermodynamic equilibrium condition between phases is assumed to be achieved within each time step. Hence, any items concerned with interphase heat transfer within the heat conservation equation are set as zero, and heat transfer equations are first solved for each phase, and the equilibrium temperature then based on the solution of these equations and the specific enthalpy of each phase. This calculation is implemented by UDFs.

One more simplification for modelling heat transfer in this study is that radiative heat transfer is neglected. This is primarily because the temperature difference between the biopile system and its surroundings is only about 5°C, the heat transfer resulting from gas flow dominates the total heat transfer. Moreover, although there are some empirical methods available to include heat radiation in bioremediation modelling (described in Equation *(1.6)*), it is difficult to obtain suitable parameters for these methods, and in the author's opinion, such methods are not accurate. Therefore, the heat governing equation of this study, Equation *(4.1)*, only accounts for heat convection, and heat conduction. Heat radiation is not involved in this study.

5.2.4 Boundary and initial conditions

(1) Boundary conditions

Although there are many choices for of boundary conditions available with FLUENT, mathematically, there are only three types of boundary conditions imposed on an ordinary differential equation or a partial differential equation:

1) Dirichlet boundary condition: this is a forced condition, also known as essential boundary conditions or first type boundary conditions. It specifies the values a solution of a differential equation on the boundary of the geometry grid. For any field variables at the boundary Γ, it gives:

$$\phi|_{\Gamma} = \phi(t) \qquad (5.4)$$

2) Neumann boundary condition: also known as natural boundary conditions or second type boundary conditions. This boundary condition gives the values of the normal derivative of a differential equation's solution on the boundary Γ of the domain.

$$\left.\frac{\partial \phi}{\partial n}\right|_{\Gamma} = g(t) \qquad (5.5)$$

3) Robin boundary condition: also known as third type boundary condition. It is a weighted combination of Dirichlet and Neumann boundary conditions.

$$\omega_1 \left.\frac{\partial \phi}{\partial n}\right|_{\Gamma} + \omega_2 \phi|_{\Gamma} = h(t) \qquad (5.6)$$

In this study, all the above boundary conditions are used. The first type boundary conditions are primarily used for illustrating the inlet boundary for the fluid (velocity inlet). The pressure outlet boundary used in this study is defined by the third type boundary condition. The boundary conditions for transport of UDSs are all set to the second type boundary conditions no matter whether it is an inlet or outlet boundary. (Refer to Section 6.3.2 for detailed settings of the boundary conditions used

in this study.)

(2) Initial conditions

In this study, the value of each field variable is set at the beginning of every simulation (Refer to Section 6.3.2 for detailed settings of the initial conditions used in this study.). This initial condition can be expressed as:

$$\phi_{(t=0)} = \phi_0 \qquad (5.7)$$

5.3 Numerical solution method

5.3.1 General

After gaining the governing partial differential equations and setting the correct FLUENT modules, it is necessary to choose a suitable discretization method, i.e. a method representing and evaluating these equations as a system of algebraic equations for the variables at a set of discrete positions on a meshed geometry and designated time. There are many discretization approaches, such as the Finite Difference and Finite Element (FE) methods, and the Finite Volume (FV) method which is employed by FLUENT, is thereby used in this study.

The FV method makes volume integration on conservation equations from the starting point. The whole solution zone is divided into a finite number of contiguous control volumes, and the governing conservation equations are solved in each control volume. At the centre of each control volume, there lies a computational node on which the variable values are calculated and stored. Different interpolations can be chosen to acquire variable values at the control volume's surface in terms of the adjacent nodal values. In a partial differential equation containing a divergence term, volume integrals are converted to surface integrals using the divergence theorem. Consequently, a set of algebraic equations for each control volume is developed, in which variable values of neighboring nodes are presented [181]. Therefore, partial differential equations are converted to a system of algebraic equations, which can be numerically solved in sequence.

The FV method is conservative, as the flux entering a given volume, i.e. the surface integrals of a variable, is identical to that leaving the adjacent volume. Another advantage of the FV method is that it can accommodate any type of grid, and hence it is suitable for complicated geometries.

Since FLUENT is used to conduct the modelling, knowledge of the numerical solution method presented below are related to the theories adopted by FLUENT, and mainly delivered by FLUENT User's Guide.

5.3.2 Numerical grid

The discrete positions at which the variables are computed are controlled by a numerical grid, which is essentially a discrete exhibition of the geometric domain upon which the problem is solved. The numerical grid separates the solution domain into a finite number of subdomians, i.e. cells, elements, control volumes. There are mainly two formations of numerical grids [181]:

(1) Structured grid

A structured grid comprises of groups of grid lines, with the specialty that lines of a single group do not cross one another and cross each line of other groups only once. This is the simplest grid structure, but its use is limited to geometrically simple solution domains.

(2) Unstructured grid

Unstructured grids are used for very complex geometries. They are made up of triangles or quadrilaterals in 2-dimensions, and tetrahedrons or hexahedra in 3-dimensions, or any other shapes in an irregular pattern. There is no restriction on the number of neighbor elements or nodes. Due to its flexibility, it can fit any arbitrary solution domain. This structure of grid is theoretically compatible with any discretization scheme, and fits the FV and FE approaches very well.

5.3.3 General discretization and linearization scheme

The general discretization and linearization scheme used in FLUENT is given in the FLUENT User's Guide [137], and briefly described below:

(1) General discretization

The discretization process of the governing equations can be demonstrated most easily by considering the unsteady conservation equation for transport of a scalar quantity ϕ. This is expressed by the following equation written in integral form for an arbitrary control volume V as follows:

$$\int_V \frac{\partial \rho \phi}{\partial t} dV + \oint \rho \phi \vec{v} \cdot d\vec{A} = \oint \Gamma_\phi \nabla \phi \cdot d\vec{A} + \int_V S_\phi dV \qquad (5.8)$$

where ρ is density, $\vec{v}$ is velocity vector, $\vec{A}$ is surface area vector, Γ_ϕ is diffusion coefficient for ϕ, $\nabla \phi$ is gradient of ϕ and S_ϕ is source of ϕ per unit volume.

Applying this to each control volume, or cell in the solution domain, discretization of Equation *(5.8)* on a given cell yields:

$$\frac{\partial \rho \phi}{\partial t} V + \sum_f^{N_{faces}} \phi_f \rho_f \vec{v}_f \cdot \vec{A}_f = \sum_f^{N_{faces}} \Gamma_\phi \nabla \phi_f \cdot \vec{A}_f + S_\phi V \qquad (5.9)$$

where N_{faces} is the number of faces enclosing the cell, ϕ_f is the value of ϕ convected through face f, $\vec{A}_f$ is the area of face f, $\rho_f \vec{v}_f \cdot \vec{A}_f$ is the mass flux through the face, $\nabla \phi_f$ is the gradient of ϕ at face f, and V is the cell volume.

(2) Linearization

The discretized scalar transport Equation *(5.9)* contains the unknown scalar variable at the cell centre as well as the unknown values in surrounding adjacent cells. Normally, this equation will be non-linear with respect to these variables. At a cell *P*, the linearized form of Equation *(5.9)* can be written as:

$$a_P \phi = \sum_{nb} a_{nb} \phi_{nb} + b \qquad (5.10)$$

where the subscript nb refers to neighbour cells, and a_P and a_{nb} are the linearized coefficients for

ϕ and ϕ_{nb}; and b is the contribution of the constant part of the source term S_c in $S = S_c + S_P\phi$.

Similar equations can be given for each cell in the computational domain. This results in a set of algebraic equations with a sparse coefficient matrix, which can be solved with any numerical computation method.

(3) Spatial discretization

The FV method calculates and stores discrete values of the scalar ϕ at the cell centres in the solution grid. However, the cell surface value ϕ_f is also required as shown in Equation *(5.9)*. In FLUENT, this value is computed by interpolating from the cell centre values. There are several interpolation schemes available, including first-order upwind, second-order upwind, power law, QUICK, etc. In this study, first-order upwind is selected, since it can give good results for most classes of flow, and is recommended for its stability [137].

By using an upwind scheme, the cell surface value ϕ_f is derived from quantities in the upstream cell, relative to the direction of the normal velocity $\vec{v}_f$ in Equation *(5.9)*. First-order results in quantities at cell faces being calculated by assuming that the cell-centre values of any field variable demonstrate a cell-averaged value, and are maintained throughout the entire cell; the face quantities are identical to the cell quantities. Hence, the face value ϕ_f is equal to the cell-centre value of ϕ in the upstream cell. This scheme has first order accuracy.

(4) Temporal discretization

Since the problems in this study are all transient simulations, the governing equations must be discretized in both space and time. Temporal discretization involves the integration of every term in the differential equations over a time step Δt. A general formulation for the time evolution of a variable ϕ is:

$$\frac{\partial \phi}{\partial t} = F(\phi) \qquad (5.11)$$

where, $F(\phi)$ consists of all spatial discretizations. An example of the temporal discretization in first-order accuracy using a backward differences scheme is:

$$\frac{\phi^{n+1}-\phi^{n}}{\Delta t}=F(\phi) \qquad (5.12)$$

where n and $n+1$ denote the value at the current time level t and value at the next time level $t+\Delta t$ respectively.

There are two kinds of time integration schemes, implicit and explicit, and the implicit scheme is adopted in this study. It is expressed as follows:

$$\frac{\phi^{n+1}-\phi^{n}}{\Delta t}=F(\phi^{n+1}) \qquad (5.13)$$

Here, "implicit" denotes that ϕ^{n+1} in a given cell, and is related to ϕ^{n+1} in neighbouring cells through $F(\phi^{n+1})$:

$$\phi^{n+1}=\phi^{n}+\Delta t F(\phi^{n+1}) \qquad (5.14)$$

(5) Evaluation of gradients and derivatives

As shown in Equation *(5.9)*, gradients are required for constructing values of a scalar at cell faces. Moreover, in some cases, the gradient $\nabla\phi$ of a given variable ϕ is also needed for discretizing the convection and diffusion terms in the flow conservation equations. Three methods are offered by FLUENT to calculate the gradient $\nabla\phi$ at the cell centre: Green-Gauss Cell based, Green-Gauss Node based and Least Squares Cell based. The Green-Gauss Cell based method is employed in this study.

By applying the Green-Gauss theorem which states that the surface integral of a scalar function is equal to the volume integral of the gradient of the scalar function, the discrete form of the gradient of scalar ϕ at the cell centre $c0$ can be acquired:

$$(\nabla\phi)_{c0} = \frac{1}{V}\sum_f \bar{\phi}_f \bar{A}_f \qquad (5.15)$$

The summation over all the faces enclosing the cell $c0$. $\bar{\phi}_f$ is computed by:

$$\bar{\phi}_f = \frac{\phi_{c0} + \phi_{c1}}{2} \qquad (5.16)$$

ϕ_{c0} and ϕ_{c1} are respectively the values of ϕ of the cell $c0$ and $c1$, $c1$ being adjacent to cell $c0$ by sharing face f.

5.3.4 Solution method

The solution methods used in this study closely depend on functions of FLUENT and are briefly explained below [137]:

The two numerical methods presented by FLUENT are a pressure-based solver and a density-based solver. Traditionally, the pressure-based approach is suitable for low-velocity incompressible flows, while the density-based approach is primarily used for high-velocity compressible flows. In this study, the pressure range used in the simulations is small, air and gas are treated as having constant density (discussed in Section 6.4.1), and flows are at low velocity. Therefore, the pressure-based approach is used in this study.

In the pressure-based solver, the velocity field is obtained from the momentum equations, and the pressure field is gained by solving a pressure or pressure correction equation, which is derived by manipulating the continuity and momentum equations in such a way that the velocity field, corrected by the pressure, satisfies the continuity. Because the governing equations are nonlinear and coupled with one another, the solution process involves iterations in which the entire set of governing equations are solved repeatedly until the solution converges.

Two pressure-based solver algorithms are available in FLUENT: a segregated algorithm, and a coupled algorithm. However, for multiphase flow which is solved by the Eulerian model, only the

segregated algorithm is suitable. Furthermore, the Eulerian multiphase flow model does not permit any pressure correction algorithms other than the SIMPLE algorithm, which is described in FLUENT User's Guide [137].

With a segregated algorithm, the individual governing equations for each solution variable (e.g., u, v, w, p, etc.) are solved one after another. Each governing equation, while being solved, is in a decoupled or segregated status from other equations. The solution steps of the segregated algorithm are shown in Figure 5.1.

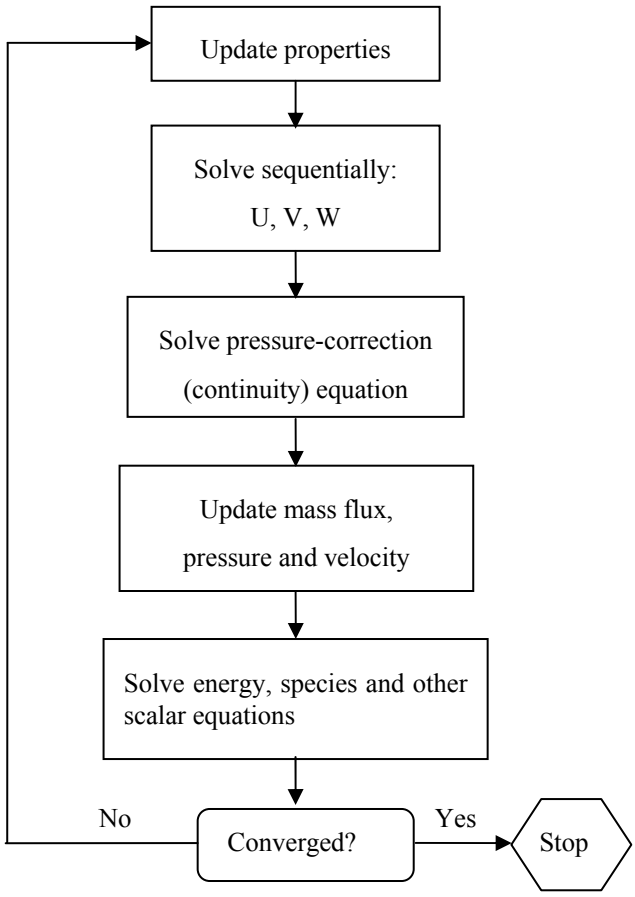

Figure 5.1 Solution steps of Pressure-based Segregated Algorithm [137]

5.3.5 Judging convergence

Although the FLUENT User's Guide recommends that it is better to judge convergence not only by examining residual levels, but also by checking the relevant integrated quantities, such as heat transfer coefficient, residual monitoring is the only feasible method provided by FLUENT for judging convergence.

For the conservation equation for a general variable ϕ, the residual R^{ϕ} computed by FLUENT's pressure-based solver, comes from the imbalance in Equation *(5.10)* summed over all the computational cells P, and is referred to as the unscaled residual.

$$R^{\phi} = \sum_{cells\ P} \left| \sum_{nb} a_{nb}\phi_{nb} + b - a_P\phi_P \right| \qquad (5.17)$$

However, since no scaling is employed, it is hard to evaluate the level of the residual defined by Equation *(5.17)*. Consequently, this residual is not practical for judging convergence. FLUENT can scale the residual by using a scaling factor which symbolizes the flow rate of ϕ through the domain. This is referred to as the scaled residual:

$$R^{\phi} = \frac{\sum_{cells\ P} \left| \sum_{nb} a_{nb}\phi_{nb} + b - a_P\phi_P \right|}{\sum_{cells\ P} \left| a_P\phi_P \right|} \qquad (5.18)$$

For the momentum conservation equations, ϕ_P is replaced by v_P, where v_P is the magnitude of velocity at cell P.

For the continuity equation, the unscaled and scaled residuals for the pressure-based solver are defined by Equations *(5.19)* and *(5.20)* respectively:

$$R^{c} = \sum_{cells\ P} \left| rate\ of\ mass\ creation\ in\ cell\ P \right| \qquad (5.19)$$

$$R^c_{scaled} = \frac{R^c_{iteration\ N}}{R^c_{iteration\ 5}} \qquad (5.20)$$

where $R^c_{iteration\ 5}$ is the largest absolute value of the continuity unscaled residual in the first five iterations.

Theoretically, in a computer with infinite precision, these residuals will reach zero when the solution converges. However for any actual computation process, the precision is finite, hence the residuals decay to some small value and then stop changing. Since the problems simulated in this study are unsteady and require extensive simulation time, the convergence criterion here requires the scaled residuals to decrease only to 10^{-3} for all equations. Although residuals in solutions closer to zero are more accurate, this value is still recommended as sufficient by FLUENT to judge convergence.

5.4 Modelling process

The general simulation steps by applying FLUENT have been introduced previously in detail. The problems concerned in this study have their own characteristics, hence some special steps are needed to simulate such cases. The following procedures direct the overall solution of the simulations in this study:

1. Creating the model geometry and grid
2. Choosing the basic solution algorithm and discretization method
3. Selecting physical models
4. Setting up phases and phase interaction
5. Setting up User Defined Scalars
6. Creating User Defined Functions
7. Specifying fluid properties

8. Specifying boundary conditions
9. Adjusting the solution control parameter
10. Hooking User Defined Functions
11. Initializing the case
12. Setting up correct convergence criterion
13. Calculating a solution for a small number of very short time steps
14. Examining the results
15. Saving the preliminary results
16. Modifying the geometry, grid, boundary conditions etc, where required
17. Setting up an appropriate increscent time step and calculating for an extended period of time
18. Saving case and data file during calculation if required

The common computation procedure of the pressure-based segregated solver is introduced in Figure 5.1. The specific computation procedures for this study using UDFs created by the author are given in Figure 5.2. The steps relevant to UDFs are those in blue in the figure below. With the exception of the UDFs mentioned in Section 5.2, some UDFs executed at the end of every time step were also developed for making records of UDSs transient information in every time step which are not given by FLUENT standard functions.

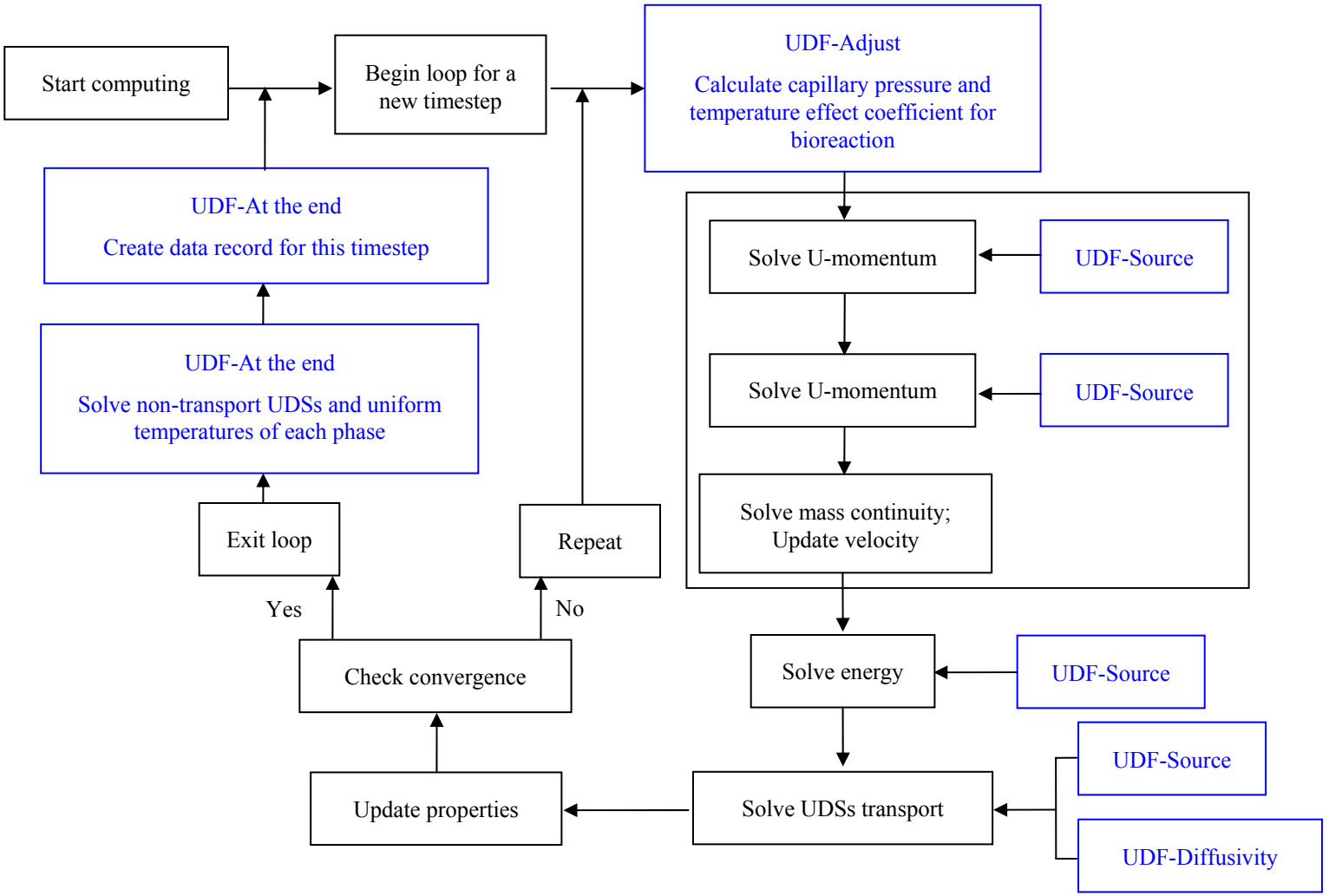

Figure 5.2 Computation procedure for the Pressure-based segregated solver with UDFs

5.5 Lessons learned in using FLUENT

During this study, the author encountered a number of issues associated with using some of FLUENT's applications. These problems were overcome by referring to relevant textbooks and the FLUENT User's Guide, consulting with experts and using online forums, accumulating information from unsuccessful attempts, and so forth. The primary points of note and relevant experiences are summarized below. Although this summary is empirical rather than theoretical, the author has realized that insightful knowledge on CFD theory is very helpful for ensuring the efficient use of FLUENT.

5.5.1 Selection of FLUENT modules

FLUENT features various built-in modules, and can simulate many issues related to fluid dynamics. When applying FLUENT to a specific problem, users must carefully choose the closest and most feasible physical and mathematical models to represent reality, especially for those problems which can not solely be simulated by using the existing models in FLUENT, otherwise, the simulation will diverge or result in an incorrect solution. The author encountered two issues of this nature. In the first, the porous media model in FLUENT appears to be capable of modelling fluid flow in biopile. However, this model can only work with a single fluid, and can not simulate multiphase flow. The second issue is encountered with FLUENT's species transport and reaction model. The reactions in this model, account only for chemical reactions, which are not considered in this study. The species, which are defined as the composition of the fluid, act as reactants and/or resultants of such reactions. This model could possibly be used for modelling contaminants transport in this study, however the UDS transport model can depict the real physical process occurring in a more straightforwardly and legibly manner, and requires less preparative work. Hence, the Eulerian multiphase model is adopted to simulate immiscible fluid flow through a porous media, and the UDS transport model is adopted to simulate contaminant transport.

5.5.2 Choice of time step

Since the problem of concern in this study is an unsteady process, temporal discretization is executed

during solving. A good way to judge the choice of time step Δt is to observe the number of iterations FLUENT needs to converge at each time step. Recommendations for choosing a suitable time step given in FLUENT User's Guide are that the ideal number of iterations per step should be 5-10. If FLUENT requires substantially more, the time step is too large. If FLUENT needs only a few iterations per time step, Δt may be increased. Thus, it is often wise to choose a conservatively small Δt for the first 5-10 time steps, and gradually increase Δt as the calculation proceeds.

It is also suggested that to get a stable computational process, that Δt should follow the relationship $\Delta t < \Delta x / u$, where Δx represents the cell size in length, and u is the velocity in the x direction [182]. By using values for the inlet air horizontal velocity of 1 m/s and 5 m/s (Section 6.3.2), and a horizontal grid cell size of 0.25m (Section 6.3.1), we can make a cursory estimation that a time step less than 0.05s can effectively ensure the computational stability.

Based on the two above criterions, the time step in this study, is initially set to 0.01s, and gradually increased to 0.5s and 1s. Although the number of iterations per time step is only one, by increasing the time step to values greater than these e.g.. 5s or 10s, the simulation will generally crash within next few time steps. Furthermore, for a number of simulations using a time step of only 1s, the calculation would proceed smoothly for a long period of time, but still would later result in. In such cases, the time step size was adjusted to a smaller value 0.5s at some point during the simulation, before the divergence could occur, and this time step size works well through all. Although a time step size of 0.5s seems extremely small in comparison with the overall simulation time which could be a number of weeks, therefore resulting in heavy computational load, it is still a very reliable choice.

5.5.3 Adjustment of relaxation factor

In the iterative solution of the algebraic equations, or the overall iterative scheme employed for handling nonlinerity, it is often desirable to speed up or to slow down the changes, from iteration to iteration, in the values of the associated variables. Depending on whether the variable changes are accelerated or slowed down, the process is called over-relaxation or under-relaxation respectively.

$$\phi = \phi_{old} + \omega \Delta \phi \qquad (5.21)$$

where ϕ is the variable value in the current iteration, ϕ_{old} is the variable value in the previous iteration, $\Delta\phi$ is the computed change in ϕ, and ω is the relaxation factor. When the relaxation factor is between 0 and 1, its effect is under-relaxation. When the relaxation factor is greater than 1, the effect is over-relaxation [137].

There are no universal rules for selecting the best value for a relaxation factor. The optimum value depends on a number of considerations, including the nature of the problem, the number of grid points, the grid spacing, the iterative procedure etc. Normally, a suitable value for the relaxation factor can be found by experience, and from exploratory computations for the given problems. In this study, the FLUENT default settings for the under-relaxation factors were accepted. When divergence was encountered after several time steps in some simulation attempts, the relevant under-relaxation factors were adjusted to both higher and lower values in an attempt to achieve a solution. In some cases adjustment of the relaxation factor either up or down still resulted in divergence. Hence, for this specific problem, although changing the relaxation factor may to some extent improve the convergence property, it cannot be relied upon to change it fundamentally.

5.5.4 Boundary conditions and fluid zone design

When using FLUENT, the author found that not only the choices for time step and relaxation factor could lead to divergence; but the selected boundary conditions could also result in solution divergence. For example, when modelling biopile treatments with suction pressure in the aeration pipes, if the pipe surface, which was also the interface of the pipe and porous media, was set as a pressure outlet boundary, the simulation crashed rapidly. This problem was solved by defining an additional fluid zone, which was solely full of gas, and contiguous to the border of soil on the pipe side, and then defining the other boundary of this fluid zone as the pressure outlet boundary.

5.5.5 Limitation of FLUENT standard features

CFD is introduced in this study by FLUENT. Although the functions of FLUENT can be extended by using UDFs to a larger extent, it still has functional limitations. Such limitations may impact or

confine the development of this model. For example, although the hydrodynamic dispersion coefficient is actually a tensor, it is treated as a scalar in all cases in FLUENT 6.2, whereas in FLUENT 6.3 this fault is ameliorated. Another deficiency is that the boundary condition of the UDS offered by FLUENT is very monotonous and rigid. Although a number of options and UDFs can be implemented in order to create some flexible boundary conditions, from the author's experiences, such functions do not work well for UDS.

5.5.6 Speeding and judging convergence

Convergence can be hindered by many factors, such as the complexity of mathematical model, a large number of computational cells, time step size, and overly conservative under-relaxation factors. In this study, by solving simulations by starting with a very small time step, a converged solution was quickly obtained. By gradually increasing the time step to 0.5s/1s, and retaining the default under-relaxation factors, the solution process also maintained a very good convergence throughout the simulation. Although using larger time steps or under-relaxation factors may theoretically lead to better convergence, they would eventually induce failure.

Although FLUENT judges convergence automatically using the convergence criterion discussed in Section 5.3.5, the author verified convergence manually by examining the variable history. In doing so, the author found in some cases that although FLUENT presented a converged solution, some of the variables were physically unreasonable. This problem was resolved by decreasing the time step size.

5.5.7 Interactive and batch execution

FLUENT can be used interactively with a Graphical User Interface (GUI) and also used in a batch mode in which the input information is obtained from a text file. The batch mode makes efficient use of computer resources by avoiding screen displays and data transfer if modelling is carried on a remotely accessed computer, which was the case in this study. Therefore, in this study, problem setup, initial calculations, and postprocessing of results were performed in interactive mode, and the large number of iterative calculations were run in batch mode, which delivered faster results than the interactive mode.

Chapter 6 Modelling Result and Discussion

6.1 Introduction

This chapter presents the results of a number of scenarios that test the ability of the model, and also simulate a series of biopile treatments with various operating conditions. The overall goal is to show that the model can reproduce the physical characteristics of the bioremediation process in a biopile, and thus help with the operation and design of biopile systems.

Section 6.2 presents a partial validation of the model for immiscible fluid flow through porous media. Section 6.3 gives a detailed description for each simulated scenario, including the geometry and grid of simulation domain, operating conditions (boundary and initial conditions), and parameters. The detailed results and discussion are given in Section 6.4.

6.2 Partial validation of fluid flow

Immiscible fluid flow in porous media is governed by a single equation which combines the variably-saturated Darcy's Law and the Eulerian multiphase model. Its validity in FLUENT was examined by means of two cases: water saturated flow and immiscible fluid flow through a 1D porous media column. The properties of porous media used for both cases are shown in Table 6.1.

Table 6.1 Properties of porous media

Porosity	0.33
Residual water saturation	0.2
n	3.97
m	1-1/n
ε *(1/Pa)*	0.00043
k (m^2)	6.8e-14

6.2.1 Saturated water flow

The geometry and grid utilized in this scenario are shown in Figure 6.1. The total column length is 0.3m. Water flows from right side to the left side with a constant Darcy velocity of 0.01m/s.

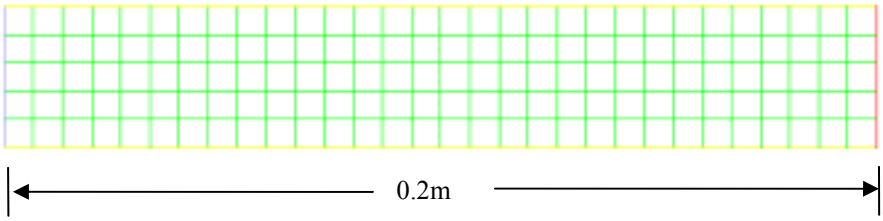

Figure 6.1 Porous media column geometry and grid

The pressure change along the column length from the FLUENT results is shown in Figure 6.2. The results directly calculated from Darcy's Law compared with those of FLUENT are listed in Table 6.2.

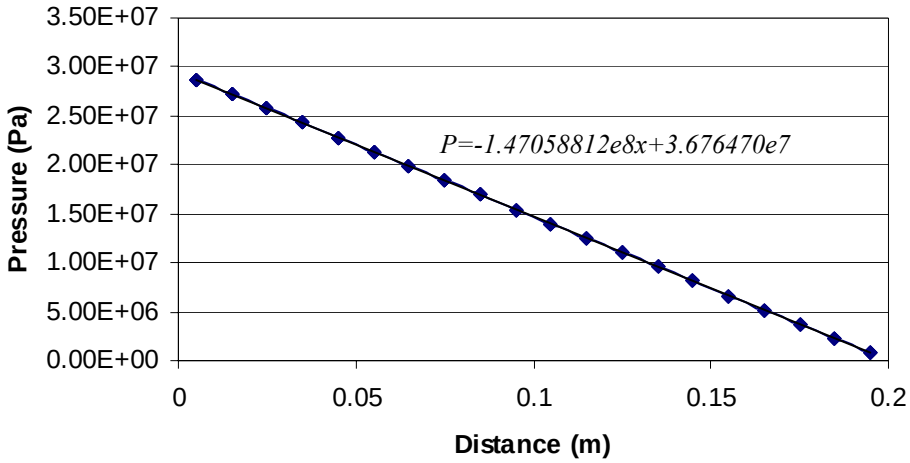

Figure 6.2 Pressure change along with column length

Table 6.2 Results compare of Darcy's Law and FLUENT

Result	Water volume of fraction	Physical velocity	$\mu q / k$ ($\Delta p = -\mu q / k * L$)
Darcy's Law	0.33	0.0303030	1.47058823
FLUENT	0.330536	0.0302538	1.47058812
Relative error	0.162%	0.162%	7.48e-8

From analysis of the above results, it is clear that the results delivered by FLUENT compare excellently with theoretically calculated solution, with only a very small relative error. Thus, the governing equation of this model works well in FLUENT for saturated flow.

6.2.2 Immiscible fluid flow

The two phases used for the immiscible fluid flow test are water and air. The meshing method used in this case is similar to that of the first case (Figure 6.1), however the solution domain is divided into 3 fluid zones as shown in Figure 6.3. Zone 1 and Zone 3 are full of air, and Zone 2 is packed with a porous media. Air flows into the column from the left side with a velocity of 0.1m/s. The actual volume fraction of air and water set for this case and the corresponding outcome after FLUENT initialization are shown in Figure 6.4 and Figure 6.5.

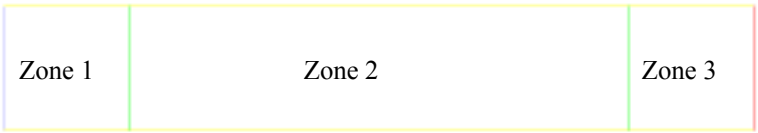

Figure 6.3 Geometry for immiscible fluid flow

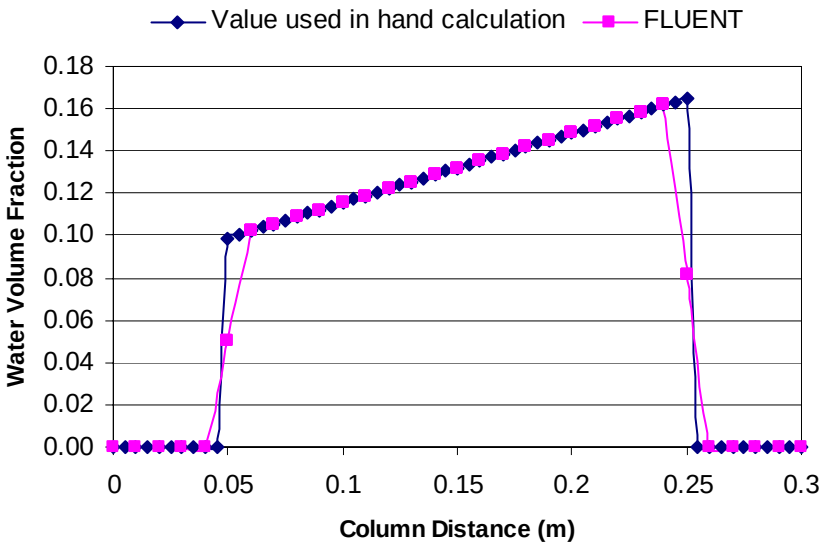

Figure 6.4 Water volume fraction in porous media zone

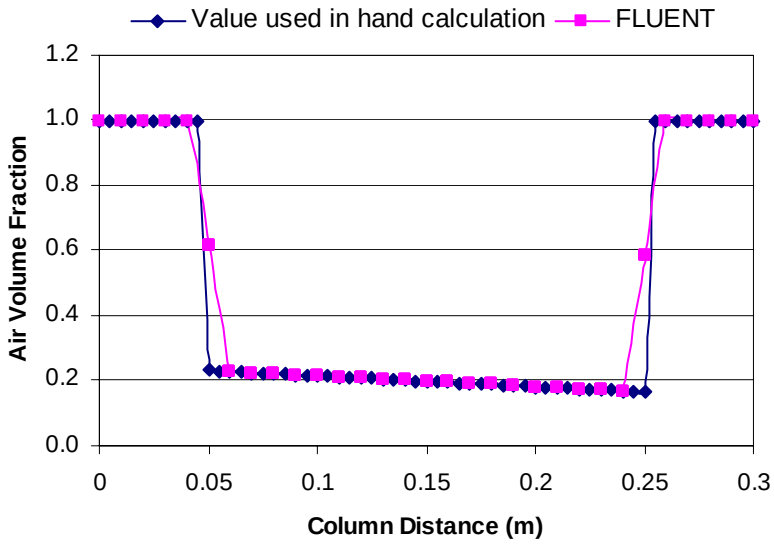

Figure 6.5 Air volume fraction in porous media zone

Although the values of air and water volume fraction change abruptly across the interfaces of the different fluid zones, FLUENT handles these as gradual changes taking place within the adjacent cells on both sides of the interfaces.

Results for the physical velocities in both phases from Darcy's Law and FLUENT are compared and shown in Figure 6.6 and Figure 6.7.

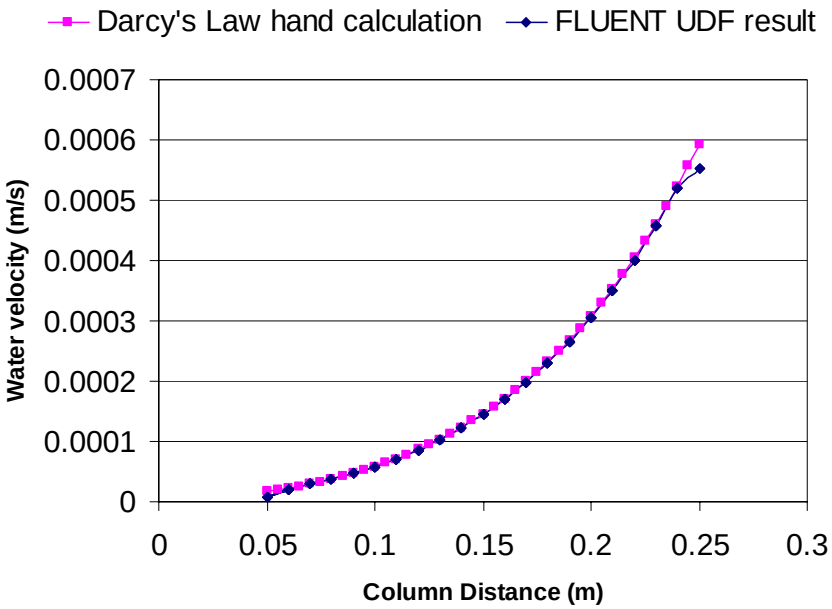

Figure 6.6 Comparison of water velocity

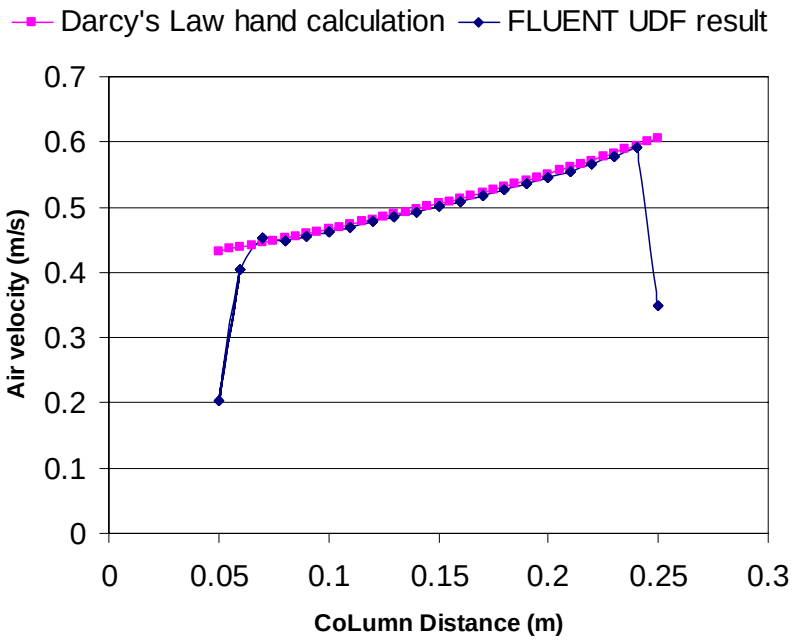

Figure 6.7 Comparison of air velocity

It is clear that the value for the water velocity obtained by FLUENT closely resembles that calculated directly from Darcy's Law, as does the air velocity, except at the boundary of the porous media zone. This is a reasonable result, since the value for the air velocity at the boundary evaluated by FLUENT is derived from the gradually changing air volume fraction shown in Figure 6.5, which is taken from interpolation of cell values on each side of the interface.

Contaminant transport, with the exception of source terms for interphase transfer and biotransformation, is modelled by the standard scalar transport equation included in FLUENT, and therefore does not need to be separately verified.

6.3 Description on simulations

6.3.1 Geometry and grid

Numerical simulations demonstrating the interaction of physical, chemical and biological procedures in biopile treatment were conducted for scenarios with three different aeration methods illustrated in Figure 6.8, Figure 6.10 and Figure 6.12. The biopile itself in each scenario is designed as a pile with a semicircular cross section. This represents a good approximation to a real pile. The radius of the pile is 1.0 m. The three different aeration methods are: non-aerated, a horizontal aeration pipe at the base of the biopile and a vertical aeration pipe through the pile centre. All simulations were carried out in two-dimensions (2D), though three-dimensions (3D) simulations were possible. It is appreciated that the 2D set-up makes the vertical pipe case somewhat conceptual, since the pipe is in fact modelled as a "slot" of infinite length along the pile.

Other than the aeration method, the numerical domains for each simulation of a single biopile were identical. Scenarios of multi-biopile layouts depicted in Figure 6.14 and Figure 6.15, were also conducted, and simulated with horizontal pipe aeration.

The grids used in this study are all unstructured as shown in Figure 6.9, Figure 6.11, Figure 6.13 and Figure 6.15. The grid information of different numerical domains distinguished by the geometry IDs of NA, HA, VA and MP is listed in Table 6.3.

A significant problem arose when conducting those simulations with suction pressure in the aeration pipes, if the pipe surface which was contiguous with soil, was defined as a pressure outlet boundary, the simulation crashed rapidly. After a number of failed attempts, the author found that if the part of the pipe which bordered the soil was defined as an additional fluid zone, and the other boundary of this zone was defined as the pressure outlet boundary, the calculation could proceed without failure.

Hence such types of fluid zones were designed in meshes for aeration scenarios and referred to as air gaps.

Table 6.3 Properties of grids used in simulations

	Geometry ID	Cells	Faces	Nodes	Fluid zones
Non-aerated	NA	2299	4718	2420	TWO: biopile and ambient surroundings
Horizontal pipe	HA	3916	7985	4070	THREE: biopile, ambient surroundings and air gap
Vertical pipe	VA	3720	7597	3876	THREE: biopile, ambient surroundings and air gap
Multi-pile	MP	11539	23454	11916	THREE: biopile, ambient surroundings and air gap

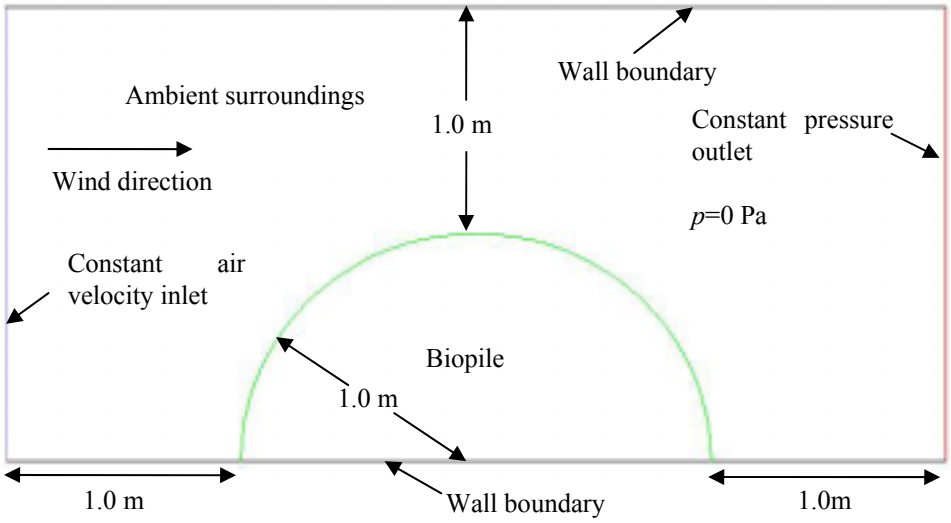

Figure 6.8 Geometry of simulations with non-aerated biopile

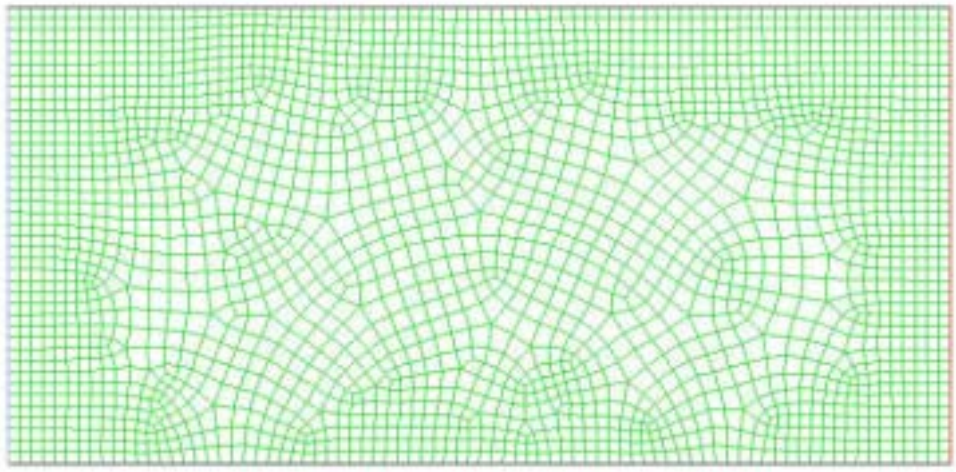

Figure 6.9 Grid of simulations with non-aerated biopile

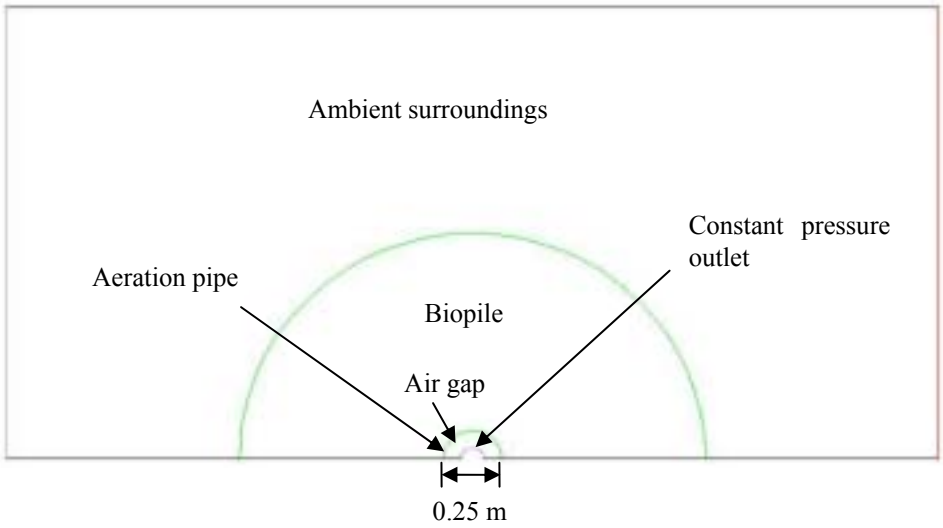

Figure 6.10 Geometry of simulations for biopile with horizontal-aeration pipe

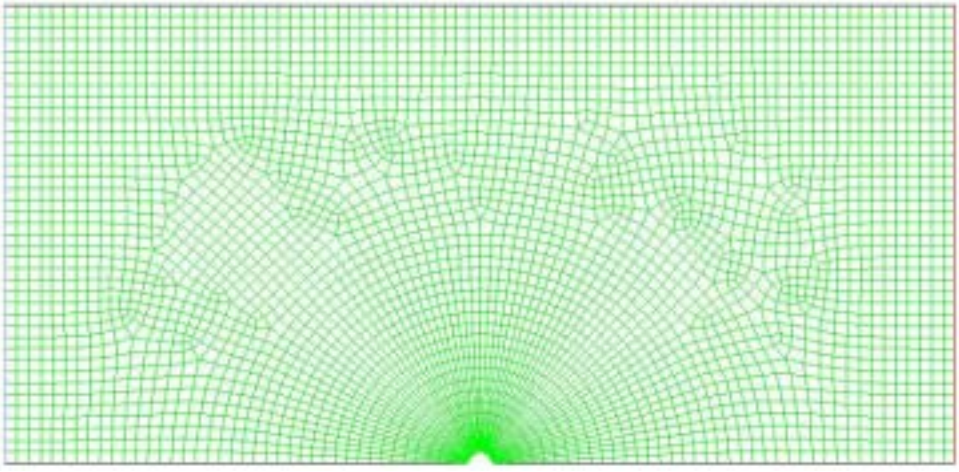

Figure 6.11 Grid of simulations for biopile with horizontal-aeration pipe

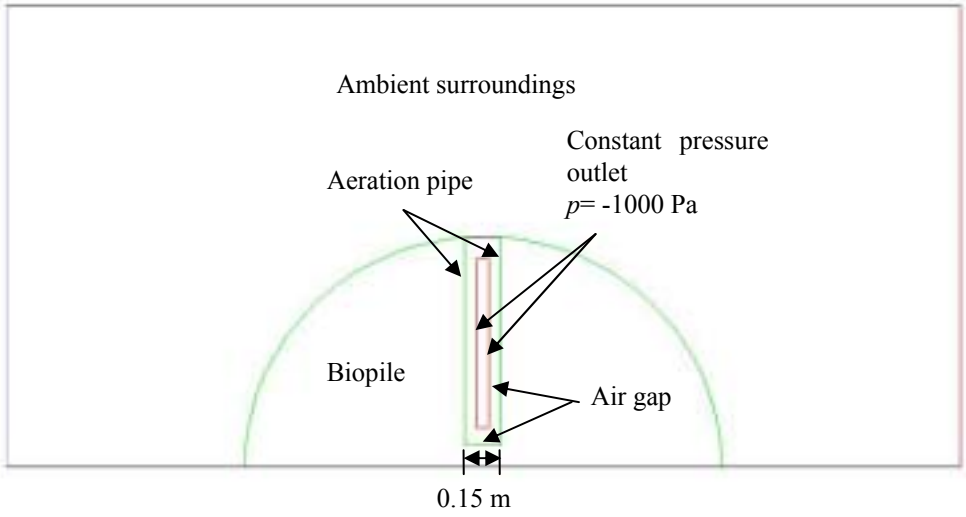

Figure 6.12 Geometry of simulations for biopile with vertical-aeration pipe

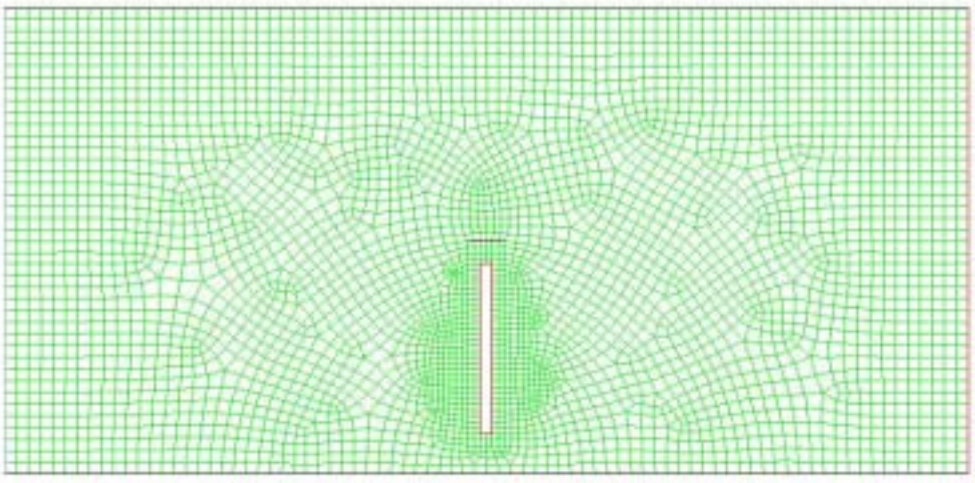

Figure 6.13 Grid of simulations for biopile with vertical-aeration pipe

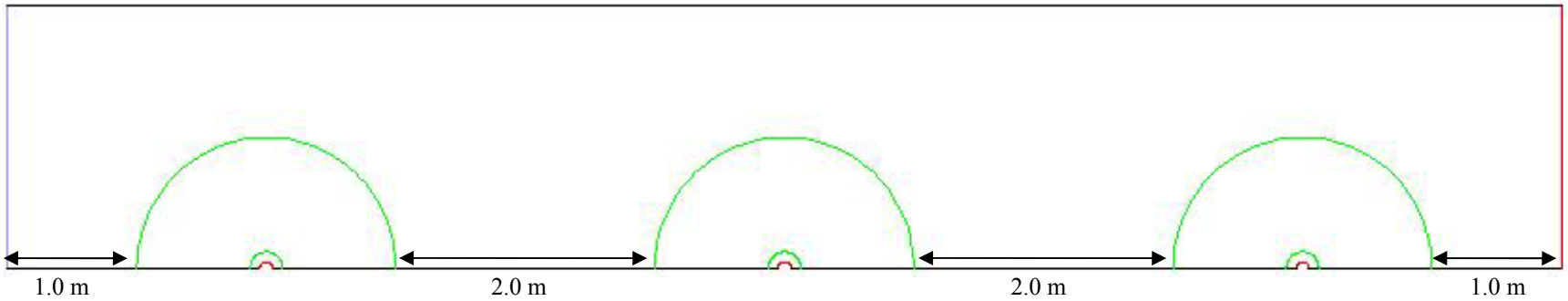

Figure 6.14 Geometry of simulations for multi-biopile

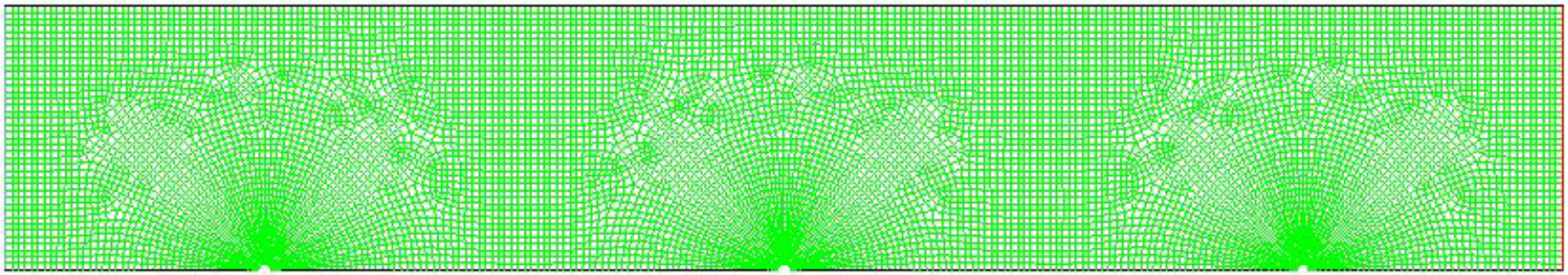

Figure 6.15 Grid of simulations for multi-biopile

6.3.2 Boundary and initial conditions

The boundary conditions used in the simulations are illustrated in Figure 6.8, Figure 6.10 and Figure 6.12. For all numerical domains, no flow conditions were employed along the entire top and bottom boundaries, which meant there was no gradient in fluid pressure and contaminant concentration, constant air velocity inlet conditions were maintained along the left boundaries, and the velocity set to be 1.0 m/s or 5.0 m/s; and the right boundaries were defined as a constant zero pressure outlet. Gravity was defined as acting vertically downwards. In simulations with an aeration pipe, a constant suction pressure of 1000 Pa was set within the pipe except where otherwise discussed. In most cases, the initial temperature of the biopile was set as 285K, with an ambient temperature 280K, and the temperature of the constant velocity inlet air also set as 280K. The atmospheric pressure for all simulations was set to 101325 Pa. The wind and temperature conditions were intended to represent conditions which might typically be found on sites in Scotland.

For modelling of contaminant transport, zero flux boundary conditions were used along the velocity inlet boundary at the left side of the numerical domain which meant that no contaminant was carried into the solution domain by fluid flow. Zero diffusive flux boundary conditions were enforced along the two pressure outlet boundaries (right side of the numerical domain and the suction pressure boundary of the pipes), which allowed the contaminant to be transported out of the solution domain with fluid flow only by advection, and not by diffusion (hydrodynamic dispersion).

At the beginning of simulations, the immobile oleic phase in the biopile system, which consisted of various organic chemicals that were not adsorbed into the soil or dissolved in the aqueous or gaseous phases, was assumed to be distributed equably within the porous media. In addition, in the organic liquid phase, the initial molar concentration of the single simulated contaminant, benzene, was set to 0.6. Benzene was selected because it is a light hydrocarbon and is volatile enough to produce interesting results in a reasonable simulation time. Furthermore, benzene has been used in many studies in this field [84, 119, 121, 156, 162, 183], hence suitable parameters were available in the literature.

The initial benzene concentration in other phases was set to be in equilibrium with its concentration in

the organic phase and calculated based on the chemical properties of benzene. Biomass was also uniformly distributed in the biopile system, with a hypothetic initial concentration of 0.0162 kg/ m^3. This figure was selected to ensure sensible bioreaction results under the control of minimum and maximum possible biomass concentrations (refer to Section 6.3.3).

The initial values of benzene concentration in each phase and biomass concentration are shown in Table 6.4. Benzene properties used in simulations are listed in Table 6.5.

Table 6.4 Initial conditions for simulations

Initial conditions	value
Benzene concentration in aqueous phase (molar fraction)	0.000248
Benzene concentration in gas phase (molar fraction)	0.06889
Benzene concentration in oleic phase (molar fraction)	0.6
Benzene sorbed in solid material (g/kg)	0.4698
Biomass concentration (kg/m^3)	0.0162

Table 6.5 Physical and chemical properties of organic compound used in simulations

Properties	Benzene
Molecular weight (g/mol)	78.1
Density (kg/m^3)	879
Vapour pressure (atm)*	0.125
Henry's coefficient (atm·L/mol)**	5.46
Air diffusion coefficient (m^2/day)***	0.76
Aqueous diffusion coefficient (m^2/day)***	9.26e-5
Organic phase molar density (mole/l)	10.07

* [184]

** [185]

*** [146]

6.3.3 Parameter estimation

The integrated simulation model requires a large amount of parameters to accurately illustrate the linked physical, chemical and biological processes occurring during biopile treatment. Most of these parameters are difficult to test in field or laboratory conditions, especially those regarding interphase species transfer and microbial metabolism rate. However, the simulation performance and the validity of the model results depend highly on these parameters. Many researchers have made reasonable estimates of such parameters, summarized by Rathfelder [109], found either directly from experiments, by fitting to laboratory data, or by estimated values used in numerical modelling. The parameters used in simulations of this study are listed in Table 6.6. Most of the parameter values adopted in this study are based on the literature review, and primarily refer to by the works of Rathfelder [109] and Abriola [94], with the exception of the specific heat [42] and thermal conductivity [180] of the soil. The bioreaction enthalpy coefficient is commonly measured as the ratio of heat to total or volatile solids removal [20], or by the ratio of heat to oxygen consumption [48, 186]. Since these are incompatible with the heat generation coefficient unit used (the heat required for benzene removal by biodegradation) in the mathematic model adopted by this study, an assumed value is used.

Table 6.6 Soil, transport and reaction parameters used in simulations

Symbol	Value	Unit	Definition
Soil properties			
n_{pore}	*0.33*	--	Porosity
Sra	*0.2*	--	Residual aqueous saturation
k	*6.8e-14*	m^2	Intrinsic permeability
n	*3.97*	--	van Genuchten equation parameter
m	*1-1/n*	--	van Genuchten equation parameter
ε	*0.00043*	*1/Pa*	van Genuchten equation parameter
Component transport			
D_g	*1.0775e-5*	*Kg/[m·s]*	Hydrodynamic dispersion for gas
D_a	1.07176e-6	Kg/[m·s]	Hydrodynamic dispersion for water

Rate limited interphase mass transfer			
K_{agc}	*5.79e-5*	s^{-1}	Mss transfer coefficient for component c from gas to aqueous phase
K_{aoc}	*5.79e-6*	s^{-1}	Mss transfer coefficient for component c from organic to aqueous phase
K_{asc}	*5.79e-5*	s^{-1}	Mss transfer coefficient for component c from soil to aqueous phase
K_{goc}	*5.79e-4*	s^{-1}	Mss transfer coefficient for component c from gas to organic phase
K^e_{agc}	*0.00360048*	--	Equilibrium partition coefficient for component c between phase aqueous and gas
K^e_{aoc}	*4.1339e-4*	--	Equilibrium partition coefficient for component c between phase aqueous and organic
K^e_{goc}	*0.11481513*	--	Equilibrium partition coefficient for component c between phase organic and gas
K_{fc}	*0.00116*	$[m^3/kg]^{nc}$	Freundlich isotherm parameter for component c (soil and aqueous)
n_c	*0.86*	--	Freundlich isotherm parameter for component c (soil and aqueous)
Bioreaction			
F_{cl}	*1/M_c (c=l)*	*mole c/kg l*	Use coefficient of component c with substrate l degradation
k_l	*1.157e-4*	*kg l/[kg biomass·s]*	Maximum specific substrate l utilization rate(mass s/ biomass)
K_{sl}	*0.5*	*mg l/ liter*	Half-saturation coefficient of component l
Y_l	*0.5*	*kg biomass/kg l*	Biomass yield coefficient for the metabolism of substrate l
K_d	*1.157407e-6*	s^{-1}	Microorganism decay coefficient
X_{min}	*1e-6*	Kg/m^3	Minimum biomass concentration
X_{max}	*0.02*	Kg/m^3	Maximum biomass concentration
Heat transfer			
C_{pa}	*4182*	*J/[kg·K]*	Specific heat of aqueous phase
k_{ta}	*0.6*	*w/[m·K]*	Thermal conductivity of aqueous phase

C_{pg}	*1006.43*	*J/[kg·K]*	Specific heat of gas phase
k_{tg}	*0.0242*	*w/[m·K]*	Thermal conductivity of gas phase
C_{ps}	*3780*	*J/[kg·K]*	Specific heat of soil phase
k_{ts}	*2*	*w/[m·K]*	Thermal conductivity of soil phase
H_l	*20000*	*J/g c*	Bioreaction enthalpy for benzene biodegradation

6.3.4 Summary of numerical work

In this study, fifteen simulations were conducted to test the capability of the model, in order to demonstrate the interaction between physical, chemical and biological processes, and determine their possible influence on remediation efficiency. With the exception of standard scenarios which followed the conditions and parameters described in Section 6.3.2 and Section 6.3.3, several other scenarios were also conducted to discover the impacts of varying initial and boundary conditions as well as some simulation parameters. Alterations in such scenarios were made on aeration patterns (suction or blowing), value of aeration pressure, chemical interphase transfer rates, initial and operating temperatures, and biomass concentration. The total simulation time of 320 hours was determined by the results of the first several simulated cases which were modelled for even longer periods of time. This simulation time ensured cogent modelling results, and therefore each subsequent simulation was carried out for a minimum of 320 hours. A description of each simulated scenario is listed in Table 6.7.

Table 6.7 List of simulated scenarios

Scenario ID	Geometry ID	Aeration arrangement	Inlet air velocity	Remark
NA1	NA	Non-aerated	1.0 m/s	
NA5	NA	Non-aerated	5.0 m/s	
HA1	HA	Horizontal pipe aeration	1.0 m/s	
HA5	HA	Horizontal pipe aeration	5.0 m/s	
VA1	VA	Vertical pipe aeration	1.0 m/s	
VA5	VA	Vertical pipe aeration	5.0 m/s	
HA5RB	HA	Horizontal pipe aeration	5.0 m/s	Initial biomass concentration reduced by 1 order of magnitude
HA5RGO	HA	Horizontal pipe aeration	5.0 m/s	Organic-gas mass transfer rate reduced by 1 order of magnitude
HA5RAG	HA	Horizontal pipe aeration	5.0 m/s	Aqueous-gas mass transfer rate reduced by 1 order of magnitude
HA5IT	HA	Horizontal pipe aeration	5.0 m/s	Initial temperature of biopile and ambient surroundings increased to 293 K and 288 K respectively
HA1SP25	HA	Horizontal pipe aeration	1.0 m/s	Suction pressure raised to 2500 Pa
HA1SP50	HA	Horizontal pipe aeration	1.0 m/s	Suction pressure raised to 5000 Pa
HA1BP	HA	Horizontal pipe aeration	1.0 m/s	Blowing pressure of 1000 Pa
HA1BPHT	HA	Horizontal pipe aeration	1.0 m/s	Blowing pressure of 1000Pa and heated air of 313 K blown in
MP5	MP	Horizontal pipes aeration	5.0 m/s	Suction pressure 1000 Pa

6.4 Results and discussion

6.4.1 General

Different operating conditions resulted in various outcomes. Variation of aeration method, which is a

fundamental operating factor, led to great diversity between contaminant distribution, temperature distribution and fluid flow pattern within a biopile.

For all aeration/non-aerated methods, the air flow patterns of the surroundings were similar, Figure 6.16 illustrates a typical flow pattern of such cases with an inlet wind speed of 1m/s. Conversely, the air flow patterns within the biopile were different in each case (Figure 6.17 for 1m/s wind speed). General flow patterns were identical despite variation of inlet velocity from 1 to 5m/s.

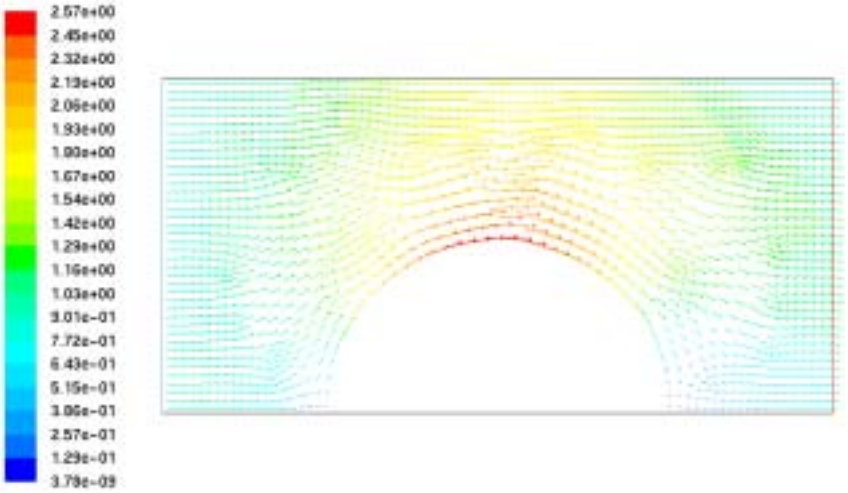

Figure 6.16 Air flow pattern in the surroundings

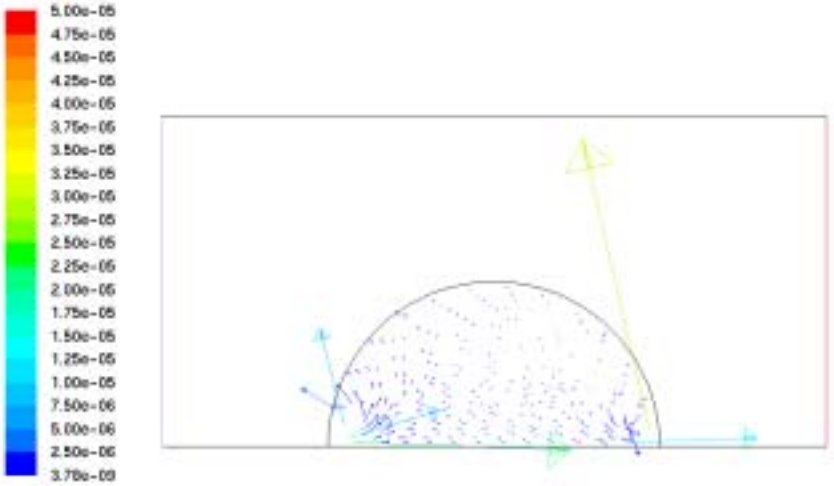

(a) Non-aerated

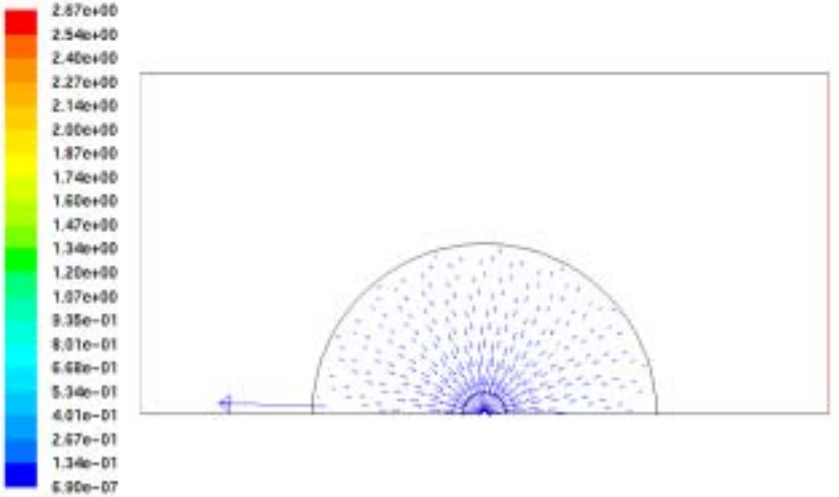

(b) Horizontal pipe suction pressure

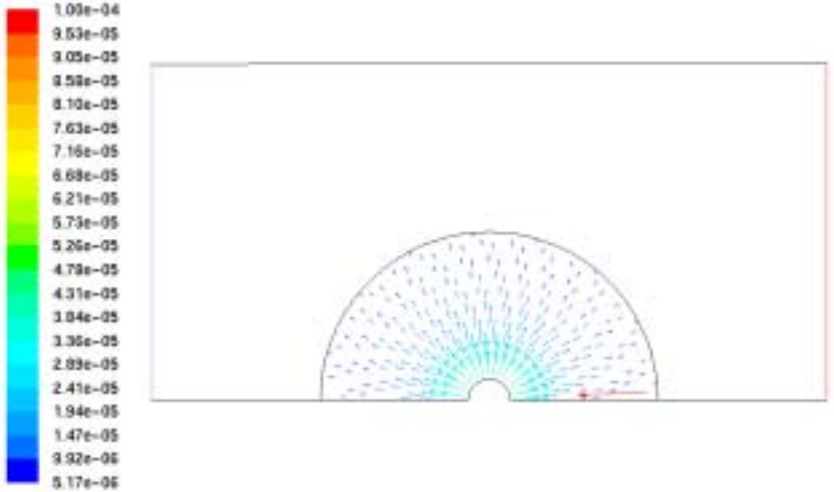

(c) Horizontal pipe blowing pressure

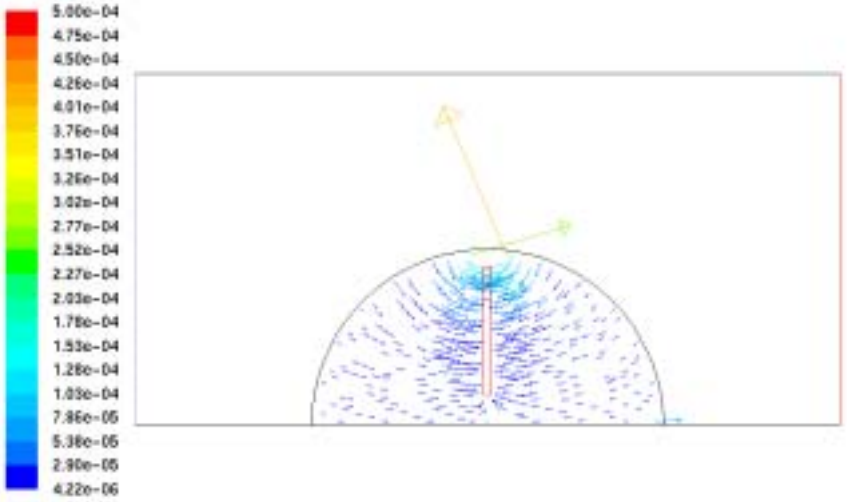

(d) Vertical pipe suction pressure

Figure 6.17 Air flow pattern within biopile

Figure 6.18--Figure 6.25 demonstrate general treatment progress for every aeration and non-aerated method. Since volatilization makes a significant contribution to benzene removal, and heat transfer takes place with fluid flow, benzene distribution and temperature distribution have different features corresponding to the various flow patterns obtained for the different aeration methods. On the other hand, for each individual aeration method, the changes of contaminant distribution and temperature distribution with time are inerratic and repeatable.

Figure 6.18--Figure 6.21 illustrate the contaminant concentration in the oleic phase only; however, the distribution pattern of contaminant concentration in other phases (gaseous, aqueous and solid phases) and its change with time are similar to those in the oleic phase for every aeration method. Figure 6.22--Figure 6.25 illustrate the temperature distribution progressions, which can be seen to have a high correlation with the gas flow patterns.

Figure 6.26 illustrates static pressure at 100 hours for scenarios NA5, HA5, VA5 and HA1SP50. These figures indicate that the range for the static pressure variation in scenarios with 1000 Pa aeration pressure is around 1000 Pa, where as this range is around 5000 Pa in scenarios with 5000 Pa aeration pressure. This status was similar for all the simulated scenarios along their running progressions. Comparing these static pressure variation ranges with absolute atmospheric pressure, 101325 Pa, these static pressure variation ranges are very small. In addition, temperature variation was also confined to a very small range, no greater than 10K in every scenario (Figure 6.22--Figure 6.25). Furthermore, gas velocity is always going to be slow enough to make incompressible assumptions valid. Therefore, the assumption of constant gas density would not lead to significant impacts on the simulation results.

Table A.3 to Table A.5 in the Appendixes give the contaminant removed by each mechanism for all scenarios, from which the contribution in percentage of biodegradation in each case was then acquired (Table A.6). This result indicates that following the treatment progression, the contribution of biodegradation on contaminant removal increases steadily. However, in terms of the current simulations, biodegradation is not the dominant approach for contaminant removal. Although the contribution of biodegradation reaches 34.56% in Scenario HA5IT at 300 hours, in all other cases it is not more than 30%. Furthermore, in most simulated scenarios, biodegradation only accounts for no

more than approximately 20% of contaminant removals in the first 200 hours of treatment. Hence, the simplification made for modelling bioreactions (described in Section 5.2.2), which actually amplifies the biodegradation effect, does not have significant impact on modelling other aspects of the biopile performance.

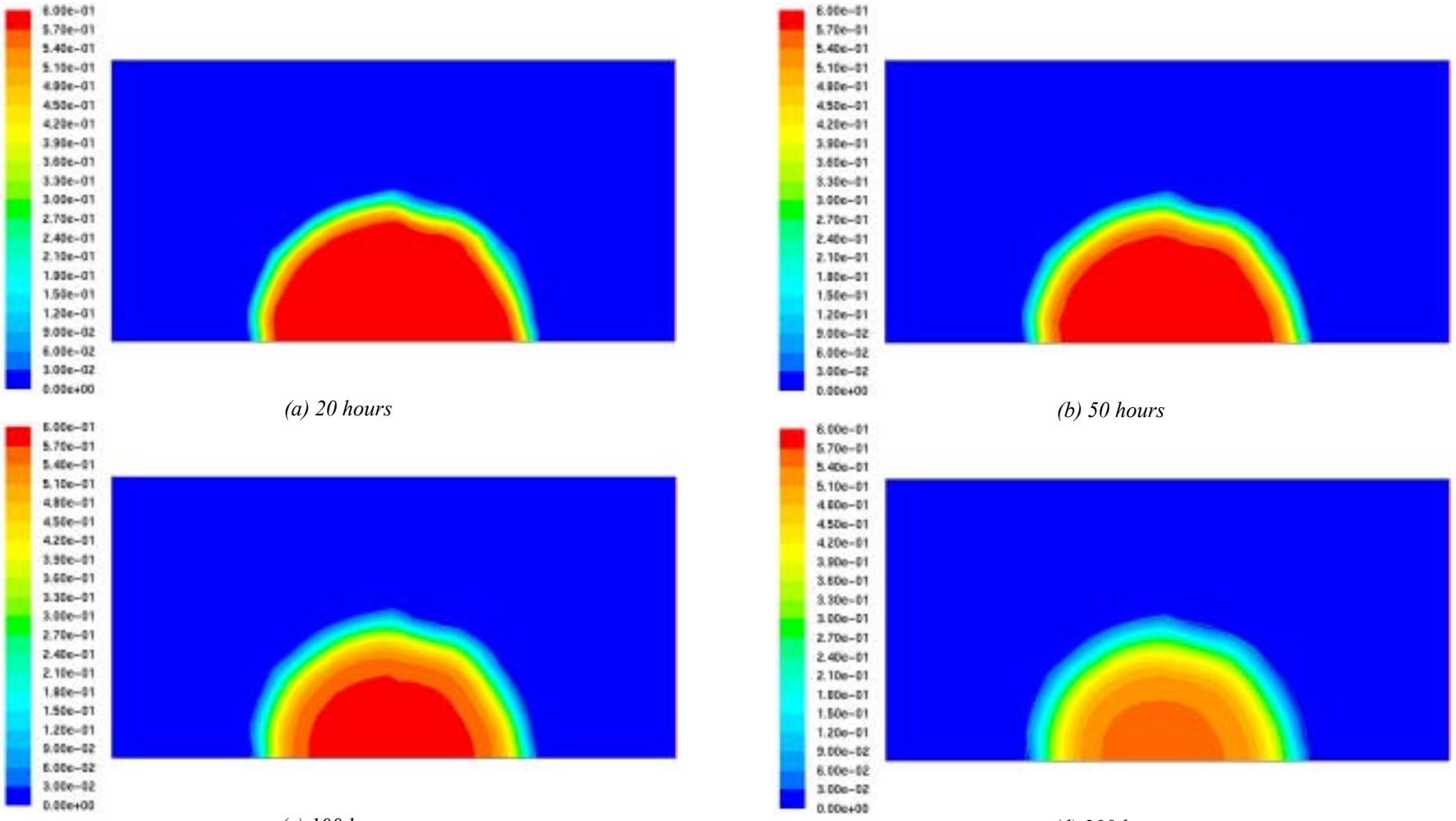

(a) 20 hours

(b) 50 hours

(c) 100 hours

(d) 200 hours

Figure 6.18 Progression of contaminant in soil predicted from Scenario NA1

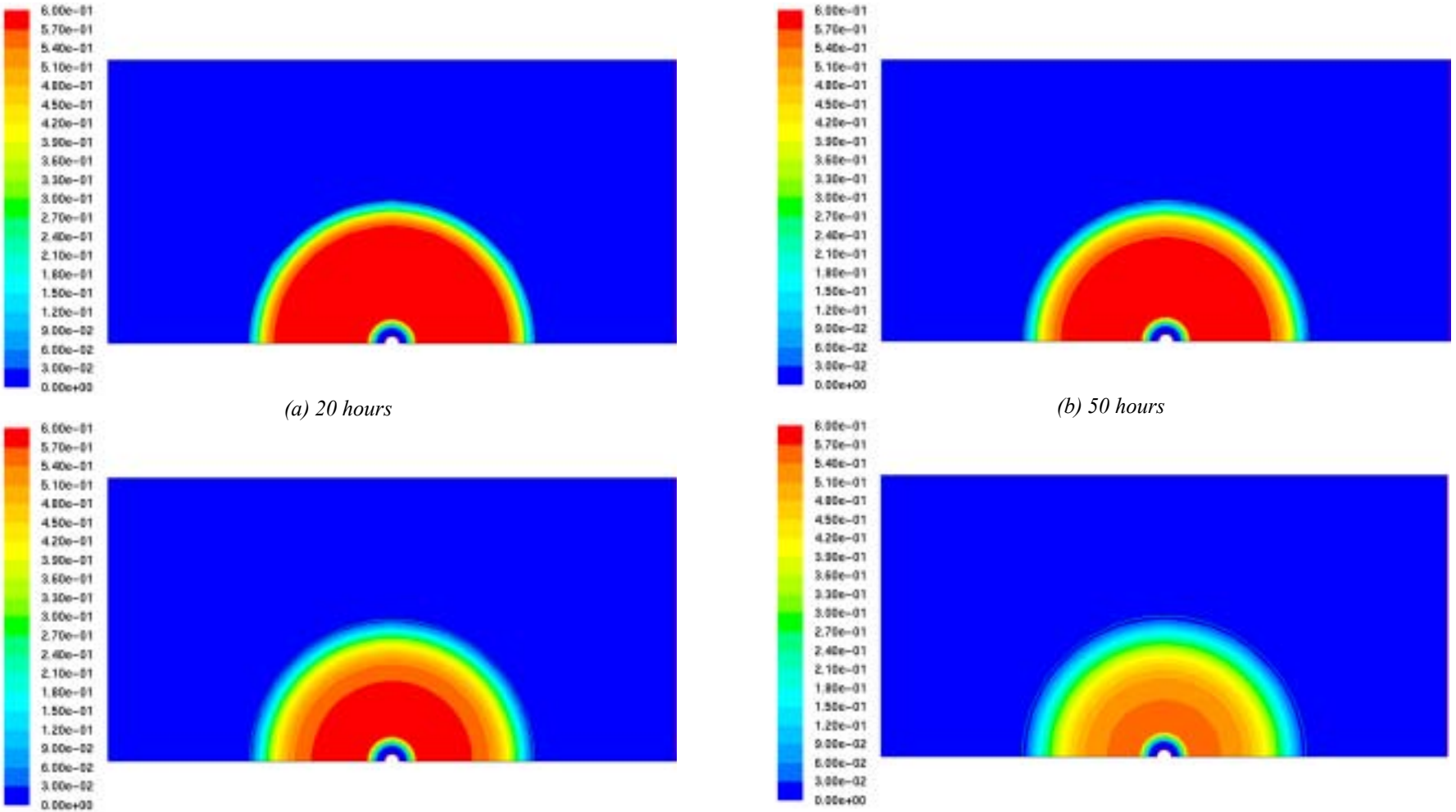

(a) 20 hours

(b) 50 hours

(c) 100 hours

(d) 200 hours

Figure 6.19 Progression of contaminant in soil predicted from Scenario HA1

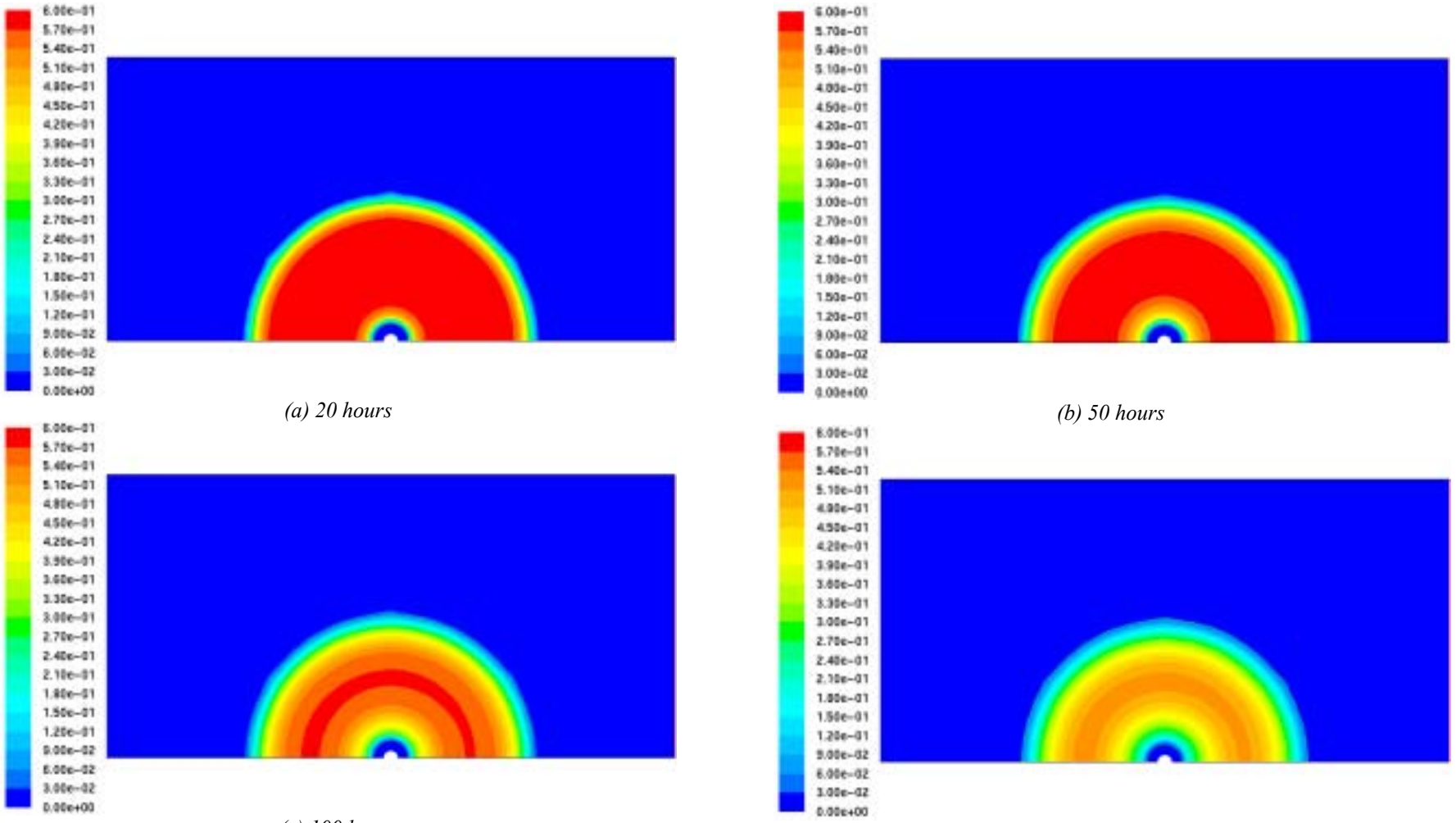

(a) 20 hours

(b) 50 hours

(c) 100 hours

(d) 200 hours

Figure 6.20 Progression of contaminant in soil predicted from Scenario HA1BP

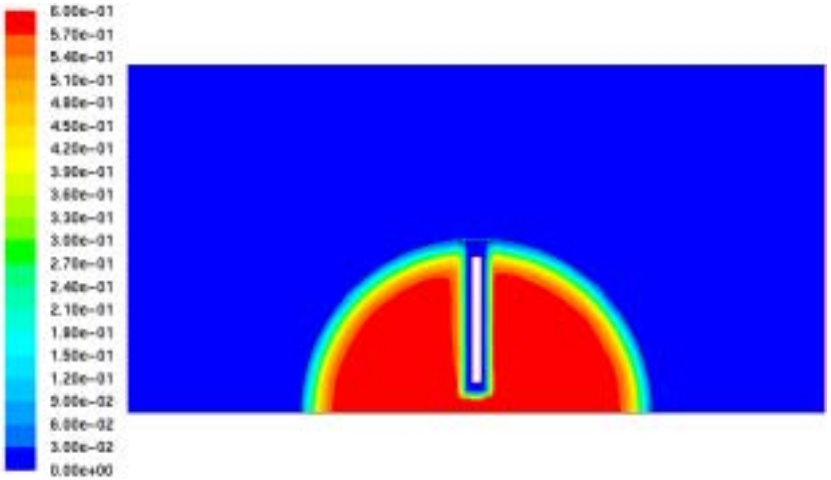

(a) 20 hours

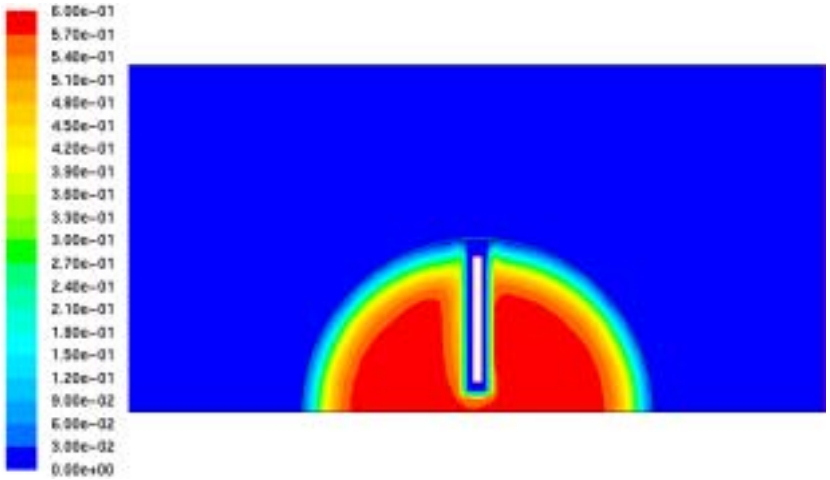

(b) 50 hours

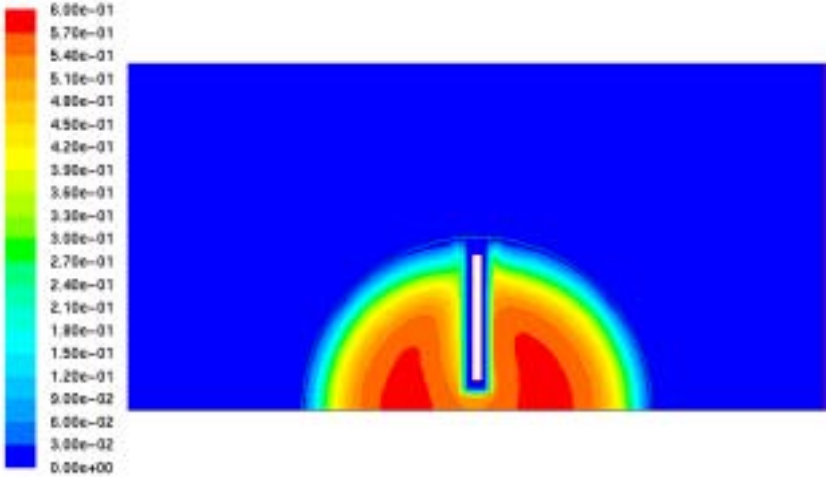

(c) 100 hours

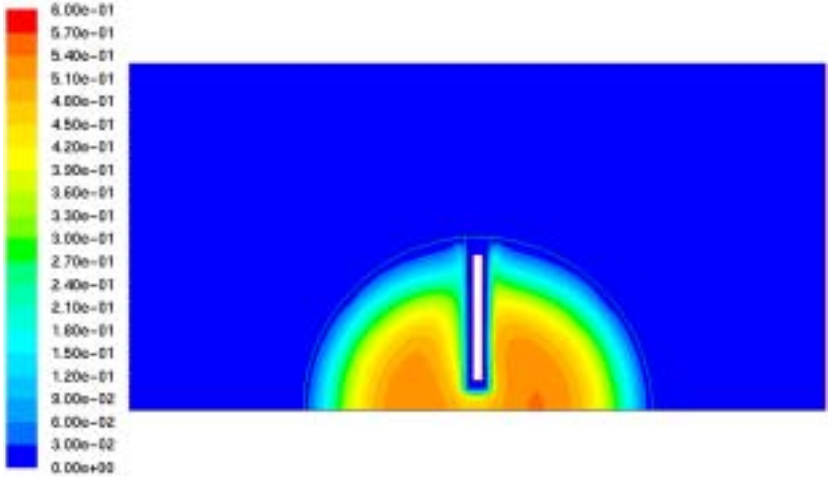

(d) 200 hours

Figure 6.21 Progression of contaminant in soil predicted from Scenario VA1

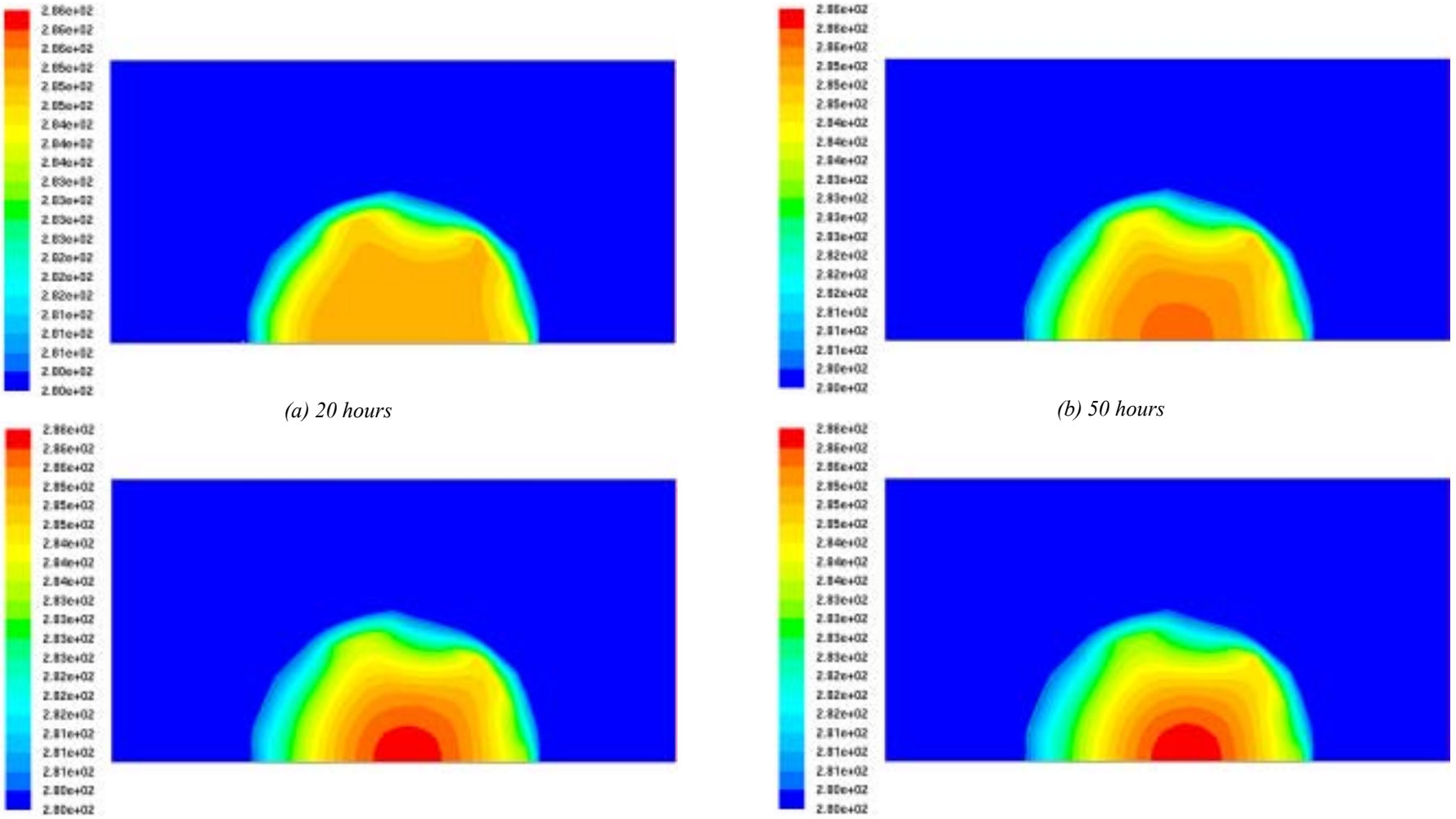

(a) 20 hours

(b) 50 hours

(c) 100 hours

(d) 200 hours

Figure 6.22 Progression of temperature distribution predicted from Scenario NA1

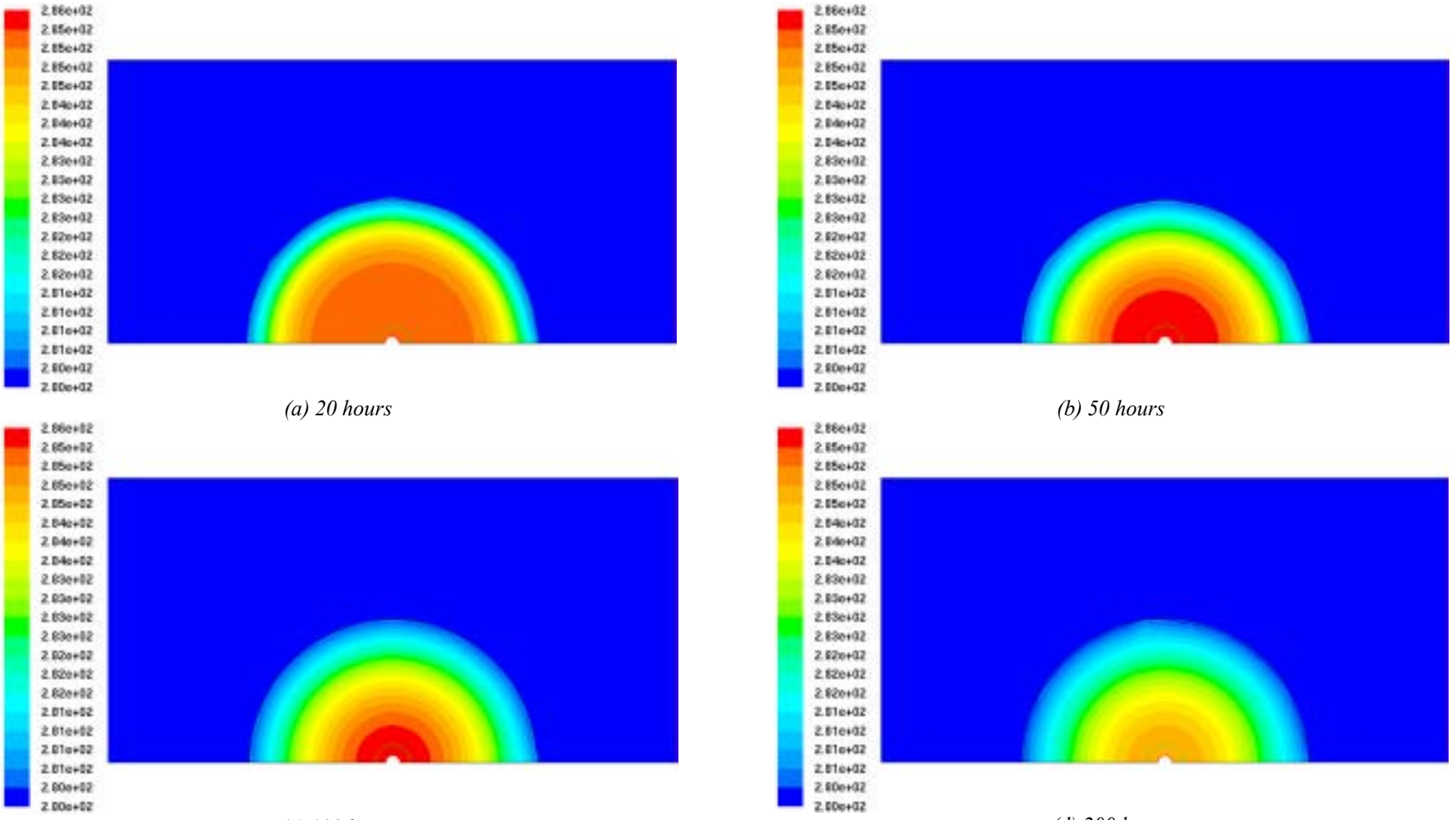

(a) 20 hours

(b) 50 hours

(c) 100 hours

(d) 200 hours

Figure 6.23 Progression of temperature distribution predicted from Scenario HA1

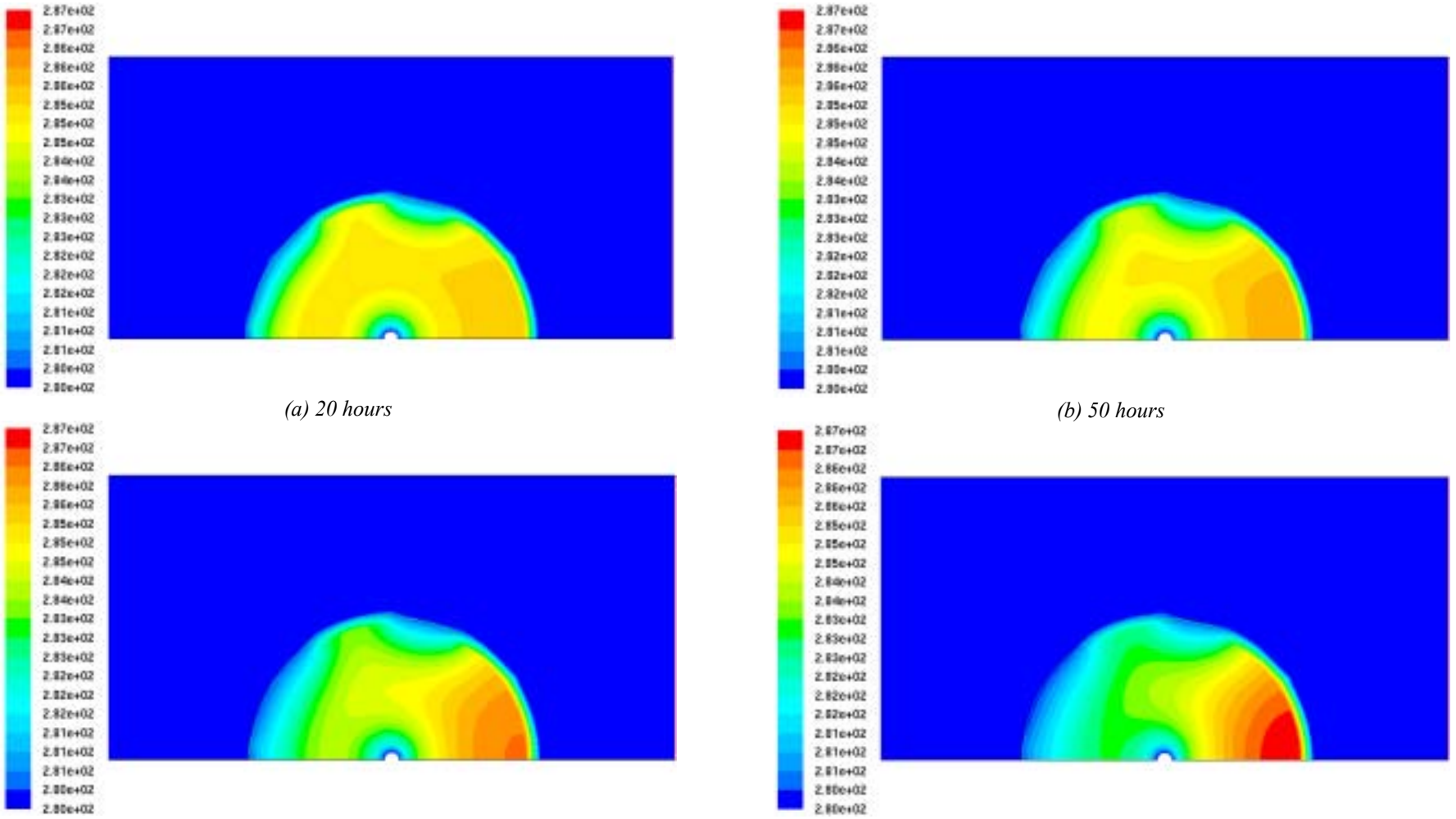

(a) 20 hours

(b) 50 hours

(c) 100 hours

(d) 200 hours

Figure 6.24 Progression of temperature distribution predicted from Scenario HA1BP

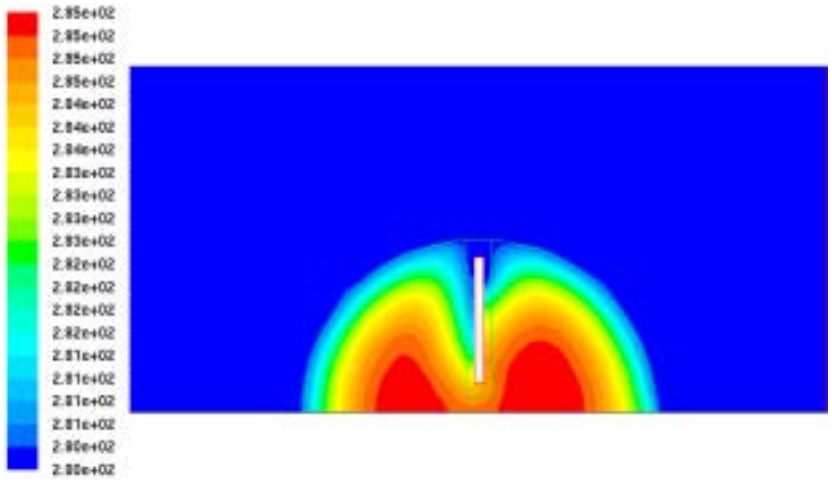

(a) 20 hours

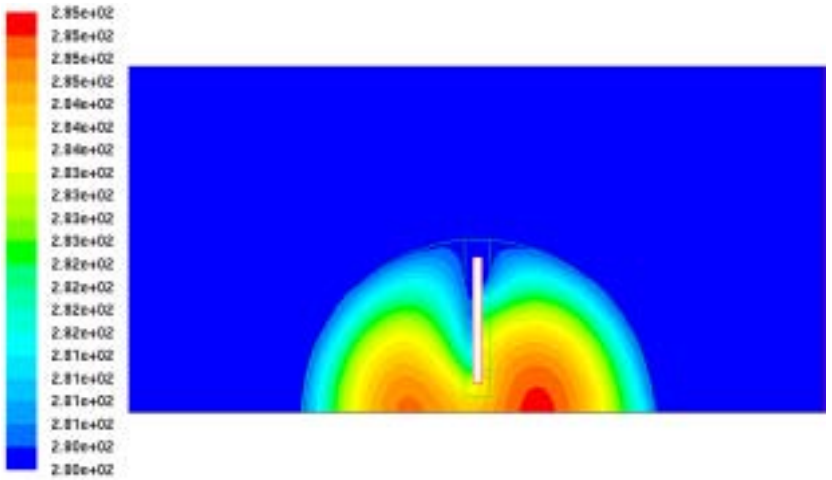

(b) 50 hours

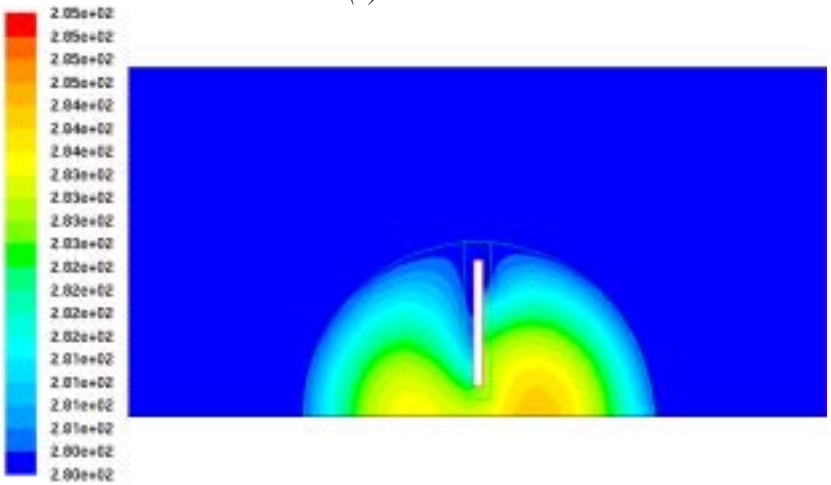

(c) 100 hours

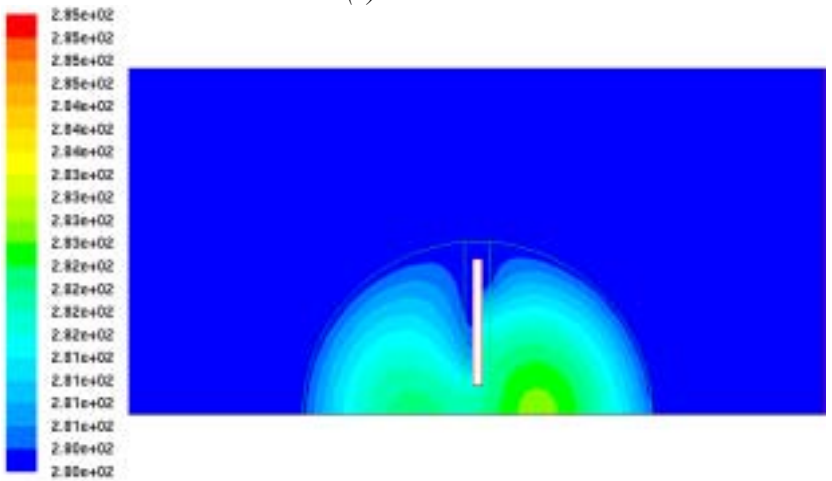

(d) 200 hours

Figure 6.25 Progression of temperature distribution predicted from Scenario VA1

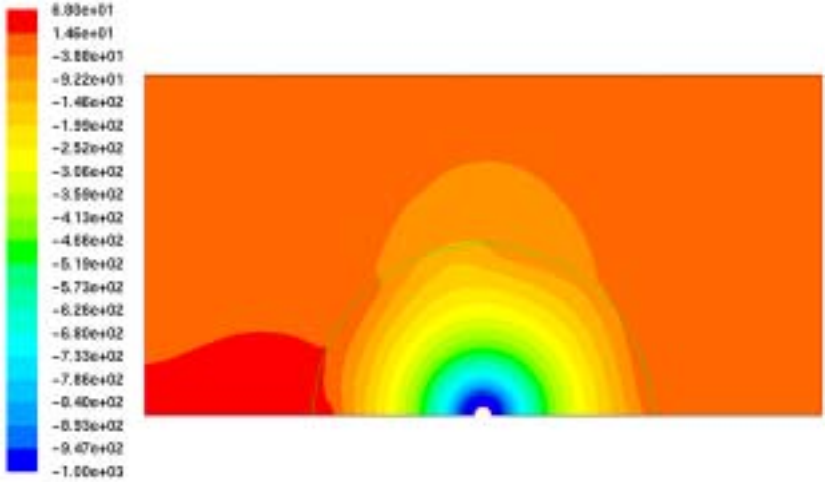

(a) Scenario HA5

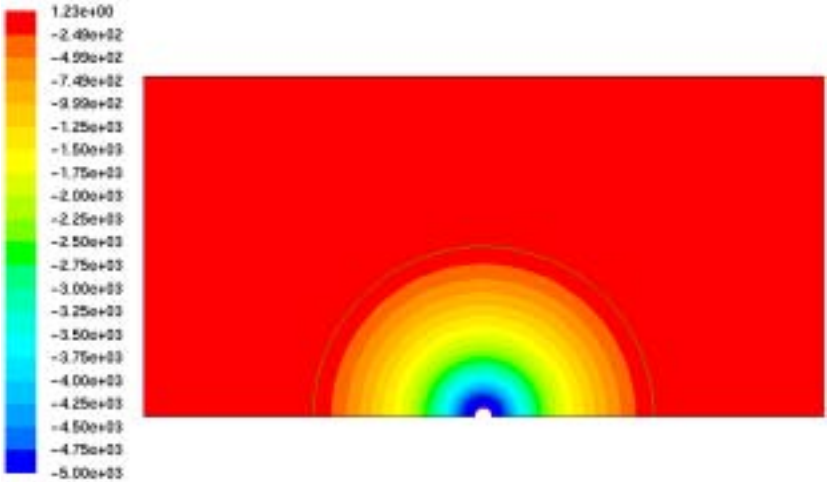

(b) Scenario HA1SP50

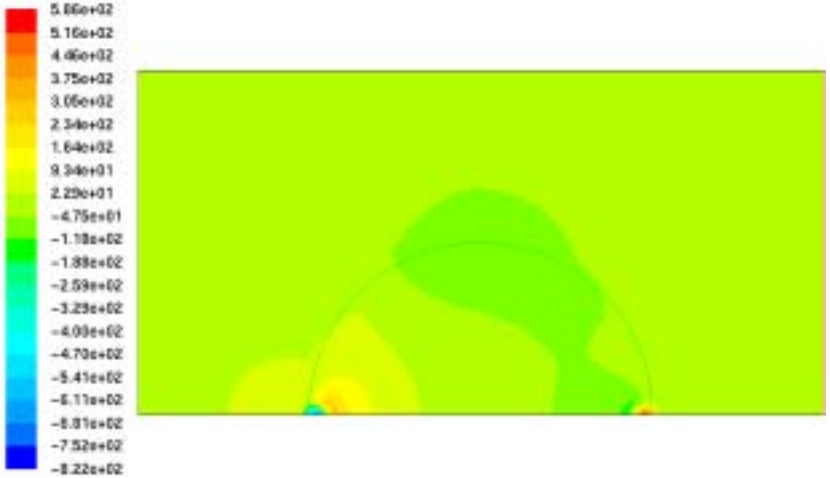

(c) Scenario NA5

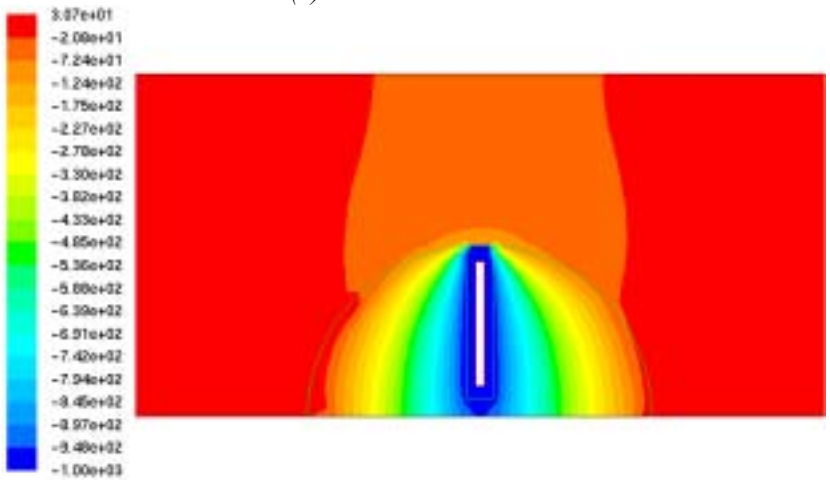

(d) Scenario VA5

Figure 6.26 Static pressure distributions at 100 hours

The results of various simulations can be compared with each other in respect of their diverse operating conditions, including wind speed, aeration method, suction pressure, temperature, initial biomass concentration and various contaminant interphase transfer rates, which will be conducted in the following sections (6.4.4-6.4.12).

6.4.2 Validity of Darcy's Law

Many experimental results prove that as the specific discharge increases, Darcy's law becomes invalid [139]. By analogy flow through conduits, a Reynolds number is defined for flow through porous media, and used to distinguish the validity of Darcy's law:

$$Re = qd / \nu \qquad (6.1)$$

where q is Darcy velocity, ν is the kinematic viscosity of the fluid and d is some characteristic length dimension of the porous matrix which should represent the elementary channels of the porous medium. The mean grain diameter is usually used as the length dimension, and some other terms such as d_{10}, d_{50} can also be referred to as a representative grain diameter [139]. No matter what d is adopted, Darcy's law is valid as long as the Reynolds number based on average grain diameter does not exceed some value between 1 and 10 [139], and the flow in the region is classified as laminar flow in porous media. This means in order to applying Darcy's law, the following requirements must be met:

$$\begin{aligned} qd / \nu &< 10 \\ q &< 10\nu / d \end{aligned} \qquad (6.2)$$

In this study the physical velocity of air in the biopile is less than 10^{-5} m/s, the physical velocity of water in biopile is less than 10^{-7} m/s, and the corresponding Darcy velocities are even less. Furthermore, depending on the material forming the biopile such as soil or sludge, the mean grain diameter is normally within the range from 10^{-4} to 1 mm, and only gravels can reach 10 mm diameter [139] which when used as the characteristic length dimension d in Equation *(6.2)*, results in the smallest upper limit of a velocity which ensures the validity of the Darcy's Law. In this study, fluid

viscosity and density are all set as constant (Table 6.8).

Table 6.8 Fluid properties

	Viscosity (Pa·s)	Density (kg/m^3)
Air	1.8×10^{-5}	1.225
Water	1.0×10^{-3}	1000

Hence, by calculation, the smallest upper limit of velocity for water is 10^{-3} m/s and for air is 1.469×10^{-2} m/s. Both are much larger than the physical velocities found by the simulations results, which support validation of Darcy's Law for all cases of this study.

6.4.3 Determination of hydrodynamic dispersion

As introduced in Section 3.4.5, the Péclet number can be used to evaluate the dominant process of hydrodynamic dispersion. The parameters and variables used to calculate Péclet numbers are all introduced in previous sections. Air and aqueous phase diffusion coefficients are listed in Table 6.5; and fluid velocities within the biopile are summarized in Section 6.4.2. The biggest possible Péclet numbers of chemical diffusion in gas and aqueous phase can be estimated using the largest possible diameter of soil:

$$Pe_g = v_g \cdot d / D_{sg} < 10^{-5}\times10^{-1} / 0.76 < 1.32\times10^{-6}$$
$$Pe_a = v_a \cdot d / D_{sa} < 10^{-7}\times10^{-1} / (9.26\times10^{-5}) < 1.08\times10^{-3}$$

It is clear that both Péclet numbers in the gas and aqueous phases are much lower than 0.3, therefore, according to Kutilek and Nielsen's conclusion described in Section 3.4.5, diffusion is the predominant process, and therefore hydrodynamic dispersion was set to air and aqueous effective diffusion coefficients in this study.

6.4.4 Wind speed

Simulations with different values of wind speed, 1 m/s and 5 m/s, were conducted for all three

aeration methods. Contaminant removals by diffusion to the atmosphere through the biopile surface are shown in Figure 6.27 to Figure 6.29. The results of non-aerated cases and vertical aeration pipe cases show that a larger wind speed can lead to slightly more contaminant loss to atmosphere. However, Figure 6.28 illustrating the results of horizontal pipe aerated cases shows that the contaminant loss to the atmosphere for both wind velocities is nearly the same, and does not directly support the above conclusion. However, since the biodegraded contaminant in the 5 m/s case is greater than that of the 1 m/s scenario (Figure 6.31), which can result in a greater contaminant concentration decrease in both the aqueous and oleic phases, this may explain the subsequent decrease in contaminant levels transferred to gas phase from aqueous and oleic phases. Hence, by considering the influence of biodegradation, the overall contaminant removal capability of biopile surface loss to the atmosphere for 5 m/s wind speed is still greater than that for 1 m/s.

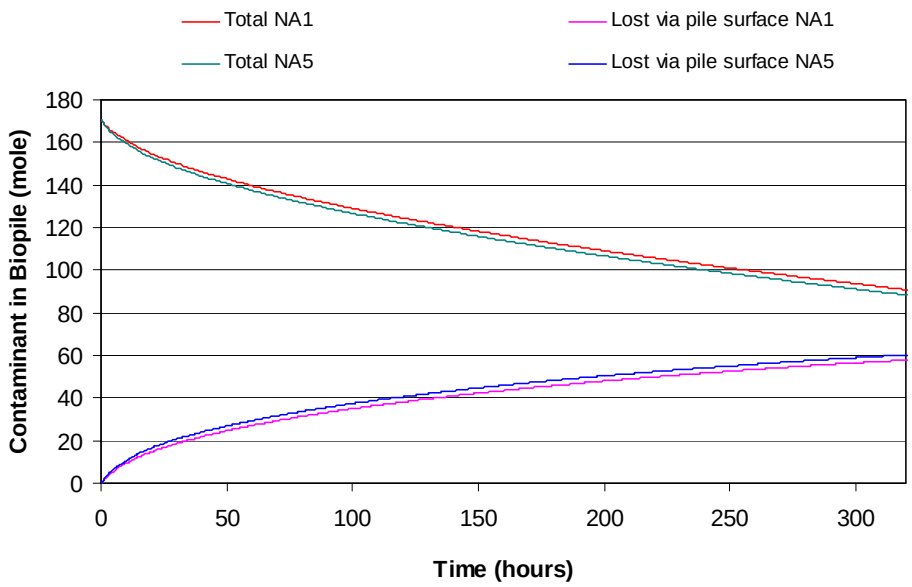

Figure 6.27 Comparison of contaminant lost via pile surfaces in Scenario NA1 and NA5

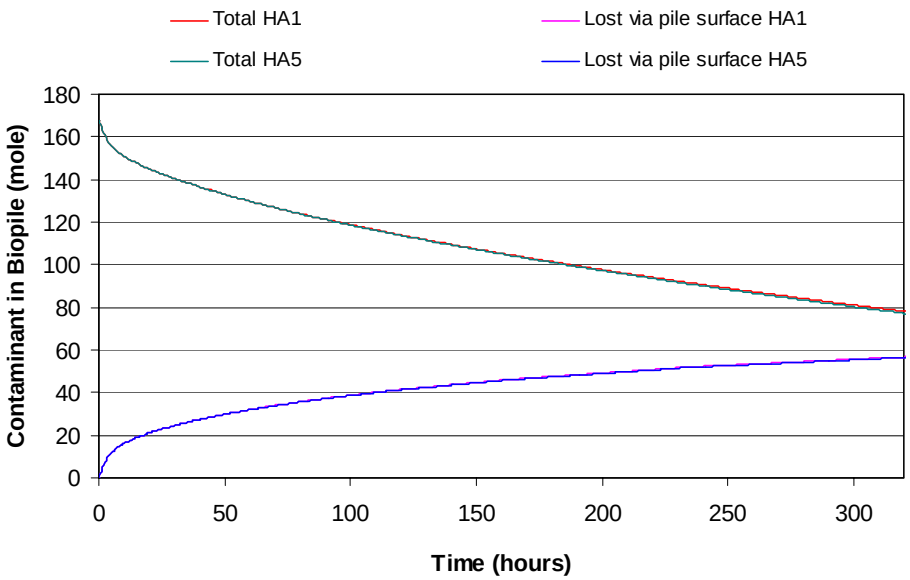

Figure 6.28 Comparison of contaminant lost via pile surfaces in Scenario HA1 and HA5

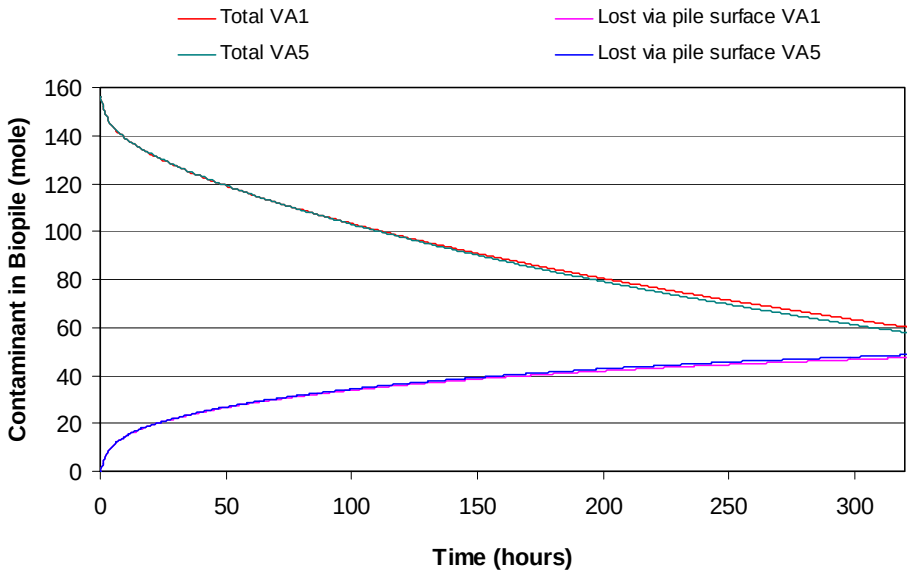

Figure 6.29 Comparison of contaminant lost via pile surfaces in Scenario VA1 and VA5

Varying the wind speed can affect not only the contaminant lost to atmosphere, but also the biodegradation rate (Figure 6.30 to Figure 6.32). In the aerated cases, the biodegraded contaminant under the 5 m/s wind speed condition is more than that with 1 m/s wind speed, while in the non-aerated cases, there is no clear difference. This is because the difference of wind speeds changes the flow pattern over the whole model domain, and alters the air flux from the surroundings into the biopile, which leads to different temperature distributions, and ultimately affects the bioremediation

rate. In the non-aerated cases, since no suction pressure was present within the biopile, the amount of ambient air flowing into the biopile is insignificant and almost has no effect on temperature. Thus, the biodegradation effect does not change as noticeably as they do in the aerated cases (refer to Table A.4 in Appendixes for detailed simulation results).

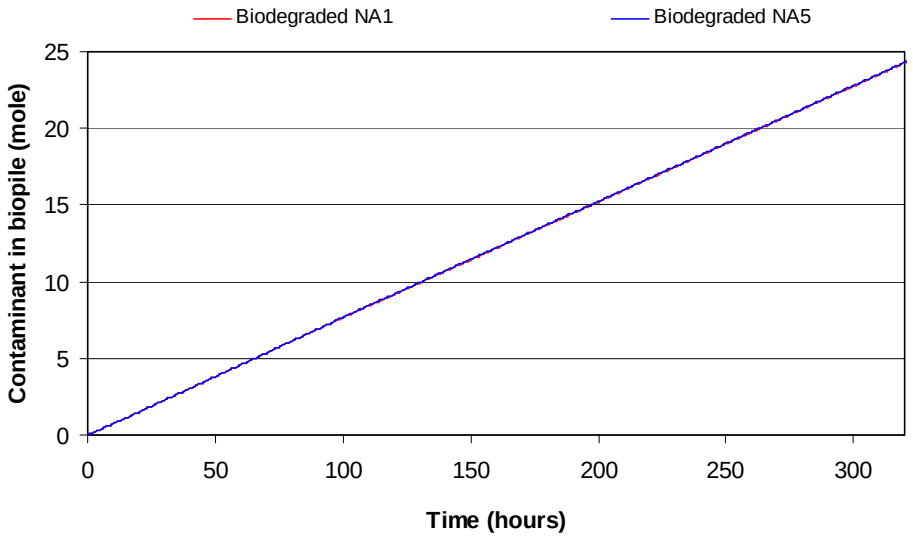

Figure 6.30 Comparison of biodegraded contaminant in Scenario NA1 and NA5

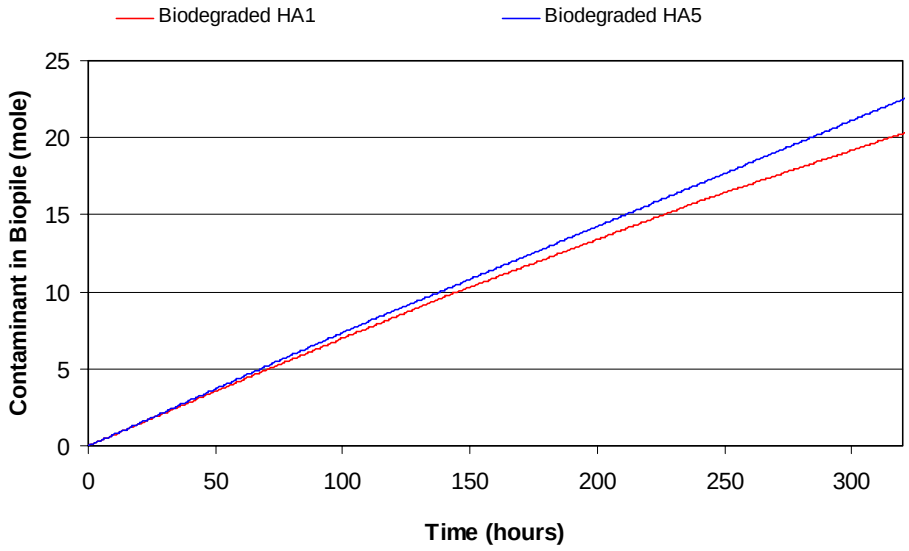

Figure 6.31 Comparison of biodegraded contaminant in Scenario HA1 and HA5

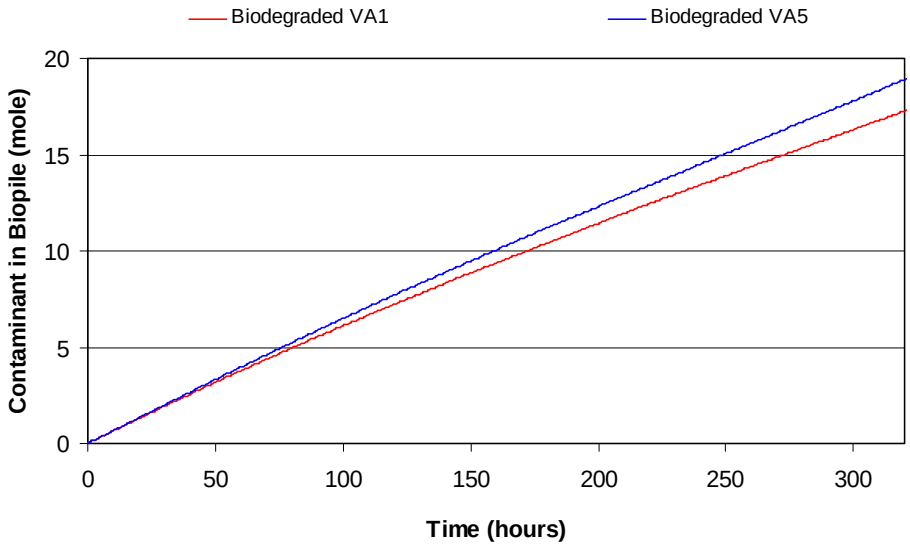

Figure 6.32 Comparison of biodegraded contaminant in Scenario VA1 and VA5

The values of the instantaneous air flux from ambient surroundings into the biopile averaged across its surface at different times are shown in Table 6.9 for Scenarios HA1, HA5, VA1 and VA5. The fluxes for the lower wind speeds (HA1 and VA1) are slightly greater than those for the higher wind speeds (HA5 and VA5). This is attributed to the fact that the higher wind speed gives rise to a lower pressure value over the surface of the pile, reducing the advective flux into the pile. This is illustrated in Figure 6.33 and Figure 6.34, where pressure contours for the 1 m/s and 5 m/s wind cases are plotted on the same scale. It can be seen that the pressure value over the pile in the 5 m/s case is in the region of -70 Pa, whereas that for the 1 m/s case is only about -1 Pa. This would clearly result in a greater net force driving air into the pile in the 1 m/s case.

Table 6.9 Instantaneous air flux across biopile surfaces in Scenario HA1, HA5, VA1 and VA5

Scenario ID	Instantaneous air flux across biopile surfaces (kg/s)					
	10 h	20 h	50 h	100 h	200 h	300 h
HA1 ($\times 10^{-6}$)	5.91	5.91	5.901	5.90	5.89	5.89
HA5 ($\times 10^{-6}$)	5.73	5.73	5.73	5.72	5.72	5.71
VA1 ($\times 10^{-5}$)	3.08	3.09	3.10	3.11	3.12	3.13
VA5 ($\times 10^{-5}$)	2.87	2.87	2.88	2.87	2.87	2.87

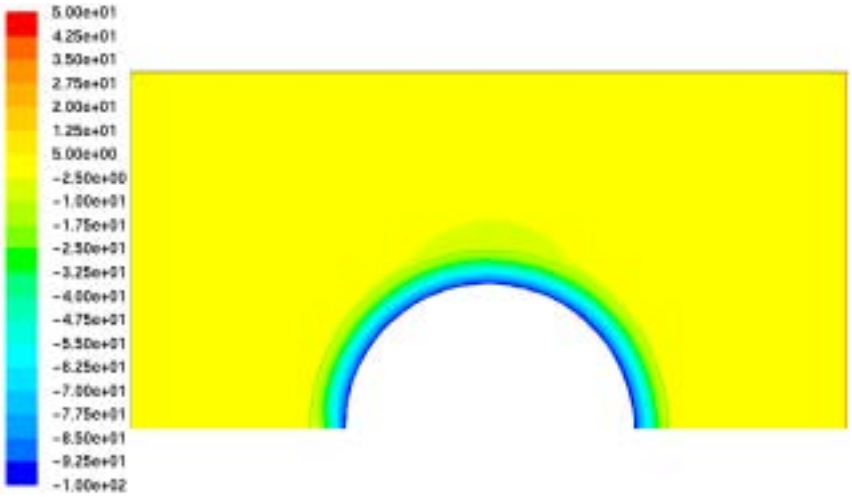

Figure 6.33 Pressure contours over horizontally-aerated biopile Scenario HA1

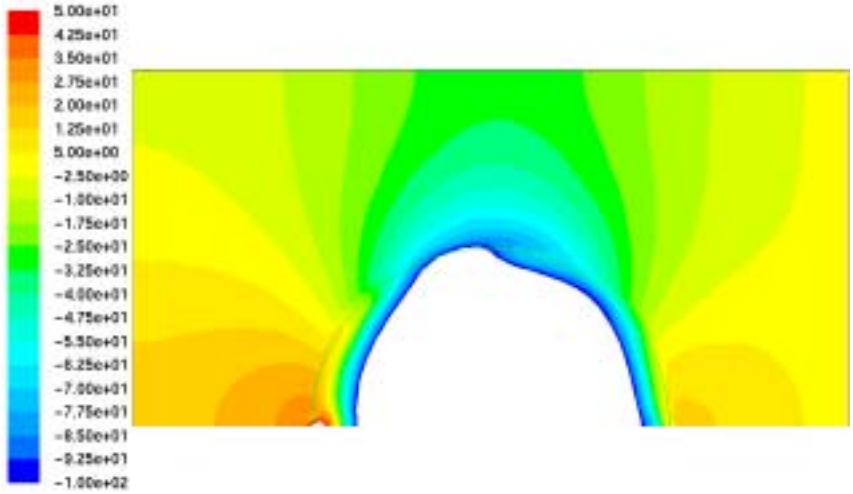

Figure 6.34 Pressure contours over horizontally-aerated biopile Scenario HA5

The decreased instantaneous air flux can directly affect the temperature change and consequently affect the bioreaction rate in the 5m/s cases. The change of average biopile temperature with time is shown in Figure 6.35. There are very clear temperature differences in the aerated biopiles (HA1 vs. HA5, VA1 vs. VA5); in contrast, the temperature differences in the non-aerated cases are very small. Figure 6.36 to Figure 6.41 illustrate the temperature distribution in the biopile for Scenario NA1, NA5, HA1, HA5, VA1 and VA5. These figures demonstrate that different inlet wind speeds affect not only the temperature value, but also the temperature distribution.

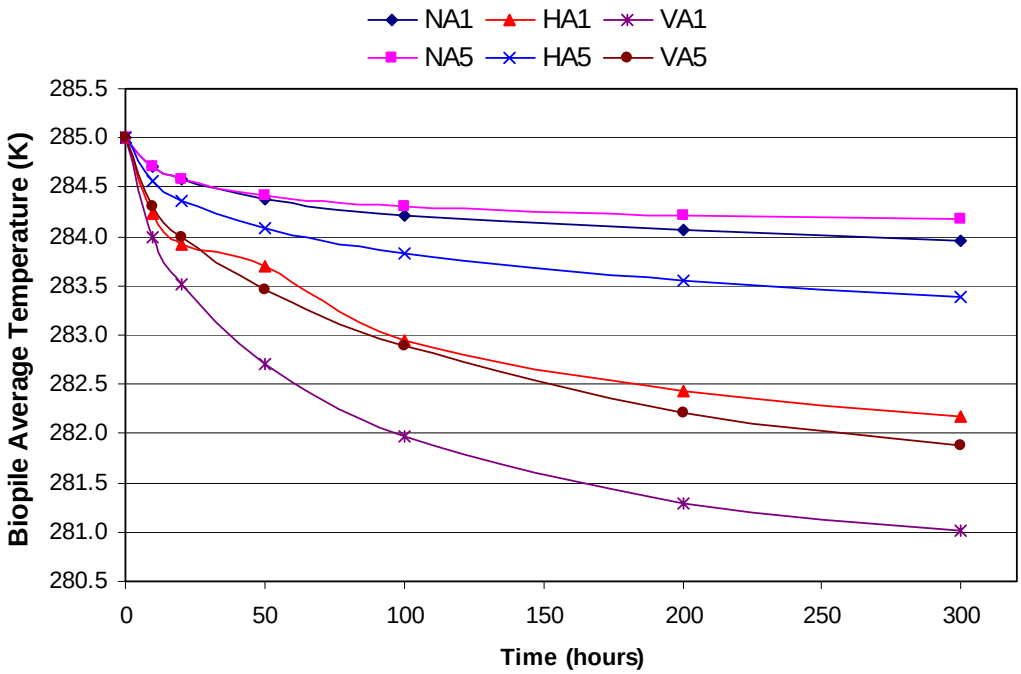

Figure 6.35 Average biopile temperature at different times

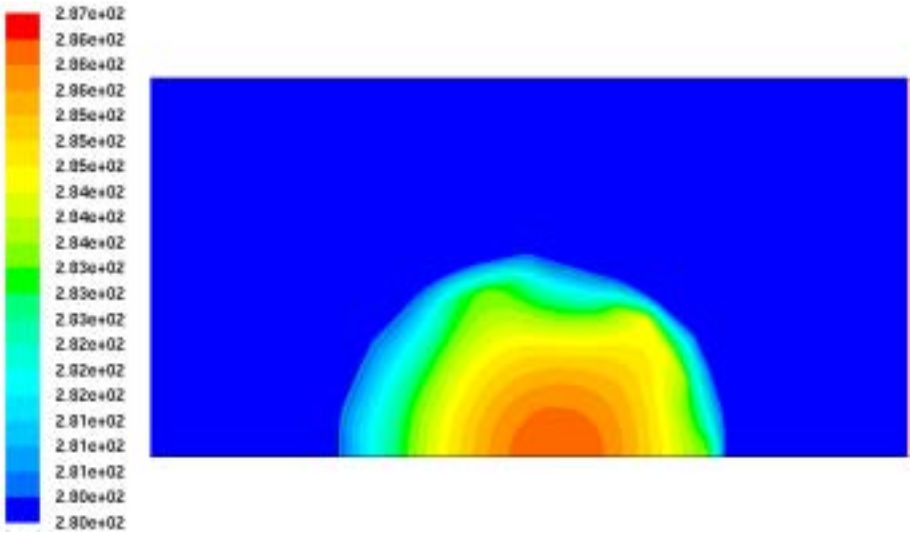

Figure 6.36 Biopile temperature distribution Scenario NA1—300 hours

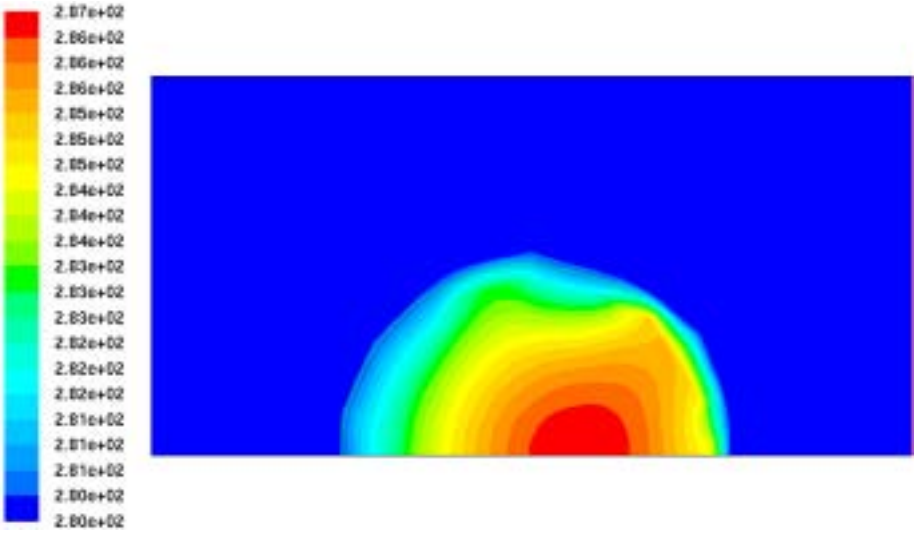

Figure 6.37 Biopile temperature distribution Scenario NA5—300 hours

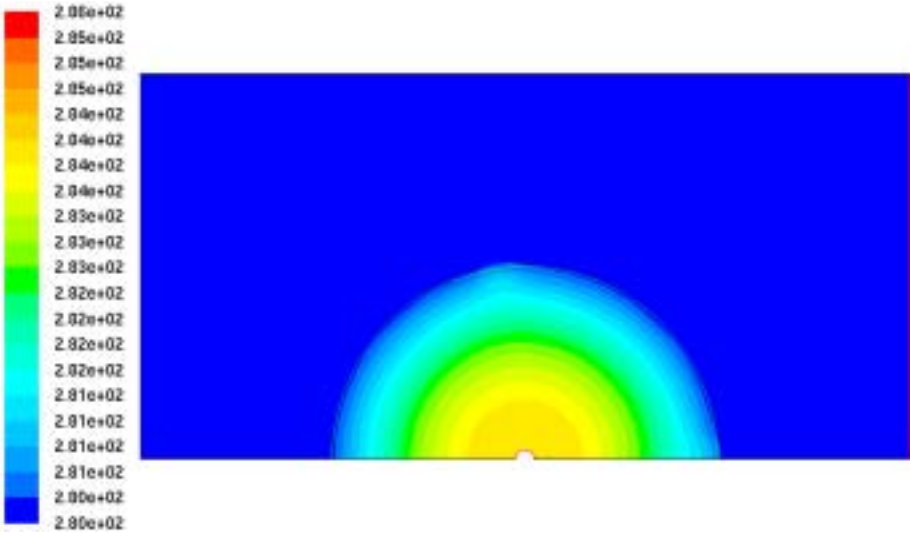

Figure 6.38 Biopile temperature distribution Scenario HA1—300 hours

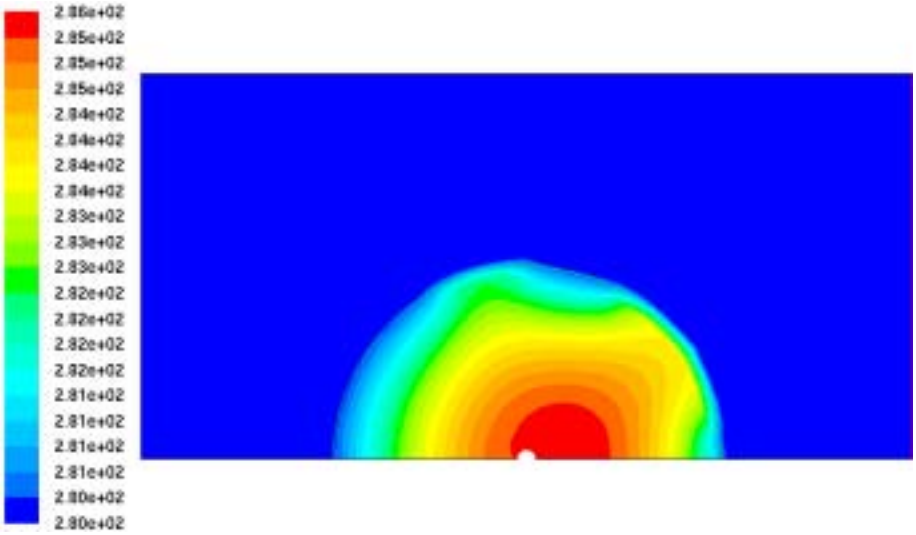

Figure 6.39 Biopile temperature distribution Scenario HA5—300 hours

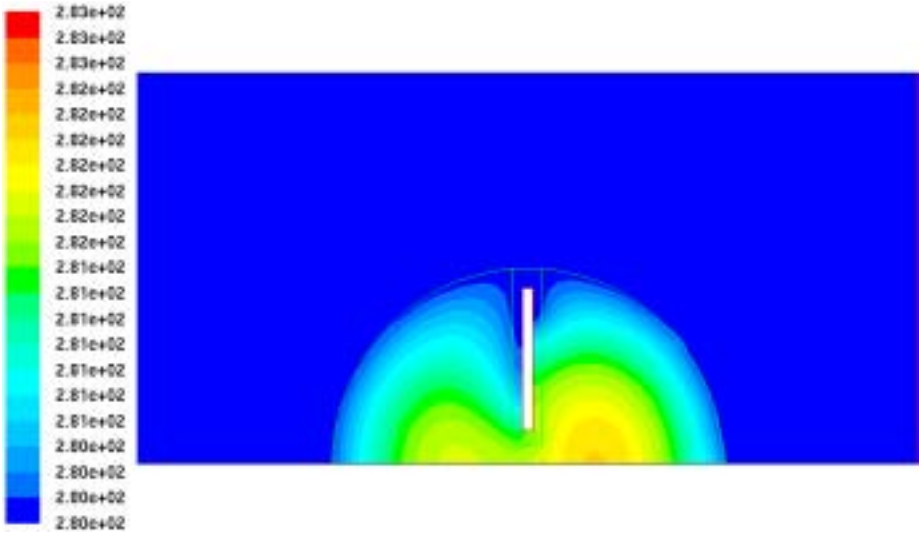

Figure 6.40 Biopile temperature distribution Scenario VA1—300 hours

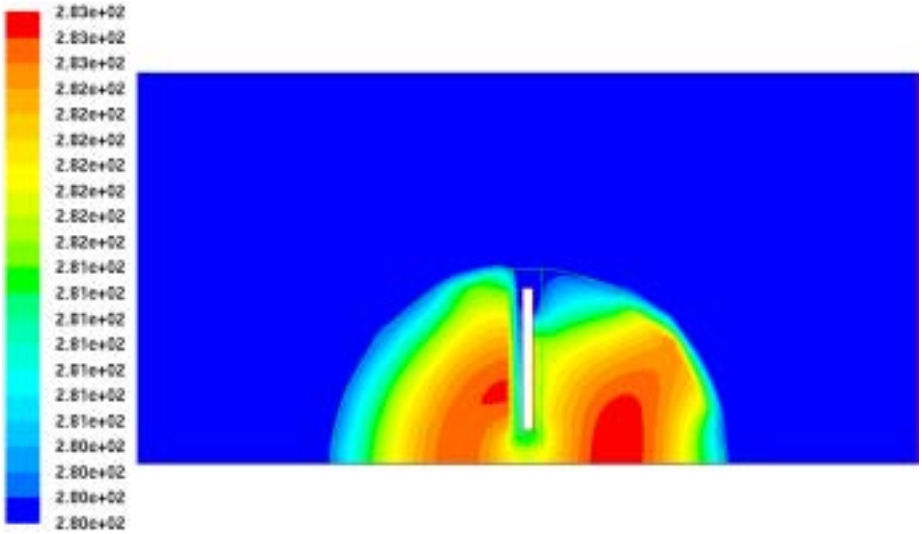

Figure 6.41 Biopile temperature distribution Scenario VA5—300 hours

A change in temperature can influence the bioreaction process, and also result in the change of biodegraded contaminant and biomass concentration. Due to higher biopile temperatures in cases with greater wind speed, a more active bioreaction takes place, consuming more organic contaminant and generating more biomass. This is shown in Figure 6.42 and Figure 6.43.

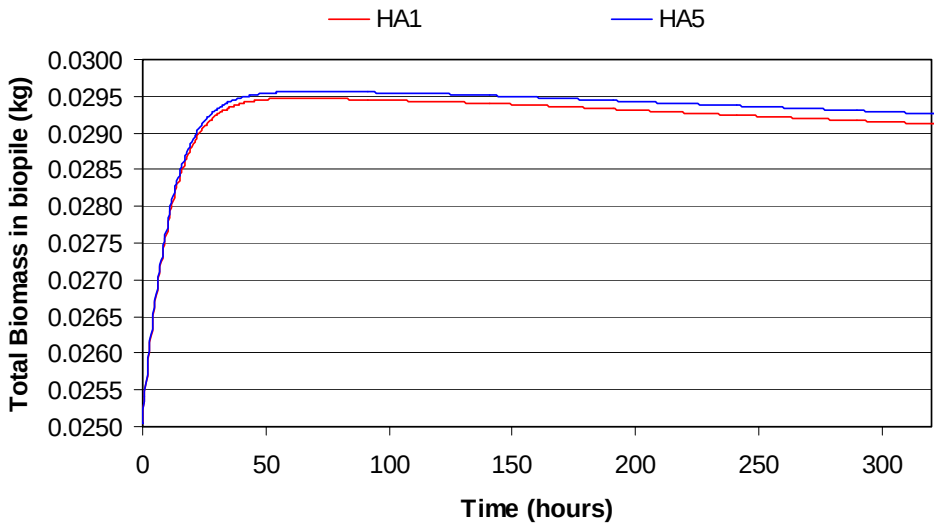

Figure 6.42 Comparison of biomass in biopiles at different times in Scenario HA1 and HA5

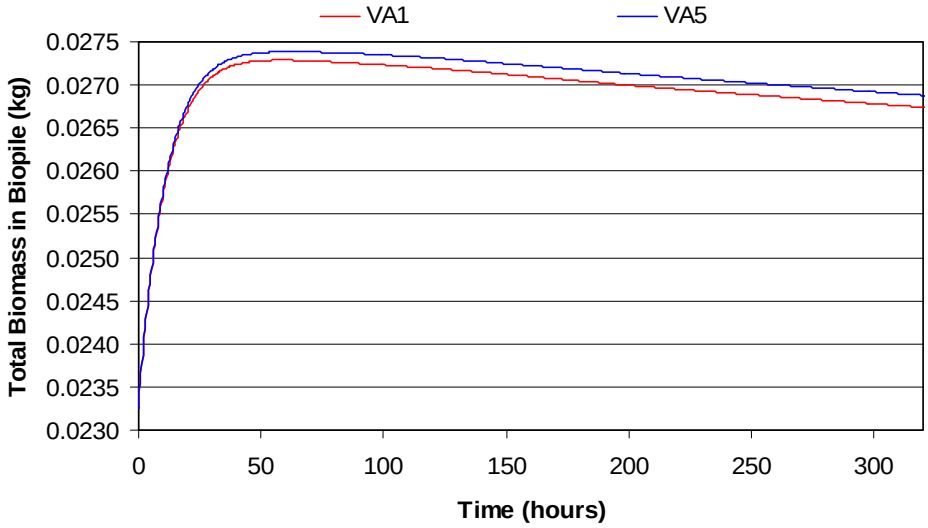

Figure 6.43 Comparison of biomass in biopiles at different times in Scenario VA1 and VA5

6.4.5 Temperature

In this study, bioreaction rate is associated with temperature. If the operating temperature of the biopile is changed, the level of contaminant removal by different approaches will also change. The values for the initial and inlet air temperatures specified in Scenario HA5IT are 8 K higher than those of Scenario HA5. Figure 6.44 compares the results of these two cases. After 320 hours of treatment, the amount of contaminant biodegraded in Scenarios HA5 and HA5IT are 22.5 moles and 35.7 moles

respectively. This difference is approximately 60%, corresponding with the fact that contaminant lost to atmosphere and through aeration pipes is slightly less in Scenario HA5IT (53.9 moles and 10.8 moles respectively) than that in Scenario HA5 (56.4 moles and 11.8 moles respectively). Overall, the total contaminant remaining in the biopiles in case HA5 is 77.2 moles, and in HA5IT is 67.4 moles, which means that 9.8 moles more contaminant is removed in the higher temperature case, which corresponds with a 6% increase of total removal efficiency. Figure 6.45 shows the progression of biomass in these two cases, demonstrating that in HA5IT with higher temperature, a faster anabolism process results in more rapid growth of microorganisms than in HA5. Furthermore, the maximum total biomass that occurs during the whole treatment process in HA5IT is greater than that in HA5, which suggests that the maximum possible biomass concentration at higher temperatures is greater than that at lower temperatures.

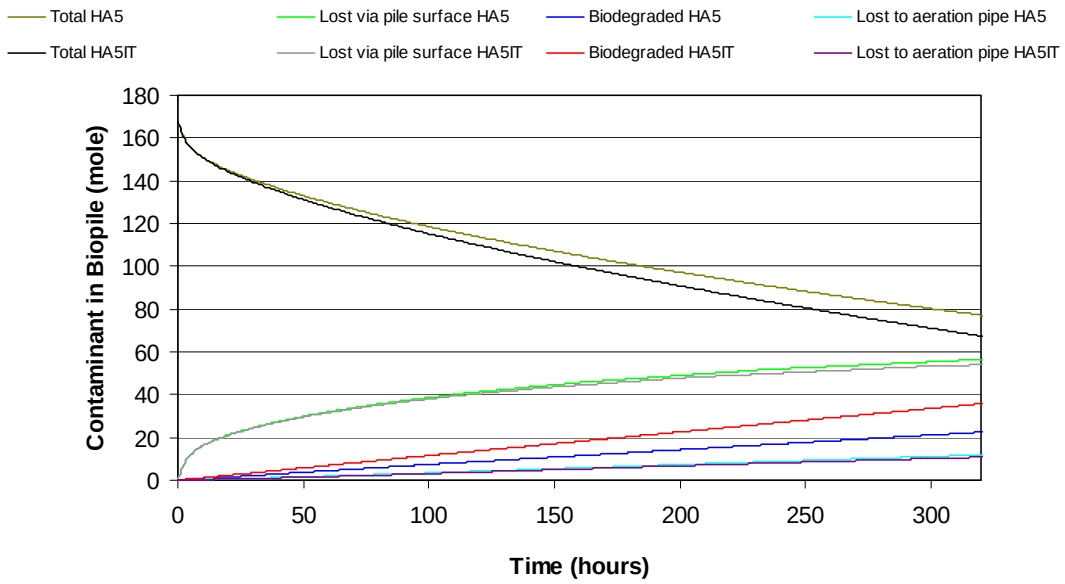

Figure 6.44 Comparison of contaminant removed by each mechanism in Scenario HA5 and HA5IT

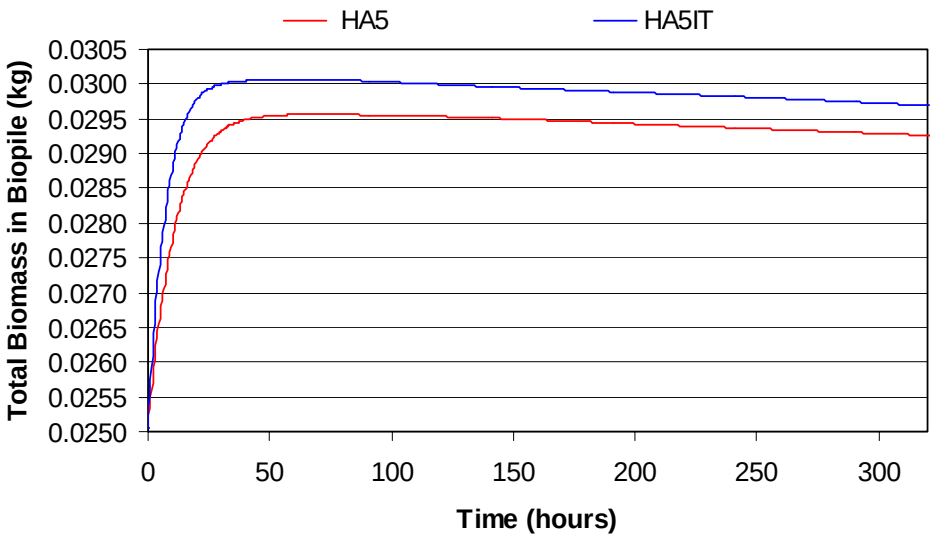

Figure 6.45 Comparison of biomass in biopiles at different times in Scenario HA5 and HA5IT

Although the above analysis seemingly concludes high temperature biopile treatment is more effective than low temperature treatment, since the optimal bioreaction temperature is 313 K (40 °C, refer to Equation *(3.24)*), the biodegradation efficiency will decrease along with temperature increase at temperatures above 313 K.

6.4.6 Biomass

Biomass has a very direct impact on the rate bioreaction. The operating conditions specified in Scenario HA5RB are identical to those of Scenario HA5 except that the initial biomass concentration is reduced by one order of magnitude (from 0.0162 kg/m^3 to 0.00162 kg/m^3). Figure 6.46 compares the results of these two cases. The amount biodegraded contaminant in Scenario HA5RB is much lower than that of HA5. In contrast with the difference between the initial biomass concentrations of one order of magnitude, the difference between levels of biodegraded contaminant after 320 hours of treatment were 0.32 moles in case HA5RB and 22.5 moles in case HA5, therefore with an order to magnitude of 2. Thus, a low initial biomass base not only directly effects on the contaminant biodegradation rate, but also contributes to slow biomass growth. Figure 6.47 clearly demonstrates this phenomenon. HA5 reached its maximum biomass after 50 hours, whereas due to the smaller initial biomass concentration, HA5RB maintained a quasi-linear biomass growth pattern during the entire process, and the biomass growth rate was much smaller than that of HA5. Thereby, the

influence of biomass on the amount of contaminant biodegraded is significant over treatment time.

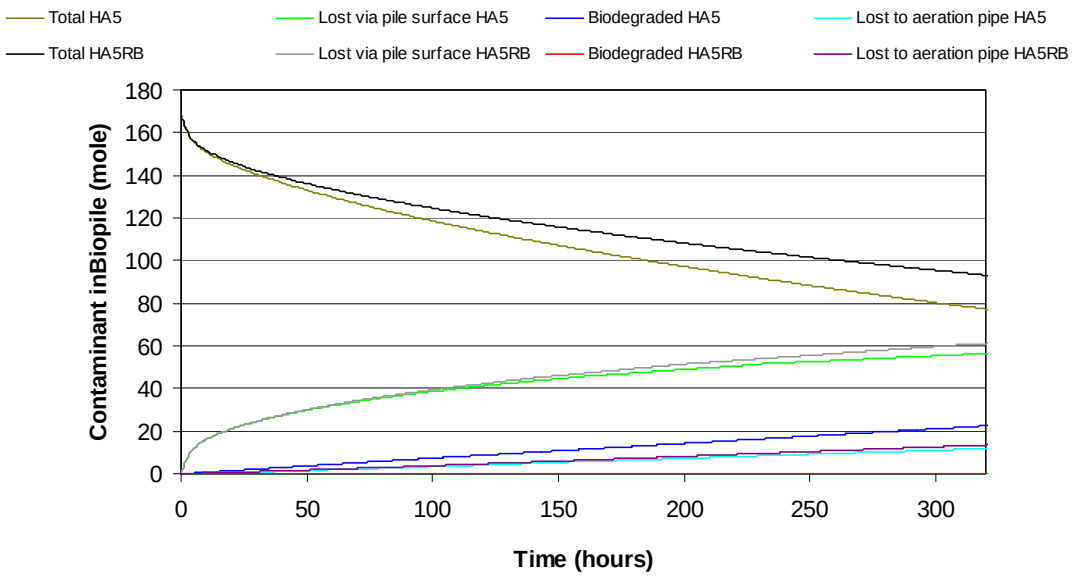

Figure 6.46 Comparison of contaminant removed by each mechanism in Scenario HA5 and HA5RB

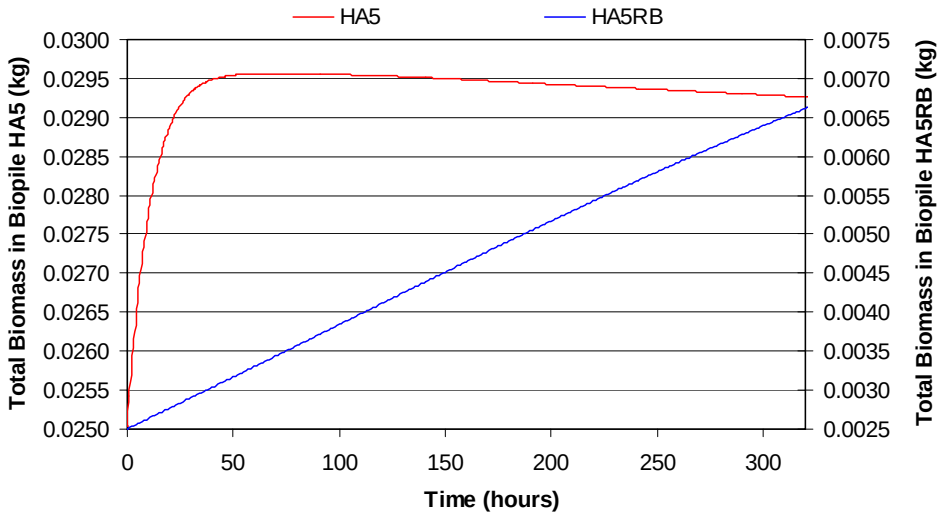

Figure 6.47 Comparison of biomass in biopiles at different times in Scenario HA5 and HA5RB

6.4.7 Contaminant interphase transfer rate

In Scenarios HA5RGO and HA5RAG, the organic-gas contaminant transfer coefficient and aqueous-gas contaminant transfer coefficient were reduced by one order of magnitude (from 5.79×10^{-4}/s to

5.79×10^{-5}/s, and from 5.79×10^{-5}/s to 5.79×10^{-6}/s respectively). Although these changes to the coefficients values are quite significant, they did not lead to any obvious impact on the level of contaminant removal (refer to Table A.3 to Table A.5 in Appendixes for detailed simulation results). In Scenario HA5RGO, not only the accumulated contaminant removed by each effect (lost via pile surface, biodegraded and lost to aeration pipe), but also the distribution of contaminant remaining in each phase and biomass are all almost identical to those of Scenario HA5 (Figure 6.48 and Figure 6.49). This phenomenon reveals that the organic-gas contaminant transfer coefficient is not the limiting factor for the contaminant removal by loss to atmosphere and aeration pipes. Instead, it is the diffusion/dispersion capability which governs this. By contrast, although the contaminant removal result found in Scenario HA5RAG is similar to that of HA5, the contaminant distributions in each phase and the biomass growth have clear differences which can be seen in Figure 6.50 and Figure 6.51.

Since the contaminant concentrations in each phase are in equilibrium at the beginning of a simulation, as the simulation proceeds, the diffusion/dispersion and biodegradation processes will decrease the contaminant concentrations in the gaseous and aqueous phases respectively, hence the trend of contaminant transfer between phase is from other phases to the gaseous and aqueous phases. The difference in results between Scenarios HA5RAG and HA5 reflects that between gaseous and aqueous phases, the normal contaminant transfer direction is from gaseous to aqueous phase. Therefore, when the aqueous-gas contaminant transfer coefficient is reduced, it is harder for the contaminant to transfer from the gas phase to aqueous phase, which leads to a more rapid decrease of contaminant concentration in the aqueous phase, and an increase of contaminant transfer to the aqueous phase from both the solid and oleic phases. In addition, a lower contaminant concentration in the aqueous phase also reduces the bioreaction activity, decelerates the microorganism production rate, and finally accelerates the decay of biomass (Figure 6.51).

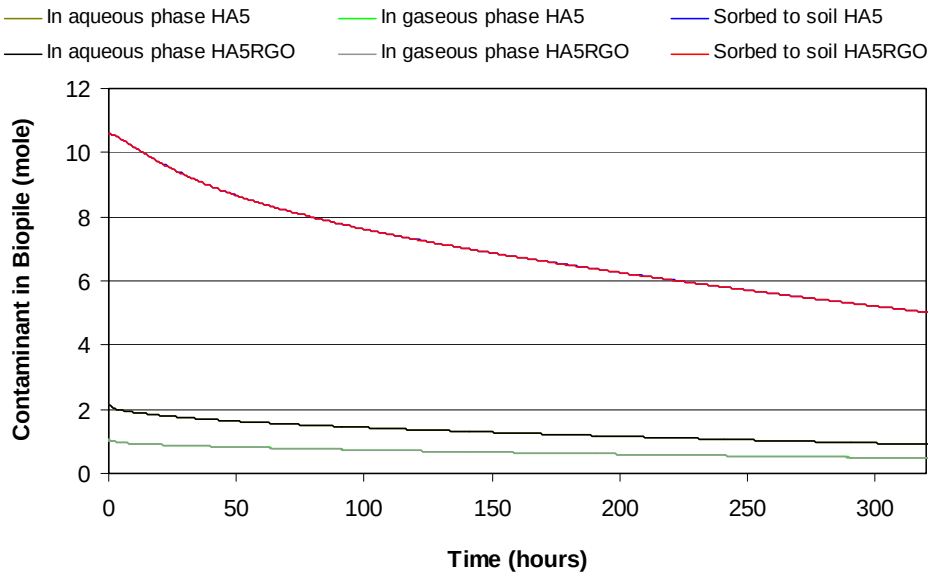

Figure 6.48 Comparison of Contaminant distributions in different phases in Scenario HA5 and HA5RGO

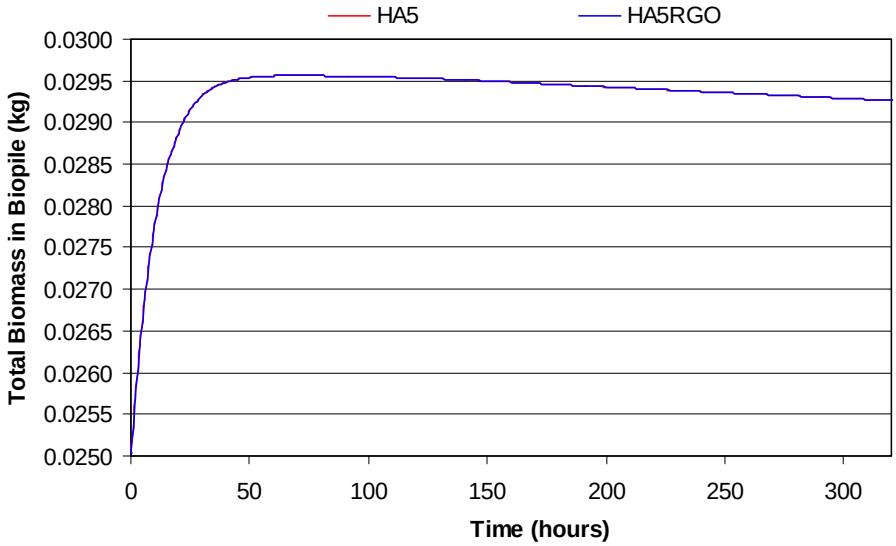

Figure 6.49 Comparison of biomass in biopiles at different times in Scenario HA5 and HA5RGO

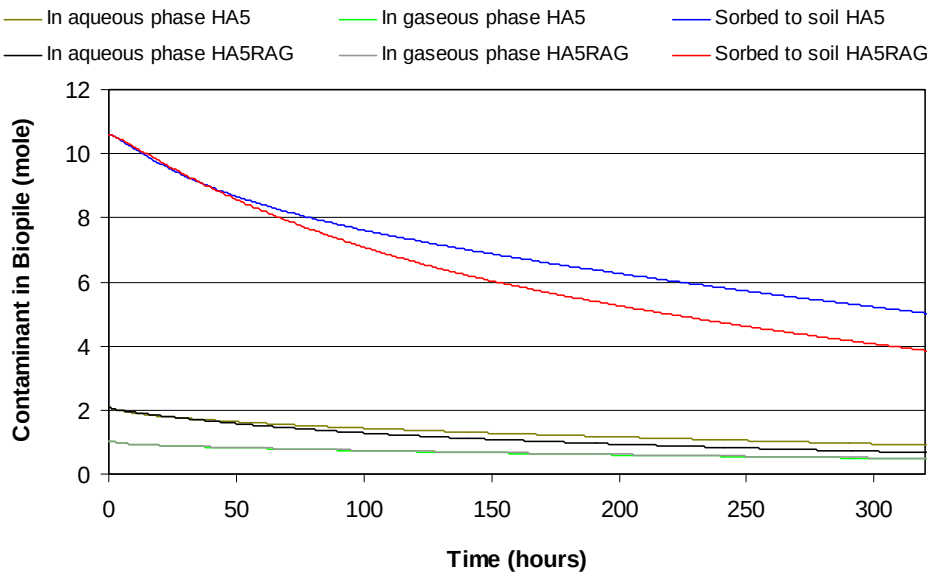

Figure 6.50 Comparison of Contaminant distributions in different phases in Scenario HA5 and HA5RAG

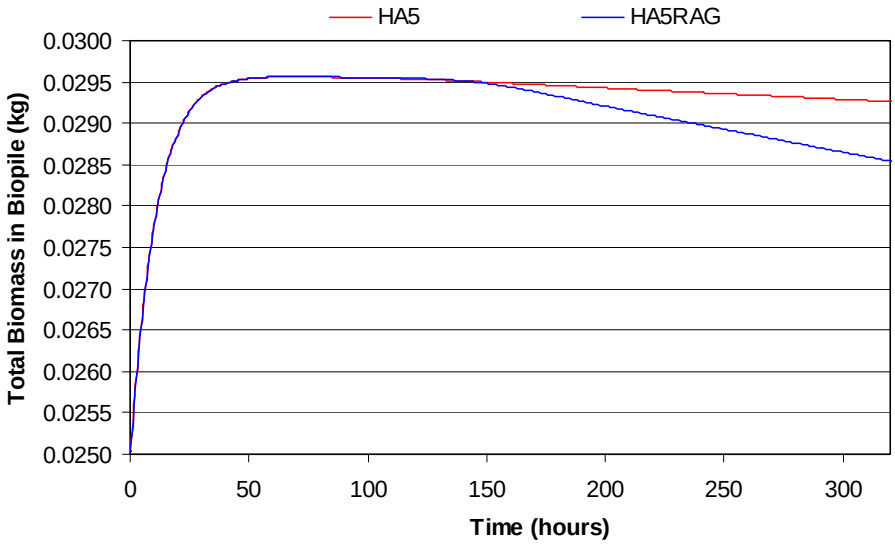

Figure 6.51 Comparison of biomass in biopiles at different times in Scenario HA5 and HA5RAG

6.4.8 Aeration method

As discussed previously, three different aeration methods are examined in this study, although the performance of each method can vary by applying different aeration pressures. Contaminant removal efficiencies of each aeration method with the same aeration pressure and wind speed are compared in Figure 6.52 to Figure 6.55. The most noticeable difference between cases is that at the same suction

pressure, the vertical pipe arrangement can remove much more contaminant though pipe loss due to the more intense air flow (Table 6.9). Contaminant loss through the pipe in the vertical pipe cases are nearly three times grater than those of the horizontal pipe cases (at 320 hours of treatment, 19.9% in Scenario VA1 compared to 7.3% in HA1, and 19.7% in VA5 compared to 7.0% in HA5). Another result simulated by Scenarios with more intense air flow is the rapid decrease of biopile temperatures, which leads to a reduction in biodegraded contaminant levels. The influence of these effects is that contaminant loss to atmosphere rapidly decreases in Scenarios VA1 and VA5, compared with Scenarios NA1, HA1 and NA5 and HA5.

In the early stages of a biopile treatment, referring to Figure 6.52 and Figure 6.54, it can be found that the amount of contaminant lost through the pile surface in Scenarios NA1 and NA5 are smaller than those of HA1, VA1 and HA5, VA5. This result is counter-intuitive, since for these aerated cases, the direction of air flow through the biopile surface is from the ambient surroundings to the biopile. An explanation for this phenomenon is that aeration enhances the fresh air (without contaminant) flow from the ambient atmosphere to the biopile via its surface, thus more rapidly decreases the contaminant concentration in the gaseous phase at the biopile surface region, and also leads to increased contaminant transfer from other phases (oleic and aqueous) to gaseous phase over a certain period of time, finally resulting in more contaminant loss through the pile surface by diffusion/dispersion. After this certain period of time has passed, the contaminant concentrations in all phases are small, and consequently less and less contaminant can transfer from other phases to the gaseous phase, thereby, contaminant transferred to the biopile surface region by diffusion/dispersion from the inner side of the biopile becomes dominant over the contaminant lost through biopile surface. Therefore, although the rates of contaminant removal by loss to surroundings in Scenarios NA1 and NA5, are smaller than those of HA1, VA1 and HA5, VA5 during the early stages of treatment, it will become larger than those of the aerated cases after a certain period of time has elapsed.

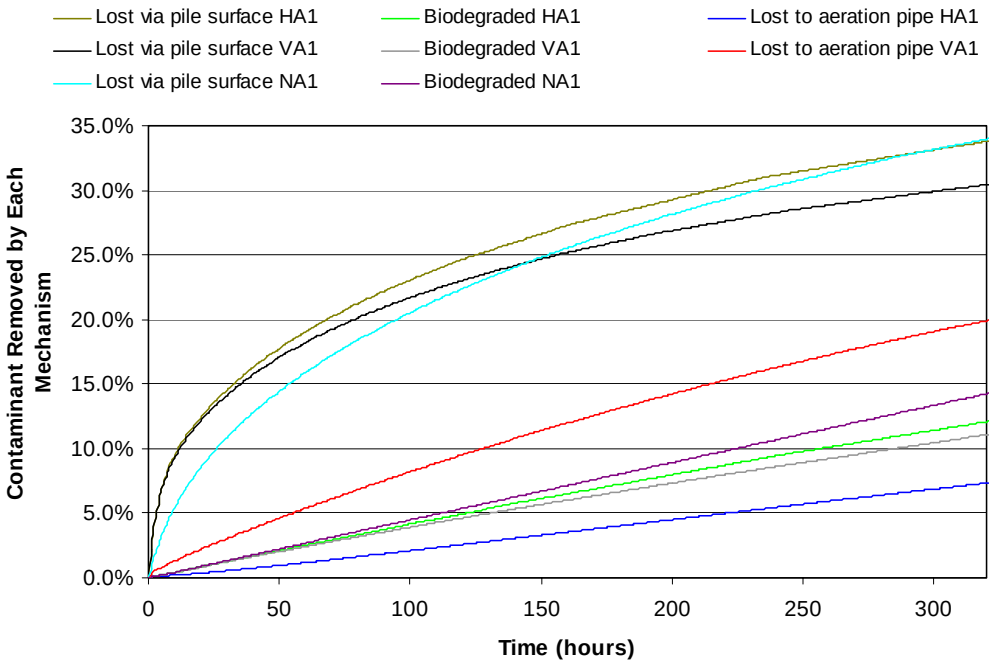

Figure 6.52 Comparison of contaminant removed by each mechanism in Scenario NA1, HA1 and VA1

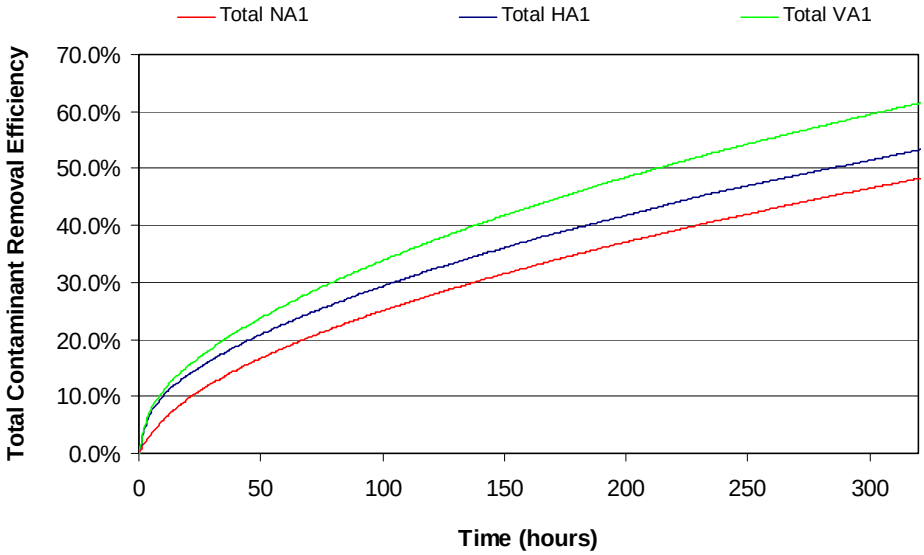

Figure 6.53 Comparison of total contaminant removal efficiency in Scenario NA1, HA1 and VA1

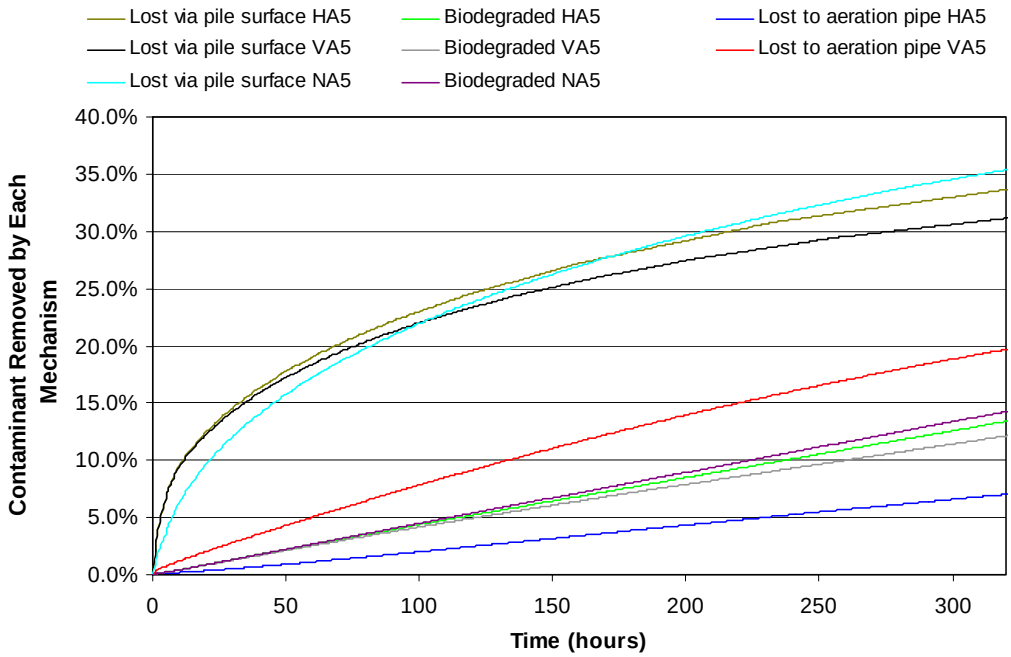

Figure 6.54 Comparison of contaminant removed by each mechanism in Scenario NA5, HA5 and VA5

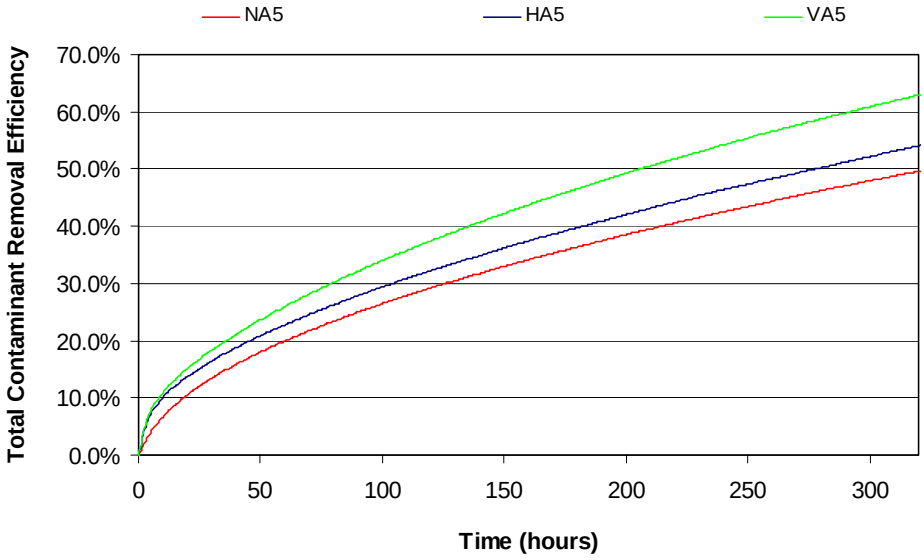

Figure 6.55 Comparison of total contaminant removal efficiency in Scenario NA5, HA5 and VA5

It has been found in general, aeration treatment can enhance the contaminant removal efficiency of a biopile. It can be concluded that the total contaminant removal efficiencies for the aerated biopiles are better than the non-aerated biopiles (at 320 hours of treatment, 48.18% in Scenario VA1 and 49.60% in VA5), and the vertical pipe aeration method (at 320 hours, 61.40% in VA1 and 62.92% in VA5) is more efficient than the horizontal pipe aeration method (at 320hours, 53.17% in Scenario HA1 and

54.04% in HA5).

6.4.9 Suction pressure

The level of contaminant removal is not only affected by the method of aeration treatment, but also by the value of aeration pressure. By increasing the suction pressure from 1000 Pa used in Scenario HA1 to 2500 Pa used in Scenario HA1SP25 and 5000 Pa in HA1SP50, the instantaneous values of air flux across the biopile surface increase also, which can be seen in Table 6.10. This consequently leads to vastly more contaminant removal through the aeration pipes, as shown in Figure 6.56. Contaminant losses due to aeration in Scenarios HA1SP25 and HA1SP50 are approximately 3 times and 5.5 times higher respectively than that found in HA1 over the whole treatment time, which results in the reduction of losses to the atmosphere in Scenarios HA1SP25 and HA1SP50. The amount of biodegraded contaminant also decreases, as the increase in air flux results in more temperature change within the pile. However, this effect is almost insignificant in these three cases, and can not be directly observed from the biodegraded contaminant mass in Figure 6.56, but can be inferred from the difference in biomass between these three cases (Figure 6.58).

Table 6.10 Instantaneous air flux across biopile surface in Scenario HA1, HA1SP25 AND HA1SP50

	Instantaneous air flux across biopile surface (kg/s)					
	10 h	20 h	50 h	100 h	200 h	300 h
HA1 ($\times 10^{-6}$)	5.91	5.91	5.90	5.901	5.89	5.89
HA1SP25 ($\times 10^{-5}$)	1.48	1.48	1.483	1.47	1.47	1.47
HA1SP50 ($\times 10^{-5}$)	2.95	2.95	2.95	2.95	2.84	2.94

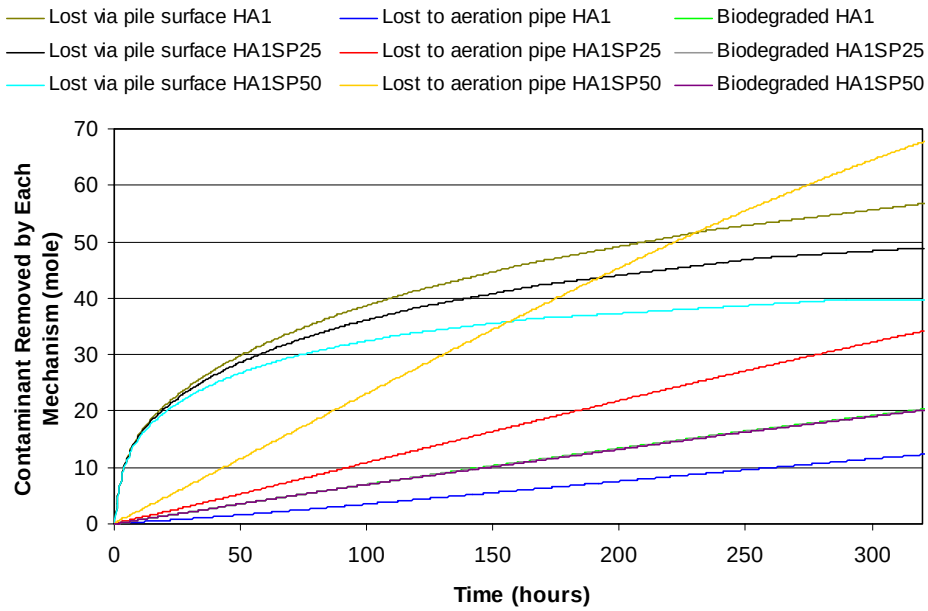

Figure 6.56 Comparison of contaminant removed by each mechanism in Scenario HA1, HA1SP25 AND HA1SP50

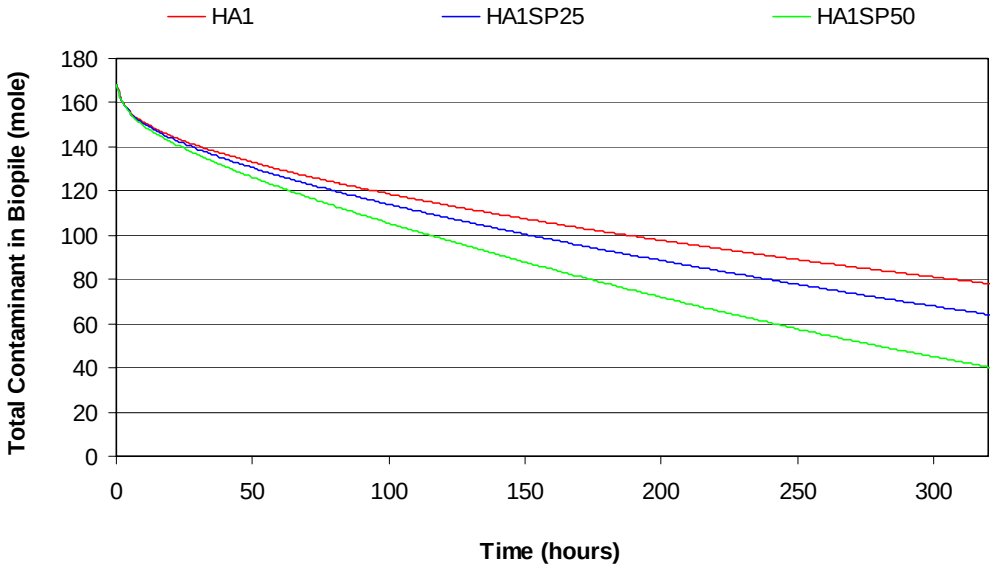

Figure 6.57 Comparison of total contaminant in biopile in Scenario HA1, HA1SP25 and HA1SP50

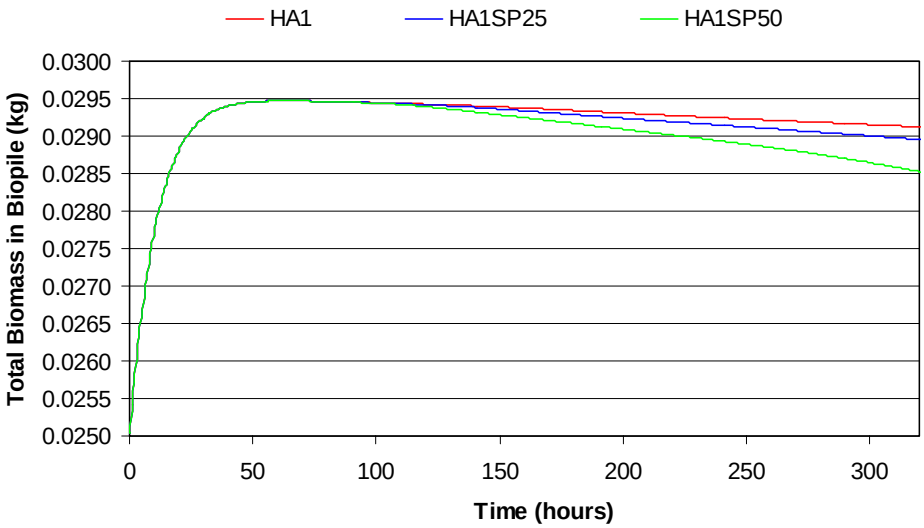

Figure 6.58 Comparison of total biomass in biopile in Scenario HA1, HA1SP25 and HA1SP50

6.4.10 Blowing and suction

For each kind of aeration pipe arrangement, the biopile treatment process can run under various aeration pressures, including both suction and blowing pressures. Scenario HA1BP is identical to HA1, except that the suction aeration pressure of 1000 Pa is changed to a blowing pressure of 1000 Pa. The difference in the results of these two cases is remarkable. At the early stages of treatment, the contaminant removal direct to the atmosphere of HA1BP is less than that of HA1, whereas the accumulation rate of contaminant lost to the atmosphere of HA1 drops off faster than that of HA1BP which means that after 170 hours of treatment the accumulation of contaminant lost to atmosphere in HA1BP becomes more than that of HA1. This difference then increases over time (Figure 6.59). The reason for this is that in HA1BP, air with lower temperature from outside surroundings enters the biopile from its centre, and not its surface. Hence, the temperature of the biopile surface region will not drop down to as low a value as that in HA1, and therefore the bioreaction at the biopile surface region in HA1BP is more active than that of HA1. This results in more contaminant transfer from the gaseous phase to the aqueous phase, and consequently reduces the diffusion/dispersion and advection to the surrounding atmosphere. The contaminant concentrations at the biopile surface region in both cases decreases with time, and thus contaminant transferred from other phases to the gaseous phase also decreases. However in Scenario HA1BP, because the air flow is from the biopile centre to its

surface, causing contaminant in the biopile centre to be transferred to the outer part by convection, this results in the accumulation rate of contaminant lost to atmosphere in HA1BP becoming greater than that of HA1.

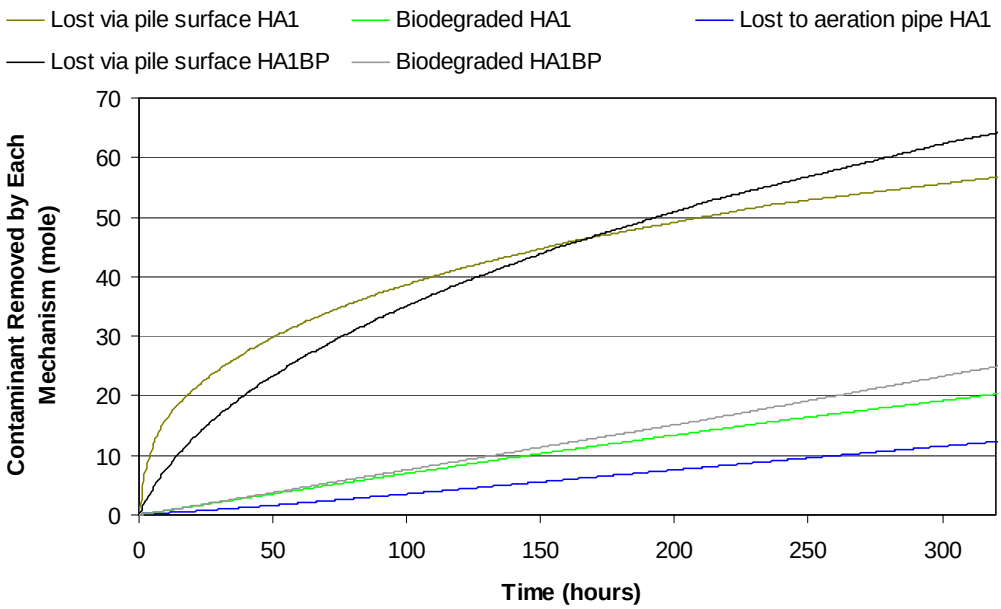

Figure 6.59 Comparison of contaminant removed by each mechanism in Scenario HA1 and HA1BP

On the other hand, although the air flux from the outside into the biopile of Scenario HA1BP is slightly more than that of HA1 (Table 6.11), the average biopile temperature decreases more in HA1 than in HA1BP. This may be because the air flux in HA1BP is distributed over a narrower range than that of HA1, so its impact on the overall bioreaction of the biopile may be less than HA1. Thus, the bioreaction in HA1BP is more intense than in HA1 (Figure 6.59), more heat is generated from bioreaction in HA1BP than in HA1 and the average biopile temperature of HA1BP is therefore higher than that of HA1 (Figure 6.60 and Figure 6.61).

Table 6.11 Instantaneous air flux across biopile surface in Scenario HA1 and HA1BP

	Instantaneous air flux across biopile surface (kg/s)					
	10 h	20 h	50 h	100 h	200 h	300 h
HA1 ($\times 10^{-6}$)	5.91	5.91	5.90	5.90	5.89	5.89
HA1BP ($\times 10^{-6}$)	6.08	6.08	6.08	6.08	6.07	6.07

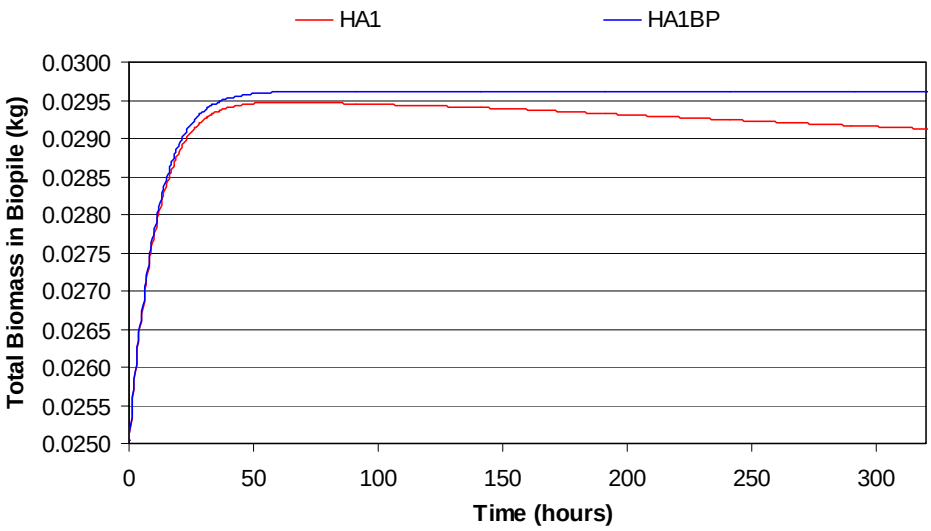

Figure 6.60 Comparison of total biomass in biopile in Scenario HA1 and HA1BP

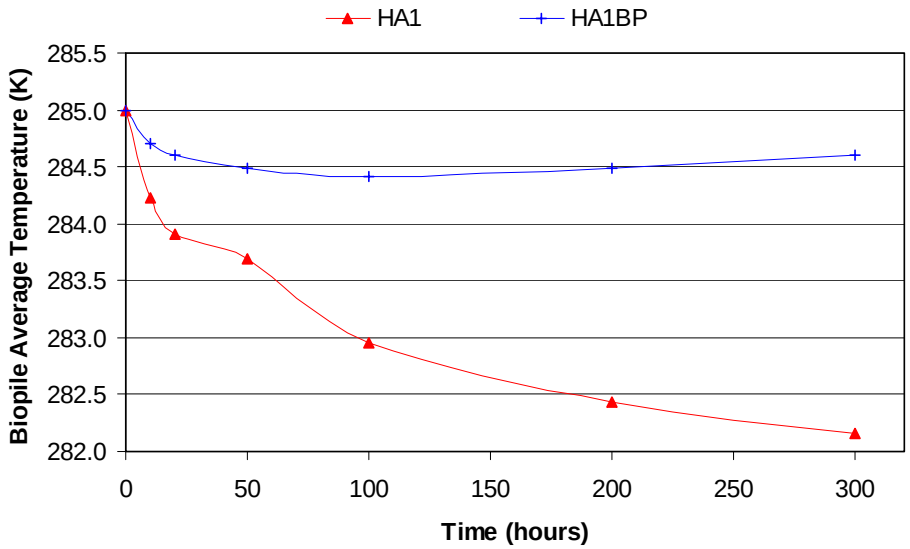

Figure 6.61 Comparison of average biopile temperature at different times in Scenario HA1 and HA1BP

The aerated cases with suction pressure have three methods of contaminant removal: loss to atmosphere, through aeration pipes, and biodegradation, whereas those with blowing pressure have only two means, with the absence of losses through aeration pipes. Thus, the overall performance of HA1BP is slightly worse than that of HA1, as shown in Figure 6.62.

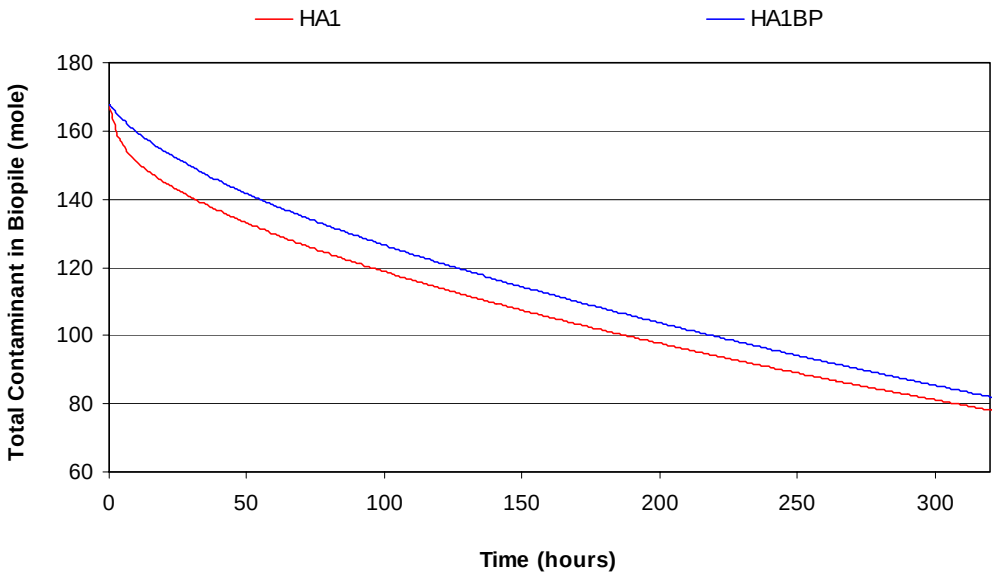

Figure 6.62 Comparison of total contaminant in biopile in Scenario HA1 and HA1BP

6.4.11 Blowing heated air

In comparison with suction aeration, an advantage of the blowing aeration condition is that the temperature of aerated air can be controlled. By blowing heated air into the biopile, the bioreaction can potentially be enhanced and the overall biopile treatment performance can be improved. In Scenario HA1BPHT, air pre-heated to 313 K was blown in the biopile. The simulation results are shown in Figure 6.63 to Figure 6.66. Although in HA1BPHT the heated air does not lead to a great improvement in biopile treatment, it does result in more biodegraded contaminant and better overall removal.

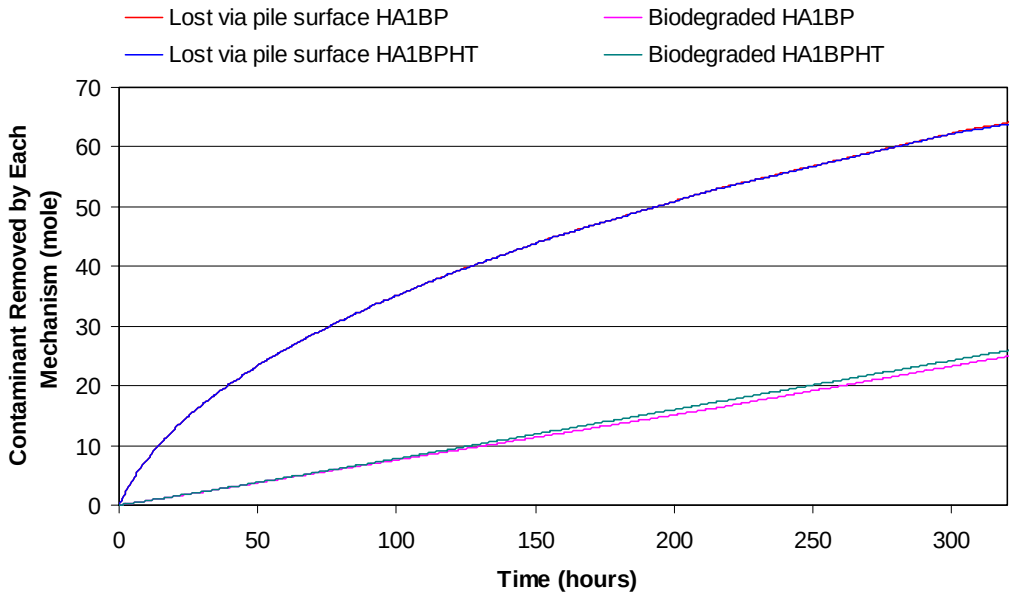

Figure 6.63 Comparison of contaminant removed by each mechanism in Scenario HA1BP and HA1BPHT

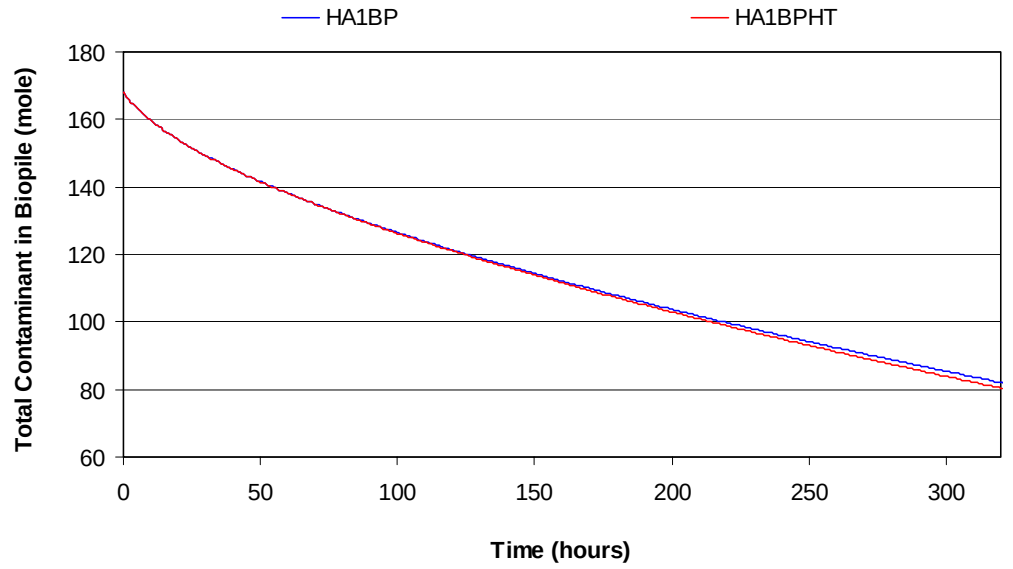

Figure 6.64 Comparison of total contaminant in biopile in Scenario HA1BP and HA1BPHT

A radical difference between Scenario HA1BPHT and the other simulations is that the biomass in this case kept growing with a very slow rate after 50 hours, unlike in most other cases where biomass levels decreased after reaching a maximum at approximately 50 hours. The warm up effect of the heated air on the biopile is clear. After decreasing slightly during the initial 50 hours of treatment, the average biopile temperature then continued to increase despite the air flux blowing into biopile being very small (around 6×10^{-6} kg air/s). Hence, if the blowing pressure is increased, a higher average

temperature of the biopile can be acquired and a greater level of biodegraded contaminant removal can be expected.

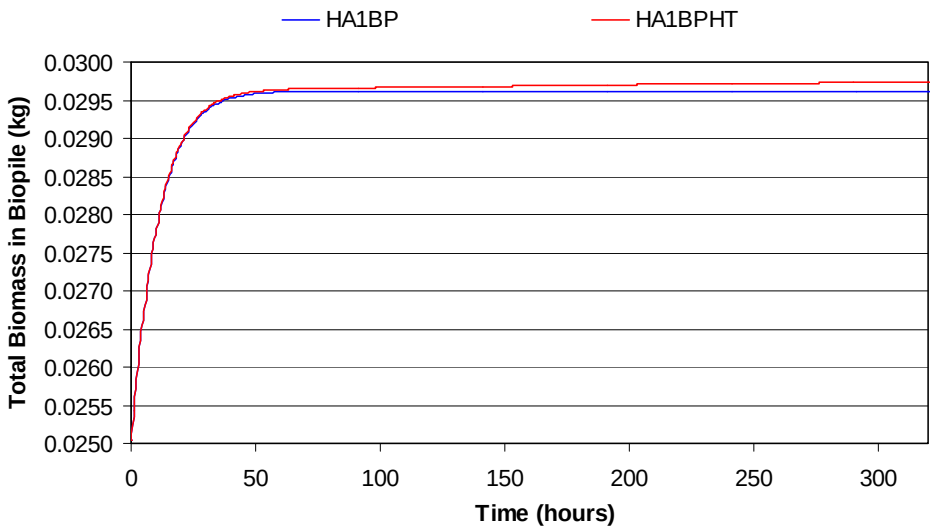

Figure 6.65 Comparison of total biomass in biopile in Scenario HA1BP and HA1BPHT

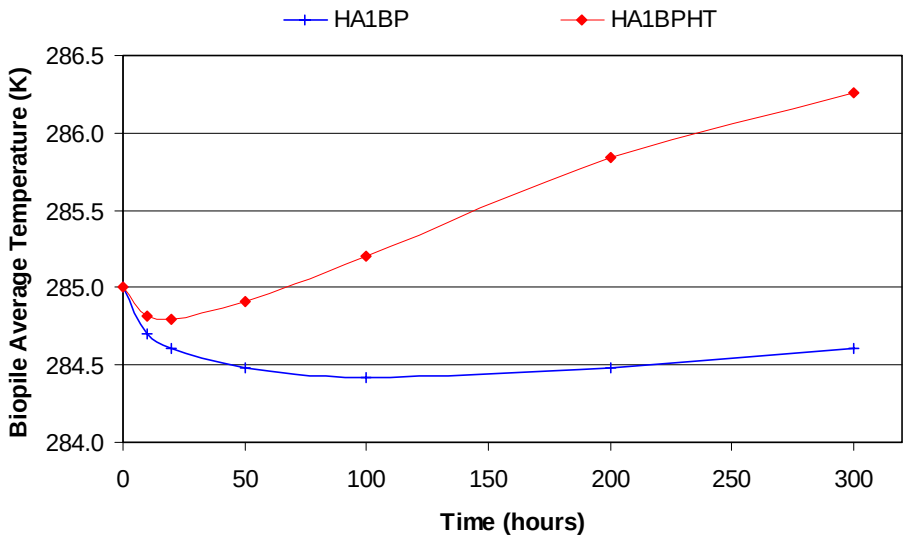

Figure 6.66 Comparison of average biopile temperature at different times in Scenario HA1BP and HA1BPHT

6.4.12 Multi-biopile simulation

Scenario MP5 simulates a multi-biopile case running with horizontal pipe aeration of 1000 Pa suction pressure. Although the resulting performances of the three contaminant removal approaches for each pile can be considered to have no different, the temperatures of each biopile do differ (Figure 6.67),

which can impact the biodegradation rate. The average biopile temperature of the biopile at the leeward side is smaller than that at the windward side (Table 6.12), which is opposite to the expected, and is another counter-intuitive result. This outcome is attributed to the fact that the air flow over the successive piles gives a greater pressure reduction in the lee of the upwind pile, reducing the flux of cool ambient air into it. This effect is lessened in the more downwind piles due to the sheltering effect of the others (Figure 6.68). Therefore, surrounding air can be more easily inhaled into a leeward biopile than a windward biopile, which ultimately results in a greater temperature drop.

Table 6.12 Average biopile temperature—multi-biopile simulation Scenario MP5

	Average biopile temperature (K)-					
	10 h	20 h	50 h	100 h	200 h	300 h
Left biopile	284.55	284.37	284.06	283.79	283.48	283.31
Middle biopile	284.53	284.33	283.99	283.68	283.31	283.08
Right biopile	284.52	284.31	283.97	283.65	283.25	283.01

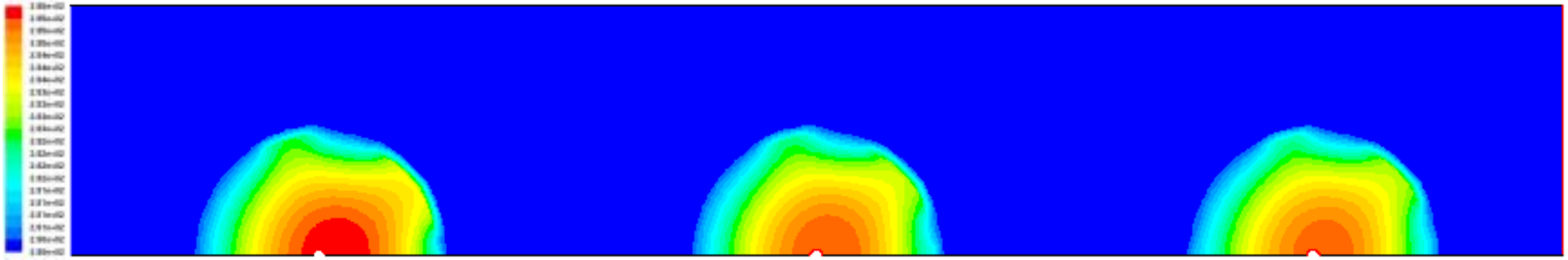

Figure 6.67 Temperature distribution of multi-biopile case at 320 hours

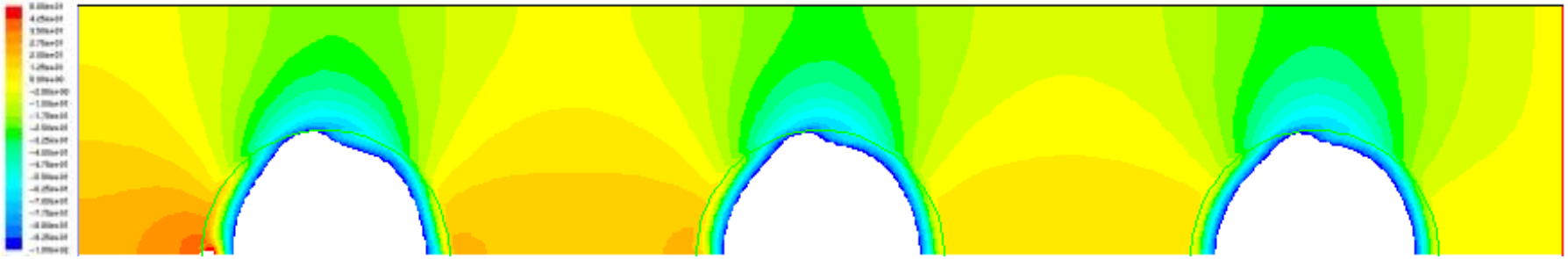

Figure 6.68 Pressure distribution of multi-biopile case at 320 hours

6.4.13 Optimal operational conditions

The effect and its action mechanism of changing every single term of the biopile operational conditions on the contaminant removal are discussed from Section 6.4.4 to Section 6.4.11, while the overall treatment efficiencies for each scenario at different times are listed in Table A.7 from which the general performance of scenarios can be compared directly and clearly.

As for the operation of a biopile, the most controllable factor among its operational conditions is the aeration method. This term includes meanings of four aspects: aerated or non-aerated, arrangement of aeration pipe, suction pressure or blowing pressure, and pressure intensity. The above sections give the discussion on the influences of these issues. It can be summarized that aeration can clearly enhance the treatment efficiency and the vertical pipe arrangement in 2D simulation which actually represents a slot along the pile is better than horizontal pipe (for example, at 250h, the removal efficiency of NA5, HA5 and VA 5 are 43.42%, 47.33% and 55.39% respectively.); suction pressure is more efficient than blowing pressure (refer to Table A.7) and as the increasing of the aeration pressure, the percentage of contaminant removal raises significantly (at 250h, 46.97% of HA1, 53.77% of HA1SP25 and 65.77% of HA1SP50).

Some other conditions which can also markedly affect the biopile performance include wind speed, biomass concentration and temperature.

A higher wind, as discussed in Section 6.4.4 , lead to more contaminant loss via pile surface and more biodegraded contaminant, but less loss to aeration pipes. However the overall efficiency of a biopile with a higher wind speed is also better than with lower wind speed, although it is very slightly (at 300h, 46.49% of NA1 vs. 47.91% of NA5, 51.41% of HA1 vs. 52.13% of HA5, 59.42% of VA1 vs. 60.84% of VA5).

Biomass concentration is an essential factor for biodegradation. As the initial biomass concentration reducing by one order of magnitude in this study (from 0.0162 kg/m^3 to 0.00162 kg/m^3), the mass of biodegraded contaminant reduces by tow orders of magnitude, the overall contaminant removal efficiency also decrease greatly (at 300h, from 52.13% of HA5 vs. 43.26% of HA5RB).

When running at a higher temperature which is not more than the optimal temperature for microbial growth, the biopile is more effective for contaminant removal than at a lower temperature and this advantage becomes more and more noticeable with the biopile progression (refer to Table A.7).

Compared with the above operational conditions, the contaminant interphase transfer rates have the worst controllability. Whilst, these transfer rates only make trivial effect on the biopile treatment. Even reduced by one order of magnitude, they can not lead to a change as much as 0.5% on the overall contaminant removal percentage (refer to Table A.7).

According to the analysis on the simulated scenarios, it can be concluded that for this study, the optimal operational conditions comprise higher wind speed (5 m/s), operational temperature close to the optimal temperature for microbial growth (initially 293K and 288K for biopile and ambient surrounding temperatures respectively), vertical aeration pipe with greater suction pressure (5000 Pa), and bigger biomass initial concentration (0.0162 kg/m^3). These optimal operational conditions can be extended to other relevant studies or used for directing lab experiments and field work, though the exact value of each condition may vary responding to the specialty of each unique case.

Chapter 7 Conclusions and Recommendations for Future Work

7.1 Conclusions

As stated in Chapter 1, the ultimate goal of this project was to investigate the feasibility of applying CFD techniques to develop a numerical model for aiding the design and operation of aerated/un-aerated biopiles for organic contaminated materials in the context of its ambient surroundings. This involved the development of relevant mathematical models, which described the physical, chemical and biological processes of the biopile treatment, incorporating such mathematic models into the commercial CFD package FLUENT, and creating complementary routines to accomplish comprehensive simulations.

In short, the aims of this research have been realised, ensuring a solid foundation for further development.

The results of a series of simulations were presented in Chapter 6 with the aim of establishing the potential usefulness of this CFD approach for application to biopile remediation treatments, and understanding the biopile performance under the interventions of surrounding environmental conditions. Such simulated scenarios covered various operating conditions, including different wind speeds, operating temperatures, initial biomass concentrations, aeration methods (including no aeration), contaminant interphase transfer rates and also a multi-biopile case. The CFD based approach gave the following reasonable results for all these simulations:

(1) The results showed that higher wind speeds could enhance the contaminant removed by losses to surroundings through the pile surfaces.

(2) By comparing the results of different aeration techniques, it can be concluded that the

efficiency of the aerated biopile was better than the non-aerated biopile, and furthermore that vertical pipe aeration was more efficient in contaminant removal than the horizontal pipe aeration method.

(3) Higher suction pressure can result in better efficiency regarding total contaminant removal and contaminant removed by losses to aeration pipes, but resulted in less removal by losses to surroundings.

(4) Blowing pressure aeration can result in greater levels of biodegraded contaminant and also more contaminant removal to surroundings during the later stages of treatment, whereas conversely suction pressure is more effective on contaminant removed by loss to surroundings during the early stages of treatment, and is more efficient in terms of on overall performance.

(5) The simulation results also demonstrated the clear dependence of bioreaction on temperature, as well as the way in which temperature could be significantly affected by wind blowing over the biopile, by the arrangement of aeration pipes and by the venting pressure used.

(6) Temperature distributions affected by fluid flow can not only influence biodegradation but also can further influence the contaminant transfer between gaseous and aqueous phases, and ultimately alter the contaminant removal by loss to atmosphere via gas flow.

Although the majority of results proved the expected theory, some counter-intuitive ones were obtained: faster average temperature decrease in the low wind velocity cases than in the higher wind velocity cases; more contaminant losses through the biopile surface encountered in the suction pressure aeration cases than in non-aerated cases in the early stages of treatment; and also greater cooling of piles downwind rather than those upwind in the multi-biopile treatment scenario. These results are reasonable despite being counter-intuitive, and indicate the potential useful insight gained by adopting the simulation approach used in this study to develop a greater understanding of the treatment process, which can then be applied when designing biopile systems.

Due to the complex nature of the biopile treatment systems, an extensive comparison of numerical results against experimental data was not possible during the time scale designated for this study. The

model also contains a large number of parameters, which influence the physics and behaviour of the whole treatment process. This ensures that the model is versatile but it also demands iteration periods to judge the effect of a change in a parameter on the biopile performance.

Although the simulation approach developed here was for an ex-situ bioremediation technique, it could also be implemented in the modelling of some in situ bioremediation processes, such as SVE and BV.

Further, it can also be concluded that the simulation approach derived from CFD is a novel way to examine the performance of a biopile in the context of its ambient surroundings. A potential function of this approach is to extend the scope of research object to the overall environmental impact, assessing not only the removal of contaminant from the biopile but also the use of energy and the effect on and of surrounding atmosphere. Thus simulations allow the total environmental footprint of the biopile to be considered.

One more advantage of this study is that the research methodology used in this study can be easily followed and repeated by others. To use this modelling approach, the author coded large amounts for fluid flow, scalars transport, heat transfer, species reaction and bioreaction, but eliminating the programming work for the numerical solutions by adopting an existing general CFD package. So that, in the author's opinion, this method allows the real problems to be focused on and sequentially can accelerate the research development in this field.

7.2 Recommendations for future work

Based on the work carried out in this thesis, the ability and full validation of the model can be tested by further simulations, and there are several aspects of the model that can be improved by further model development.

7.2.1 Further tests

(1) Multi-contaminant – this model was developed for a multi-contaminant bioremediation process,

whereas in the simulations of this work, only single contaminant cases were conducted. To model multi-contaminant cases, a similar procedure to that of the single contaminant case, can be followed to establish a model for each contaminant, and models for all different contaminants can then be solved simultaneously.

(2) Gas density – in this study, the density of gaseous phase was set to be constant. This approach was selected in order to incorporate with proper boundary conditions in FLUENT, and ameliorate computational convergence. Although this method was proved to be a reasonable and practical assumption, it is also worth considering the nature compressibility of gas in this model, especially when modelling more intense aeration pressure boundary conditions. In such cases, gas velocity may be no longer slow enough to ensure the validity of incompressible assumptions.

(3) More complex bioreaction model – as described previously, simulations on the bioreaction rate in this study neglected the effects of oxygen and nutrients, and some inhibition functions. These features can be incorporated in subsequent simulations. Meanwhile, more resultants of bioreaction can also be considered. By collaborating with multi-contaminant modelling, more insightful numerical results can be obtained. For instance, oxygen consumption and carbon dioxide generation can be modeled as dynamic processes occurring during bioreaction, and these changes of mass can subsequently affect the gas flow.

(4) Validation by experiment – due to time restrictions, validation by comparison of numerical results against experiment data was not possible. However, this work is certainly necessary and can reliably prove whether the model is correct and accurately simulates reality. Furthermore, many parameters used in this study were arbitrary, and real experimental data can offer reliable parameters for an actual scenario.

(5) 3D simulation – this may be obligatory for some biopile cases whose geometry and aeration settings can not be properly simplified to a 2D form. The modelling approach adopted by this study could be easily extended from a 2D simulation to 3D simulation. However, it is important to note that 3D simulations require significantly more computational time and resources than

2D cases, which restricts the potential use of 3D modelling.

7.2.2 Model developments for more complex features

(1) Water, moisture and vapour – in addition to gas and heat transfer between the biopile system and its surroundings, water can be introduced as a material than transfers from one phase to another. There are several mechanisms of water transfer. These include: water accumulation within a biopile due to rainfall; moisture loss of the biopile by evaporation taking place at the pile surface; and gas flow through the surroundings as well as biopile itself resulting in humidity transfer. The water exchange (either in aqueous phase or in gaseous phase) has an important influence not only on the biopile's mass balance, but also its heat balance. Foremost, water loss or gain directly changes the contaminant concentration, and consequentially affects the contaminant interphase transfer. Furthermore, the occurrence of evaporation and/or condensation can affect both temperature and the energy balance. Hence, water transfer is a very significant aspect that should be integrated within the current model, which could potentially be accomplished by incorporating suitable UDFs in FLUENT, if reliable mathematic models are available.

(2) Heat radiation – a suitable heat radiation model, though not considered in this study, can incorporate into simulations for more comprehensive modelling. The simplest empirical model for heat radiation described in Chapter 1 could be adopted and implemented by UDFs if more sophisticated models prove too difficult to assemble.

(3) Parameters at different temperature – some parameters of this model vary with temperature, despite being set as constant in this study. Such parameters are primarily the chemical or physical properties of matters, such as Henry's coefficient of the contaminant, vapour pressure, and possibly the contaminant interphase transfer rate. By considering the relationship of these parameters and temperate, the model can produce more accurate results.

(4) Mobile oleic phase – in this study, in order to simplify the whole system and save computational resources, the oleic phase was treated as immobile. In the majority of cases, this

assumption is valid, however under some circumstances, the oleic phase is highly saturated and can flow through the soil. In such cases, the oleic phase should be defined as a real phase and its flow governing equations should be solved in a similar way as those modelling the gaseous and aqueous phase flows.

(5) More dynamic models on biodegradation – a number of dynamic models for biodegradation were introduced in Chapter 1, though only the Monod type expression was adopted in this study. It would be preferable to integrate all of these models in the programme, which would allow future researchers to select either one for a special case, or compare the results of each dynamic model.

(6) Turbulent flow – this study only accounts for laminar flows, which has been proved as a valid assumption for fluid flow within the biopiles for all the simulated scenarios. However, flow in the surroundings of the biopile may in fact be turbulent, and if aeration is more intense, the laminar assumption for flow in a porous media might no long be valid, and consequently an inertial loss on momentum would occur. Hence, designing for turbulent flow and an inertial loss is preferred for a strong fluid flow case simulation.

In addition to the suggested works introduced above, two further aspects of study are also worth subsequent investigation. Firstly, implementing the simulation approach to model in situ bioremediation applications in order to test the feasibility of the modelling approach to a broader extent; and secondly, linking the mathematical models formulated in this study with a variety of CFD software packages other than FLUENT, to determine whether other softwares may be more suitable and capable of simulating the model developed in this study.

References

1. Campagnolo, J. F.; Akgerman, A., Modeling of soil vapor extraction (SVE) systems - part I and part II. *Waste Management* **1995,** *15*, 379-397.

2. Kaluarachchi, J. J.; Mesbah-Ul Islam, K. M., Thermal venting to recover less-volatile hydrocarbons from the unsaturated zone, 1. Theory. *Journal of Contaminant Hydrology* **1995,** *17*, (293-311).

3. Mesania, F. A.; Jennings, A. A., Modeling soil pile bioremediation. *Environmental Modelling & Software* **2000,** *15*, 411-424.

4. Dupont, R. R.; Bruell, C. J.; Marley, M. C.; Downey, D. C.; Norris, R. D.; Huling, S. G.; Pivetz, B., *Innovative Site Remediation Technology*. 1998; Vol. 1.

5. L.Li; Cunningham, C. J.; Pas, V.; Philp, J. C.; Barry, D. A.; Anderson, P., Field trial of a new aeration system for enhancing biodegradation in a biopile. *Waste Management* **2004,** *24*, 127-137.

6. Cookson, J. T., *Bioremediation Engineering, Design and Application*. McGraw-Hill, Inc.: 1995.

7. Martin, I.; Bardos, P., *A review of Full Scale Treatment Technologies for the Remediation of Contaminated soil.* EPP Publications: Lansing MI, 1996.

8. Patterson, B. M.; Davis, G. B.; Briegel, D., Use of respirometry Test to Monitor Bioventiong Remediation of Hydrocarbon Contaminated Soil. In *Contaminated Site Remediation: Challenges posed by Urban and Industrial Contaminants*, Johnston, C. D., Ed. CSIRO: Perth Australia, 1999.

9. Buchanan, M.; Gilessman, S. R., How compost fertilization affects soil nitrogen and crop yield. *Biocycle* **1991,** *32*, 72-76.

10. Garcia, C.; Gernandez, T.; Costa, F., Composted vs. uncomposted organics. *Biocycle* **1992,** *33*, 70-72.

11. Golueke, C. G., *Composting-A Study of the Process and its Principles*. Rodale Press: Emmaus, PA, 1973.

12. Schlegel, A. J., Effect of composted manure on soil chemical properties and nitrogen use by gain sorghum. *Journal of Production Agriculture* **1992,** *5*, 153-157.

13. Wilson, G. B.; Dalmat, D., Measuring compost stability. *Biocycle* **1986,** *27*, 34-37.

14. U.S. Environmental Protection Agency *How to evaluate alternative cleanup technologies for underground storage tank sites. A guide for corrective action plan reviewers*; EPA 510-B-95-007; Washington, DC, 1995.

15. von Fahnestock, F. M.; Smith, L. A.; Wickramanayake, G. B.; Place, M. C.; Kratzke, R. J.; Major, W. R.; M.Walker, A.; Wollenberg, J. P.; Carsley, M. J.; Dinh, P. V.; Ta, N. T. *Technical Memorandum: Biopile Design and Constrauction Manual*; TM-2189-ENV; Naval Facilities Engineering Service Center: Port Hueneme, CA, 1996.

16. Diaz, M. J.; Madejon, E.; Lopez, F.; Lopez, R.; Cabrera, F., Optimization of the rate vinasse/grape marc for co-composting process. *Process Biochemistry* **2002,** *37*, 1143-1150.

17. Kulcu, R.; Yaldiz, O., Determination of aeration rate and kinetics of composting some agricultural wastes. *Bioresource Technology* **2004,** *93*, 49-57.

18. Rynk, R.; Kamp, M.; Willson, G. B.; Singley, M. E.; Richard, T. L.; Kolega, J. J.; Gouin, F. R.; Laliverty, L.; kay, D.; Murpy, D. W.; Hoitink, H. A. J.; Brinton, W. F., *On-Farm Composting Handbook*. North Regional Agricultural Engineering Service: Ithaca, NY, USA, 1992.

19. Brodie, H. L.; Carr, L. E.; Condon, P., A comparison of static pile and turned windrow methods for poultry litter compost production. . *Compost Science and Utilization* **2000,** *8*, 178-189.

20. Haug, R. T., *The Practical Handbook of Composting Engineering*. Lewis Publishers: Boca Raton, FL, USA, 1993.

21. Wiley, J. S.; Pierce, G. W. In *A preliminary study of high rate composting*, Proc. Am. Soc. Civil Engineering, 1995; 1995; pp 1-28.

22. Keener, H. M.; Elwell, D. L.; Ekinci, K.; Hoitink, H. A. J., Composting and value-added utilization of manure from a swine finishing facility. *Compost science & utilization* **2001,** *9*, (4), 312-321.

23. Vining, M. A. Bench-Scale Compost Reactors System and The Self Heating Capabilities. Texas A&M University, 2002.

24. Troeh, F. R.; Thompson, L. M., *Soil and Soil Fertility*. Iowa State University Press: 2005.

25. NFESC *Biopile Remediation*; Naval Facilities Engineering Service Center: 2004.

26. Liang, C.; Das, K. C.; McClendon, R. W., The influence of temperature and moisture contents regimes on the aerobic microbial activity of a biosolids composting blend. *Bioresource Technology* **2003,** *86*, 131-137.

27. Bari, Q. H.; Koening, A., Effect of air recirculation and reuse on composting of organic solid waste. *Resources Conservation and Recycling* **2001,** *33*, 93-111.

28. Barrington, S.; Choiniere, D.; Trigui, M.; Knight, W., Compost convective airflow under passive aeration. *Bioresource Technology* **2003,** *86*, 259-266.

29. Fernandes, L.; Zhan, W.; Patni, N. K.; Jui, P. Y., Temperature distribution and variation in passively aerated static compost piles. *Bioresource Technology Journal* **1994,** *48*, (3), 257-263.

30. Sartaj, M.; Fernandes, L.; Patni, N. K., Performance of forced, passive and natural aeration methods for composting manure slurries. *Transactions of the ASAE* **1997,** *40*, (2), 457-463.

31. Diaz, L. F.; Savage, G. M.; Eggerth, L. L.; Golueke, C. G., *Composting and Recycling*. Lewis Publishers: Boca Raton, FL, USA, 1993.

32. Zhu, N. W.; Deng, C. Y.; Xiong, Y. Z.; Qian, H. Y., Performance characteristics of three aeration systems in the swine manure composting. *Bioresource Technology* **2004,** *95*, (3), 319-326.

33. Shi, W.; Norton, J. M.; Miller, B. E.; Pace, M. G., Effects of aeration and moisture during windrow composting on the nitrogen fertilizer values of dairy waste composts. *Applied Soil Ecology* **1999,** *11*, (1), 17-28.

34. Rhykerd, R.; Crews, B.; McInnes, K.; Weaver, R. W., Impact of bulking agents, forced aeration, and tillage on remediation of oil-contaminated soil. *Bioresource Technology* **1999,** *67*, (3), 279-285.

35. Hwang, E. Y.; Park, J. S.; Kim, J. D.; Namkoong, W., Effects of aeration mode on the composting of diesel-contaminated soil. *J. Ind. Eng. Chem.* **2006,** *12*, (5), 694-701.

36. Godoy-Faundez, A.; Antizar-Ladislao, B.; Reyes-Bozo, L.; Camano, A.; Saez-Navarrete, C., Bioremediation of contaminated mixtures of desert mining soil and sawdust with fuel oil by aerated in-vessel composting in the Atacama Region (Chile). *J. Hazard. Mater.* **2008,** *151*, (2-3), 649-657.

37. Yeung, P. Y.; Johnson, R. L.; Xu, J. G., Biodegradation of petroleum hydrocarbons in soil as affected by heating and forced aeration. *J. Environ. Qual.* **1997,** *26*, (6), 1511-1516.

38. Cegarra, J.; Alburquerque, J. A.; Gonzalvez, J.; Tortosa, G.; Chaw, D., Effects of the forced ventilation on composting of a solid olive-mill by-product ("alperujo") managed by mechanical turning. *Waste Management* **2006,** *26*, (12), 1377-1383.

39. Mason, I. G., Mathematical modelling of the composting process: A review. *Waste Management* **2006,** *26*, 3-21.

40. Scholwin, F.; Bidlingmaier, W. In *Fuzzifying the composting process: a new model based control strategy as a device for achieving a high grade and consistent product quality*, the Fourth International Conference of ORBIT Association on Biological Processing of Organics: Advances for a Sustainable Society, Perth, Australia, 2003; Perth, Australia, 2003; pp 739-751.

41. Seki, H., Stochastic modeling of composting processes with batch operation by the Fokker-Planck equation. *Transactions of ASAE* **2000,** *43*, (11), 169-179.

42. Kishimoto, M.; Preechaphan, C.; Yoshida, T.; Taguchi, H., Simulation of an aerobic composting of activated sludge using a statistical procedure. *NURCEN Journal* **1987,** *3*, 113-124.

43. Bongochgetsakul, N.; Ishida, T., A new analytical approach to optimizing the design of large-scale composting systems. *Bioresource Technology* **2008,** *99*, (6), 1630-1641.

44. Kodres, C. A., Coupled water and air flows through a bioremediation soil pile. *Environmental Modelling and Software* **1999,** *14*, 37-47.

45. Ekinci, K.; Keener, H. M.; Elwell, D. L.; Michel, F. C., Effects of aeration strategies on the composting process: Part II. Numerical modeling and simulation. *Transactions of the ASAE* **2005,** *48*, (3), 1203-1215.

46. Lin, Y. P.; Huang, G. H.; Lu, H. W.; He, L., Modeling of substrate degradation and oxygen consumption in waste composting processes. *Waste Management* **2008,** *28*, (8), 1375-1385.

47. Sole-Mauri, F.; Illa, J.; Magri, A.; Prenafeta-Boldu, F. X.; Flotats, X., An integrated biochemical and physical model for the composting process. *Bioresource Technology* **2007,** *98*, 3278-3293.

48. Kaiser, J., Modelling composting as a microbial ecosystem: A simulation approach. *Ecological Modelling* **1996,** *91*, (1-3), 25-37.

49. Stombaugh, D. P.; Nokes, S. E., Development of a biologically based aerobic composting simulation mode. *Transactions of ASAE* **1996,** *39*, (1), 239-250.

50. Richard, T. L.; Walker, L. P., Modeling the temperature kinetics of aerobic solid-state biodegradation. *Biotechnology Progress* **2006,** *22*, (1), 70-77.

51. Petric, I.; Selimbasic, V., Development and validation of mathematical model for aerobic composting process. *Chemical Engineering Journal* **2008,** *139*, (2), 304-317.

52. Robinzon, R.; Kimmel, E.; Krasovitski, B.; Avnimelech, Y., Estimation of Bulk Parameters of a Composting Process in Windrows. *Journal of agricultural engineering research* **1999,** *73*, 113-121.

53. Higgins, C. W.; Walker, L. P., Validation of a new model for aerobic organic solids decomposition: simulations with substrate specific kinetics. *Process Biochemistry* **2001,** *36*, (8-9), 875-884.

54. Keener, H. M.; Marugg, C.; Hansen, R. C.; Hoitink, H. A. J., Optimizing The Efficiency Of The Composting Process. *Science And Engineering Of Composting : Design, Environmental, Microbiological And Utilization Aspects* **1993**, 59-94.

55. Das, K.; Keener, H. M., Numerical model for the dynamic simulation of a large scale composting system. *Transactions Of The Asae* **1997,** *40*, (4), 1179-1189.

56. Gomes, A. P.; Pereira, F. A., Mathematical modelling of a composting process, and validation with experimental data. *Waste Management & Research* **2008,** *26*, (3), 276-287.

57. Briski, F.; Vukovic, M.; Papa, K.; Gomzi, Z.; Domanovac, T., Modelling of composting of food waste in a column reactor. *Chemical Papers* **2007,** *61*, (1), 24-29.

58. Ndegwa, P. M.; Thompson, S. A.; Merka, W. C., A dynamic simulation model of in-situ composting of caged layer manure. *Compost Science & Utilization* **2000,** *8*, (3), 190-202.

59. Ekinci, K.; Keener, H. M.; Elwell, D. L.; Michel, F. C., Effects of aeration strategies on the composting process: Part I. Experimental studies. *Transactions of the ASAE* **2004,** *47*, (5), 1697-1708.

60. Ekinci, K.; Keener, H. M.; Michel, F. C.; Elwell, D. L., Modeling composting rate as a function of temperature and initial moisture content. *Compost Science & Utilization* **2004,** *12*, (4), 356-364.

61. Finger, S. M.; Hatch, R. T.; Regan, T. M., Aerobic microbial growth in semi-solid matrices: heat and mass transfer limitations. *Biotechnology and Bioengineering* **1976,** *18*, 1193-1218.

62. Kim, D. S.; Kim, J. O.; Lee, J. J., Aerobic composting performance and simulation of mixed sludges. *Bioprocess Engineering* **2000,** *22*, (6), 533-537.

63. IUPAC, *Compendium of Chemical Terminology*. 2nd ed.; Blackwell Scientific Publications: Oxford, 1997.

64. Smith, R.; Eilers, R. G. *Numerical simulation of activated sludge composting*; EPA-600/2-8C-191; USEPA: Cincinnati, OH, USA, 1980.

65. Mohee, R.; White, R. K.; Das, K. C., Simulation model for composting cellulosic (Bagasse) substrates. *Compost Science & Utilization* **1998,** *6*, (2), 82-92.

66. Rosso, L.; Lobry, J. R.; Flandrois, J. P., An Unexpected Correlation Between Cardinal Temperatures Of Microbial-Growth Highlighted By A New Model. *J. Theor. Biol.* **1993,** *162*, (4), 447-463.

67. Ratkowsky, D. A.; Lowry, R. K.; McMeekin, T. A.; Stokes, A. N.; Chandler, R. E., Model For Bacterial Culture-Growth Rate Throughout The Entire Biokinetic Temperature-Range. *J. Bacteriol.* **1983,** *154*, (3), 1222-1226.

68. Nielsen, H.; Berthelsen, L., A model for temperature dependency of thermophilic composting process rate. *Compost Science & Utilization* **2002,** *10*, (3), 249-257.

69. Hamelers, H. V. M., Modeling composting kinetics: A review of approaches. *Reviews in Environmental Science & Bio/Technology* **2004,** *3*, 331-342.

70. Saucedocastaneda, G.; Gutierrezrojas, M.; Bacquet, G.; Raimbault, M.; Viniegragonzalez, G., Heat-Transfer Simulation In Solid Substrate Fermentation. *Biotechnology And Bioengineering* **1990,** *35*, (8), 802-808.

71. VanderGheynst, J. S.; Walker, L. P.; Parlange, J. Y., Energy transport in a high-solids aerobic degradation process: Mathematical modeling and analysis. *Biotechnology Progress* **1997,** *13*, (3), 238-248.

72. Bach, P. D.; nakasaki, K.; Shoda, M.; kubota, H., Thermal balance in composting operations. *Journal of Fermentation Technology* **1987,** *65*, (2), 199-209.

73. Nakasaki, K.; Kato, J.; Akiyama, T.; Kubota, H., A New Composting Model And Assessment Of Optimum Operation For Effective Drying Of Composting Material. *Journal Of Fermentation Technology* **1987,** *65*, (4), 441-447.

74. Vanlier, J. J. C.; Vanginkel, J. T.; Straatsma, G.; Gerrits, J. P. G.; Vangriensven, L., Composting Of Mushroom Substrate In A Fermentation Tunnel - Compost Parameters And A Mathematical-Model. *Neth. J. Agric. Sci.* **1994,** *42*, (4), 271-292.

75. Baehr, A. L.; Hult, M. F., Evaluation Of Unsaturated Zone Air Permeability Through Pneumatic Tests. *Water Resources Research* **1991,** *27*, (10), 2605-2617.

76. Massmann, J. W.; Madden, M., Estimating Air Conductivity And Porosity From Vadose-Zone Pumping Tests. *Journal Of Environmental Engineering-Asce* **1994,** *120*, (2), 313-328.

77. Edwards, K. B.; Jones, L. C., Air Permeability From Pneumatic Tests In Oxidized Till. *Journal Of Environmental Engineering-Asce* **1994,** *120*, (2), 329-347.

78. Mohr, D. H.; Merz, P. H., Application Of A 2d Air-Flow Model To Soil Vapor Extraction And Bioventing Case-Studies. *Ground Water* **1995,** *33*, (3), 433-444.

79. Schwarze, R.; Mothes, J.; Obermeier, F.; Schreiber, H., Numerical modeling of soil bioventing processes - Fundamentals and validation. *Transport in Porous Media* **2004,** *55*, (3), 257-273.

80. Roy, W. R.; Griffin, R. A., An Analytical Model For Insitu Extraction Of Organic Vapors. *J. Hazard. Mater.* **1991,** *26*, (3), 301-317.

81. Zaidel, J.; Russo, D., Analytical Models Of Steady-State Organic-Species Transport In The Vadose Zone With Kinetically Controlled Volatilization And Dissolution. *Water Resources Research* **1993,** *29*, (10), 3343-3356.

82. DePaoli, D. W., Design equations for soil aeration via bioventing. *Separations Technology* **1996,** *6*, (2), 165-174.

83. El-Beshry, M. Z.; Gierke, J. S.; Bedient, P. B., Practical modeling of SVE performance at a jet-fuel spill site. *Journal Of Environmental Engineering-Asce* **2001,** *127*, (7), 630-638.

84. Rahbeh, M. E.; Mohtar, R. H., Application of multiphase transport models to field remediation by air sparging and soil vapor extraction. *J. Hazard. Mater.* **2007,** *143*, 156-170.

85. Wilson, D. J.; Conrad, S. H.; Hagan, E.; Mason, W. R.; Peplinski, W. In *The pore level spatial distribution and saturation of organic liquids in porous media*, NWWA Conference on Petroleum hydrocarbons and organic chemicals in groundwater, Dublin, OH, 1988; National Water Well Association: Dublin, OH, 1988; pp 107-132.

86. Gannon, K.; Wilson, D. J.; Clarke, A. N.; Jr., R. D. M.; Clarke, J. H., Soil Clean Up by in-situ Aeration. II. Effects of Impermeable Caps, Soil Permeability, and Evaporative Cooling *Separation Science and Technology* **1989,** *24*, (11), 831-862.

87. Gomez-lahoz, C.; Rodriguez-maroto, J. M.; Wilson, D. J., Soil Clean Up by in-situ Aeration. VI. Effects of Variable Permeabilities. *Separation Science and Technology* **1991,** *26*, (2), 133-163.

88. Rodriguez-maroto, J. M.; Wilson, D. J., Soil Clean Up by in-situ Aeration. VII. High-Speed Modeling of Diffusion Kinetics *Separation Science and Technology* **1991,** *26*, (6), 743-760.

89. Rodriguez-maroto, J. M.; Gomez-lahoz, C.; Wilson, D. J., Soil Clean Up by in-situ Aeration. VIII. Effects of System Geometry on Vapor Extraction Efficiency *Separation Science and Technology* **1991,** *26*, (8), 1051-1064.

90. Osejo, R. E.; Wilson, D. J., Soil Clean Up by in-situ Aeration. IX. Diffusion Constants of Volatile Organics and Removal of Underlying Liquid *Separation Science and Technology,* **1991,** *26*, (12), 1433-1466.

91. Roberts, L. A.; Wilson, D. J., Soil Clean up by in-situ Aeration. XI. Cleanup Time Distributions for Statistically Equivalent Variable Permeabilities. *Separation Science and Technology* **1993,** *28*, (8), 1539-1559.

92. Mutch Jr., R. D.; Wilson, D. J., Soil Clean Up by in-situ Aeration. IV. Anisotropic Permeabilities *Separation Science and Technology* **1990,** *25*, (1), 1-29.

93. Benson, D. A.; Huntley, D.; Johnson, P. C., Modeling vapor extraction and general transport in the presence of NAPL mixtures and nonideal conditions. *Ground Water* **1993,** *31*, (3), 437-445.

94. Abriola, L. M.; Lang, J.; Rathfelder, K. *Michigan soil vapor extraction remediation (MISER) model: a computer program to model soil vapor extraction and bioventing of organic chemicals in unsaturated geological material*; U.S. Environmental Protection Agency: 1997.

95. Pennington, S. V.; Jimack, P. K.; McFarlane, K., Adaptive numerical simulation of the remediation of soil contamination by in-situ gas venting. *Computational Geosciences* **1999,** *3*, (2), 135-160.

96. Rathfelder, K.; Yeh, W. W. G.; Mackay, D., MATHEMATICAL SIMULATION OF SOIL VAPOR EXTRACTION SYSTEMS - MODEL DEVELOPMENT AND NUMERICAL EXAMPLES. *Journal of Contaminant Hydrology* **1991,** *8*, (3-4), 263-297.

97. Schulenberg, J. W.; Reeves, H. W., Axi-symmetric simulation of soil vapor extraction influenced by soil fracturing. *Journal of Contaminant Hydrology* **2002,** *57*, (3-4), 189-222.

98. Lingineni, S.; Dhir, V. K., Modeling Of Soil Venting Processes To Remediate Unsaturated Soils. *Journal Of Environmental Engineering-Asce* **1992,** *118*, (1), 135-152.

99. Stephanotos, B. N. In *Modeling the transport of gasoline vapors by an advective-diffusion unsaturated zone model*, Petroleum Hydrocarbons and Organic Chemicals in Groundwater: Prevention, Detection and Restoration, Houston, TX, 1988; National Water Well Association: Houston, TX, 1988; pp 591-611.

100. Baehr, A. L.; Hoag, G. E.; Marley, M. C., Removing volatile contaminants from the unsaturated zone by inducing advective air-phase transport *Journal of Contaminant Hydrology* **1989,** *4*, (1), 1-26.

101. Kaluarachchi, J. J.; Parker, J. C., Modeling multicomponent organic chemical transport in three-fluid-phase porous media. *Journal of Contaminant Hydrology* **1990,** *5*, (4), 349-374.

102. Webb, S. W.; Phelan, J. M., Effect of soil layering on NAPL removal behavior in soil-heated vapor extraction. *Journal Of Contaminant Hydrology* **1997,** *27*, (3-4), 285-308.

103. Travis, B. J.; Rosenberg, N. D., Modeling in situ bioremediation of TCE at Savannah River: Effects of product toxicity and microbial interactions on TCE degradation. *Environmental Science & Technology* **1997,** *31*, (11), 3093-3102.

104.Yoon, H.; Werth, C. J.; Valocchi, A. J.; Oostrom, M., Impact of nonaqueous phase liquid (NAPL) source zone architecture on mass removal mechanisms in strongly layered heterogeneous porous media during soil vapor extraction. *Journal of Contaminant Hydrology* **2008,** *100*, (1-2), 58-71.

105. Abriola, L. M., MODELING MULTIPHASE MIGRATION OF ORGANIC-CHEMICALS IN GROUNDWATER SYSTEMS - A REVIEW AND ASSESSMENT. *Environmental Health Perspectives* **1989,** *83*, 117-143.

106. Abriola, L. M.; Pinder, G. F., A Multiphase Approach To The Modeling Of Porous-Media Contamination By Organic-Compounds .2. Numerical-Simulation. *Water Resources Research* **1985,** *21*, (1), 19-26.

107. Reeves, H. W.; Abriola, L. M., AN ITERATIVE COMPOSITIONAL MODEL FOR SUBSURFACE MULTIPHASE FLOW. *Journal of Contaminant Hydrology* **1994,** *15*, (4), 249-276.

108. Abriola, L. M.; Chen, Y. M., Mathematical modeling of BTX: Biotransformation and transport in the subsurface. *Environmental Health Perspectives* **1995,** *103*, 85-88.

109. Rathfelder, K. M.; Lang, J. R.; Abriola, L. M., A numerical model (MISER) for the simulation of coupled physical, chemical and biological processes in soil vapor extraction and bioventing systems. *Journal of Contaminant Hydrology* **2000,** *43*, (3-4), 239-270.

110. Rathfelder, K. M.; Abriola, L. M.; Taylor, T. P.; Pennell, K. D., Surfactant enhanced recovery of tetrachloroethylene from a porous medium containing low permeability lenses - 2. Numerical simulation. *Journal of Contaminant Hydrology* **2001,** *48*, (3-4), 351-374.

111. Bradford, S. A.; Rathfelder, K. M.; Lang, J.; Abriola, L. M., Entrapment and dissolution of DNAPLs in heterogeneous porous media. *Journal of Contaminant Hydrology* **2003,** *67*, (1-4), 133-157.

112. Phelan, T. J.; Lemke, L. D.; Bradford, S. A.; O'Carroll, D. M.; Abriola, L. M., Influence of textural and wettability variations on predictions of DNAPL persistence and plume development in saturated porous media. *Adv. Water Resour.* **2004,** *27*, (4), 411-427.

113. Taylor, T. P.; Rathfelder, K. M.; Pennell, K. D.; Abriola, L. A., Effects of ethanol addition on micellar solubilization and plume migration during surfactant enhanced recovery of tetrachloroethene. *Journal of Contaminant Hydrology* **2004,** *69*, (1-2), 73-99.

114. Lemke, L. D.; Abriola, L. M.; Goovaerts, P., Dense nonaqueous phase liquid (DNAPL) source zone characterization: Influence of hydraulic property correlation on predictions of DNAPL infiltration and entrapment. *Water Resources Research* **2004,** *40*, (1).

115. Mesbah-Ul Islam, K. M.; Kaluarachchi, J. J., Thermal venting to recover less-volatile hydrocarbons from the unsaturated zone, 2. Model applications. *Journal of Contaminant Hydrology* **1995,** *17*, 313-331.

116. Mohammed, N.; Allayla, R. I., Modeling transport and biodegradation of BTX compounds in saturated sandy soil. *J. Hazard. Mater.* **1997,** *54*, (3), 155-174.

117. El-Kadi, A. I., Modeling hydrocarbon biodegradation in tidal aquifers with water-saturation and heat inhibition effects. *Journal Of Contaminant Hydrology* **2001,** *51*, (1-2), 97-125.

118. Huang, Y. F.; Huang, G. H.; Wang, G. Q.; Lin, Q. G.; Chakma, A., An integrated numerical and physical modeling system for an enhanced in situ bioremediation process. *Environmental Pollution* **2006,** *144*, (3), 872-885.

119. Prommer, H.; Barry, D. A.; Davis, G. B., A one-dimensional reactive multi-component transport model for biodegradation of petroleum hydrocarbons in groundwater. *Environmental Modelling & Software* **1999,** *14*, (2-3), 213-223.

120. Prommer, H.; Davis, G. B.; Barry, D. A., Geochemical changes during biodegradation of petroleum hydrocarbons: field investigations and biogeochemical modelling. *Organic Geochemistry* **1999,** *30*, (6), 423-435.

121. Barry, D. A.; Prommer, H.; Miller, C. T.; Engesgaard, P.; Brun, A.; Zheng, C., Modelling the fate of oxidisable organic contaminants in groundwater. *Adv. Water Resour.* **2002,** *25*, (8-12), 945-983.

122. Zysset, A.; Stauffer, F.; Darcos, T., MODELING OF REACTIVE GROUNDWATER TRANSPORT GOVERNED BY BIODEGRADATION. *WATER RESOURCES RESEARCH* **1994,** *30*, (8), 2423-2434.

123. Gallo, C.; Manzini, G., 2-D numerical modeling of bioremediation in heterogeneous saturated soils. *Transport In Porous Media* **1998,** *31*, (1), 67-88.

124. Rashid, M.; Kaluarachchi, J. J., A simplified numerical algorithm for oxygen- and nitrate-based biodegradation of hydrocarbons using Monod expressions. *Journal Of Contaminant Hydrology* **1999,** *40*, (1), 53-77.

125. Mulder, H.; Breure, A. M.; Rulkens, W. H., Prediction of complete bioremediation periods for PAH soil pollutants in different physical states by mechanistic models. *Chemosphere* **2001,** *43*, (8), 1085-1094.

126. Li, K. Y.; Xu, T.; Cawley, W. A.; Colapret, J. A.; Bonner, J. S.; Ernest, A.; Verramachaneni, P. B., Field-Test And Mathematical-Modeling Of Bioremediation Of An Oil-Contaminated Soil .2. Mathematical-Modeling. *Waste Management* **1994,** *14*, (7), 571-579.

127. Cornelissen, G.; Sijm, D., An energy budget model for the biodegradation and cometabolism of organic substances. *Chemosphere* **1996,** *33*, (5), 817-830.

128. Barnes, D. L.; McWhorter, D. B., Uncertainty in predicting the rate of mass removal created by soil vapor extraction systems. *Journal of Soil Contamination* **2000,** *9*, (1), 13-29.

129. Furman, A., Modeling coupled surface-subsurface flow processes: A review. *Vadose Zone Journal* **2008,** *7*, (2), 741-756.

130. Datta, A. K., Porous media approaches to studying simultaneous heat and mass transfer in food processes. I: Problem formulations. *Journal of food engineering* **2007,** *80*, 80-95.

131. Vafai, K., Convective flow and heat transfer in variable porosity media. *Jorunal of fluid Mechanics* **1984,** *147*, 233-259.

132. Vafai, K.; Tien, C. L., Boundary and inertia effects on flow and heat transfer in porous media. *International Journal of Heat and Mass Transfer* **1981,** *24*, (195-203).

133. Khaled, A.-R. A.; Vafai, K., The role of porous media in modeling flow and heat transfer in biological tissues. *International Journal of Heat and Mass Transfer* **2003,** *46*, 4989-5003.

134. Lian, G. P.; Thiru, A.; Parry, A.; Moore, S., CFD simulation of heat transfer and polyphenol oxidation during tea fermentation. *Computers And Electronics In Agriculture* **2002,** *34*, (1-3), 145-158.

135. Pak, A.; Mohammadi, T.; Hosseinalipour, S. M.; Allahdini, V., CFD modeling of porous membranes. *Desalination* **2008,** *222*, (1-3), 482-488.

136. Saidi, M. S.; Hajaligol, M. R.; Mhaisekar, A.; Subbiah, M., A 3D modeling of static and forward smoldering combustion in a packed bed of materials. *Appl. Math. Model.* **2007,** *31*, (9), 1970-1996.

137. FLUENT, *FLUENT 6.2 User's Guide*. Lebanon, NH, USA, 2005.

138. Hubbert, M. K., The theory of ground water motion. *Journal of geology* **1940,** *48*, 785-944.

139. Bear, J., *Dynamics of fluids in porous media*. Elsevier: New York, 1972.

140.Botset, A. G., Flow of gas-liquid mixtures through consolidated sand *Trans. A. I. M. E.* **1940,** *136*, 91-108.

141. Richards, L. A., Capillary conduction of liquids in porous mediums. *Physics* **1931,** *1*, 318-333.

142. van Genuchten, M. T., A closed-form equation for predicting the hydraulic conductivity of

unsaturated soils. *Soil Sci. Soc. AM. J.* **1980,** *44*, 892-898.

143. Parker, J. C.; Lenhard, R. J.; Kuppusamy, T., A parametric model for constitutive properties governing multiphase flow in porous media. *Water resources research* **1987,** *23*, (4), 618-624.

144. Kaluarachchi, J. J.; Parker, J. C., Multiphase flow with a simplified model for oil entrapment. *Trans. in porous media* **1992,** *7*, 1-14.

145. Adenekan, A. E.; Patzek, T. W.; Pruess, K., Modeling of multiphase transport of multicomponent organic contaminants and hear in the subsurface. *Water resources research* **1993,** *29*, (11), 3727-3740.

146. Schwarzenbach, R.; Gschwend, P. M.; Imboden, D. M., *Environmental Organic Chemistry*. John Wiley: New York, 1993.

147. Weber, W. J. J.; McGinley, P. M.; Katz, L. M., Sorption phenomena in subsurface systems: concepts, models and effects on contaminant fate and transport. *Water resources* **1991,** *25*, (5), 499-528.

148. Welty, J. R.; Wicks, C. E.; Wilson, R. E., *Fundamentals of momentum, heat, and mass transfer*. John Wiley & Sons: New York, 1984.

149. Weber, W. J. J.; DiGiano, F., *Process dynamics in environmental systems*. John Wiley: New York, 1996.

150. Roberts, P. V.; Hopkins, G. D.; Munz, C.; Riojas, A. H., Evaluation two-resistance models for air stripping of volatile organic organic contaminants in a countercurrent packed column. *Environmental Science & Technology* **1985,** *19*, (2), 164-173.

151. Munz, C.; Roberts, P. V., The ratio of gas-phase to liquid-phase mass transfer coefficients in gas-liquid contacting processes. In *Gas Transfer at water surfaces*, Brutsaert, W.; Jirka, G. H., Eds. D. Reidel Publishing Company: Dordrecht, 1983; pp 35-45.

152. Tchobanoglous, G.; Burton, F. L.; H. D. Stensel, *Wastewater engineering: treatment and reuse*. 4 ed.; McGraw-Hill Boston, 2002; Vol. 1.

153. Monod, J., The growth of bacterial cultures. *Annual review of microbiology* **1949,** *3*, 371-394.

154. Lawrence, A. W.; McCarty, P. L., Unified basis for biological treatment design and operation. Journal of the sanitary engineering division. *Proceedings of ASCE* **1970,** *96*, (SA3), 757-778.

155. Bailey, J. E.; Ollis, D. F., *Biochemical Engineering Fundamentals*. McGraw-Hill: New York, 1986.

156. Chen, Y. M.; Abriola, L. M.; Alvarez, P. J. J.; Anid, P. J.; Vogel, T. M., Modeling transport and biodegradation of benzene and toluene in sandy aquifer material: comparisons with experimental measurements. *Water resources research* **1992,** *28*, (7), 1847-2833.

157. Williamson, K. J.; McCarty, P. L., A model of substrate utilization by bacterial films. *Journal of the Water Pollution Control Federation* **1976,** *48*, (1), 9-24.

158. Huesemann, M. H.; Moore, K. O., The effect of soil type, crude oil type and loading, oxygen, and commercial bacteria on crude oil bioremediation kinetics as measured by soil respirometry. In *Hydrocarbon Bioremediation*, Hinchee, R. E.; Alleman, B. C.; Hoeppel, R. E.; Miller, R. N., Eds. Lewis Publishers: Boca Raton, 1994.

159. Mu, D. Y.; Scow, K. M., Effect of Trichloroethylene (TCE) and toluene concentrations of TCE and toluene biodegradation and the population density of TCE and toluene degraders in soil. *Applied and environmental microbiology* **1994,** *60*, (7), 2661-2665.

160. Speitel, G. E.; Alley, E. R., Bioremediation of unsaturated soils contaminated with chlorinated solvents. *J. Hazard. Mater.* **1991,** *28*, (81-90).

161. Wood, B. D.; Dawson, C. N.; Szecsody, J. E.; Streile, G. P., Modeling contaminant transport and biodegradation in a layered porous medium system. *Water resources research* **1994,** *30*, (6), 1833-1845.

162. Chiang, C. Y.; Salanitro, J. P.; Chai, E. Y.; Colthart, J. D.; Klein, C. L., Aerobic biodegradation

of benzene, toluene, and xylene in a sandy aquifer - data analysis and computer modeling. *Ground Water* **1989,** *27*, (6), 823-834.

163. Leahy, J. G.; Olsen, R. H., Kinetics of toluene degradation by toluene-oxidizing bacteria as a function of oxygen concentration, and the effect of nitrate. *FEMS MICROBIOLOGY ECOLOGY* **1997,** *23*, 23-30.

164. Fan, S.; Scow, K. M., Biodegradation of trichloroethylene and toluene by indigenous microbial populations in soil. *Applied and environmental microbiology* **1993,** *56*, (9), 1911-1918.

165. Holman, H.-Y.; Tsang, Y. W., Effects of soil moisture on biodegradation of petroleum hydrocarbons. In *In Situ Aeration: Air Sparging, Bioventing, and Related Remediation* Hinchee, R. E.; Miller, R. N.; Johnson, P. C., Eds. Battelle Press: Columbus, 1995; pp 323-332.

166. Davis, M. L.; Cornwell, D. A., *introduction to environmental engineering*. 3 ed.; WCB/McGraw-Hill: New York, 1998.

167. Chen, Y. M. Mathematical Modeling of In-Situ Bioremediation of Volatile Organics in Variably Saturated Aquifers. PHD, University of Michigan, 1996.

168. Spitz, K.; Moreno, J., *A practical guide to groundwater and solute transport modeling*. John Wiley & Sons. Inc: New York, 1996.

169. Drever, J. I., *The geochemistry of natural waters: surface and groundwater*. Prentice-Hall Inc.: New Jersey, 1997.

170. Millington, R. J.; Quirk, J. P., Permeability of porous solids. *Trans. of the Faraday society* **1961,** *57*, 1200-1207.

171. Kutilek, M.; Nielsen, D. R., *Soil Hydrology*. Margot Rohdenburg, Catena Verlag GmbH Reiskirchen, 1994.

172. Litchfield, C. D., In situ bioremediation: Basis and practices. In *Biotreatment of Industrial and Hazardous Waste*, Levin, M.; Gealt, M., Eds. McGraw-Hill: New York, 1993; pp 167-195.

173. Minkowycz, W. J.; Haji-Sheikh, A.; Vafai, K., On departure from local thermal equilibrium in porous media due to a rapidly changing heat source: the Sparrow number. *International journal of heat and mass transfer* **1999,** *42*, 3373-3385.

174. Rees, D. A. S.; Pop, I., Vertical free convection boundary layer flow in a porous medium using a thermal nonequilibrium model. *Journal of porous media* **2000,** *3*, 31-44.

175. Wong, W. S.; Rees, D. A. S.; Pop, I., Forced convection past a heated cylinder in a porous medium using a thermal nonequilibrium model: Finite Péclet number effects. *International Journal of Thermal Sciences* **2004,** *43*, 213-220.

176. Botterill, J. S. M., *Fluid-bed heat transfer*. Academic Press: London, 1975.

177. Michaelides, E. E., *Particles, bubbles and drops - their motion, heat and mass transfer*. World Scientific Publishing Co. Pte. Ltd.: Singapore, 2006.

178. Soo, S. L., *Fluid Dynamics of multiphase systems*. Blaisdell Publishing Company: Waltham, 1967.

179. Jennings, A. A., A vapor extractioin teaching module based on AIRFLOW/SVE. *Environmental Modelling & Software* **1998,** *12*, (4), 335-353.

180. Chandrakanthi, M.; Mehrotra, A. K.; Hettiaratchi, J. P. A., Thermal conductivity of leaf compost used in biofilters: An experimental and theoretical investigation. *Environmental pollution* **2005,** *136*, 167-174.

181. Ferziger, J. H.; Peric, M., *Computational methods for fluid dynamics*. New York, 1996; Vol. Springer-Verlag.

182. Sarker, M. A. Application of CFD to modelling local features in a river: free surface flow over broad-crested weir and modification of crump weir for fish passage. Cranfield University, 2000.

183. Yang, J. W.; Cho, H. J.; Choi, G. Y.; Lee, S. H. In *Cost-effective monitoring for a soil vapor*

extraction (SVE) system. A simplified modeling and gas sensor test, 2001; 2001; pp 201-210.

184. Mackay, D.; Shiu, W. Y.; Ma, K.-C., *Illustrated Handbook of Physical-Chemical Properties and Environmental Fate for Organic Chemicals*. CRC Press Inc: London, 1993.

185. Verschueren, K., *Handbook of Environmental Data on Organic Chemicals*. Chapman and Hall: London, 1983.

186. Harper, E.; Miller, F. C.; Macauley, B. J., Physical management and interpretation of an environmentally controlled composting ecosystem. *Australian Journal of Experimental Agriculture* **1992,** *32*, (5), 657-667.

Appendixes

A UDSs list

Table A.1 UDSs description and features

UDS NO.	Description	Phase depend on	transport?
0	Capillary pressure	Water	No
1	Benzene concentration in aqueous	Water	Yes
2	Benzene concentration in gas	Gas	Yes
3	Benzene concentration in solid	Mixture	No
4	Benzene concentration in organic	Mixture	No
5	Biomass concentration	Mixture	No
6	Temperature effect on reaction	Mixture	No

B UDFs

```
#include "udf.h"


/* soil property */

#define porosity 0.33         /*soil property porosity*/

#define sat_0_w 0.2           /*soil property residual water saturation*/

#define n 3.97                /* VAN GENUCHTEN parameter n, used for capillary pressure and relative conductivity*/

#define m (1-1/3.97)          /* VAN GENUCHTEN parameter m=1-1/n*/

#define alpha_w 0.00043       /* VAN GENUCHTEN parameter alpha  [1/Pa]*/

#define solid_density 1700000  /*g/m3*/

#define k_sat 6.8e-14         /* k: (intrinsci) permeability [L2]     K: hydraulic conductivity [l/T ]=k rho gravity/nu */

#define mu_w 1.0e-3           /* mu: (dynamic) viscosity [n s/m2] or [Pa s] */

#define mu_a 1.8e-5


/* oil volume fraction in pore */

#define saturo 0.05


/* equilibrium partition coefficient for benzene*/

#define KEgo  0.11481513 /* calculated  KE.xls*/

#define KEao  4.1339e-4  /* calculated  KE.xls*/

#define KEag  0.00360048  /* calculated  KE.xls*/

#define KEsa  0.00116   /* [(mg/g)/(mg/l)^(Fn)]*/

#define Fn 0.86


/* benzene  transfer coefficient */
```

```
#define Kao 5.79e-6

#define Kog 5.79e-4

#define Kag 5.79e-5

#define Kas 5.79e-5


/*material property */

#define Mben 78100.0     /*    benzene molar mass [mg/mole]*/

#define Mxylene 106200   /*    benzene molar mass [mg/mole]*/

#define rhoa_mole 55.56  /* water molar density [mole/l]*/

#define rhooM 10.07  /* oil molar density[mole/l]*/

#define rhoa 1000.0 /*water density [kg/m^3] or [g/liter] or [mg/cm^3]*/

#define rhog 1.225   /* gas density [kg/m^3] or [g/liter] or [mg/cm^3]*/

#define rhos 1700   /* soil density [kg/m^3] or [g/liter] or [mg/cm^3]*/

#define rhoo 880   /* oil density  */

#define Maqueous 0.018       /* aqueous molar mass [kg/mole]       */

#define Mgas 0.02896       /* gas molar mass  [kg/mole]      */


/* biodegradation for benzene                   */

#define kb  1.157e-5   /*    [1/T]*/

#define Ksb 0.5   /*    [mg/l]*/

#define Yb 0.5     /*    [g/g]*/


/* biomass decay */

#define Kd 1.157407e-6       /* biomass decay coefficient  [1/T]*/

#define Xmin 1e-6    /* min biomass concentration */

#define Xmax 0.02    /* max biomass concentration */

#define Latent_heat_water 2272  /* J/g  latent heat of water */

#define Bioheat 2e4  /* J/g TS estimated */
```

```
/* get zone id and domain id */
#define pile_zone_id 3     /*zone-id get from BC panel*/
#define pileground1_zone_id 13
#define pileground2_zone_id 14
#define outlet_zone_id 10
#define waterdomainid 3   /*domain-id get from Phases panel*/
#define gasdomainid 2
#define soildomainid 4

/*****************************************************************/
/*  calculate capillary pressure, based on water content                    */
/*  and temperature effect on bioreaction at the beginning of every time step      */
/*****************************************************************/

int last_ts = -1;   /*  Global variable.  Time step is never <0 */

DEFINE_ADJUST(cap_press_and_t_effect, domain)
{
 int curr_ts;
 curr_ts=N_TIME;
 if (last_ts != curr_ts)        /*check if it is the start of a time step*/
  {
   Thread *pile_thread_mixture;
   Thread *pile_thread_water;
   Thread *c_thread;
   Domain *waterdomain;
   int water_domain_index;
```

```
cell_t cell;


last_ts = curr_ts;


waterdomain=Get_Domain(waterdomainid);  /*** gets the domain ID for the water domain ***/

water_domain_index=PHASE_DOMAIN_INDEX(waterdomain); /*** this is the phase domain index for the waterdomain ***/

    /*** printf("waterdomain = %d \n", waterdomain);   ***/

pile_thread_mixture=Lookup_Thread(domain, pile_zone_id);  /*** this is the mixture thread id of the pile in the mixture domain ***/

pile_thread_water=THREAD_SUB_THREAD(pile_thread_mixture, water_domain_index);  /* this is the water thread id in the pile */


thread_loop_c(c_thread, waterdomain)  /*** loop over all threads in the water domain ***/

{

 if (c_thread == pile_thread_water)  /*if the thread id is the same as the water thread id in the pile then loop over all cells in this thread */

  {

   begin_c_loop(cell, c_thread)   /* calculate the capillary pressure*/

     {

      real a, sat_w, relsat_w, SSwm, SSwmn;


      a=C_VOF(cell, c_thread);


      if (a<=porosity*sat_0_w)

         a=porosity*sat_0_w+0.00000001;


      if (a>porosity)

         a=porosity;
```

```
          if (a>=porosity)
            C_UDSI(cell,c_thread,0)=0;
          else
          {
            /* capillary pressure */
            sat_w=a/porosity;
            relsat_w=(sat_w-sat_0_w)/(1-sat_0_w);
            SSwm=pow((1/relsat_w),(1/m))-1;
            SSwmn=pow(SSwm,(1/n));
            C_UDSI(cell,c_thread,0)=-1*SSwmn/alpha_w;

            /* T influence factor*/
            if (0<=C_T(cell,c_thread)<=353.15)
              C_UDSI(cell,THREAD_SUPER_THREAD(c_thread),6)=(C_T(cell,c_thread)-
273.15)*(80-(C_T(cell,c_thread)-273.15))/1600;
            else
              C_UDSI(cell,THREAD_SUPER_THREAD(c_thread),6)=0;
          }
        }
      end_c_loop(cell, c_thread)
    }
  }
 }
}

/************************************************************/
/* Source term for water flow momentum x direction          */
/************************************************************/
```

```
DEFINE_SOURCE(water_x,c,t,dS,eqn)
{
 real con, source, a, sat_w, relsat_w, Swm1, Swm2, rel_k_w;

 a=C_VOF(c,t);

 if (a<=porosity*sat_0_w)
  a=porosity*sat_0_w+0.00000001;

 if (a>porosity)
  a=porosity;

 if (a>=porosity)
   rel_k_w=1;
 else
  {sat_w=a/porosity;
  relsat_w=(sat_w-sat_0_w)/(1-sat_0_w);
  Swm1=1-pow(relsat_w,(1/m));
  Swm2=1-pow(Swm1,m);
  rel_k_w=sqrt(relsat_w)*pow(Swm2,2);
  }

 source = -1*C_VOF(c,t)*C_VOF(c,t)*C_U(c,t)*mu_w/(k_sat*rel_k_w)-
C_VOF(c,t)*C_UDSI_G(c,t,0)[0];
 dS[eqn] = -1*C_VOF(c,t)*C_VOF(c,t)*mu_w/(k_sat*rel_k_w);

 return source;
```

```
}


/************************************************************/
/* Source term for water flow momentum y direction          */
/************************************************************/

DEFINE_SOURCE(water_y,c,t,dS,eqn)
{

 real con, source, a, sat_w, relsat_w, Swm1, Swm2, rel_k_w;

 a=C_VOF(c,t);

 if (a<=porosity*sat_0_w)
  a=porosity*sat_0_w+0.00000001;

 if (a>porosity)
  a=porosity;

 if (a>=porosity)
   rel_k_w=1;
 else
  {sat_w=a/porosity;
  relsat_w=(sat_w-sat_0_w)/(1-sat_0_w);
  Swm1=1-pow(relsat_w,(1/m));
  Swm2=1-pow(Swm1,m);
  rel_k_w=sqrt(relsat_w)*pow(Swm2,2);
```

```
  }

  source = -1*C_VOF(c,t)*C_VOF(c,t)*C_V(c,t)*mu_w/(k_sat*rel_k_w)-
C_VOF(c,t)*C_UDSI_G(c,t,0)[1];
  dS[eqn] = -1*C_VOF(c,t)*C_VOF(c,t)*mu_w/(k_sat*rel_k_w);

  return source;
}

/************************************************************/
/* Source term for air flow momentum x direction            */
/************************************************************/

DEFINE_SOURCE(air_x,c,t,dS,eqn)
{
  real con, source, a, b,sat_w, relsat_w, relsat_a, Stm1, rel_k_a;

  b=C_VOF(c,t);   /* vol fraction of air */

  a=porosity-b;   /* vol fraction of water */

  if (a<=porosity*sat_0_w)
    a=porosity*sat_0_w+0.00000001;

  if (a>porosity)
    a=porosity;
```

```
 if (a>=porosity)
  {
   source=0;
   dS[eqn]=0;
  }
 else
  {
  sat_w=a/porosity;
  relsat_w=(sat_w-sat_0_w)/(1-sat_0_w);
  relsat_a=1-relsat_w;

  Stm1=1-pow(relsat_w,(1/m));

  rel_k_a=sqrt(relsat_a)*pow(Stm1,(2*m));

  source = -1*C_VOF(c,t)*C_VOF(c,t)*C_U(c,t)*mu_a/(k_sat*rel_k_a);
  dS[eqn] = -1*C_VOF(c,t)*C_VOF(c,t)*mu_a/(k_sat*rel_k_a);
  }

 return source;
}

/************************************************************/
/* Source term for water flow air y direction               */
/************************************************************/

DEFINE_SOURCE(air_y,c,t,dS,eqn)
```

```
{
 real con, source, a, b,sat_w, relsat_w, relsat_a, Stm1, rel_k_a;

 b=C_VOF(c,t);   /* vol fraction of air */

 a=porosity-b;   /* vol fraction of water */

 if (a<=porosity*sat_0_w)
  a=porosity*sat_0_w+0.00000001;

 if (a>porosity)
  a=porosity;

 if (a>=porosity)
  {
   source=0;
   dS[eqn]=0;
  }
 else
  {
  sat_w=a/porosity;
  relsat_w=(sat_w-sat_0_w)/(1-sat_0_w);
  relsat_a=1-relsat_w;

  Stm1=1-pow(relsat_w,(1/m));

  rel_k_a=sqrt(relsat_a)*pow(Stm1,(2*m));
```

```
   source = -1*C_VOF(c,t)*C_VOF(c,t)*C_V(c,t)*mu_a/(k_sat*rel_k_a);
   dS[eqn] = -1*C_VOF(c,t)*C_VOF(c,t)*mu_a/(k_sat*rel_k_a);
  }

 return source;
}



/************************************************************/
/* species source term for aqueous phase                    */
/************************************************************/

DEFINE_SOURCE(aqueous_CBT,c,t,dS,eqn)
{
 Thread *mt;
 Thread *gt;
 Domain *gd;
 int gas_domain_index;
 real sao, sag, sas, Bioab, source;

 mt=THREAD_SUPER_THREAD(t);

 gd=Get_Domain(gasdomainid);
 gas_domain_index=PHASE_DOMAIN_INDEX(gd);
 gt=THREAD_SUB_THREAD(mt, gas_domain_index);

 sao= Kao*(KEao * C_UDSI_M1(c,mt,4)-C_UDSI_M1(c,t,1));   /* Kao*(Keao*Xo-Xa)*/
 sag= Kag*(KEag * C_UDSI_M1(c,gt,2)-C_UDSI_M1(c,t,1));      /* Kag*(Keag*Xg-Xa)*/
```

```
 sas=    Kas*(pow(C_UDSI_M1(c,mt,3)/KEsa,1/Fn)/(rhoa_mole*Mben)-C_UDSI_M1(c,t,1));       /*
Kas*[(ws/kesa)^(1/n)/species molar mass/water molar density-Xa)*/



 Bioab=-
1/(Mben/1000000)*C_UDSI_M1(c,mt,5)*kb*C_UDSI(c,mt,6)*Maqueous*(C_UDSI_M1(c,t,1)/(C_U
DSI_M1(c,t,1)+Ksb/Mben/rhoa_mole));   /*bioab=Bac*Ma water molar mass */

 /*                                                                                    Bioab=-
1/(Mben/1000000)*C_UDSI_M1(c,mt,5)*kb*Maqueous*(C_UDSI_M1(c,t,1)/(C_UDSI_M1(c,t,1)+K
sb/Mben/rhoa_mole));  */    /*bioab=Bac*Ma  water  molar  mass  WITHOUT  TEMPERATURE
EFFECT*/



/*   source=porosity*(sao+sag+sas)*rhoa;  *//*porosity*E*water molar mass=porosity* water molar
density*(sao+sag+sas)*water molar mass=porosity *(sao+sag+sas)*water mass density*/

 source=porosity*(sao+sag+sas)*rhoa+Bioab;



 dS[eqn] = 0;



 return source;

}




/************************************************************/

/* Species source term for gas phase                        */

/************************************************************/



DEFINE_SOURCE(gas_C,c,t,dS,eqn)

{

 Thread *mt;

 Thread *wt;

 Domain *wd;

 int water_domain_index;
```

```
  real sga, sgo, source;

  mt=THREAD_SUPER_THREAD(t);

  wd=Get_Domain(waterdomainid);
  water_domain_index=PHASE_DOMAIN_INDEX(wd);
  wt=THREAD_SUB_THREAD(mt, water_domain_index);

  sga= -1*Kag*(KEag * C_UDSI_M1(c,t,2)-C_UDSI_M1(c,wt,1));
  sgo= -1*Kog*(C_UDSI_M1(c,t,2)/KEgo-C_UDSI_M1(c,mt,4));

  source=porosity*(sga*rhoa_mole*1000+sgo*rhooM*1000)*Mgas;  /* SI:  *1000 */

  dS[eqn] = 0;

  return source;
}



/************************************************************/
/* Species in solid and organic phases                      */
/* calculate at the end of every time step and record files  */
/************************************************************/

DEFINE_EXECUTE_AT_END(biomassT_in_a_and_species_in_o_and_s_and_files)
{
  /* variables for first function */
  Domain *md;
```

```
Thread *pmt;
Domain *wd;
Thread *pwt;
Domain *gd;
Thread *pgt;
Domain *sd;
Thread *pst;

int soil_domain_index;
int water_domain_index;
int gas_domain_index;

cell_t c;

real ssa, source_solid,a,soa, sog, source_organic, source_bio;

/* variables for second function */
Thread *pilegroundmt;
face_t f;
cell_t  c0;
Thread *t0;

/*variables for the third function */

FILE *fp1, *fp2, *fp3; /*file pointer*/
float outletinfile, biodegradeinfile, cinallt0, cinalltp;
real cinwater, cingas, cinsoil, cinorg;
```

```
/*Variables for the fourth function */

real conbiodeg,conoutlet,cpipeoutints;
Thread *outletmt, *outletgt;

/*variables for the fifth fucntion*/

int fun5;
real totalpipeout, biomass,cinall;

biomass=0.0;

cinwater=0.0;  /*3re function */
cingas=0.0;
cinsoil=0.0;
cinorg=0.0;

conbiodeg=0.0;  /*4th function */
conoutlet=0.0;

c0=-1;          /* 2nd funciton */
t0=NULL;

md = Get_Domain(1);   /* mixture domain if multiphase */  /*1st function */

wd=Get_Domain(waterdomainid);
water_domain_index=PHASE_DOMAIN_INDEX(wd);
```

```
  gd=Get_Domain(gasdomainid);

  gas_domain_index=PHASE_DOMAIN_INDEX(gd);


  sd=Get_Domain(soildomainid);

  soil_domain_index=PHASE_DOMAIN_INDEX(sd);


  pmt=Lookup_Thread(md, pile_zone_id);  /*** this is the mixture thread id of the pile in the mixture domain ***/


  /* FIRST FUNCTION: calculte the contaminant concentration in solid and organic and biomass */


  begin_c_loop(c,pmt)

   {

      pwt=THREAD_SUB_THREAD(pmt, water_domain_index);

      pgt=THREAD_SUB_THREAD(pmt, gas_domain_index);

      pst=THREAD_SUB_THREAD(pmt, soil_domain_index);


      /* calculate species in solid phase */


      if (C_UDSI(c,pwt,1)<0)

         a=0;

      else a=C_UDSI(c,pwt,1);


      ssa=                    -1*Kas*(pow(C_UDSI_M1(c,pmt,3)/KEsa,1/Fn)/(rhoa_mole*Mben)-
C_UDSI_M1(c,pwt,1));

      source_solid=porosity*ssa*rhoa_mole*1000; /* SI: rhoa_mole* 1000= 5556mole/cubic meter */

      C_UDSI(c,pmt,3)=                    source_solid                    *Mben*
CURRENT_TIMESTEP/solid_density+C_UDSI_M1(c,pmt,3);
```

```
      /* calculate species in organic phase */


      sog= Kog*(C_UDSI_M1(c,pgt,2)/KEgo-C_UDSI_M1(c,pmt,4));

      soa=-1* Kao*(KEao * C_UDSI_M1(c,pmt,4)-C_UDSI_M1(c,pwt,1));

      source_organic=porosity*(soa*rhoa_mole+sog*rhooM);


C_UDSI(c,pmt,4)=source_organic*CURRENT_TIMESTEP/(porosity*saturo*rhooM)+C_UDSI_M1(
c,pmt,4);


      /* biomass concentration */


    /*
source_bio=C_UDSI_M1(c,pmt,5)*(Yb*kb*(C_UDSI_M1(c,pwt,1)/(C_UDSI_M1(c,pwt,1)+Ksb/Mb
en/rhoa_mole))*(1-(C_UDSI_M1(c,pmt,5)/Xmax))-Kd*(1-(Xmin/C_UDSI_M1(c,pmt,5))));   */      /*
without T influence */


source_bio=C_UDSI_M1(c,pmt,5)*(Yb*kb*C_UDSI(c,pmt,6)*(C_UDSI_M1(c,pwt,1)/(C_UDSI_M1
(c,pwt,1)+Ksb/Mben/rhoa_mole))*(1-(C_UDSI_M1(c,pmt,5)/Xmax))-Kd*(1-
(Xmin/C_UDSI_M1(c,pmt,5))));    /*with T influence */

      C_UDSI(c,pmt,5)=C_UDSI_M1(c,pmt,5)+source_bio*CURRENT_TIMESTEP;


    /* part of THE FOURTH FUNCTION */



conbiodeg=conbiodeg+C_UDSI_M1(c,pmt,5)*C_UDSI(c,pmt,6)*(C_UDSI_M1(c,pwt,1)/(C_UDSI_
M1(c,pwt,1)+Ksb/Mben/rhoa_mole))*C_VOLUME(c,pmt);  /* With T effect */

    /*
conbiodeg=conbiodeg+C_UDSI_M1(c,pmt,5)*(C_UDSI_M1(c,pwt,1)/(C_UDSI_M1(c,pwt,1)+Ksb/
Mben/rhoa_mole))*C_VOLUME(c,pmt); */


   }

  end_c_loop(c,pmt)
```

```
conbiodeg=conbiodeg*1/(Mben/1000000)*kb*CURRENT_TIMESTEP;

/* SECOND FUNCTION: pile ground face uds value to cell value */

pilegroundmt=Lookup_Thread(md, pileground1_zone_id);

begin_f_loop(f,pilegroundmt)
  {
    if (BOUNDARY_FACE_THREAD_P(pilegroundmt))
    {
     c0 = F_C0(f,pilegroundmt);
     t0 = THREAD_T0(pilegroundmt);

     F_UDSI(f,pilegroundmt,3)=C_UDSI(c0,t0,3);
     F_UDSI(f,pilegroundmt,4)=C_UDSI(c0,t0,4);
     F_UDSI(f,pilegroundmt,5)=C_UDSI(c0,t0,5);

    }
 }
end_f_loop(f,pipemt)

pilegroundmt=Lookup_Thread(md, pileground2_zone_id);

begin_f_loop(f,pilegroundmt)
  {
    if (BOUNDARY_FACE_THREAD_P(pilegroundmt))
    {
     c0 = F_C0(f,pilegroundmt);
```

```
      t0 = THREAD_T0(pilegroundmt);


      F_UDSI(f,pilegroundmt,3)=C_UDSI(c0,t0,3);

      F_UDSI(f,pilegroundmt,4)=C_UDSI(c0,t0,4);

      F_UDSI(f,pilegroundmt,5)=C_UDSI(c0,t0,5);


    }

  }

 end_f_loop(f,pipemt)


 /* THIRD FUNCTION: create 3 record files if the previous time is 0.0 second */


 if(PREVIOUS_TIME==0.0)

  {

   if((fp1=fopen("outletandbio.txt","wt+"))==NULL)  /* create 1st file te record contaminant flow at at outlet boundary and biodegrade in pile */

    {

     printf("Cannot open file strike any key exit!");


    }


   fprintf(fp1,"T, cinwater, cingas, cinsoil, cinorg, cinall, totaloutlet, totalbiodegrade, totalpipeout, biomass, outletints, biodegradeints, pipeoutints\n");

   fprintf(fp1,"0.0 0.0 0.0 0.0 0.0 0.0 0.0 0.0 0.0 0.0 0.0 0.0 0.0 0.0\n");


   fclose(fp1);


   if((fp2=fopen("threetemp.txt","wt+"))==NULL)     /* a temporary file used to record tatal contaminant and total flowout and total degrade */
```

```
  {
    printf("Cannot open file strike any key exit!");

  }

  begin_c_loop(c,pmt)
  {
    pwt=THREAD_SUB_THREAD(pmt, water_domain_index);
    pgt=THREAD_SUB_THREAD(pmt, gas_domain_index);
    pst=THREAD_SUB_THREAD(pmt, soil_domain_index);

    /*calculate contaminant in each phases, degraded by bioreaction and biomass */

    cinwater=cinwater+C_UDSI_M1(c,pwt,1)*C_VOF_M1(c, pwt)*C_VOLUME(c,pmt);
    cingas=cingas+C_UDSI_M1(c,pgt,2)*C_VOF_M1(c, pgt)*C_VOLUME(c,pmt);
    cinsoil=cinsoil+C_UDSI_M1(c,pmt,3)*(1-C_VOF_M1(c, pwt)-C_VOF_M1(c, pgt))*C_VOLUME(c,pmt);
    cinorg=cinorg+C_UDSI_M1(c,pmt,4)*C_VOLUME(c,pmt);

  }
  end_c_loop(c,pmt)

  cinwater=cinwater*rhoa_mole*1000;
  cingas=cingas*rhog/Mgas;
  cinsoil=cinsoil/Mben*1000*rhos;
  cinorg=cinorg*saturo*porosity*rhooM*1000;

  cinallt0=cinwater+cingas+cinsoil+cinorg;
```

```
    cinalltp=cinallt0;


    outletinfile=0.0;

    biodegradeinfile=0.0;


    fprintf(fp2,"%e %e %e %e\n",cinallt0,cinalltp,outletinfile, biodegradeinfile);


    fclose(fp2);


    cinwater=0.0;

    cingas=0.0;

    cinsoil=0.0;

    cinorg=0.0;


    if((fp3=fopen("contaminantbalance.txt","wt+"))==NULL) /* data file to record contaminant status
along with the time */

     {

       printf("Cannot open file strike any key exit!");


     }


    fprintf(fp3,"T, cinwater, cingas, cinsoil, cinorg, cinall, totaloutlet, totalbiodegrade, totalpipeout,
biomass\n");


    fclose(fp3);

   }


   /* Fourth FUNCTION: Print to file to record contaimant flow at at outlet boundary and biodegrade
in pile */
```

```
outletmt=Lookup_Thread(md, outlet_zone_id);


begin_f_loop(f,outletmt)
  {
    if (BOUNDARY_FACE_THREAD_P(outletmt))
    {
     outletgt=THREAD_SUB_THREAD(outletmt, gas_domain_index);


     conoutlet=conoutlet+F_UDSI(f,outletgt,2)*CURRENT_TIMESTEP*F_FLUX(f,outletgt);
    }
 }
end_f_loop(f,pipemt)


conoutlet=conoutlet/Mgas;


 if((fp2=fopen("threetemp.txt","rt"))==NULL)  /* a temporary file used to record tatal contaminant and total flowout and total degrade */
  {
   printf("Cannot open file strike any key exit!");


  }
 rewind(fp2);
 fscanf(fp2,"%e%e%e%e",&cinallt0,&cinalltp,&outletinfile, &biodegradeinfile);
 fclose(fp2);


 outletinfile=outletinfile+conoutlet;
 biodegradeinfile=biodegradeinfile+conbiodeg;
```

```
begin_c_loop(c,pmt)
 {
  pwt=THREAD_SUB_THREAD(pmt, water_domain_index);
  pgt=THREAD_SUB_THREAD(pmt, gas_domain_index);
  pst=THREAD_SUB_THREAD(pmt, soil_domain_index);

  /*calculate contaminant in each phases, degraded by bioreaction and biomass */

  cinwater=cinwater+C_UDSI(c,pwt,1)*C_VOF(c, pwt)*C_VOLUME(c,pmt);
  cingas=cingas+C_UDSI(c,pgt,2)*C_VOF(c, pgt)*C_VOLUME(c,pmt);
  cinsoil=cinsoil+C_UDSI(c,pmt,3)*(1-C_VOF(c, pwt)-C_VOF(c, pgt))*C_VOLUME(c,pmt);
  cinorg=cinorg+C_UDSI(c,pmt,4)*C_VOLUME(c,pmt);
  biomass=biomass+C_UDSI(c,pmt,5)*C_VOLUME(c,pmt);
 }
end_c_loop(c,pmt)

 cinwater=cinwater*rhoa_mole*1000;
 cingas=cingas*rhog/Mgas;
 cinsoil=cinsoil/Mben*1000*rhos;
 cinorg=cinorg*saturo*porosity*rhooM*1000;
 cinall=cinwater+cingas+cinsoil+cinorg;

 cpipeoutints=cinalltp-cinall-conoutlet-conbiodeg;

 totalpipeout=cinallt0-cinall-outletinfile-biodegradeinfile;

if((fp2=fopen("threetemp.txt","wt+"))==NULL)
```

```
  {
    printf("Cannot open file strike any key exit!");

  }

  fprintf(fp2,"%e %e %e %e\n",cinallt0,cinall,outletinfile, biodegradeinfile);

  fclose(fp2);

  if((fp1=fopen("outletandbio.txt","at"))==NULL)  /* create 1st file te record contaminant flow at at outlet boundary and biodegrade in pile */
  {
    printf("Cannot open file strike any key exit!");
  }

  fprintf(fp1,"%.2f %e %e %e %e %e %e %e %e %e %e %e\n", CURRENT_TIME, cinwater, cingas, cinsoil, cinorg, cinall, outletinfile, biodegradeinfile, totalpipeout, biomass,conoutlet,conbiodeg,cpipeoutints);

  fclose(fp1);

  /* THE FIFTH FUNCTION: record contaminant status with the time */

  fun5= (int) floor(CURRENT_TIME) % 3600;

  if((real)fun5<=CURRENT_TIMESTEP)
    {

    if((fp3=fopen("contaminantbalance.txt","at+"))==NULL)
```

```
    {
      printf("Cannot open file strike any key exit!");


    }


  /* fprintf(fp3,"T, cinwater, cingas, cinsoil, cinorg, cinall, totaloutlet, totalbiodegrade, totalpipeout, biomass\n");*/

   fprintf(fp3,"%.2f %e %e %e %e %e %e %e %e\n",CURRENT_TIME, cinwater, cingas, cinsoil, cinorg, cinall, outletinfile, biodegradeinfile, totalpipeout, biomass);

   fclose(fp3);

 }

}




/************************************************************************/

/* average temperature in every cell at the end of every time step      */

/************************************************************************/


/*DEFINE_ON_DEMAND(tempera)*/

DEFINE_EXECUTE_AT_END(tempera_at_end)

{

   /*   average temperature of each phase in every cell   */


  Domain *d=Get_Domain(1);   /* mixture domain for multiphase */

  Domain *gasdomain=Get_Domain(gasdomainid);  /*gas domain pointer*/

  int phase_domain_index, gas_domain_index;

  real vcr, vcrt,t;

  Thread *subthread;

  Thread *gasthread;
```

```
  Thread *thread_pile_mixture = Lookup_Thread(d,pile_zone_id);  /*get mixture thread in pile */
  cell_t c_pile;

  begin_c_loop(c_pile, thread_pile_mixture)    /* loops over cells in mixture thread of pile  */
   {
    vcr=0;
    vcrt=0;

    sub_thread_loop(subthread, thread_pile_mixture, phase_domain_index)
     {
      vcr=vcr+C_VOF(c_pile,subthread)*C_CP(c_pile,subthread)*C_R(c_pile,subthread);
vcrt=vcrt+C_VOF(c_pile,subthread)*C_CP(c_pile,subthread)*C_R(c_pile,subthread)*C_T(c_pile,sub
thread);
     }

    t=vcrt/vcr;

    sub_thread_loop(subthread, thread_pile_mixture, phase_domain_index)
     {
      C_T(c_pile,subthread)=t;
     }
   }
  end_c_loop(c_pile, thread_pile_mixture)
}

/************************************************************/
/* Source term for heat transfer  in aqueous phase                                  */
```

```
/* Source comes from bioreaction                                        */

/************************************************************/


DEFINE_SOURCE(heat,c,t,dS,eqn)

{

  real Bioa, source;


  Bioa=-
1/(Mben/1000000)*C_UDSI_M1(c,THREAD_SUPER_THREAD(t),5)*kb*C_UDSI(c,THREAD_SU
PER_THREAD(t),6)*Mben/1000*(C_UDSI_M1(c,t,1)/(C_UDSI_M1(c,t,1)+Ksb/Mben/rhoa_mole));
/*species mass degradated by bioreaction, bioab=Bac*Mc c molar mass */


  source=-1*Bioa*Bioheat;


  dS[eqn] = 0;


  return source;

}




/************************************************************/

/* Define diffusivity of UDS dependent on water                         */

/*                                                                      */

/************************************************************/


DEFINE_DIFFUSIVITY(water_diff,c,t,i)

{

    real diff;

    Domain *domain;
```

```
    Thread *pile_thread_mixture;

    Domain *waterdomain;

    int water_domain_index;


    domain = Get_Domain(1);  /* returns fluid domain pointer       */

    pile_thread_mixture=Lookup_Thread(domain, pile_zone_id);


    waterdomain=Get_Domain(waterdomainid);  /*** gets the domain ID for the water domain ***/

    water_domain_index=PHASE_DOMAIN_INDEX(waterdomain); /*** this is the phase domain index for the waterdomain ***/


    if (t == pile_thread_mixture || t == THREAD_SUB_THREAD(pile_thread_mixture, water_domain_index))


      diff=1.07176e-6*pow(C_VOF(c,THREAD_SUB_THREAD(pile_thread_mixture, water_domain_index)),(7/3))/pow(porosity,2);


    else


      diff= 1.07176e-6;


    return diff;

}




/************************************************************/

/* Define diffusivity of UDS dependent on gas                */

/*                                                           */

/************************************************************/
```

```
DEFINE_DIFFUSIVITY(air_diff,c,t,i)

{

    real diff;

    Domain *domain;

    Thread *pile_thread_mixture;

    Domain *gasdomain;

    int gas_domain_index;


    domain = Get_Domain(1);  /* returns fluid domain pointer       */

    pile_thread_mixture=Lookup_Thread(domain, pile_zone_id);


    gasdomain=Get_Domain(gasdomainid);  /*** gets the domain ID for the water domain ***/

    gas_domain_index=PHASE_DOMAIN_INDEX(gasdomain); /*** this is the phase domain index
for the waterdomain ***/


    if (t == pile_thread_mixture || t == THREAD_SUB_THREAD(pile_thread_mixture,
gas_domain_index))


      diff=1.0775e-5*pow(C_VOF(c,THREAD_SUB_THREAD(pile_thread_mixture,
gas_domain_index)),(7/3))/pow(porosity,2);


    else


      diff=1.0775e-5;


    return diff;

}
```

C Brief simulation results

Table A.2 Total contaminant in biopile at the beginning of each scenario

Scenario ID	Total contaminant in biopile (mole)
NA1	170.38
NA5	170.38
HA1	167.83
HA5	167.83
VA1	155.85
VA5	155.85
HA5RB	167.83
HA5RGO	167.83
HA5RAG	167.83
HA5IT	167.83
HA1SP25	167.83
HA1SP50	167.83
HA1BP	167.83
HA1BPHT	167.83
MP5-left pile	167.83
MP5-middle pile	167.83
MP5-right pile	167.83

Table A.3 Accumulative contaminant removed by loss via pile surface at different times

Scenario ID	Accumulative contaminant removed by loss via pile surface at different times (mole)							
	10 h	20 h	50 h	100 h	150 h	200 h	250 h	300 h
NA1	9.184	14.543	24.543	34.939	42.239	47.954	52.561	56.468
NA5	10.592	16.375	26.789	37.361	44.695	50.405	54.994	58.863
HA1	15.900	20.869	29.764	38.649	44.661	49.114	52.847	55.593
HA5	15.910	20.878	29.724	38.554	44.537	48.955	52.604	55.350
VA1	14.526	18.947	26.544	33.778	38.458	41.884	44.547	46.607
VA5	14.578	19.044	26.780	34.254	39.101	42.746	45.542	47.693
HA5RB	15.906	20.909	29.966	39.384	45.994	51.441	55.561	59.681
HA5RGO	15.781	20.829	29.696	38.533	44.519	48.940	52.590	55.337
HA5RAG	15.756	20.520	29.176	38.233	44.414	49.131	53.232	55.979
HA5IT	15.897	20.832	29.512	37.941	43.598	47.718	50.594	53.341
HA1SP25	15.668	20.408	28.540	36.094	40.789	44.054	46.801	48.351
HA1SP50	15.292	19.675	26.676	32.404	35.523	37.313	38.686	39.662
HA1BP	7.550	12.722	23.291	35.046	43.807	50.873	56.778	62.271
HA1BPHT	7.550	12.722	23.291	35.045	43.802	50.856	56.720	62.189
MP5-left pile	15.856	20.841	29.736	38.589	44.575	48.991	52.624	55.371
MP5-middle pile	15.844	20.828	29.722	38.577	44.567	48.990	52.655	55.402
MP5-right pile	15.823	20.800	29.678	38.596	44.571	48.885	52.573	56.770

Table A.4 Accumulative biodegraded contaminant at different times

Scenario ID	Accumulative biodegraded contaminant at different times (mole)							
	10 h	20 h	50 h	100 h	150 h	200 h	250 h	300 h
NA1	0.717	1.473	3.788	7.629	11.406	15.182	18.959	22.735
NA5	0.717	1.474	3.789	7.652	11.436	15.212	18.989	22.766
HA1	0.689	1.400	3.525	6.964	10.288	13.378	16.416	19.163
HA5	0.700	1.434	3.668	7.326	10.791	14.225	17.658	21.091
VA1	0.634	1.277	3.156	6.091	8.843	11.418	13.888	16.291
VA5	0.643	1.307	3.294	6.471	9.452	12.289	15.035	17.782
HA5RB	0.007	0.014	0.035	0.076	0.122	0.173	0.228	0.291
HA5RGO	0.700	1.434	3.668	7.326	10.791	14.225	17.658	21.091
HA5RAG	0.700	1.434	3.669	7.327	10.852	14.286	17.719	21.152
HA5IT	1.076	2.225	5.727	11.551	17.044	22.537	28.030	33.524
HA1SP25	0.689	1.400	3.525	6.964	10.208	13.298	16.344	19.091
HA1SP50	0.689	1.400	3.525	6.956	10.101	13.191	16.249	18.996
HA1BP	0.705	1.451	3.739	7.554	11.330	15.107	19.145	23.265
HA1BPHT	0.709	1.462	3.805	7.761	11.871	15.991	20.111	24.231
MP5-left pile	0.700	1.434	3.666	7.320	10.786	14.219	17.652	21.085
MP5-middle pile	0.700	1.431	3.648	7.279	10.746	14.179	17.613	21.046
MP5-right pile	0.699	1.431	3.647	7.268	10.736	14.169	17.603	21.036

Table A.5 Accumulative contaminant removed by loss to aeration pipes at different times

Scenario ID	Accumulative contaminant removed by loss to aeration pipes at different times (mole)							
	10 h	20 h	50 h	100 h	150 h	200 h	250 h	300 h
NA1								
NA5								
HA1	0.347	0.614	1.591	3.523	5.528	7.561	9.564	11.523
HA5	0.340	0.591	1.521	3.368	5.306	7.264	9.181	11.052
VA1	2.007	3.411	7.167	12.763	17.726	22.165	26.140	29.704
VA5	1.848	3.138	6.672	12.180	17.193	21.707	25.742	29.337
HA5RB	0.401	0.708	1.758	3.773	5.941	8.167	10.402	12.637
HA5RGO	0.327	0.577	1.515	3.375	5.338	7.296	9.214	11.087
HA5RAG	0.348	0.613	1.461	3.134	4.958	6.873	8.790	10.681
HA5IT	0.287	0.494	1.361	3.100	4.930	6.730	8.468	10.125
HA1SP25	1.085	2.090	5.303	10.836	16.372	21.818	27.105	32.168
HA1SP50	2.322	4.581	11.476	23.023	34.382	45.307	55.450	64.443
HA1BP								
HA1BPHT								
MP5-left pile	0.315	0.567	1.500	3.375	5.323	7.295	9.231	11.124
MP5-middle pile	0.330	0.586	1.528	3.409	5.355	7.307	9.244	11.134
MP5-right pile	0.357	0.619	1.603	3.481	5.434	7.402	9.336	11.226

Table A.6 Biodegradation contribution to the total contaminant removal at different times

Scenario ID	Biodegradation contribution to the total contaminant removal at different times (%)							
	10 h	20 h	50 h	100 h	150 h	200 h	250 h	300 h
NA1	7.24	9.20	13.37	17.92	21.26	24.05	26.51	28.70
NA5	6.34	8.26	12.39	17.00	20.37	23.18	25.67	27.89
HA1	4.07	6.12	10.11	14.17	17.01	19.10	20.83	22.21
HA5	4.13	6.26	10.51	14.88	17.80	20.19	22.23	24.11
VA1	3.69	5.40	8.56	11.57	13.60	15.13	16.42	17.59
VA5	3.77	5.56	8.96	12.23	14.38	16.01	17.42	18.76
HA5RB	0.04	0.06	0.11	0.18	0.23	0.29	0.34	0.40
HA5RGO	4.16	6.28	10.52	14.88	17.79	20.19	22.22	24.10
HA5RAG	4.17	6.35	10.69	15.05	18.02	20.32	22.22	24.09
HA5IT	6.23	9.45	15.65	21.96	25.99	29.27	32.18	34.56
HA1SP25	3.95	5.86	9.43	12.92	15.15	16.80	18.11	19.17
HA1SP50	3.76	5.46	8.46	11.15	12.63	13.77	14.72	15.43
HA1BP	8.54	10.24	13.83	17.73	20.55	22.90	25.22	27.20
HA1BPHT	8.58	10.31	14.04	18.13	21.32	23.92	26.18	28.04
MP5-left pile	4.15	6.28	10.50	14.85	17.77	20.17	22.20	24.08
MP5-middle pile	4.15	6.26	10.45	14.78	17.71	20.12	22.15	24.03
MP5-right pile	4.14	6.26	10.44	14.73	17.68	20.11	22.14	23.63

Table A.7 Accumulative total contaminant removal at different time

Scenario ID	Accumulative total contaminant removal at different times (%)							
	10 h	20 h	50 h	100 h	150 h	200 h	250 h	300 h
NA1	5.81	9.40	16.63	24.98	31.49	37.06	41.98	46.49
NA5	6.64	10.48	17.95	26.42	32.94	38.51	43.42	47.91
HA1	10.09	13.63	20.78	29.28	36.03	41.74	46.97	51.41
HA5	10.10	13.65	20.80	29.34	36.13	41.97	47.33	52.13
VA1	11.02	15.17	23.66	33.77	41.72	48.42	54.27	59.42
VA5	10.95	15.07	23.58	33.95	42.19	49.24	55.39	60.84
HA5RB	9.72	12.89	18.92	25.76	31.02	35.62	39.44	43.26
HA5RGO	10.02	13.61	20.78	29.34	36.14	41.98	47.35	52.14
HA5RAG	10.01	13.45	20.44	29.01	35.88	41.88	47.51	52.32
HA5IT	10.28	14.03	21.81	31.34	39.07	45.87	51.89	57.79
HA1SP25	10.39	14.24	22.27	32.11	40.14	47.17	53.77	59.35
HA1SP50	10.91	15.29	24.83	37.17	47.67	57.09	65.77	73.35
HA1BP	4.92	8.44	16.11	25.38	32.85	39.31	45.24	50.97
HA1BPHT	4.92	8.45	16.15	25.51	33.17	39.83	45.78	51.49
MP5-left pile	10.05	13.61	20.80	29.37	36.16	42.01	47.37	52.18
MP5-middle pile	10.05	13.61	20.79	29.35	36.15	41.99	47.38	52.18
MP5-right pile	10.06	13.61	20.81	29.40	36.19	41.98	47.38	53.05

D Publications

Conference Proceedings:

Crapper, M.; Wu, T. In *The significance of ambient atmosphere and temperature on ex-situ remediation of hydrocarbon contaminated soil: a computational fluid dynamics modelling approach*, Water and Sanitation in International Development and Disaster Relief, Edinburgh, UK, 2008; pp 296-307.

Crapper, M.; Wu, T. In *A computational approach to modelling ex-situ bioremediation*, The 4th European Bioremediation Conference, Chania, Greece, 2008; ISBN 978-960-8475-12-0.

Journal Papers:

Wu, T.; Crapper, M., A Computational Fluid Dynamics based model of the ex-situ remediation of hydrocarbon contaminated soils. *Desalination*, in press.

Wu, T.; Crapper, M., Simulation of biopile processes using a hydraulics approach. *Journal of Hazardous Materials*, under review.